Novel Interactions of SYNPO2 in Skeletal and Smooth Muscles

D I S S E R T A T I O N

zur
Erlangung des Doktorgrades (Dr. rer. nat.)
der
Mathematisch-Naturwissenschaftlichen Fakultät
der
Rheinischen Friedrich-Wilhelms-Universität Bonn

vorgelegt von

Marvin Aßent

aus

Wesel

Bonn, Mai 2024

Angefertigt mit Genehmigung der Mathematisch-Naturwissenschaftlichen Fakultät der Rheinischen Friedrich-Wilhelms-Universität Bonn

Gutachter/Betreuer: Prof. Dr. Dieter O. Fürst

Gutachter: Priv.-Doz. Dr. Gregor Kirfel

Tag der Promotion: 26.08.2024

Erscheinungsjahr: 2024

Parts of this work have previously been published in scientific journals:

Research articles:

Lohanadan, K.*, **Assent, M.***, Linnemann, A., Schuld, J., Heukamp, L. C., Krause, K., Vorgerd, M., Reimann, J., Schänzer, A., Kirfel, G., Fürst, D. O., Van der Ven, P. F. M. (2023). Synaptopodin-2 Isoforms Have Specific Binding Partners and Display Distinct, Muscle Cell Type-Specific Expression Patterns. *Cells*, 13(1), 85. DOI: 10.3390/cells13010085
* equal contribution

Mao, Y., Schneider, R., Ven, P. F. M. van der, **Assent, M.**, Lohanadan, K., Klämbt, V., Buerger, F., Kitzler, T. M., Deutsch, K., Nakayama, M., Majmundar, A. J., Mann, N., Hermle, T., Onuchic-Whitford, A. C., Zhou, W., Margam, N. N., Duncan, R., Marquez, J., Khokha, M., Hildebrandt, F. (2021). Recessive Mutations in SYNPO2 as a Candidate of Monogenic Nephrotic Syndrome. *Kidney International Reports*, 6(2), 472–483. DOI: 10.1016/j.ekir.2020.10.040

Poster presentations:

Assent, M., Lohanadan, K., Schuld, J., Linnemann, A., Van der Ven, P.F.M., Fürst, D.O. (2023). Synaptopodin-2 Isoforms: Expression patterns and specific binding partners. *European Muscle Conference* (EMC) 2023, Florence, Italy.



Abstract

Synaptopodin-2 (SYNPO2), a multiadapter protein from the synaptopodin family highly abundant in mammalian muscle cells, associates with Z-discs and dense bodies in skeletal and smooth muscle cells. It is involved in processes responsible for signaling, maintenance, and protein homeostasis. SYNPO2 interacts with a variety of proteins, including F-actin, α-actinin, filamin C, BAG3 and VPS18 of which the latter two link SYNPO2 to the CASA machinery and membrane vesicle trafficking.

in this work, the transcriptional coactivators YAP1 and TAZ were identified as novel interaction partners for two distinct structural elements of SYNPO2, its PDZ domain and its PPPY motif. Biochemical experiments were conducted to investigate the relationship between SYNPO2, YAP1/TAZ, and BAG3. These results demonstrate that SYNPO2 can act as a platform to constitute a ternary complex with BAG3 and YAP1/TAZ. Both, YAP1 and TAZ were found to independently bind to the PDZ domain and the PPPY motif of SYNPO2. Additional assays reveal YAP1 and TAZ to compete with BAG3 for binding to the PPPY motif, as BAG3 can displace YAP1 and TAZ.

Bimolecular fluorescence complementation (BiFC) assays demonstrate that SYNPO2-YAP1 complexes localize to Z-discs and dense bodies in skeletal and smooth muscle cells, respectively. Furthermore, peptide binding assays and co-immunoprecipitations (co-IPs) performed in this thesis revealed that SYNPO2 phosphorylation near its PPPY motif not only affected a molecular switch of BAG3 to replace YAP1 at this site, but also indicated an impaired to abolished SYNPO2 targeting to the actin cytoskeleton in both, skeletal and smooth muscle cells. In addition, fluorescence microscopic analyses quantifying the fraction of nuclear YAP1 in skeletal muscle cells suggest the regulation of YAP1 activity to be mediated by overexpressing BAG3, but not SYNPO2. It is speculated that SYNPO2 may stabilize YAP1/TAZ in the cytoplasm along the Hippo signaling core axis, whereas may BAG3 promote their activation. Taken together, these findings provide new insights into a potential regulatory role of SYNPO2 for the Hippo signaling pathway proteins YAP1/TAZ and linking them to BAG3-mediated autophagy in skeletal muscle cells.

Zusammenfassung

Synaptopodin-2 (SYNPO2), ein Multiadapterprotein der Synaptopodin-Familie, das mit Z-Scheiben in Skelettmuskeln und dense bodies in glatten Muskeln assoziiert. Es ist unter anderem für die Signalübertragung, die Erhaltung und die Proteinhomöostase der Skelettmuskulatur verantwortlich. SYNPO2 interagiert als Multiadapterprotein mit einer Vielzahl von Proteinen, darunter F-Actin, α-Actinin, Filamin C, BAG3 und VPS18, von denen die letzten beiden SYNPO2 mit dem CASA-Komplex und der Membran-Vesikel-Transportmaschinerie verbinden. In dieser Arbeit wurden die Transkriptionskofaktoren YAP1 und TAZ als neue Interaktionspartner zweier Bindestellen von SYNPO2, die PDZ-Domäne und das PPPY-Motiv, identifiziert. Durch proteinbiochemische Experimente wurden Protein-Protein-Wechselwirkungen zwischen SYNPO2, YAP1/TAZ und BAG3 untersucht. Diese zeigten, dass SYNPO2 als Plattform für die Bildung eines ternären Komplexes mit BAG3 und YAP1 bzw. TAZ dient. Darüber hinaus wurde festgestellt, dass YAP1 und TAZ unabhängig voneinander an die PDZ-Domäne und das PPPY-Motiv von SYNPO2 binden können. Weiterhin konnte beobachtet werden, dass YAP1 und TAZ mit BAG3 um die Bindung an das PPPY-Motiv konkurrieren und BAG3 sowohl YAP1 als auch TAZ verdrängen kann. Durch bimolekulare Fluoreszenzkomplementationsexperimente (BiFC) wurde veranschaulicht, dass SYNPO2-YAP1-Komplexe in Z-Scheiben in Skelett- bzw. dense bodies in Glattmuskelzellen lokalisiert sind. Peptidinteraktionsassays und Co-Immunpräzipitationen in dieser Arbeit zeigten, dass SYNPO2-Phosphorylierungen nahe dem PPPY-Motiv nicht nur einen Austausch von YAP1 durch BAG3 an dieser Bindestelle verhindern, sondern auch Lokalisation von SYNPO2 mit dem Actinzytoskelett in Skelett- und Glattmuskelzellen beeinträchtigen können. Weitere mikroskopische Experimente zur Bestimmung des Anteils an aktivem, nukleärem YAP1 in Skelettmuskelzellen deuteten darauf hin, dass eine Regulierung der YAP1-Aktivität durch die Überexpression von BAG3, nicht aber von SYNPO2 vermittelt wird. Dadurch wurde vermutet, dass SYNPO2 die Hippo-Signalwegeffektoren YAP1/TAZ im Zytoplasma stabilisieren könnte, während BAG3 diese aktiviert. Zusammenfassend vermitteln die Ergebnisse dieser Arbeit einen neuen Einblick in eine potentiell regulatorisches, SYNPO2-vermitteltes Zusammenspiel von Hippo-Signalwegeffektoren YAP1/TAZ und deren Assoziierung mit BAG3-vermittelter Autophagie durch die CASA-Maschinerie in Skelettmuskelzellen.

Change. But start slowly, because
direction is more important than speed
- *Paolo Coelho* -

Acknowledgements

First and foremost, I want to express my sincere gratitude to everyone who helped me complete this thesis; it has been a long and challenging journey for me that was also incredibly rewarding:

Most importantly, I would like to give special thanks to Prof. Dieter O. Fürst for giving me the opportunity to work on this fascinating topic, and for always being available to help with any problems. I am extremely grateful for his trust, his advice, and our lively discussions, especially in the field of biochemistry!

Thanks to PD Dr. Gregor Kirfel, who contributed to this work as my reviewer with his valuable pieces of honest advice regarding academic writing, microscopic analyses, and his recommendation to switch to Ultegra.

I want to extend my sincere thanks to my colleague and supervisor Dr. Peter van der Ven for his valuable insights and expertise in cell biology. His pragmatically simple solutions to complex problems and his willingness to support me have made working in this field of research much more enriching.

I want to thank my fellow coworkers Dr. Keerthika Lohanadan and Lorena Heil for making institute life much more enjoyable. Working with you has been an absolute pleasure thanks to your companionship, your scientific advice, and your moral support. (And - of course - your support with Aperol Spritz...). Moreover, a dedicated shoutout to the (former) scientists of the Haas Lab, specifically Alexandra Jünger-Leif and Dr. Thomas Haubenthal, as well as La(u)ra Pöttgen, Tobi(a)s Dummin and Ariane Schleinitz. I appreciate your professional scientific expertise, but what is more important to me is the fact that we became friends and spent so much time together.

In addition, I want to thank our lab technicians, especially Babette Bockmühl, Corina Mirschkorsch, and Karin Bois for putting up with my crazy schedule, sticky proteins, and my unorthodox protocols. Your patience and hard work helped to achieve fruitful results for this work. Special gratitude to all collaboration partners from the Warscheid group in Würzburg, but also Kristina Djinović-Carugo from Vienna for performing additional experiments, supportive information, and lots of additional data!

I really appreciate the immense support of all my other friends, family, and especially my girlfriend. Thank you all! Your aid has kept me going even during many moments of doubt. All the valuable time we spent, all moments of laughter, happy memories we share together in various corners of the globe, and all of your encouragement have been the perfect antidote.

As parts of this work were a team effort, I am truly grateful for the collaborative spirit that surrounded me in this work group. I am truly thankful for each person who contributed to both my academic and personal growth during these tremendous six years.

Contents

1 Introduction **1**

1.1 Vertebral muscle tissues . . . 1

1.1.1 Smooth muscle: Overview and function . . . 1

1.1.2 Striated muscle: Overview and function . . . 2

1.2 Subcellular organization of the smooth muscle cell . . . 4

1.2.1 Structural features of the smooth muscle actin cytoskeleton . . . 5

1.2.2 Dense bodies and dense plaques . . . 6

1.3 Organization of skeletal muscle . . . 8

1.3.1 Structural features of the skeletal muscle cytoskeleton . . . 9

1.3.2 The Z-disc and its associated proteins . . . 12

1.4 Protein network of Z-disk and dense bodies . . . 14

1.4.1 α-actinin . . . 14

1.4.2 The synaptopodin protein family member SYNPO2 . . . 15

1.4.3 BAG3 and its role in autophagy at the Z-disk . . . 20

1.4.4 The transcriptional coactivation factors YAP1 and TAZ . . . 22

1.5 WW domains . . . 24

1.6 Aims of this study . . . 25

2 Materials and Methods **27**

2.1 Materials . . . 27

2.1.1 Chemicals . . . 27

2.1.2 Antibiotics . . . 27

2.1.3 Media, buffers, and solutions . . . 28

2.1.4 Consumables . . . 30

2.1.5 Antibodies . . . 31

2.1.6 Kits . . . 32

2.1.7 Bacterial strains . . . 32

2.1.8 Software & Tools . . . 33
2.2 Methods in Molecular Biology . . . 34
2.2.1 Plasmid DNA isolation . . . 34
2.2.2 Agarose gel electrophoresis . . . 34
2.2.3 Polymerase chain reaction (PCR) . . . 35
2.2.4 Amplicon isolation from PCRs and clean-up from agarose gels . . . 36
2.2.5 Restriction endonuclease treatment . . . 36
2.2.6 Ligation . . . 37
2.2.7 Transformation of bacterial cells . . . 37
2.3 Methods in Protein Biochemistry . . . 38
2.3.1 Recombinant protein expression . . . 38
2.3.2 Affinity chromatography purification of GST-tag recombinant proteins 39
2.3.3 Affinity chromatography purification of His-tagged recombinant proteins . . . 40
2.3.4 Denaturing purification of His-tagged recombinant proteins . . . 40
2.3.5 Tandem Affinity Purification (TAP) of PDZ domains . . . 41
2.3.6 Spectrophotometric determination of protein concentrations . . . 41
2.3.7 Protein pulldown assay . . . 42
2.3.8 Protein crosslinking assay . . . 43
2.3.9 Co-immunoprecipitations (co-IP) . . . 43
2.3.10 Co-immunoprecipitations (co-IP) with YAP1/TAZ constructs . . . 44
2.3.11 Competitive binding assay . . . 44
2.3.12 Peptide interaction assay . . . 45
2.3.13 SDS-Polyacrylamide gel electrophoresis (SDS-PAGE) . . . 45
2.4 Methods in Cell Biology . . . 49
2.4.1 Cultivation of mammalian cells . . . 49
2.4.2 C2C12 murine myoblast cell line . . . 49
2.4.3 A7r5 smooth muscle-like cell line . . . 49
2.4.4 Cell density measurements . . . 50
2.4.5 Transient transfection of myoblasts via electroporation (Nucleofection) 50
2.4.6 Transient transfection of cells via chemical compounds (JetPRIME) 51
2.4.7 Bimolecular fluorescence complementation assay (BiFC) . . . 51

2.4.8 Fixation of cells with paraformaldehyde 52
2.4.9 Electrical pulse stimulation (EPS) 52
2.4.10 Immunofluorescence staining of cells for microscopy 52
2.4.11 Confocal laser scanning microscopy (CLSM) 53
2.5 Computational Biology and *in silico* analyses 54
2.5.1 Nuclear translocation measurements of YAP1 54
2.5.2 Colocalization analyses 55
2.5.3 Line plot analyses 55
2.5.4 In-Gel quantification of GST-Pulldowns 56
2.5.5 Quantification of co-IPs 56
2.5.6 Statistical Analyses 56

3 Results **57**
3.1 PDZ domain interactions of SYNPO2 57
3.1.1 The PDZ domain of SYNPO2 remains in a monomeric state 58
3.1.2 YAP1 harbors a C-terminal motif that interacts with SYNPO2 . . . 60
3.1.3 SYNPO2 functions as an adapter protein, forming a ternary complex with BAG3, and YAP1/TAZ 63
3.1.4 YAP1 and BAG3 bind SYNPO2 simultaneously, but independently 66
3.2 The relationship between SYNPO2, BAG3, and YAP1/TAZ 74
3.2.1 SYNPO2 harbors a novel binding motif for both YAP1 and TAZ independent of the PDZ domain 74
3.2.2 BAG3 competes with both YAP1 and TAZ for the PPPY motif in SYNPO2 *in vitro* 78
3.3 YAP1 and SYNPO2 have distinct interaction patterns in smooth and skeletal muscle cells 84
3.3.1 SYNPO2-YAP1 complexes are recruited to dense bodies in smooth muscle cells 85
3.3.2 SYNPO2-YAP1 complexes are recruited to Z-discs in skeletal muscle cells 92
3.4 SYNPO2 interactions with BAG3, YAP1, and TAZ are regulated via phosphorylation 98

3.4.1 Phosphorylations in SYNPO2 regulate binding of different WW domains . . . 99
3.4.2 Phosphorylations in SYNPO2 facilitate a replacement of YAP1 isoforms by BAG3 *in vitro* . . . 101
3.5 SYNPO2 phosphorylations specifically regulate its recruitment to the actin cytoskeleton in muscle cells . . . 105
3.5.1 SYNPO2 associates with the actin cytoskeleton in a phosphorylation-dependent manner . . . 106
3.5.2 Phosphorylations of SYNPO2 regulate its binding to α-actinin *in vitro* 111
3.6 YAP1 activation regulation in muscles . . . 115
3.6.1 BAG3, but not SYNPO2 overexpression facilitates YAP1 activation in skeletal muscle cells . . . 115
3.6.2 Muscle damage exerted by EPS regulates YAP1 activation in skeletal muscle cells . . . 119
3.7 Novel mutations in human SYNPO2 abrogate binding to α-actinin, eventually leading to disease . . . 122

4 Discussion **125**
4.1 Novel interactors bind to the PDZ domain of SYNPO2 . . . 125
4.2 YAP1 and TAZ interactions with the PPPY motif of SYNPO2 . . . 129
4.3 SYNPO2 phosphorylations regulate binding of WW domain-containing proteins to its PPPY motif . . . 132
4.4 Regulation of YAP1 in smooth and skeletal muscle cells . . . 136
4.5 Novel SYNPO2 mutations and their role for human disease . . . 139

Appendix A **I**
Abbreviations . . . I
Amino acid code . . . V
SI-Prefixes . . . VI
List of Units . . . VI

Appendix B **VII**
Motifs and domain classes . . . VII

Appendix C **IX**

Supplementary Figures IX

Appendix D **XVII**

Sequences and primers XVII

Appendix E **XXII**

Vector maps XXII

Appendix F **XXXIII**

Suppliers, manufacturers, developers and publishers XXXIII

List of Tables

2.1 Antibiotics . . . 27
2.2 Solutions for the cultivation of bacterial strains . . . 28
2.3 Solutions for mammalian cell culture . . . 28
2.4 Media for mammalian cell culture . . . 29
2.5 General buffers . . . 29
2.6 Protein purification buffers . . . 30
2.7 Primary antibodies . . . 31
2.8 Secondary antibodies and conjugates . . . 31
2.9 Commercially available kits . . . 32
2.10 Strains used in molecular cloning and protein biochemistry . . . 32
2.11 Software and computational tools . . . 33
2.12 DNA marker list . . . 34
2.13 *Phusion* PCR . . . 35
2.14 *FIREPol* PCR . . . 36
2.15 Recombinant protein chimeras and expression conditions . . . 38
2.16 Tris-glycine SDS gel composition . . . 46
2.17 Bis-Tris SDS gel composition . . . 46

3.1 SYNPO2 Phosphorylation sites in muscle cells upon mechanical stress . . . 98

B.1 PDZ domain classes . . . VII
B.2 WW domain groups . . . VII
B.3 YAP1/TAZ phosphorylation sites and kinases . . . VIII

D.1 α-actinin cloning primer sequences . . . XVII
D.2 SYNPO2 cloning primer sequences . . . XVII
D.3 YAP1 and TAZ cloning primer sequences . . . XVII
D.4 SYNPO2L cloning primer sequences . . . XVIII

E.1 Company list XXXIII

List of Figures

1.1 Electron micrograph from a transverse section of relaxed-state porcine trachealis muscle fixed *in situ*. 2
1.2 Electron micrograph and schematic outline of the sarcomeric organization in striated muscles. 3
1.3 Schematic illustration of a smooth muscle cell 5
1.4 Schematic transversal section model of a dense plaque 7
1.5 Illustration of a skeletal myofiber 8
1.6 Schematic outline of the sarkomer 11
1.7 Overview of the α-actinin-2 dimer conformation 15
1.8 Overview of the synaptopodin protein family members SYNPO, SYNPO2, and SYNPO2L 16
1.9 Prediction of protein disorder in SYNPO2a 17
1.10 Structure of the PDZ-peptide complex of SYNPO2 and VPS18 19
1.11 Overview of the protein BAG3 20
1.12 BAG3-mediated macroautophagy via CASA machinery 21
1.13 Overview of the transcriptional coactivators YAP1 and TAZ 22

3.1 SEC elution profiles of SYNPO2 and SYNPO2L during purification 59
3.2 PDZ domains of SYNPO2 and SYNPO2L remain in a monomeric state . . 60
3.3 Protein alignment of positively screened ligands for SYNPO2 61
3.4 *In silico* motif prediction and PDZ domain interactors 61
3.5 YAP1 interacts with the PDZ domain of SYNPO2 *in vitro* 62
3.6 SYNPO2, YAP1 and BAG3 form a ternary complex 64
3.7 SYNPO2, TAZ and BAG3 form a ternary complex 65
3.8 YAP1 does not engage in PPIs with BAG3 67
3.9 Overview of YAP1 constructs for overexpression in muscle cells 68
3.10 YAP1 overexpression in smooth muscle cells 69

3.11 YAP1 overexpression in skeletal muscle cells 70
3.12 YAP1 overexpression in C2C12 cells with regard to nuclear targeting 71
3.13 Nuclear translocation of overexpressed YAP1 in smooth and skeletal muscles 73
3.14 Protein alignment of human group I WW domains 75
3.15 SYNPO2 coprecipitates with YAP1 constructs lacking the PDZ-BM 76
3.16 SYNPO2 coprecipitates with TAZ constructs lacking the PDZ-BM 77
3.17 Competitive binding assays of BAG3 and YAP1--1 78
3.18 Competitive binding assays of BAG3 and YAP1--2 79
3.19 Competitive binding assays of BAG3 and TAZ 80
3.20 Overview of C-terminal pseudo-PPXY motifs in human SYNPO2 81
3.21 Co-IPs of SYNPO2(664--1093) and YAP1 82
3.22 Co-IPs of SYNPO2(664--1093) and TAZ 83
3.23 Schematic overview of SYNPO2 isoforms predominantly expressed in striated muscle tissue 84
3.24 Overview of transiently transfected BiFC constructs 85
3.25 BiFC assays of YAP1--1 and SYNPO2 in smooth muscle cells 86
3.26 BiFC assays of YAP1--2 and SYNPO2 in smooth muscle cells 87
3.27 SYNPO2-YAP1 colocalization with α-actinin in smooth muscle cells 88
3.28 Overview of transiently transfected SYNPO2 truncation constructs 89
3.29 Overexpression of SYNPO2 constructs in smooth muscle cells 90
3.30 Line plot measurements of SYNPO2 and α-actinin 91
3.31 Overexpression of SYNPO2 constructs in smooth muscle cells 93
3.32 SYNPO2-YAP1 colocalization with the Z-disc epitope of titin in skeletal muscle cells 94
3.33 Overview of transiently transfected SYNPO2 truncation constructs 94
3.34 Overexpression of SYNPO2 truncation constructs in skeletal muscle cells . 95
3.35 Line plot measurements of SYNPO2 and the Z-disc epitope of titin 96
3.36 Overview of Phosphomimetic substitute of serine and threonine 99
3.37 Peptide binding assay of WW domain to the PPPY motif in SYNPO2 . . . 100
3.38 Competitive binding assay of YAP1-WW12 and BAG3 102
3.39 Competitive binding assay of YAP1-WW1 and BAG3 103
3.40 Schematic overview of SYNPO2 phosphomimetic mutants 105

3.42 Line plot measurements of SYNPO2 and α-actinin 107
3.41 Overexpressing SYNPO2 mutant constructs in smooth muscle cells 108
3.43 Overexpressing SYNPO2 mutant constructs in skeletal muscle cells 109
3.44 Line plot measurements of SYNPO2 and the Z-disc epitope of titin 110
3.45 Protein alignment of the N-terminal SYNPO2 α-actinin-binding region . . . 111
3.46 Co-IPs of SYNPO2 with different α-actinin isoforms 112
3.47 Quantifying α-actinin isoform binding upon phosphorylation in SYNPO2 . . 113
3.48 Overview of transiently transfected SYNPO2 constructs 116
3.49 Nuclear translocation of endogenous YAP1 in smooth and skeletal muscle cells 117
3.50 Nuclear translocation of overexpressed YAP1 in smooth and skeletal muscle cells 118
3.51 Nuclear translocation of endogenous YAP1 in mechanically damaged C2C12 myotubes 119
3.52 YAP1 localization in skeletal muscle cells under mechanical stress 120
3.53 Protein pulldown assay of SYNPO2 with α-actinins 123
3.54 Quantifying α-actinins bound to SYNPO2 exon 6 constructs 124

4.1 Possible binding modes between YAP/TAZ and SYNPO2 130

C.1 Species of PDZ-PDZ dimer complexes X
C.2 Protein crosslinks using the PDZ domain of SYNPO2 with increased ionic strength X
C.3 SYNPO2 constructs for biochemistry and cell biology experiments XI
C.4 YAP1 constructs for biochemistry and cell biology experiments XII
C.5 TAZ constructs for biochemistry and cell biology experiments XII
C.6 BiFC experiment of analyzed ROIs in A7r5 smooth muscle-like cells XIII
C.7 BiFC experiment of analyzed ROIs in A7r5 smooth muscle-like cells XIV
C.8 BiFC experiment of analyzed ROIs in C2C12 myotubes XV
C.9 BiFC experiment of analyzed ROIs in C2C12 myotubes XVI

C.10 Sequence alignment of SYNPO2 proteins from different species XVIII
C.11 Sequence alignment of human α-actinin isoforms XIX
C.12 Sequence alignment of human YAP1 and TAZ isoforms XX
C.13 Sequence alignment of human SYNPO2 constructs utilized XXI

C.14 pETW1-EEF plasmid XXIII
C.15 pETW2-T7 plasmid XXIV
C.16 pGEX-6P plasmid XXV
C.17 pGEX-W2-hybrid plasmid XXVI
C.18 pEGFP-N1Pd plasmid XXVII
C.19 pEGFP-C1Pd plasmid XXVIII
C.20 pVenus1-C plasmid XXIX
C.21 pVenus2-C plasmid XXX
C.22 pVenus1-N3 plasmid XXXI
C.23 pVenus2-N3 plasmid XXXII

Chapter 1

Introduction

1.1 Vertebral muscle tissues

The vertebral musculature, as a multifaceted system, is responsible for a versatile repertoire of physiological functions. By generating force and movement through contraction, muscles account for a wide range of activities including locomotion, feeding and digestion, vascular constrictions, and respiration. From basal vertebrates, important muscle tissue groups further developed, including (cardio-)vascular, cranial, neck, pectoral, and forelimb/fin muscles, in the clades of *Actinopterygii* and *Sarcopterygii* (Diogo & Abdala, 2010). Over time, the vertebral musculature became more complex due to evolutionary transitions, subdivisions, and reversions of muscle groups in developed vertebrates. With this development, the role of muscular tissues emerged in maintaining posture and stability, protecting internal organs, respiration, and regulating body temperature in homoiothermic animals (Diogo & Abdala, 2010; Donadon & Santoro; 2021). Due to differences in cellular organization and function, vertebral muscles are classified into three major types: Smooth muscle tissue, and striated muscle tissue which, in turn, may be further subdivided into skeletal and heart muscles. Each of these muscle types possesses a distinct structural and functional profile, which is addressed in detail in the following sections.

1.1.1 Smooth muscle: Overview and function

Smooth muscles are distinguished from striated muscles due to their morphology, capability to maintain the muscle tone for extended periods, and the ability to involuntarily contract (Hafen *et al.*, 2023). In humans and other vertebrates, the smooth

muscle tissue is part of organ walls in the gastrointestinal tract, functioning in intestinal peristalsis, the bladder, or the cardiovascular system regulating vasoconstriction (Hafen *et al.*, 2023). At the cellular level, smooth muscle cells are interspersed with an alternating pattern of thick and thin filaments (myofilaments) that are not organized in sarcomeres (Kelly & Rice, 1969). These myofilaments consist of bundles of actin microfilaments, called thin filaments, and bundles of myosin, called thick filaments (Lowy & Small, 1970; Murphy, 1976). On light microscopic examination, the cytoplasm of these cells will appear mostly homogeneous (smooth), but in electron microscopy, it features a non-striated pattern of actin and myosin filaments (Kelly & Rice, 1969). However, structures such as electron-dense plaques anchoring actin filament bundles can be observed within smooth muscle cells (Bond & Somlyo, 1982). Due to their dark appearance in electron microscopy imaging, these structures were previously termed as dense bodies (Fig. 1.1).

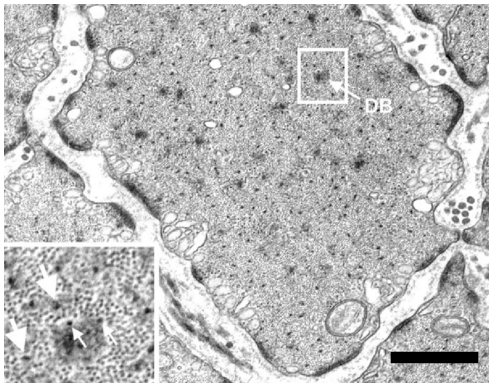


Fig. 1.1: Electron micrograph from a transverse section of relaxed-state porcine trachealis muscle fixed *in situ*. Dense bodies (DB). (Bottom left) The magnified portion from the dense body. Lattice-arranged Actin-containing thin filaments, intermediate filaments (small arrows) and myosin-containing thick filaments (large arrows) surrounding the dense body. Taken and modified from Herrera *et al.* (2005). Scale bar: 1 µm.

1.1.2 Striated muscle: Overview and function

Cardiac and skeletal muscles both showcase a distinct organizational pattern essential to their functions (Mukund & Subramaniam, 2019). Striated muscles ensure voluntary, precise force generation and transmission through myofibrils comprised of an intricately arranged network of myofilaments consisting of actin and myosin (Clark *et al.*, 2002).

These myofilaments are arranged in alternating arrays of sarcomeres, which represent the elementary contractile units of striated muscles. Using polarized light microscopy, the cross-striated appearance of the sarcomere organization becomes visually apparent (Hanson & Huxley, 1954; Huxley, 1957) (Fig. 1.2): The sarcomeric arrangement is based on darker, anisotropic and lighter, isotropic regions, called the A-band and the I-band, respectively.

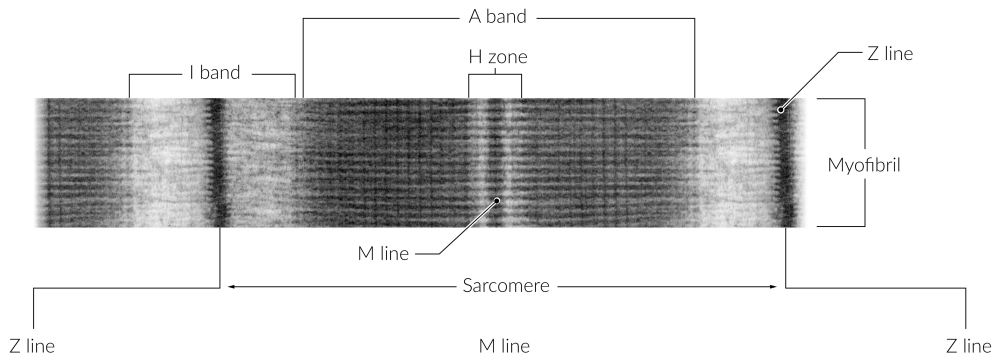


Fig. 1.2: Electron micrograph and schematic outline of the sarcomeric organization in striated muscles. (Upper panel) Using electron microscopy, the differential appearance of each region of the sarcomere can be visualized. (Lower panel) Outline of myosin myofilaments (rose) and actin myofilaments (blue). Note, that in the Z-disc (Z-line), actin myofilaments are anchored and primarily crosslinked via α-actinin. Adapted from AMBOSS GmbH. https://amboss.com. Accessed March 01, 2024

The I-band, consisting of actin microfilaments, is bisected by the Z-disc bordering each of the sarcomeres. In the Z-disc, actin myofilaments are rigidly anchored. The A-band contains both, myosin and actin myofilaments and is bisected by the H-zone, where only myosin can be found. In the middle of the H-zone, the M-band is located, where myosin myofilaments are cross-connected (Huxley, 1957; Huxley, 1963). While the heart musculature is responsible for cardiac output and blood circulation, special emphasis should be placed on the skeletal musculature, facilitating thermoregulation as well as voluntary movements for locomotion and posture maintenance (Lieber & Fridén, 2000; Mukund & Subramaniam, 2019).

1.2 Subcellular organization of the smooth muscle cell

Together with other components of the cytoskeleton - addressed in later sections - human smooth muscle cells possess a specialized contractile apparatus, a conjointly arranged network of actin and myosin myofilaments. Associated with myofilaments, actin-binding proteins including α-actinin, tropomyosin, caldesmon, calponin, filamin, dystrophin, and ARP2/3 play an eminent role in the structural integrity of the smooth muscle contractile machinery (Fürst *et al.*, 1986; North *et al.*, 1994b; Terasaki *et al.*, 2002; Gunning *et al.*, 2008; Lehman & Morgan, 2012). The myosin filaments, consisting of the force-generating motor protein smooth muscle myosin II, associated with myosin light chain kinase (MLCK), and myosin light chain phosphatase (MLCP), represent the foundation of smooth muscle contractility and its modulation (Somlyo & Somlyo, 2003). The unique smooth muscle contraction shall be briefly described: In response to specific stimuli, the smooth muscle contraction mechanism is initiated by an intracellular increase of calcium (Ca^{2+})-concentration. These stimuli are either a membrane depolarization through neuronal action potentials, receptor-agonistic agents (e.g. angiotensin II, norepinephrine), or mechanical activation through stretch (Webb, 2003). Receptor-operated or voltage-gated Ca^{2+}-channels (VGCCs) facilitate a Ca^{2+}-release from either the sarcoplasmic reticulum (SR) or a transfer through the sarcolemma upon stimulation. A phospholipase C (PLC) and 1,4,5-innositoltriphosphate (IP_3)-mediated signal cascade causes the SR, a specialized organelle that stores Ca^{2+}-ions, to release Ca^{2+} into the cytosol (Webb, 2003). The influx of calcium across the sarcolemma is facilitated by L-type VGCCs located in special structures at the membrane, called *caveolae* (Hafen *et al.*, 2023; Webb, 2003). *Caveolae*, flask-shaped invaginations at the smooth muscle sarcolemma, contain the actin-associated protein calveolin (Fig. 1.3) (Gabella & Blundell, 1978; Taggart, 2001). In the cytosol, Ca^{2+} binds the protein calmodulin to form a complex which activates the MLCK. The smooth muscle-specific 20-kDa myosin light chain (MLC_{20}) is phosphorylated by activated MLCK. The activated ATPase subunit of myosin hydrolyzes ATP which, in turn, triggers cross-bridge cycling along actin filaments resulting in force development through contraction (Taggart, 2001; Webb, 2003). In contrast, the smooth muscle relaxation is initiated by the removal of Ca^{2+}-ions from the cytoplasm, which is facilitated by

Ca^{2+}/Mg^{2+}-ATPases in the sarcolemma and in the SR. Closed VGCCs circumvent a Ca^{2+}-reentry into the cell during relaxation. The decrease of cytosolic Ca^{2+} activates a MLCP-mediated dephosphorylation of MLC, causing it to detach from the actin filaments, resulting in relaxation of the cell.

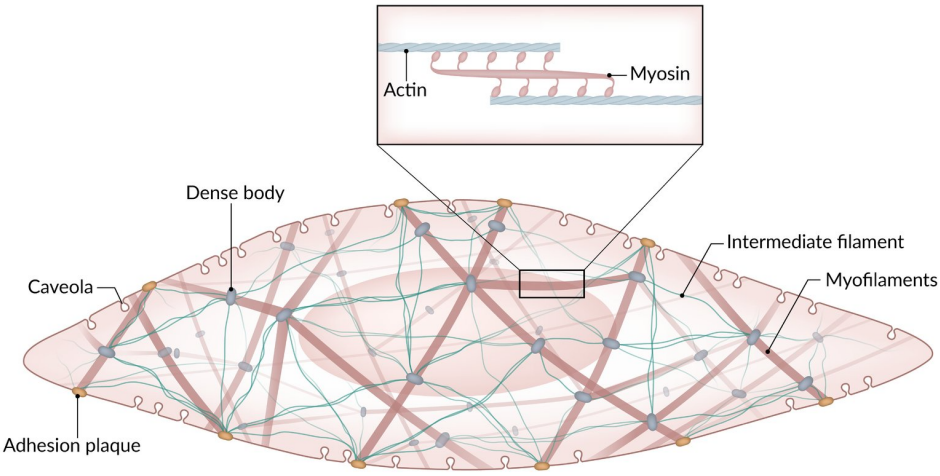


Fig. 1.3: Schematic illustration of a smooth muscle cell. Important cytosolic and sarcolemmal structures such as *caveolae*, dense bodies, and adhesion plaques are outlined. Contractile actin (blue) and myosin (red) filaments, but also intermediate filaments (green) represent smooth muscle cytoskeleton components which maintain the structural integrity and secure functionality. Adapted from AMBOSS GmbH. https://amboss.com. Accessed March 01, 2024.

1.2.1 Structural features of the smooth muscle actin cytoskeleton

The cytoskeleton of the smooth muscle cell exhibits distinctive structural features that account for its unique contractile properties: In addition to myofilaments of the contraction machinery, cortical non-muscle actin-containing filaments, intermediate filaments, and the microtubule system comprise the smooth muscle cytoskeleton. These cytoskeletal components function in maintaining cell shape, mechanical resistance, and sustaining cellular transport processes (Gao, 2022). The actin filaments of the contractile apparatus are composed of the smooth muscle-specific isoforms α- and γ-actin. These isoforms predominate in vascular and gastrointestinal smooth muscle tissue, respectively (Fatigati & Murphy, 1984; Kim *et al.*, 2008; Lehman & Morgan, 2012; Gao, 2022). However, non-muscle γ-actin and β-actin expressed in smooth muscle were found to polymerize into *non-muscle* actin filaments

distinct from the contractile apparatus. These non-muscle actin filaments, organized at the cell cortex and along the longitudinal axis of the cell, transmit contractile forces exerted from the myofilament apparatus to the extracellular matrix (ECM) (Tang & Tan, 2003; Gunst & Zhang, 2008; Yamin & Morgan, 2012). The intermediate filament network spans the whole the cell, promoting structural integrity of the cell and maintaining its shape (Small & Gimona, 1998). In particular, intermediate filaments represent a heterogeneous subfamily of cytoskeletal filaments: proteins that self-assemble into intermediate filaments can be divided into six major groups based on biochemical properties and sequence homologies (Tang, 2008). Smooth muscle intermediate filaments are predominantly composed of the type III intermediate filament proteins desmin and vimentin (Frank & Warren, 1981; Johansson *et al.*, 1997; Small & Gimona, 1998). In order to conjointly sustain aforementioned functions in the smooth muscle cell, these cytoskeletal components are interconnected by specialized structures called dense bodies.

1.2.2 Dense bodies and dense plaques

Dense bodies are electron-dense structures in smooth muscles crucial for spatially organizing and cross-linking the contractile myofilament apparatus and connecting it with other cytoskeleton components (Draeger *et al.*, 1989). By providing a semi-rigid framework to which actin myofilaments are attached, dense bodies can be functionally compared to Z-discs in skeletal muscle cells (Bond & Somlyo, 1982). Dense bodies also function in cross-connecting vimentin and desmin intermediate filaments (Draeger *et al.*, 1990). Spatial codistribution of the intermediate filaments and the cytoskeletal actin filaments occurs at the dense bodies, connecting them with the contractile actin filament machinery (Small & North, 1995; Yamin & Morgan, 2012). Non-muscle α-actinin, namely α-actinin-1 is the primary component of dense bodies. It cross-links actin filaments and anchors them to the dense bodies, scaffolding structural integrity of both non-contractile non-muscle actin and contractile myofilaments (Waites *et al.*, 1992). Another protein accumulated in dense bodies and associated with actin filament binding is calponin, a 34-kDa protein responsible for regulating the contractile activity of smooth muscle myofilaments (Takahashi *et al.*, 1988; North *et al.*, 1994b; Winder *et al.*, 1998; Roman *et al.*, 2013). Thus, dense bodies can be

considered not only fundamental structures for smooth muscle contraction and force transmission, but also as an integral link of the contractile apparatus with both the cytoskeletal components actin and intermediate filaments.

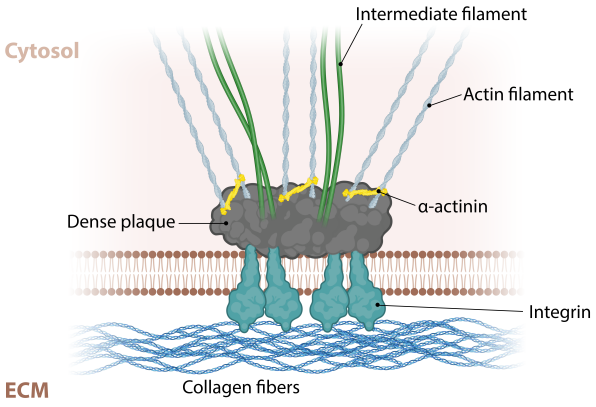


Fig. 1.4: Schematic transversal section model of a dense plaque. Attached at the cell membrane, dense plaques connect the ECM with the actin filaments (blue) of the contractile apparatus. Dense plaques are composed of integrins, organized at the interface between ECM components like Collagen (dark blue) and dense plaque proteins, such as α-actinin (yellow) which cross-connects actin, filamin, vinculin, and dystrophin. Created with Biorender.com. Based on Sit *et al.*, 2019.

Dense plaques, historically discovered as dense structures in electron microscopy, were classified as a type of integrin-enriched adhesion site, located at the sarcolemma (North *et al.*, 1993; Morgan *et al.*, 2007) (Fig. 3.1). Their incorporation of both, myofilaments and intermediate filaments, as well as their longitudinal extent within the cell distinguishes them from both, adherens junctions and focal adhesions (FAs) (Couchman & Rees, 1979; Small, 1985; Burridge *et al.*, 1987; Dorland & Huveneers, 2017). Similar to the latter, dense plaques establish contact between the contractile myofilament network and the ECM, as both harbor a similar subset of proteins including dystrophin, vinculin, α-actinin, talin or filamin (Draeger *et al.*, 1990; Turner *et al.*, 1991; North *et al.*, 1993). To date, no advances have been made to comparatively analyze the adhesome of dense plaque to FAs in detail (Sit *et al.*, 2019). However, both dense plaques and FAs, are structures responsible for force transmission and smooth muscle cell contraction along the ECM (Gunst & Tang, 2000).

1.3 Organization of skeletal muscle

In healthy humans, skeletal muscles amount to approx. 22–35% of the total body mass in women and men, respectively (Janssen *et al.*, 2000). A skeletal muscle consists of large multinucleated cells which are longitudinally oriented to their force generation axis and attached to the skeleton via tendons (Lieber, 1993; Dave *et al.*, 2023). The muscle and its substructures are compassed by sheaths of connective tissue, the mysia, of which the epimysium layers around the muscle fiber (Clark *et al.*, 2002). These muscle fibers are organized in bundles of fascicles bordered by the perimysium and supplied by blood vessels. Each fascicle subdivides into endomysium-enclosed muscle fibers, syncytia of multinucleated muscle cells developed from fused myoblasts during myogenesis (Alberts *et al.*, 2002, pp. 918–919; Clark, 2002).

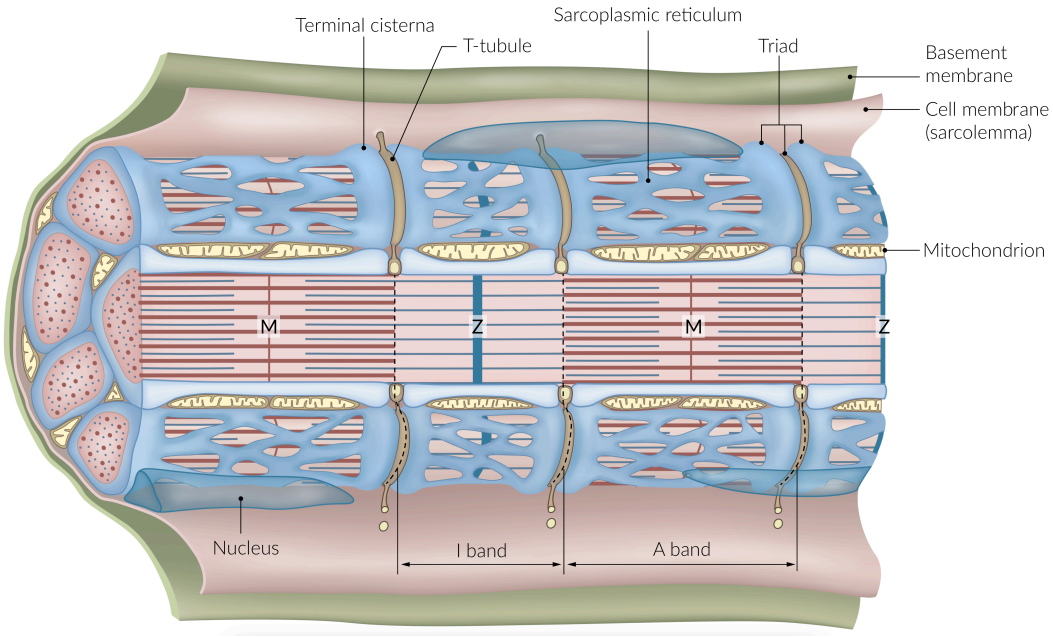


Fig. 1.5: Illustration of a skeletal myofiber Different structures of the myofiber and myofibril are outlined. In the sarcomeres, the contractile units of myofibrils, the M-line (M) and Z-disc (Z) are denoted. Taken from AMBOSS GmbH. https://amboss.com. Accessed March 01, 2024.

In each myofiber, subcellular arrays of sarcomeres are arranged in myofibrils (see 1.1.2; Fig. 1.5). A plasma membrane called sarcolemma encasing each myofiber invaginates into the myofiber cytoplasm (sarcoplasm), constituting a system of transverse tubules (T-tubules). Perpendicular to the sarcolemma, they encompass each myofibril at the intersection of the A- and the I-band. (Bennett *et al.*, 2006). The T-tubular membranes

incorporate dihydropyridine receptors (DHPRs), a specialized type of VGCC (Fosset *et al.*, 1983; Curtis & Catterall, 1984; De Jongh *et al.*, 1991). T-tubules are opposed by two adjacent, junctional sites of the SR (jSR), the terminal *cisternae* (TCs), where skeletal muscle-specific, DHPR-interacting ryanodine receptors (RyR1) are located (Block *et al.*, 1988). Both, DHPRs and RyRs are capable of releasing Ca^{2+} into the cytosol of the myofiber (DeFelice, 1993; Meissner & Lu, 1995). The interface of neighboring jSRs and a T-tubule is referred to as triad. A triad represents a highly specialized substructure linking the T-tubule and the SR, of which the latter is specialized in Ca^{2+}-storage and release (Fig. 1.5) (Alberts *et al.*, 2015, p. 920; Cretiou *et al.*, 2018).These structures are instrumental in excitation-contraction coupling (EC) in the skeletal muscle allowing for force generation, whereas other structural building blocks involved in this process are elaborated in the following sections.

1.3.1 Structural features of the skeletal muscle cytoskeleton

This section places special emphasis on the cytoskeletal components that contribute to the structural integrity and function of human skeletal myofibers. The skeletal muscle cytoskeleton interconnects structures, such as nuclei, mitochondria, T-tubules, SR, and myofibrils, of which the latter are anchored to the basal lamina (Stromer, 1998; Carlsson, 2001). In general, the cytoskeleton consists of actin filaments, microtubules, and intermediate filaments. However, due to the compartmentalization of these components in skeletal muscle, the cytoskeleton can be sectioned into intrasarcomeric and extrasarcomeric elements (Stromer, 1998; Carlsson, 2001; Clark, 2002).

Notable structures of the extrasarcomeric cytoskeleton are costameres, vinculin-rich, force-transducing structures that link myofibrils to the sarcolemma and eventually to the basal lamina (Pardo *et al.*, 1983; Campbell & Stull, 2003). Apart from dystroglycans and integrins in the sarcolemmal membrane, costameres harbor a variety of proteins, such as talin, dystrophin, and -alpha-actinin, incorporating intermediate filaments and non-muscle γ-actin filaments (Williams & Bloch, 1999; Patel & Lieber, 1997; Rybakova *et al.*, 2000). Structures associated to the costameres are dimers of the Z-disc protein filamin-C and dystrophin-glycoprotein complexes (DGCs), both instrumental in

myofiber integrity (Zhang *et al.*, 2007; Ervasti & Campbell, 1991; Milner *et al.*, 1996). In costameres, vinculin and -alpha-actinin interact with two species of non-muscle γ-actin filaments: non-contractile actin filaments lined at the cortex and contractile actin myofilaments linked to the myofibrils (Renley *et al.*, 1998; Rybakova *et al.*, 1996; Pandey *et al.*, 2018). In addition, desmin and vimentin intermediate filaments link myofibrils directly to the costameres by forming a honeycomb-like network wrapped around the myofibrillar periphery of Z-discs (Granger & Lazarides, 1979). Together, these extrasarcomeric cytoskeletal components represent an intricate network that provides structural rigidity through myofibrillar anchoring during contraction.

The intrasarcomeric cytoskeleton of skeletal muscle cells consists of specialized, contractile myofilaments based on actin and myosin filaments (see section 1.1.2). The actin-containing myofilaments, bundles of polymerized skeletal muscle α-actin, possess a specific polarity (Cretiou *et al.*, 2018). In sarcomeres, the "plus"-ends of the actin myofilaments are anchored in the adjacent Z-discs, while their "minus"-ends are oriented towards the M-line. The structural stability of actin myofilaments is safeguarded by the actin-associated capping proteins CapZ and tropomodulin, bound to plus- and minus-ends, respectively (Fig. 1.6; upper panel) (Maruyama *et al.*, 1977a; Fowler *et al.*, 1993; Swist *et al.*, 2020). Attached along the actin filaments, actin-associated troponin complexes and tropomyosin polymers are responsible for the Ca^{2+}-dependent regulation of myofilament contraction (Clark *et al.*, 2002) (Fig. 1.6; lower left panel). The myosin-based myofilaments are arranged in a bipolar manner as well. They are anchored in the M-line of the sarcomeres, with myosin head domains oriented towards adjacent Z-discs. In developed skeletal muscles, these myofilaments consist of a muscle-specific myosin, skeletal muscle myosin II, with an ATPase domain located in the myosin heads (Ojima, 2019) (Fig. 1.6; lower right panel).

Furthermore, titin, often referred to as the "third contractile" filament protein in vertebrate striated muscles, is also localized in the sarcomere (Labeit & Kolmerer, 1995; Herzog, 2018). As the largest human protein identified, it spans the sarcomere halves from the M-line to the adjacent Z-disc and is associated with a variety of functions including contribution to force generation, mechanosensing, and sarcomere stabilization (Maruyama *et al.*, 1977b; Herzog *et al.*, 2006; Colomo *et al.*, 1997; Novak & Truskinovsky, 2015). In order for skeletal muscles to generate force, these structural and

regulatory components operate in a highly organized manner: An action potential from a motor neuron in proximity to the myofiber depolarizes the sarcolemmal membrane.

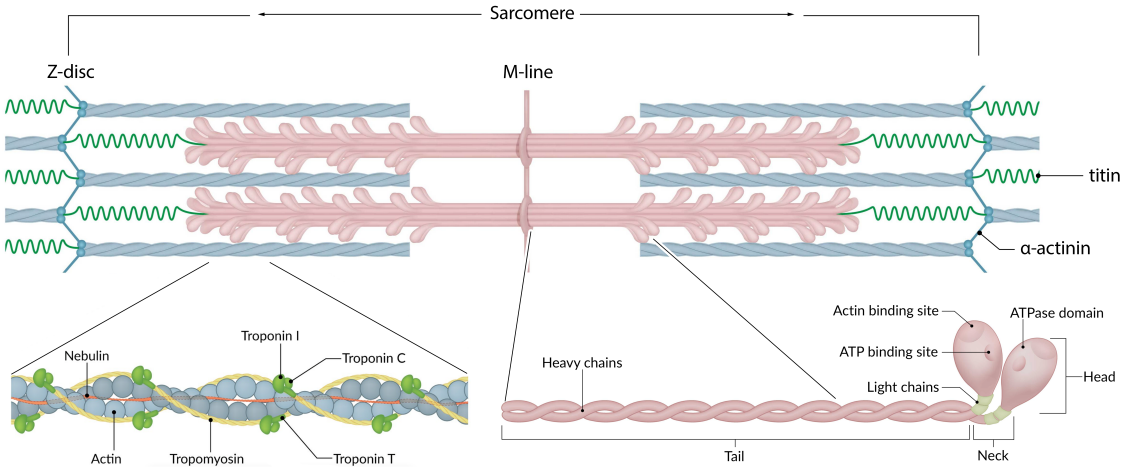


Fig. 1.6: Schematic outline of the sarkomer Anchored in the Z-disc, actin filament bundles (blue) are associated with the proteins nebulin, tropomyosin, and troponin complex proteins (I, T, C). Myosin filaments (red), anchored in the M-line, are composed of myosin dimers, harboring an ATPase in each head domain of a myosin molecule. Taken and adapted from AMBOSS GmbH. https://amboss.com. Accessed March 01, 2024.

The depolarization propagates along the invaginated T-tubules, triggering a DHPR-RyR-mediated Ca^{2+}-release from the SR into the cytosol (Alberts *et al.*, 2015, pp. 920–922; Cretiou *et al.*, 2018). A vast elevation of the cytosolic Ca^{2+}-ion levels triggers Ca^{2+}-ions to bind to troponins on the actin filaments. This binding facilitates a Ca^{2+}-mediated conformational change of tropomyosin. The actin myofilaments now become accessible for myosin heads. The myosin ATPases hydrolyze bound ATP molecules, initiating a cross-bridge cycling of myosin heads along the actin myofilaments. As a result, the sarcomeres shorten towards the M-band and force is generated; The muscle is contracting (Alberts *et al.*, 2015, p. 922; Pham & Puckett, 2023). However, the cytosolic Ca^{2+}-levels increase only transiently, because Ca^{2+} is translocated from the cytosol into the SR lumen in an ATP-hydrolyzing manner. This process is facilitated by a SR membrane complex, the sarco-/endoplasmic reticulum calcium ATPase (SERCA) which inactivates the contractile apparatus and initiates muscle relaxation (Melzer *et al.*, 1984; Primeau *et al.*, 2018).

1.3.2 The Z-disc and its associated proteins

Appearing as a dense, confined structure in electron micrographs, the Z-disc portray a complex, highly-organized scaffold within sarcomeres, as they anchor the minus-ends of actin myofilaments and harbor numerous accessory proteins (Takahashi & Hattori, 1989; Clark, 2002; Luther, 2009). The actin myofilaments are cross-linked by α-actinin dimers, organized in a lattice-like network which appears as a distinct, small-square form in transverse electron-micrographs of relaxed skeletal muscles (Goldstein *et al.*, 1987; Yamaguchi *et al.*, 1985). In vertebral skeletal muscles, numerous efforts have been made to resolve the spatial ultrastructure of the Z-disc which was prescinded as a two to seven layer model (Goldstein *et al.*, 1990; Luther, 2000; Luther, 2009; Wang *et al.*, 2021). Its immense intricacy in native vertebral skeletal muscles was further elucidated proposing the existence of different conformational states that varied from approx. 80 to 100 nm in Z-disc thickness (Wang *et al.*, 2021). Foundation of this complexity are the building blocks of the Z-disc. Apart from titin which extends into Z-discs with its N-terminal end, the filamentous actin-binding protein nebulin has been identified as key element anchored in the Z-disc (Gregorio,1998; Kruger *et al.*, 1991). Similar to titin, nebulin functions as length-determining factor of sarcomere lengths, additionally essential for sarcomere assembly, structure, and function (Littefield & Fowler, 2008; McElhinny *et al.*, 2003; Luther, 2009). In addition to aforementioned key proteins associated to the structural integrity maintenance of Z-discs in adult skeletal muscles, a variety of other proteins, such as myotilin, calcineurin, calsarcins, PDZ and LIM domain proteins (PDLIMs), muscle LIM protein (MLP) and zyxin contribute to a signaling function of the Z-disc in response to mechanical stress (Frank *et al.*, 2006; Luther, 2009; Clark *et al.*, 2002; Yu & Luo, 2006; Noureddine & Gehmlich, 2023). Other proteins associated to actin myofilaments, such as troponin and tropomyosin are not present in Z-discs (Ohtsuki, 1974; Trombitás *et al.*, 1993).

Despite its structural rigidity, the Z-disc is a highly dynamic structure also involved in signaling processes. In response to mechanical stress and damage, its intricate structure is safeguarded by the Z-disc proteins titin, and NRIP in order to maintain sarcomeric integrity and function (Swist *et al.*, 2020; Chen *et al.*, 2015). In fluorescence recovery after photobleaching (FRAP) experiments, distinct mobility characteristics of Z-disc proteins were identified, proposing a dynamic turnover of Z-disc components with a

cytoplasmic pool (Wang *et al.*, 2005). Moreover, it was demonstrated that these tightly regulated dynamics are modified by phosphorylations of numerous Z-disc proteins by protein kinases like the protein kinase C (PKC) (Reimann *et al.*, 2017). The following sections focus on the Z-disc- and dense body-associated proteins relevant for this thesis.

1.4 Protein network of Z-disk and dense bodies

1.4.1 α-actinin

α-actinin, an actin filament crosslinking member of the spectrin protein family, is a ubiquitously expressed protein in eukaryotic cells (Blanchard *et al.*, 1989; Sjöblom *et al.*, 2008; Liem, 2016). Human α-actinin is encoded by a set of four different genes, *ACTN1–ACTN4*. Abundant in almost all tissues, α-actinin-1 and α-actinin-4 have been described as Ca^{2+}-sensitive isoforms, whereas α-actinin-2 and α-actinin-3 are Ca^{2+}-insensitive isoforms, are expressed in striated muscle tissue (Burridge & Feramisco, 1981; Otto, 1994). Yet, there is a Ca^{2+}-insensitive, specific splice variant of α-actinin-1 that is expressed in smooth muscles (Waites *et al.*, 1992; Burridge & Feramisco, 1981). Together with the Ca^{2+}-insensitive α-actinins, this isoform is referred to as muscle α-actinin, whereas the Ca^{2+}-sensitive isoforms 1 and 4 are often referred to as non-muscle α-actinins (Foley & Young, 2013; Foley & Young, 2014). In both, smooth and striated muscle, α-actinin is localized to dense bodies and Z-discs. In contrast, the non-muscle α-actinin isoforms (1 and 4) are associated with cell matrix contacts, such as FAs, as well as cell-cell contacts (Sjöblom *et al.*, 2008; Foley & Young, 2014). α-actinins form antiparallel, rod-shaped dimers with a molecular mass of approx. 200 kDa (Fig. 1.7). The overall structure of a monomer consists of an actin-binding domain (ABD), a central region with four consecutive spectrin repeats (SR) often referred to as rod-domains, and a C-terminal Calmodulin-like domain (CAMD) with two paired Ca^{2+}-binding helix-loop-helix motifs, named EF-hands (EF12 and EF34) (Baron *et al.*, 1987; Blanchard *et al.*, 1989; Ribeiro *et al.*, 2014; Foley & Young, 2014).

An aligned pairing of basic SR 1 and 2 with acidic SR 3 and 4, with additional interactions between SR 2 and 3 facilitates the dimerization of α-actinin molecules (Djinović-Carugo *et al.*, 1999; Ylänne *et al.*, 2001; Sjöblom *et al.*, 2008). Due the ABDs present on the opposite sides of dimer molecules, α-actinins primarily function in bundling and crosslinking of actin filaments in a (bi-)polar manner (Fig. 1.9; B and C) (Djinović-Carugo *et al.*, 1999; Taylor *et al.*, 2000). The sensitivity to Ca^{2+}-ions of isoforms 1 and 4 inhibits binding to actin filaments in the presence of high Ca^{2+}-levels, facilitated by Ca^{2+}-dependent binding of the CAMDs to their proximal ABDs - an effect

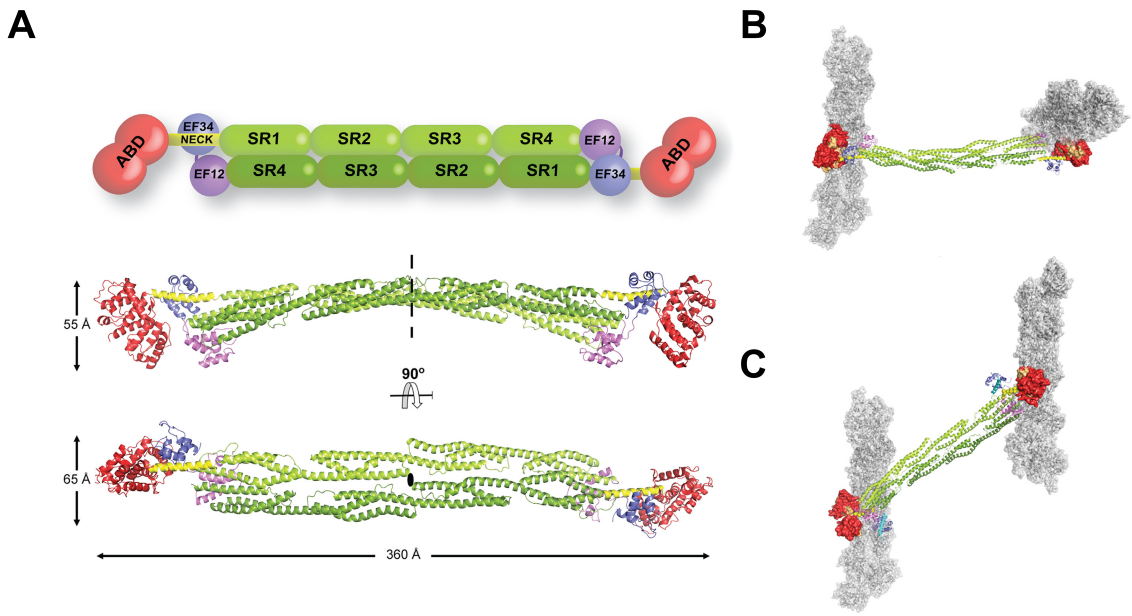


Fig. 1.7: Overview of the α-actinin-2 dimer conformation. (A) Schematic outline of the dimeric α-actinin-2 domain architecture. Actin-binding domain (ABD), EF-hand pairs (EF12, EF34) and spectrin repeats (SR). (Lower panels) Spatial reconstruction of the dimeric α-actinin-2 complex partially assembled from two α-actinin-2 halves. (B) Model of the dimeric α-actinin-2 complex superimposed on F-actin and (C) model of the dimeric α-actinin-2 complex linking antiparallel F-actin filaments, bound with a Z-disc portion of titin. Taken and modified from Ribeiro *et al.*, 2014.

which is not exhibited by muscle α-actinins (Blanchard *et al.*, 1989; Sjöblom *et al.*, 2008). Muscle α-actinins are involved in interactions via a phosphatidylinositol 4,5-biphosphate (PIP_2) and phosphatidylinositol 3,4,5-triphosphate (PIP_3)-dependent mechanism, allowing for α-actinins to adopt conformational changes and interact with both, titin and smooth muscle titin (smitin) (Young & Gautel, 2000; Chi *et al.*, 2005).

Apart from titin and smitin, as major component of the FAs, Z-discs, and dense bodies, muscle α-actinins also rigidly anchor actin filaments to variety of other proteins including vinculin, myopalladin, or the functionally versatile synaptopodin family protein synaptopodin-2 (SYNPO2) (Kroemker *et al.*, 1994; Bang *et al.*, 2001; Chi *et al.*, 2008; Linnemann *et al.*, 2010; Grison *et al.*, 2017) (see sections 1.2 and 1.3).

1.4.2 The synaptopodin protein family member SYNPO2

SYNPO2/myopodin, first described in avian muscle as fesselin, belongs to the synaptopodin protein family along with synaptopodin (SYNPO) and synaptopodin-2-like (SYNPO2L/tritopodin) (Leinweber *et al.*, 1999; Weins *et al.*, 2001).

Encoded by the genes *SYNPO*, *SYNPO2* and *SYNPO2L*, the proline-rich podin proteins are expressed in adult muscle tissues and associate to the actin cytoskeleton, binding to α-actinin and to F-actin via independent binding regions (Kremerskothen *et al.*, 2005; Linnemann, 2011, pp. 143–151; Leinweber *et al.*, 1999; Pham & Chalovich, 2006; Faul *et al.*, 2007; Linnemann *et al.*, 2010). A characteristic feature of these proteins is their homology in three regions, termed podin homology regions and denoted H1, H2, and H3 (Fig. 1.8) (Linnemann, 2011, p. 61). In humans, SYNPO2 encompasses different isoforms which attribute to the presence of two alternative transcription start sequences and alternative splicing of exons in the *SYNPO2* gene (Lin *et al.*, 2001; Linnemann, 2011, pp. 60–62). To date, six SYNPO2 isoforms have been discovered, subdivided into long and short isoforms, denoted *a, b, c* and *d, e, f*, respectively (Linnemann, 2011, pp. 65–66; De Ganck *et al.*, 2008; Linnemann *et al.*, 2010).

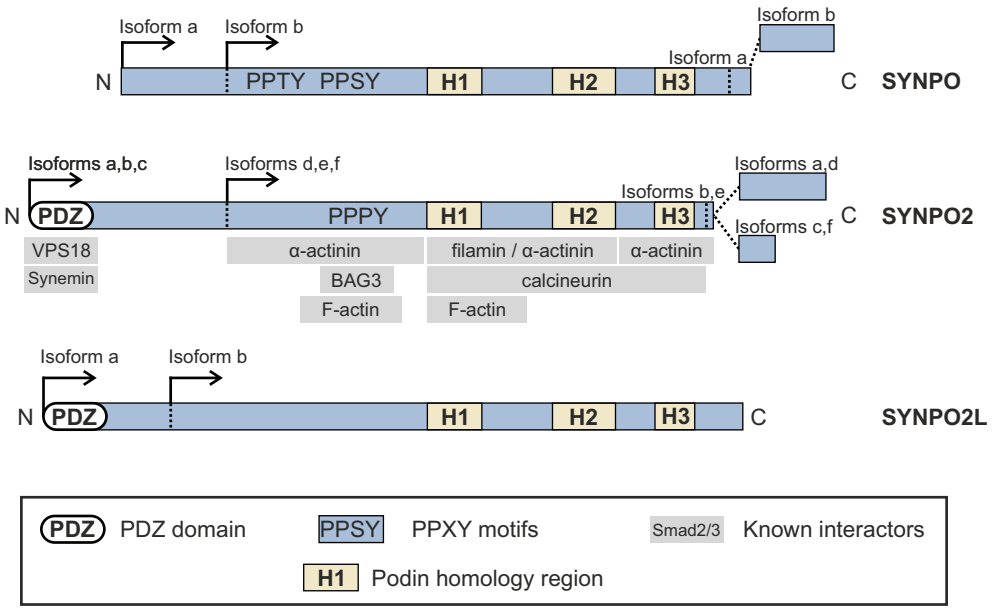


Fig. 1.8: Overview of the synaptopodin protein family members SYNPO, SYNPO2, and SYNPO2L. Isoforms from alternative transcription starts and alternative spicing variants are denoted above. Characteristic features of the synaptopodin family proteins, such as the homology regions (yellow - H1, H2, H3) and the PDZ domain (white) are outlined. Binding regions of SYNPO2 interaction partners are outlined in gray.

However, the existence of an additional isoform was proposed (Zheng & Song, 2023). The long SYNPO2 isoforms harbor an N-terminal region of the protein which encompasses a PDZ domain comprising the amino acids 6–88, whereas in the short isoforms, this region is missing (De Ganck *et al.*, 2008; Schroeter *et al.*, 2008) (Fig. 1.8).

Still, large portions of the SYNPO2 molecule remain intrinsically disordered (Fig. 1.9) (Chalovich & Schroeter, 2010). In striated muscle tissues, SYNPO2b (heart) and SYNPO2e (skeletal) were found to be predominantly expressed, whereas smooth muscle cells mainly express the SYNPO2a isoform (Linnemann, 2011; Lohanadan *et al.*, 2023). SYNPO2 primarily localizes to the Z-discs in striated muscles, while in smooth muscle cells, it was found to localize to dense bodies (Weins *et al.*, 2001; Linnemann, 2011). SYNPO2 is a multifaceted protein not only engaged in protein-protein interactins (PPIs) with actin and α-actinin, but also interacting with the structural protein filamin A/C, or with zyxin in smooth muscle focal adhesions (Schroeter & Chalovich, 2005; Linnemann *et al.*, 2010; Yu & Luo, 2006). The proteins calmodulin, calsarcin-2, and the phosphatase calcineurin, all instrumental for Ca^{2+}-dependent skeletal and smooth muscle regulatory functions, have been identified to associate with SYNPO2 as well (Faul *et al.*, 2007; Lohanadan, 2023; Kolakowski *et al.*, 2004).

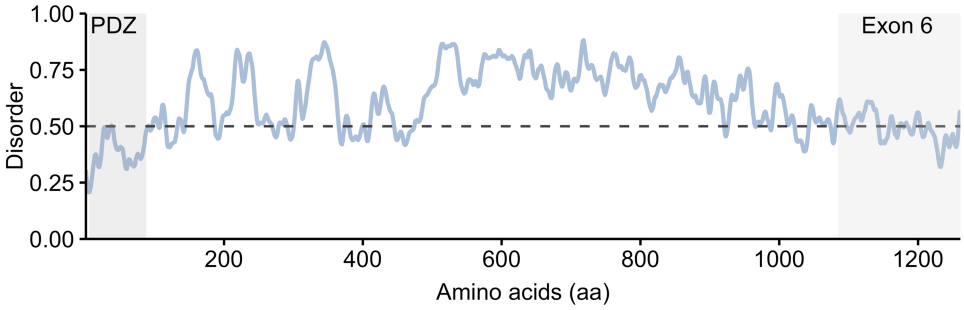


Fig. 1.9: Prediction of protein disorder in SYNPO2a. The prediction was performed using the IUPred3 server (Erdõs *et al.*, 2021). Disorder probability values above 0.5 indicate a predicted disorder at the corresponding residue site (dashed line). Gray-colored regions represent the PDZ domain and the exon 6 of SYNPO2.

SYNPO2 has been linked to the chaperone-assisted selected autophagy (CASA) machinery, responsible for maintaining protein quality control and protein homeostasis in skeletal muscle cells under mechanical stress, by binding to both BAG3 and the vacuolar protein sorting-associated protein 18 homolog (VPS18) (Ulbricht *et al.*, 2013). In addition to that, specific interactions of SYNPO2 were found to be phosphorylation-dependent: It was demonstrated that phosphorylation of SYNPO2 at two specific sites near the PPPY motif via protein kinase A (PKA) and Ca^{2+}/calmodulin dependent kinase II (CaMKII) mediated its interaction with the adapter protein 14-3-3β (Faul *et al.*, 2005; Faul *et al.*, 2007).

1.4.2.1 The PDZ domain

The N-terminal portion of SYNPO2 consists of a PDZ domain which represents a group of structurally domains engaging in PPIs. PDZ domains, found in almost all kingdoms of life, encompass approx. 90 amino acids and are involved in signaling processes (Lee & Zheng, 2010; Muley *et al.*, 2019). Previously termed as DHR domains, the name PDZ derives from proteins first discovered to harbor this domain: post synaptic density protein (PSD95), *Drosophila* disc large tumor suppressor (Dlg1), and zonula occludens-1 protein (ZO-1) (Ponting & Phillips, 1995; Kennedy, 1995). In a stricter sense, PDZ domains are composed of five to six β-strands, as well as a long and a short α-helix, adopting a globular, tertiary structure (Fig. 1.11) (Cabral *et al.*, 1996; Lee *et al.*, 2009). The PDZ β-strands as well as the α-helices are consecutively termed β A-E and α A & α B. PDZ domains comprise a binding cleft that adjoins a carboxylate-binding loop containing a highly conserved, canonical XΦGΦ motif located between the α B and β A secondary structures (Kennedy, 1995; Fanning & Andersson, 1996; Songyang *et al.*, 1997). Interestingly, in the PDZ domains of SYNPO2 and SYNPO2L, this motif is composed of the amino acids P-W-G-F (Bezerra, 2015).

A characteristic feature of PDZ domains is the PPI with ligands by recognizing specific C-terminal motifs often limited to a few amino acids (Songyang *et al.*, 1997). These PDZ-binding motifs (PDZ-BM) have been classified into consensus motifs clusters (classes I–IV) according to the specificity and/or adopted conformation of four terminal ligand residue positions, reversely denoted from P_{-3} to the C-terminal P_0 (Songyang *et al.*, 1997). These classes were further subdivided into 16 binding subclasses comprising motifs with additional amino acids (Tonikian *et al.*, 2008) (see Appendix C). Recognizing C-terminal PDZ-BM classes bound to the PDZ binding cleft is referred to as canonical binding, whereas perpendicular binding has been reported for the PDZ domains of syntenin, and SYNPO2 that recognize ligands via two terminal amino acids (Fig. 1.11) (Sugi *et al.*, 2007; Grembecka *et al.*, 2006; Bezerra, 2015). Additionally, a study revealed that PDZ domains may recognize amino acids anterior to canonical ligand motifs (Zeng *et al.*, 2016). Moreover, a variety of PDZ domains recognize internal peptides, represented by short linear motifs (SLIMs), internal β-hairpin loops, and cyclic peptides, tremendously extending the versatility of possible PDZ-peptide recognition patterns (Mu *et al.*, 2014; Gee *et al.*, 1998; Hillier *et al.*, 1999).

Apart from PDZ-peptide or PDZ-phospholipid interactions observed, some PDZ domains engage in PDZ-PDZ interactions through dimerization (Gallardo *et al.*, 2010; Chang *et al.*, 2011). This phenomenon was first discovered and further characterized

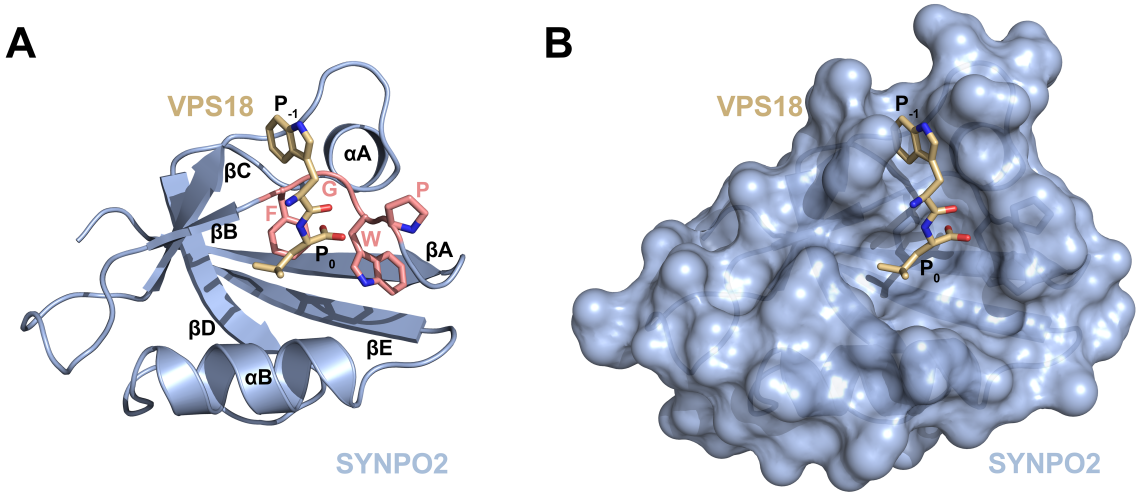


Fig. 1.10: Structure of the PDZ-peptide complex of SYNPO2 and VPS18. (A) Cartoon representation showing the PDZ domain architecture of SYNPO2 (slate blue), harboring 5 β-sheets A-E and 2 α-helices A, B. The altered XΦGΦ motif of the carboxylate loop in SYNPO2, consists of the motif sequence PWGF (peach). The two C-terminal amino acids of VPS18 (yellow), denoted as P_{-1} and P_0 engage in perpendicular binding to the PDZ domain. (B) Surface representation of the PDZ-peptide complex. The structures obtained were refined with a resolution of 2.35 Å (Bezerra, 2015), courtesy of K. Djinović-Carugo.

between skeletal muscle α1 syntrophin (SNT1) and the neuronal nitric oxide synthase (nNOS) which both specifically interact through their PDZ domains (Brenman *et al.*, 1996, Hillier *et al.*, 1999). In some cases, the peptide binding properties are preserved while PDZ domains engage in homo- or heterodimerization (Xu *et al.*, 1998; Ivarsson *et al.*, 2013) (see Appendix C). It is proposed that PDZ dimerization: (1) facilitates the assembly of multimeric protein complexes required for signaling, (2) enhances the binding specificity of a protein through heteromeric PDZ-PDZ interactions, or (3) mediates regulatory functions through occupying the peptide binding site (Wu *et al.*, 2007; Xu *et al.*, 1998; Hillier *et al.*, 1999; Purbey *et al.*, 2008). In order to shed light on the variety of SYNPO2's functions and its involvement in PDZ domain-mediated, Z-disc-associated signaling processes, it is fundamental to investigate its PDZ domain C-terminal peptide binding properties, to identify new interaction partners, as well as to study engagement in PDZ domain dimerization processes.

1.4.3 BAG3 and its role in autophagy at the Z-disk

BAG3 belongs to the Hsp/Hsc70-regulating B-cell lymphoma-2-associated athanogene (BAG) cochaperone family and a multifunctional scaffold protein which, as part of the CASA machinery, interacts with SYNPO2 (see section 1.4.2) (Takayama *et al.*, 1997; Takayama *et al.*, 1999; Ulbricht *et al.*, 2013). Furthermore, BAG3 was found to be engaged in processes responsible for cellular integrity, cell signaling, maintenance, and proteostasis which has been extensively studied with respect to Z-disc integrity in striated muscle cells (Behl, 2011; Behl, 2016; Ulbricht *et al.*, 2013; Arndt *et al.*, 2010; Klimek *et al.*, 2017).

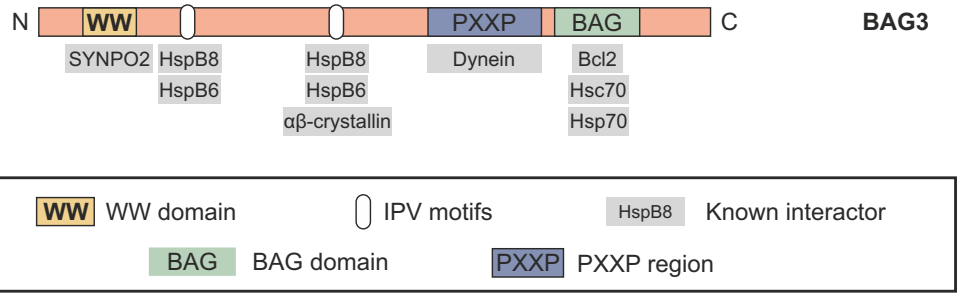


Fig. 1.11: Overview of the protein BAG3. Characteristic features, such as the WW domain (yellow), IPV motifs (white ovals), the SH3 domain-binding PXXP motif (blue), and the BAG domain (green) are outlined. Binding sites of BAG3 interaction partners are outlined in gray.

Human BAG3 is a protein with 575 amino acids and harbors regions including a WW domain, a pair of IPV motifs that independently link BAG3 to the chaperones HspB6 and HspB8, and a BAG domain at its C-terminus (Fig. 1.11) (Takayama *et al.*, 1999; Carra *et al.*, 2008; Fuchs *et al.*, 2009; Fang *et al.*, 2019). Its N-terminal WW domain recognizes PPXY motifs of (1) SYNPO2, (2) Hippo signaling pathway kinases, (3) and the mammalian target of rapamycin complex (mTORC)-regulating cochaperone hamartin (TSC1), whereas the BAG domain associates with the ATPase domain of the heat-shock proteins Hsc70/Hsp70 (Ji *et al.*, 2019; Ulbricht *et al.*, 2013; Takayama *et al.*, 1999). BAG3 is the key element for BAG3-mediated macroautophagy, a process which involves the SQSTM1-mediated recognition and formation of LC3-coated autophagic degradation vesicles (autophagosomes) facilitated by the CASA complex prior to sequestering and degrading ubiquitinylated client proteins (Fig. 1.12) (Garmerdinger *et al.*, 2009; Arndt *et al.*, 2010; Höhfeld *et al.*, 2021). In the CASA

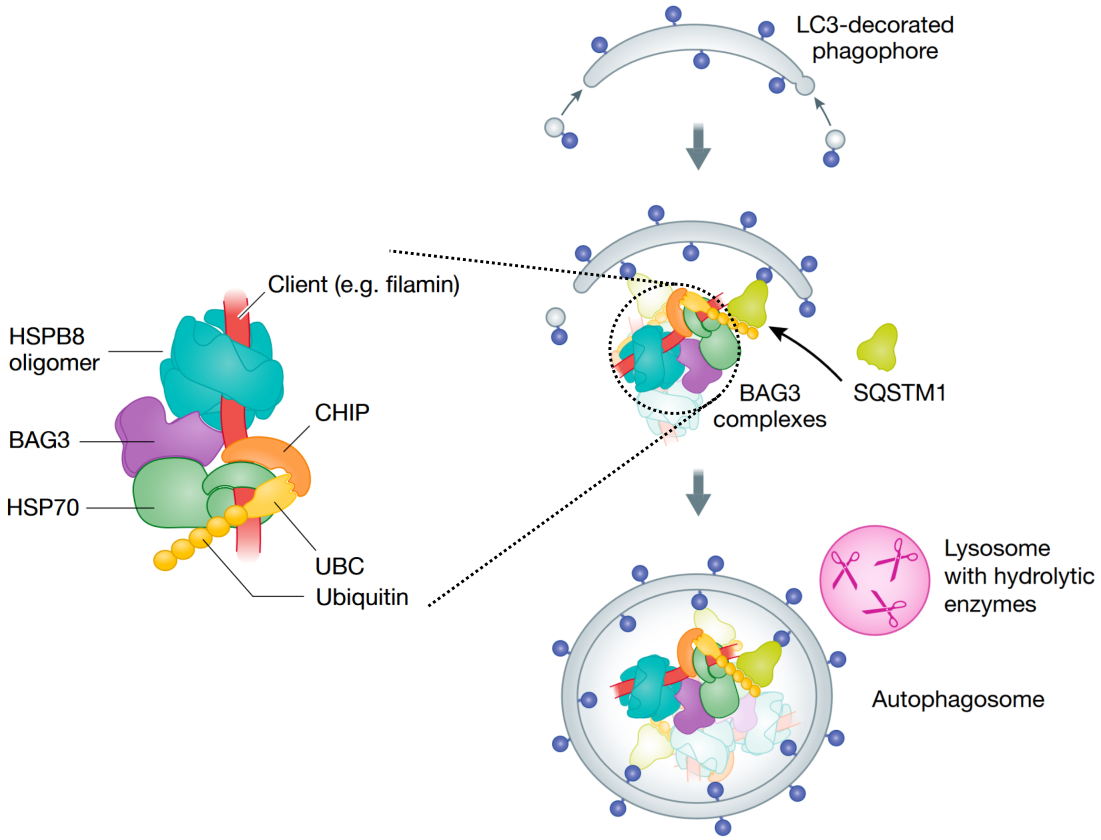


Fig. 1.12: BAG3-mediated macroautophagy via CASA machinery. (Left panel) Formation of the BAG3-mediated chaperone complex recruited with a client protein (red). (Right panel) Induction of autophagosome formation and autolysosomal degradation of client proteins initiated by accessory proteins recognizing LC3-coated phagophores. Taken and adapted from Höhfeld *et al.*, 2021.

complex, BAG3 is associated to small heat-shock proteins (sHSPs), Hsp70/Hsc70, the client protein ubiquitin ligase CHIP, and ubiquitin-conjugating enzymes (UBCs) (Fig. 1.12) (Carra *et al.*, 2008; Arndt *et al.*, 2010; Arndt *et al.*, 2007; Rauch & Gestwicki, 2014; Crippa *et al.*, 2016). The formation of the autophagosomes, requires involvement of SYNPO2 as an adapter between BAG3 and VPS18 (Ulbricht *et al.*, 2013; Klimek *et al.*, 2017).

In skeletal muscle cells, BAG3 safeguards the Z-disc integrity by monitoring the protein quality of cytoskeletal components. The mechanosensitive Z-disc protein filamin C, prone to unfolding or aggregation under mechanical stress, is one of the CASA machinerie's clients in muscle cells (Ulbricht *et al.*, 2013). Once filamin C undergoes stress-induced, conformational changes, the CASA machinery mediates the sequestering and degradation by binding to filamin C (Ulbricht *et al.*, 2013; Klimek *et al.*, 2017).

1.4.4 The transcriptional coactivation factors YAP1 and TAZ

The Yes-associated protein 1 (YAP1) was first characterized as proline-rich protein associated to the YES1 kinase (Sudol 1994; Sudol *et al.*, 1995). Its paralog, the transcriptional coactivator with PDZ-binding motif (TAZ), also named WWTR1, was first described as 14-3-3-binding protein (Kanai *et al.*, 2000). Both proteins function as transcriptional coactivators in the Hippo signaling pathway capable of regulating cell proliferation and development, also involved in tumorigenesis, and with respect to muscle tissues, responsible for myogenesis, muscle fiber size and protein homeostasis (Dong *et al.*, 2007; Watt *et al.*, 2010; Watt *et al.*, 2015; Goodman *et al.*, 2015; Esteves de Lima *et al.*, 2016).

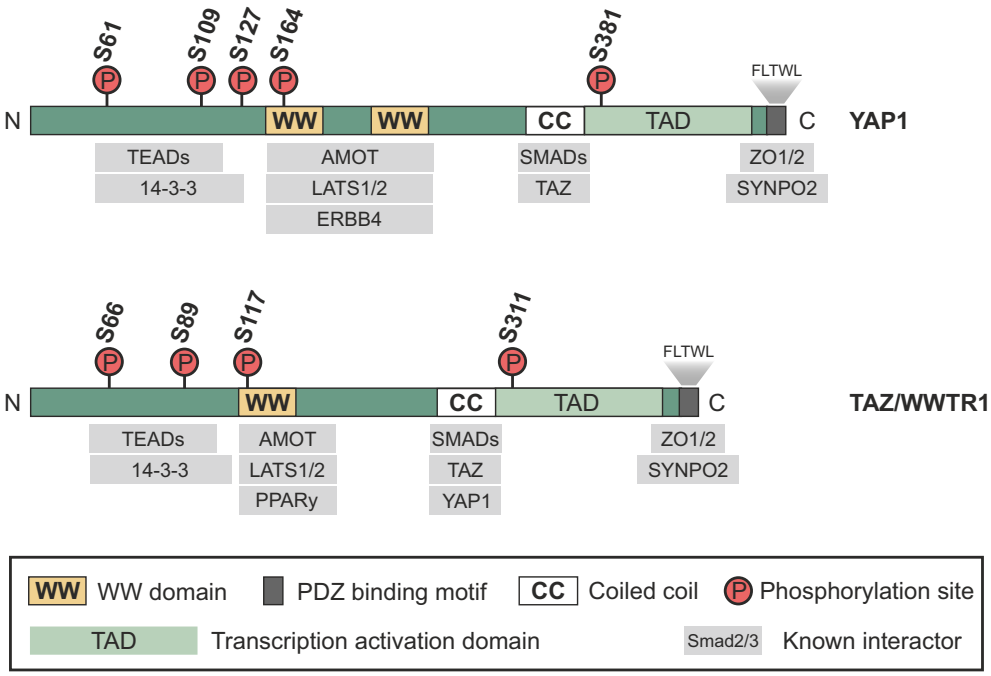


Fig. 1.13: Overview of the transcriptional coactivators YAP1 and TAZ. Characteristic features, such as the WW domain (yellow), coiled-coil regions (white - CC), the transcription activation domain (green - TAD), and the C-terminal PDZ-BM (dark gray) are outlined. Binding sites of YAP1 and TAZ interaction partners are outlined in gray. LATS1/2 phosphorylation sites are shown in red with the corresponding phospho-acceptor.

YAP1/TAZ share structural elements, such as a C-terminal transcription activation domain (TAD), one or two N-terminal WW domains recognizing proline-rich motifs, and a coiled-coil region anterior to the TAD (Sudol *et al.*, 1995; Gaffney *et al.*, 2012; Hong & Guan, 2012). Furthermore, both proteins contain a PDZ-BM at their

C-terminal ends, potentially promoting nuclear translocation of YAP1/TAZ (Fig. 1.13) (Oka *et al.*, 2010; Oka & Sudol, 2009). In humans, eight YAP1 isoforms have been identified which differ in the presence of a single or tandem WW domains, and alterations in the TAD (YAP1α–δ), while only one TAZ isoform is known (Gaffney *et al.*, 2012; Sudol, 2013). As critical effectors of the Hippo signaling pathway, YAP1/TAZ coactivate transcription of target genes by engaging in PPIs with transcriptional enhancer factor proteins (TEADs) in the nucleus (Sudol *et al.*, 2001; Zhao *et al.*, 2008; Wackerhage *et al.*, 2014). Apart from a PDZ-BM-mediated import of YAP/TAZ into the nucleus, numerous models and other regulatory pathways for a nuclear translocation have been discovered (Kofler & Kapus, 2023). A key mechanism of YAP1/TAZ regulation is mediated through a phosphorylation signaling cascade via the Hippo signaling kinases MST1/2 and LATS1/2 (Oka *et al.*, 2008; Sudol & Harvey, 2010). In particular, LATS1/2 specifically phosphorylates HXRXXS motifs in YAP1/TAZ, e.g. the amino acids S127 of YAP1 and S89 of TAZ, which promotes a cytoplasmic retention leading to 14-3-3-interaction-mediated degradation of YAP1/TAZ (Fig. 1.13) (Zhao *et al.*, 2007; Oka *et al.*, 2008; Lei *et al.*, 2008). Though, Hippo signaling kinases or related phosphatases mediate a variety of site-specific (de)phosphorylations, capable of both, positively or negatively regulating YAP1/TAZ activity (see Appendix B). In skeletal muscle cells, YAP1 and TAZ were found to regulate proliferation, myogenesis and mechanotransduction in different manners, but were in turn regulated by components of the Z-disc, such as filamin C (Watt *et al.*, 2010; Dupont *et al.*, 2011; Jeong *et al.*, 2010; Jeon *et al.*, 2014; Knyazeva *et al.*, 2020). More recently, YAP1 was found to associate with BAG3/Hsp70 potentially linking it to autophagy via the CASA machinery (Ulbricht *et al.*, 2013; Baldan *et al.*, 2021).

1.5 WW domains

The WW domain, encompassing approx. 40 amino acids, is a structurally characteristic region of YAP1, TAZ, and BAG3. Notably, this domain was first identified upon characterizing PPIs between YAP1 and the YES1 kinase (see section 1.4.4) (Sudol, 1994; Sudol *et al.*, 1995). The general WW domain structure is composed of three distinct elements: (1) a pair of highly conserved tryptophans which are separated by 20–25 amino acids and further denominated the "WW" domain, (2) three consecutive antiparallel β-sheets forming a hydrophobic core, (3) a conserved LP motif N-terminally located of the anterior tryptophan (Jäger *et al.*, 2001; Jäger *et al.*, 2007; Jäger *et al.*, 2009). These WW domain characteristics allow for specific ligand binding by recognizing SLIMs, in particular proline-rich stretches of amino acids, first described for the WW domain of YAP1 (Chen & Sudol, 1995; Macias *et al.*, 1996). According to the types of proline-rich motifs recognized, WW domains were subdivided into different classes (see Appendix B) (Salah *et al.*, 2012). In general, it was previously proposed that WW domain-containing proteins may function as a platform for multi-protein complexes, involved in various cellular processes, such as transcription, spicing, or ubiquitylation, elemental for cell differentiation, apoptosis, and tumor control (Ingham *et al.*, 2005; Salah *et al.*, 2012).

1.6 Aims of this study

The human Z-disc and dense body-associated, proline-rich adapter protein SYNPO2 interacts with a variety of proteins, including F-actin, α-actinin, VPS18, and BAG3. Prime aim of this work is to elucidate the role of SYNPO2 and its involvement in signaling networks in smooth and skeletal muscle cells. Hence, identifying novel interaction partners of SYNPO2 as well as characterizing their interaction with SYNPO2 at a cellular level is instrumental to unravel its function in Z-disc-associated signaling processes and involvement in BAG3-mediated autophagy (Ulbricht *et al.*, 2013). A pivotal structural element of SYNPO2 is its PDZ domain capable of binding C-terminal motifs of potential ligands and of dimerizing with other PDZ domains. In order to investigate these types of PDZ domain-mediated binding for SYNPO2, protein crosslinking assays and size exclusion chromatography (SEC) experiments should be carried out. Based on previous studies from Bezerra (2015) which investigated the interactions between VPS18, synemin and the PDZ domain of SYNPO2, this thesis should further utilize an *in silico* prediction dataset analysis to identify novel potential ligands such as YAP1/TAZ. Potential interactions between SYNPO2, YAP1 and TAZ should be investigated via biochemical pulldown assays and co-immunoprecipitation (co-IPs). Additionally, the interaction between YAP1 and SYNPO2 was to be characterized via bimolecular fluorescence complementation (BiFC) assays in smooth and skeletal muscle cells. Subsequent colocalization studies target to investigate the association of SYNPO2-YAP1 complexes with components of the actin cytoskeleton of these muscle cells. The WW domain, a structural feature shared between BAG3, YAP1, and TAZ recognizes proline-rich motifs, such as the PPPY motif of SYNPO2. Peptide binding assays and competitive binding assays should be performed to assess the relationship between SYNPO2, BAG3, YAP1, and TAZ. Moreover, previous studies highlighted that some SYNPO2 phosphorylations near the PPPY motif were upregulated under mechanical stress, while others affected its interaction with 14-3-3 proteins (Hoffman *et al.*, 2015, Potts *et al.*, 2017, Faul *et al.*, 2005). This thesis compasses to put emphasis on these SYNPO2 phosphorylations affecting its interactions with BAG3, YAP1, and TAZ: Additional co-IPs should elucidate this putative link of SYNPO2 to BAG3, the key player of the CASA machinery, and the Hippo pathway

effectors YAP1/TAZ. To investigate the regulatory effects of SYNPO2 and BAG3 overexpression on the activity of YAP1 in smooth and skeletal muscle cells, fluorescence microscopy-based localization studies should be carried out monitoring YAP1 nuclear translocation.

Chapter 2

Materials and Methods

2.1 Materials

2.1.1 Chemicals

All chemicals were supplied by Roth AG, VWR Chemicals GmbH, Thermo Fisher Scientific, AppliChem GmbH, Merck KGaA, Avantor Performance Materials, Th. Geyer GmbH & Co. KG, ASV–innovative Chemie GmbH, Köhler GmbH, and Schlüter GmbH.

2.1.2 Antibiotics

Tab. 2.1: Antibiotics

Substance name	**Working concentration (mg/mL)**
Carbenicillin	100
Chloramohenicol	34
Kanamycin	50
Tetracycline	10

2.1.3 Media, buffers, and solutions

All of the solutions, buffers, and media used have been autoclaved or have been filtered through 0.45 µm pore filters. Solutions used in fast protein liquid chromatography (FPLC) experiments have been filtered through membranes with a pore size of 0.2 µm.

2.1.3.1 Media and solutions for bacterial cell culture

Tab. 2.2: Solutions for the cultivation of bacterial strains

Name	**Ingredient**
5052 solution	0.5% (w/v) glycerol, 0.5% (w/v) D-glucose, and 0.2% (w/v) α-lactose monohydrate
LB medium	1% (w/v) tryptone, 0.5% (w/v) yeast extract, 0.5% (w/v) NaCl
NPS	50 mM Na_2HPO_4, 50 mM KH_2PO_4, 25 mM $(NH_4)SO_4$
SOC medium	2% (w/v) tryptone, 0.5% (w/v) yeast extract, 0.5% (w/v) NaCl, 2.5 mM KCl, 10 mM $MgCl_2$, 10 mM $MgSO_4$, 20 mM D-glucose
ZY medium	1% (w/v) N-Z-amine or tryptone, 0.5% (w/v) yeast extract

2.1.3.2 Solutions and media for mammalian cell culturing

Tab. 2.3: Solutions for mammalian cell culture

Product name	**Manufacturer**
2.5% trypsin 100×	Gibco, Thermo Fisher Scientific
L-glutamine 200 mM	Gibco, Thermo Fisher Scientific
FCS for C2C12-growth medium (GM)	Sigma-Aldrich
FCS for A7r5-growth medium (GM)	Gibco, Thermo Fisher Scientific
DMEM GlutaMax 1×	Gibco, Thermo Fisher Scientific
DMEM 1X×	Gibco, Thermo Fisher Scientific
DPBS (supplemented with Ca2+ and Mg) 10×	Gibco, Thermo Fisher Scientific
HS	Gibco, Thermo Fisher Scientific
MEM NEAA 100×	Gibco, Thermo Fisher Scientific
Penicillin/streptomycin 100×	Gibco, Thermo Fisher Scientific

Tab. 2.4: Media for mammalian cell culture

Name	Ingredients
A7r5-growth medium (GM)	DMEM, 10% (v/v) FCS, 1% (v/v) penicillin/ streptomycin, 2% (v/v) L-glutamine
C2C12-differentiation medium (DM)	DMEM Glutamax, 2% (v/v) HS, 1% (v/v) penicillin/ streptomycin, 1% (v/v) MEM NEAA
C2C12-growth medium (GM)	DMEM Glutamax, 15% (v/v) FCS, 1% (v/v) penicillin/ streptomycin, 1% (v/v) MEM NEAA
NGS/BSA solution	10% (w/v) NGS, 5% (w/v) BSA in 1× PBS
Nucleofection Solution I	120 mM NaH_2PO_4, 5 mM KCl, 15 mM $MgCl_2$, pH 7.2
Nucleofection Supplement	50 mM Na-succinate in H_2O
PBS-EDTA	0.5 mM EDTA in PBS
PFA solution	4% (v/v) PFA in 1× DPBS

2.1.3.3 Buffers

Tab. 2.5: General buffers

Name	Ingredient
Bis-Tris Buffer (7×)	2.5 M Bis-Tris, 1.5 M HCl, pH 6.7 ± 0.1
Membrane blocking buffer	5% (w/v) milk powder in TBST
MES running buffer	50 mM MES, 50 mM Tris, 0.1% (w/v) SDS, 1 mM EDTA
PBS	137 mM NaCl, 2.7 mM KCl, 8.1 mM Na_2HPO_4, 1.5 mM K_2HPO_4, pH 7.4
PBST	0.05% (v/v) Tween 20 in PBS, pH 7.4
SDS sample buffer (5×)	60 mM Tris, 15% (w/v) SDS, 30% (w/v) glycerol, 7.5% (v/v) 2-ME, 0.1% (w/v) bromophenol blue, pH 6.8
TAE buffer	40 mM Tris, 20 mM acetic acid, 1 mM EDTA
TBE buffer	89 mM Tris, 89 mM boric acid, 2 mM EDTA, ph 8.0
TBS	50 mM Tris, 0.15 M NaCl, pH 7.9
TBST	0.05% (v/v) Tween 20 in TBS, pH 7.9
Transfer buffer	25 mM Tris, 192 mM glycine, 20% (v/v) methanol, pH 8.6 ± 0.2
Transfer buffer	25 mM Tris, 192 mM glycine, 20% (v/v) methanol, pH 8.6 ± 0.2
Tris running buffer (Lämmli)	25 mM Tris, 0.192 M glycine, 0.1% (w/v) SDS

Tab. 2.6: Protein purification buffers

Name	**Ingredient**
BAG3 lysis buffer	20 mM Na_2HPO_4, 0.5 M NaCl, 20 mM imidazole, 1 mM PMSF, pH 7.4 (Fontanella *et al.*, 2010)
BAG3 elution buffer	20 mM Na_2HPO_4, 0.5 M NaCl, 300 mM imidazole, pH 7.4 (Fontanella *et al.*, 2010)
Bis-Tris Buffer (7×)	2.5 M Bis-Tris, 1.5 M HCl, pH 6.7 ± 0.1
co-IP buffer	1% (w/v) BSA, 1×*Protease Inhibitor Cocktail* in PBS
co-IP buffer X	0.05% (v/v) Triton X-100 in co-IP buffer
co-IP buffer T	0.001% (v/v) Tween 20, 20 mM GSH in co-IP buffer
co-IP buffer NT	0.5% (v/v) NP-40, 0.001% (v/v) Tween 20, 20 mM GSH in co-IP buffer
DENAT buffer	50 mM Na_2HPO_4, 8 M Urea, 20 mM imidazole, pH 8.0
GSH elution buffer	50 mM Tris-HCl, 0.15 M NaCl, 1 mM EDTA, 1 mM DTT, 10 mM reduced GSH, pH 8.0
GSH lysis buffer	1% (v/v) Triton X-100, 1 mM EDTA, 2 mM $MgCl_2$ in PBS
GSH wash buffer	1× PBS
NTA elution buffer	50 mM Na_2HPO_4, 0.3 M NaCl, 300 mM imidazole, pH 8.0
NTA lysis buffer	1% (v/v) Triton X-100 in NTA wash buffer
NTA wash buffer	50 mM Na_2HPO_4, 0.3 M NaCl, 20 mM imidazole, ph 8.0
PDZ buffer	50 mM K_2HPO_4, 0.5 M NaCl, pH 7.0
SYNPO2 NTA lysis buffer	1% (v/v) Triton X-100, 2% (v/v) lauroylsarkosine in NTA wash buffer
TAP wash buffer 1	50 mM K_2HPO_4, 0.5 M NaCl, pH 7.0
TAP wash buffer 2	50 mM K_2HPO_4, 0.15 M NaCl, pH 7.0
TAP lysis buffer	50 mM K_2HPO_4, 0.5 M NaCl, 1% (v/v) Triton X-100, 2% (v/v) N-lauroyl sarcosinate, 40 mM CHAPS, pH 7.0
WW elution buffer	50 mM Tris-HCl, 0.1 M NaCl, 1 mM EDTA, pH 7.8

2.1.4 Consumables

All consumables, such as reaction tubes, pipette tips, scrapers, serological pipette tips, dishes, microscopic slides, and plates were used from Sarstedt, Starlab, TPP, Eppendorf, Greiner, Invitrogen, Thermo Fisher Scientific and Qiagen. Prepacked affinity resins for purifications of recombinant proteins were used from Invitrogen, Cube Biotech and Macherey-Nagel.

2.1.5 Antibodies

Tab. 2.7: Primary antibodies

Name	Epitope	Species	Usage	Dilution	Origin
BM75.2	actinin (pan)	mouse IgG	IF	1:50 – 200	Sigma-Aldrich
GAPDH	GAPDH	mouse IgG1	WB	1:1000	Calbiochem/Merck KGaA
GST	GST	rabbit IgG	WB	1:10000	Proteintech
HH9	SYNPO2 HH	mouse IgG1	IF	1:1	Linnemann, 2010
phospho-YAP	YAP1 p-S127	rabbit IgG	WB	1:1000	Cell Signaling Technology
T12	titin (Z-disk)	mouse IgG1	IF	1:50	Fürst *et al.*, 1988
T7	T7-peptide	mouse IgG2b	co-IP, WB	1:10000	Novagen
XR1B	Xin	mouse IgG1	co-IP	see 2.3.7	Van der ven, 2006
YAP-63.7	YAP1	mouse IgG2a	IF, WB	1:100	Santa Cruz Biotechnology
YL1/2	EEF-peptide	rat IgG2a	IF, WB	1:800	Invitrogen

Tab. 2.8: Secondary antibodies and conjugates

Name	Epitope	Donor	Usage	Dilution	Origin
GAM IgG1 Alexa 594	mouse IgG1	Goat	IF	1:100	Jackson Immuno
GAM IgG1 Cy5	mouse IgG1	Goat	IF	1:300	Jackson Immuno
GAM IgG2a Alexa 594	mouse IgG2a	Goat	IF	1:300	Jackson Immuno
GAM-HRP	mouse IgG	Goat	WB	1:10000	Jackson Immuno
GAM-IRDye680RD	mouse IgG	Goat	WB	1:10000	Li-COR Biotechnology
GAM-IRDye800CW	mouse IgG	Goat	WB	1:10000	Li-COR Biotechnology
GAR-HRP	rabbit IgG	Goat	WB	1:10000	Jackson Immuno
GAR-IRDye680RD	rabbit IgG	Goat	WB	1:10000	Li-COR Biotechnology
GAR-IRDye800CW	rabbit IgG	Goat	WB	1:10000	Li-COR Biotechnology
GARat-IRDye800CW	rabbit IgG	Goat	WB	1:10000	Li-COR Biotechnology
GST-HRP	GST	Goat	WB	1:10000	Jackson Immuno
T7-HRP	T7-peptide	Goat	WB	1:10000	Merck KGaA

2.1.6 Kits

Tab. 2.9: Commercially available kits

Product name	**Method**	**Manufacturer**
Amaxa Cell Line Nucleofector Kit V	Mammalian cell transfections	Lonza Group
2× *Phusion HF PCR Master Mix*	High-fidelity PCR	Thermo Fisher Scientific
JetPRIME transfection reagent	Mammlian cell transfetions	Polyplus, Sartorius
NucleoSpin Gel and PCR Clean up	Agarose gel and PCR clean-up	Macherey-Nagel
NucleoSpin Gel and PCR Clean up	Agarose gel and PCR clean-up	Macherey-Nagel
NucleoSpin Plasmid EasyPure	Plasmid DNA purification	Macherey-Nagel
Pierce SuperSignal West Pico PLUS	Western Blot Immunodetection	Thermo Fisher Scientific

2.1.7 Bacterial strains

Tab. 2.10: Strains used in molecular cloning and protein biochemistry

Strain name	**Genotype**	**Manufacturer**
E. coli JM109	*end*A1 *rec*A1 *gyr*A96 *hsd*R17($r_k^- m_k^+$) *rel*A1*sup*E44 Δ(*lac-pro*AB) [F´*tra*D36 *pro*AB *laq*I^{q}ZΔM15] *thi*	Agilent, Stratagene
E. coli One Shot TOP10	F$^-$ *mcr*A Δ(*mrr-hsd*RMS-*mcr*BC) φ80*lac*ZΔM15 Δ*lac*X74 *rec*A1 *ara*D139 Δ(*ala-leu*) 7697 *gal*U *gal*K *rps*L (Str^r)*end*A1 *nup*G λ-	Invitrogen, Thermo Fisher Scientific
E. coli ArcticExpress (DE3)RIL	*E. coli* B F$^-$*omp*T *hsd*S($r_B^- m_B^-$) *dcm*$^+$Tet^r *gal* λ(DE3) *end*A Hte [cpn10 cpn60 Gent^r][*arg*U *ile*Y *leu*W Str^r]	Agilent, Stratagene
E. coli BL21 CP (DE3)pLysS	*E. coli* B F$^-$ *omp*T *hsd*S(r_B^- m_B^-) *gal* λ(DE3) [*pLys*S Cam^r]	Agilent, Stratagene

2.1.8 Software & Tools

For computational biology methods and *in silico* data analyses, following software and computational tools were used:

Tab. 2.11: Software and computational tools

Product name	**Version**	**Developer**
A plasmid editor (ApE)	2.054b	Davis & Jorgensen, 2022
CorelDRAW	22.0 & 23.0	Corel Corporation
GraphPad Prism 7	7.0.0	GraphPad Software, Inc.
Image Lab	6.1	Bio-Rad Laboratories
ImageJ/FIJI	2.14.0/1.54f	Schindelin *et al.*, 2012
JalView	2.11.3.0	Waterhouse *et al.*, 2009
MacTEX	2024/10.03.0	MacTeX TeXnical working group
Microsoft Office Excel	16.17	Microsoft Corp.
Microsoft Office Word	16.17	Microsoft Corp.
Odyssey	3.0	Li-COR Biotechnology
Photoshop 2024	25.0.0	Adobe Inc.
Quantity One	4.6	Bio-Rad Laboratories
R	4.3.2	R Core Team
RStudio	2023.06.0+421	Posit PBC
SnapGene	7.2.0	GSL Biotech LLC
TexSHOP	5.12	Richard Koch, 2000
Zen Blue	3.4	Carl Zeiss AG

2.2 Methods in Molecular Biology

2.2.1 Plasmid DNA isolation

The *NucleoSpin Plasmid EasyPure Kit* (Macherey-Nagel) was used to isolate plasmid DNA from bacterial cells according to the manufacturer's instructions. Isolated plasmid DNA was resuspended in 50 µL AE elution buffer and stored at -20 °C.

2.2.2 Agarose gel electrophoresis

To distinguish DNA fragments of varying lengths, isolated and purified DNA samples were separated via agarose gel electrophoresis. Agarose was diluted in 1× TAE buffer to achieve a final concentration of 0.5–2.0% (w/v). Concentrations were adjusted depending on the expected DNA fragment sizes. To resolve differences in DNA fragment sizes of less than 50 bp, higher concentrations of agarose were used. Therefore, 5.0% (w/v) agarose was diluted in TBE buffer. Solutions were heated until the agarose was fully dissolved. Ethidium bromide was added in a dilution of 1:10000 (v/v) before casting the gels. Prior to loading, samples were prepared by adding loading dye to a final concentration of 1× *MassRuler DNA* loading dye (Thermo Fisher Scientific). A DNA size marker with fragments of known lengths was used to assess the fragment sizes of the separated DNA fragments (Table 11).

Tab. 2.12: DNA marker list

DNA size marker name	**Manufacturer**
100 bp DNA Ladder Ready to Load	Solis Biodyne
1 kb DNA Ladder Ready to Load	Solis Biodyne
MassRuler DNA Ladder Mix	Thermo Fisher Scientific
pUC19 Marker ready-to-use	Carl Roth AG

Electrophoretic separation was performed with 1× TAE buffer accordingly at a voltage of 5 –10 V per cm gel length. DNA fragments were detected using the *XR Gel Doc* gel documentation system (Bio-Rad Laboratories) and analyzed via *Quantity One Software*

or *Image Lab* (see section 2.1.7). Bands corresponding to indented sizes were cut out and subsequently cleaned up for further preparation (see section 2.2.4).

2.2.3 Polymerase chain reaction (PCR)

The polymerase chain reaction (PCR) is a molecular biological technique using enzymes to amplify specific DNA sequences (Mullis *et al.*, 1986). These generated DNA amplicons could be used for molecular cloning, e.g. insertion into a plasmid, or in combination with cDNA synthesis to analyze the expression of certain mRNAs. Specific DNA sequences for molecular cloning were amplified with a *Phusion High-Fidelity Polymerase* used in a commercially available 2× *Phusion High-Fidelity PCR Master Mix* (Thermo Fisher Scientific) according to the manufacturer's instructions with following modifications: The final reaction volume was 20 µL, and optional DMSO was used to enhance primer binding.

Tab. 2.13: *Phusion* PCR

Component	**Volume (µL)**	**Final concentration**
Template DNA	1	approx. 10 ng
Forward Primer	0.5	0.5 µM
Reverse Primer	0.5	0.5 µM
DMSO	0.6	3% (v/v)
2× *Phusion Master Mix*	10	1×
Nuclease-free Water	7.4	-

All reactions were performed according to the manufacturer's instructions. Primer annealing temperatures were set to 3 °C above the primer melting temperatures, which were calculated via the *Oligo Calc Tool* (Kibbe, 2007) using a Nearest Neighbor algorithm. Analytical PCRs were performed with a *FIREPol DNA Polymerase* in a 5× *FIREPol Master Mix* (Solis Biodyne) according to the manufacturer's instructions with following modifications: The final reaction volume was 20 µL and the sample composition is stated below.

Elongation times were set to 30 s per PCR with 35 cycles performed. The annealing temperatures were set 3 °C below the primer melting temperatures, which were

calculated as described above. Generally, the reaction steps were performed in a *PCR Thermocycler T3000* (Biometra, Analytik Jena). PCR amplicons from PCRs used in molecular cloning were analyzed as described above and purified as described in the following section. Analytical PCRs were separated using 5% (w/v) agarose gels were used and eventually visualized as previously described (see section 2.2.2).

Tab. 2.14: *FIREPol* PCR

Component	**Volume (µL)**	**Final concentration**
Template DNA	1	approx. 10 ng
Forward Primer	0.5	0.5 µM
Reverse Primer	0.5	0.5 µM
5× *FIREPol Master Mix*	4	1×
Nuclease-free Water	14	-

2.2.4 Amplicon isolation from PCRs and clean-up from agarose gels

After agarose gel electrophoresis or PCR, obtained DNA fragments were processed using either a *NucleoSpin Gel and PCR Clean-up Kit* or the *NucleoSpin Gel and PCR Clean-up XS Kit* (Macherey-Nagel) according to the manufacturer's manual.

2.2.5 Restriction endonuclease treatment

Before combining DNA fragments, overlapping complementary 5'-ends were generated using commercially available restriction endonucleases (Thermo Fisher Scientific) which cleave DNA at a sequence-specific site. Primarily, *Mlu*I and *Sal*I restriction endonucleases were used simultaneously and buffer recommendations from the *DoubleDigest Calculator* (Thermo Fisher Scientific) were used. For an analytic endonuclease digest, approx. 200 ng of DNA was used to digest in a 10 µL reaction volume. Per restriction endonuclease, 1 U of enzyme was used according to the manufacturer's instruction with appropriate buffer concentrations. The restriction digests were incubated at 37 °C for 2 h. Analyses were carried out as described previously (see section 2.2.2) to determine correct DNA fragment sizes and yield. DNA fragments used for molecular cloning were prepared preparative

endonuclease digests. Here, 2–5 µg of plasmid DNA were digested in a 20 µL reaction volume according to the manufacturer's manual and incubated for 16 h at 37 °C. The digested fragments obtained were analyzed as previously described (see section 2.2.2).

2.2.6 Ligation

DNA fragments with complementary cohesive 5'-ends were joined together to create plasmids with newly inserted genes. The *T4 DNA Ligase* (Thermo Fisher Scientific) catalyzes the formation of a covalent phosphodiester bond between these DNA fragments. Reactions fusing a vector and a target gene to be inserted according to the manufacturer's instructions with following modifications: The ligation reaction was incubated 2–10 h at 20–25 °C, referred to as room temperature (RT).

2.2.7 Transformation of bacterial cells

Introduction of recombinant plasmid DNA was performed according to the chemically competent bacterial cells manufacturer's manual with following modifications: 300–400 µL SOC medium were used after the heat shock protocol. Cell-medium mixtures were plated onto LB agar plates containing appropriate antibiotics for selection and incubated at 37 °C.

2.3 Methods in Protein Biochemistry

2.3.1 Recombinant protein expression

Tab. 2.15: Recombinant protein chimeras and expression conditions

Recombinant protein	Bacterial strain	Induction method	Expression
GST	BL21	Autoinduction	see below
GST-hsSYNPO2(1085–1261)	BL21	0.3 mM IPTG	3 h at 16 °C
GST-hsTAZ1(fl)	Arctic Express	0.5 mM IPTG	16 h at 16 °C
GST-hsTAZ1(ΔC)	BL21	0.5 mM IPTG	16 h at 16°C
GST-hsTAZ1(ΔN)	Arctic Express	0.5 mM IPTG	16 h at 16 °C
GST-hsYAP1-1(fl)	Arctic Express	Autoinduction	see below
GST-hsYAP1-1(ΔC)	Arctic Express	0.5 mM IPTG	16 h at 16 °C
GST-hsYAP1-1(ΔC)	BL21	0.5 mM IPTG	16 h at 16 °C
GST-hsYAP1-2(fl)	BL21	0.5 mM IPTG	16 h at 16 °C
GST-hsYAP1(ΔN)	Arctic Express	0.5 mM IPTG	16 h at 16 °C
GST-hSYNPO2(1–85)-His-EEF	BL21	Autoinduction	see below
GST-hSYNPO2L(1–85)-His-EEF	BL21	Autoinduction	see below
His-EEF-hsACTN1(fl)	BL21	Autoinduction	see below
His-EEF-hsACTN2(fl)	BL21	Autoinduction	see below
His-EEF-hsACTN3(fl)	BL21	Autoinduction	see below
His-EEF-hsBAG3(fl)	BL21	Autoinduction	see below
His-EEF-hsBAG3(fl) WAWA	BL21	Autoinduction	see below
His-GST-TEV-hsBAG3 WAWA (17–67)	BL21	0.2 mM IPTG	5 h at 30°C
His-GST-TEV-hsBAG3-WW (17–67)	BL21	0.2 mM IPTG	5 h at 30°C
His-GST-TEV-hsYAP1-WW1 (165–209)	BL21	0.2 mM IPTG	5 h at 30°C
His-GST-TEV-hsYAP1-WW12 (165–271)	BL21	0.2 mM IPTG	5 h at 30°C
His-GST-TEV-hsYAP1-WW2 (229–271)	BL21	0.2 mM IPTG	5 h at 30°C
T7-His-hsACTN1(fl)	BL21	Autoinduction	see below
T7-His-hsACTN2(fl)	BL21	Autoinduction	see below
T7-His-hsACTN3(fl)	BL21	Autoinduction	see below
T7-His-hsACTN4(fl)	BL21	Autoinduction	see below
T7-His-hsSYNPO2(1–809)	BL21	0.3 mM IPTG	3 h at 16 °C
T7-His-hsSYNPO2(527–663) DDDD	BL21	Autoinduction	see below
T7-His-hsSYNPO2(527–663) TSDD	BL21	Autoinduction	see below
T7-His-hsSYNPO2(527–663) WT	BL21	Autoinduction	see below
T7-His-hsSYNPO2(664–1093)	Arctic Express	0.5 mM IPTG	16 h at 16 °C
T7-His-hsSYNPO2b(fl)	BL21	0.3 mM IPTG	3 h at 16°C

The production of recombinant proteins for experiments was either carried out in LB medium with IPTG-induced expression or in ZYM-5052 autoinduction medium (Studier, 2005) depending on the protein to be expressed. Expression protocols using LB medium were followed according to the expression strain supplier's instructions with modifications (Tab. 2.15). For expression via autoinduction, cells were grown in ZYM-5052 medium to an OD_{600} of 1.5–2.0 at 37 °C with agitation. After an incubation for 30 min at 4 °C, cultures were shifted to the expression incubation at 16 °C for 16–20 h. All cultured cells were harvested by centrifugation with 5250×g for 30 min at 4 °C and stored at -20 °C.

If not stated otherwise, all steps in the following protein purification protocols and biochemical assays were carried out on ice or at 4 °C, all buffers were ice-cold.

2.3.2 Affinity chromatography purification of GST-tag recombinant proteins

Pellets from bacterial expression cultures harvested were resuspended in GSH lysis buffer supplemented with a final concentration of 0.1 mg · mL^{-1} lysozyme and 1× *Protease Inhibitor Cocktail* (Roche). Per 100 mL of bacterial cell culture pellet, 5 mL of GSH lysis buffer were used. To reduce viscosity due to genomic DNA, *Pierce Nuclease* (Thermo Fisher Scientific) was added 1:5000, incubated for 40 min and samples were sonicated with a *UP100* sonotrode (Hielscher Ultrasonics) for 5 min (cycle 0.6, amplitude 100%). The samples were centrifuged at 13000×g for 30 min and incubated with *PureCube Glutathione Agarose* beads (Cube Biotech) pre-equilibrated with GSH wash buffer for 120 min After separating the beads by centrifugation at 1500×g for 3 min, the supernatant was removed by aspiration. The beads were washed three times with 10 bead volume equivalents of GSH wash buffer, separated by centrifugation and eventually resuspended in 1–2 mL GSH wash buffer. Resuspended beads were loaded into a column and the buffer was removed by gravity flow. Proteins bound to the beads were eluted with GSH elution buffer and fractionated in 500–1000 µL, WW domain constructs fused to GST were eluted with WW elution buffer, instead. The proteins to be used for experiments were stored on ice. The proteins to be used for experiments were stored on ice. Purity and concentrations of were determined via SDS-PAGE and spectrophotometry (see section 2.3.5 and 2.3.12).

2.3.3 Affinity chromatography purification of His-tagged recombinant proteins

Pellets from bacterial expression cultures harvested were resuspended in NTA lysis buffer supplemented with a final concentration of 0.1 mg · mL^{-1} lysozyme and 1× *Protease Inhibitor Cocktail*. Pellets with SYNPO2 constructs expressed were resuspended in SYNPO2 NTA lysis buffer, pellets with expressed BAG3 constructs were resuspended in BAG3 lysis buffer (Tab.2.15). Per 100 mL of bacterial cell culture pellet, 5 mL of lysis buffer were used, respectively. *Pierce Nuclease* was added 1:5000, incubated for 40 min, and samples were sonicated as previously described. The samples were centrifuged at 13000×g for 30 min and incubated with *PureCube Ni-Indigo Agarose* beads (Cube Biotech) pre-equilibrated with NTA wash buffer for 90 min. After separating the beads by centrifugation at 1500×g for 3 min, the supernatant was removed by aspiration. The beads were washed three times with 10 bead volume equivalents of NTA wash buffer, separated by centrifugation and eventually resuspended in 1–2 mL NTA wash buffer. Resuspended beads were loaded into a column and the buffer was removed by gravity flow. Proteins bound to the beads were eluted with NTA elution buffer and fractionated in 500–1000 µL. The proteins were stored on ice until used for experiments. The proteins to be used for experiments were stored on ice. Purity and concentrations of were determined via SDS-PAGE and spectrophotometry.

2.3.4 Denaturing purification of His-tagged recombinant proteins

Due to low solubility, some SYNPO2 constructs (amino acids 527–663), referred to as SYNPO2(527–663) were purified with a different approach. All initial steps were carried out as described in section 2.3.3, with following modifications: after centrifugation, pellets were soaked in DENAT buffer for 30 min at RT with agitation. Soaked pellets were combined with supernatants from the initial centrifugation after cell disruption and incubated with *PureCube Ni-Indigo Agarose* pre-equilibrated with NTA wash buffer for 90 min. The proteins to be used for experiments were stored on ice. Purity and concentrations of were determined via SDS-PAGE and spectrophotometry.

2.3.5 Tandem Affinity Purification (TAP) of PDZ domains

Pellets from bacterial cell cultures harvested were resuspended in TAP lysis buffer supplemented with a final concentration of 0.2 mg · mL^{-1} lysozyme and 1× *Protease Inhibitor Cocktail*. Per 100 mL of bacterial cell culture pellet, 5 mL of GSH lysis buffer were used. *Pierce Nuclease* was added 1:5000. Cell pellets were resuspended in a beaker with magnetic stirrer for 40 min and sonicated as described above (see section 2.3.2). The samples were centrifuged with an *Optima L-100XP* preparative ultracentrifuge (Beckman & Coulter) at 35.000×g for 30 min. The supernatant was loaded onto a *GSTrap HP column* (Cytiva) equilibrated with 5 column volumes of TAP wash buffer 1 with a flow of 0.3–0.4 mL · min^{-1} using a *REGLO ICC* peristaltic pump (Ismatec). The column was washed on an *ÄKTA Purifier* Fast Liquid Protein Chromatography (FPLC) machine (Pharmacia, Cytiva) with gradient of TAP wash buffer 1 and TAP wash buffer 2 at a flow rate of 1–2 mL · min^{-1}. The gradient was selected to decrease salinity to 150 mM NaCl for subsequent elution and protease cleavage. The proteins were eluted in TAP 3C buffer and 3C protease (1 mg · mL^{-1}) was added 1:50 to cleave the GST-tag. The protease was incubated for at least 16 h. To separate the PDZ domains from cleaved GST-tag, samples were subsequently applied to a *Superdex 75 prep-grade* size exclusion chromatography (SEC) column (Cytiva) equilibrated with PDZ buffer. The proteins to be used for experiments were stored on ice. Purity and concentrations of were determined via SDS-PAGE and spectrophotometry.

2.3.6 Spectrophotometric determination of protein concentrations

Purity and concentration of purified recombinant proteins was determined via UV-vis spectrophotometry using the NanoPhotometer NP80 (Implen). Absorbances at 280 and 260 nm were measured to determine protein and DNA contaminant concentrations, respectively. Corrected protein concentrations accounting for DNA contamination of samples were calculated as follows:

$$Protein\ concentration\ (mg \cdot mL^{-1}) = \frac{1.55 \cdot A_{280} - 0.76 \cdot A_{260}}{Path\ length\ (cm)} \tag{2.1}$$

If there were no tryptophans present in purified recombinant proteins to provide a sufficient read-out of the absorbance at 280 nm, absorbances at 205 and 280 nm were measured instead. Subsequently, protein concentrations were calculated as follows:

$$Protein\ concentration\ (mg \cdot mL^{-1}) \ = \ \frac{A_{205}}{27 + \frac{A_{260}}{A_{205}}} \tag{2.2}$$

Finally, molar protein concentrations were then calculated:

$$Molar\ concentration\ (mol \cdot L^{-1}) \ = \ \frac{Protein\ concentration(mg \cdot mL^{-1})}{Molecular\ mass\ (Da)} \tag{2.3}$$

2.3.7 Protein pulldown assay

To assess interactions between proteins *in vitro*, a protein pulldown assay was carried out. In principle, a bait protein is immobilized to affinity beads by means of a GST-tag fused to its N-terminus. The immobilized bait protein is then probed with potential ligand proteins, which eventually result in interactions with some of the probed ligands. Interacting probes bound to the bait protein are immobilized as well. However, if no interaction occurs, probes will be retracted in the mobile phase. The elution of immobilized interacting complexes allows for the specific detection of both the bait protein and the interacting ligand using SDS-PAGE and immunoblotting. The bait proteins were purified incubated with *Protino Glutathione Agarose 4B* (Macherey-Nagel) as previously described (see section 2.3.2). Per ligand, a bed volume of 25 µL bait-coupled beads was used. Prior to probing, the beads were washed three times with 10 bed volumes of PBS. Subsequently, purified ligand proteins were incubated in a final volume of 400 µL PBS with final concentrations up to 5 µM for 1 h at 4 °C. After three wash steps with 10 bed volumes of PBS, proteins were eluted with 50 µL of pre-heated SDS sample buffer. Experimental outcomes were determined via SDS-PAGE, immunoblotting, and immunodetection (see section 2.3.12, 2.3.14, and 2.3.15).

2.3.8 Protein crosslinking assay

Interacting proteins which are in close proximity to each other can be chemically linked using a crosslinking reagent like EGS. These reagents carry chemically active groups that react with specific residues on polypeptide chains. Covalently crosslinked proteins will migrate in an SDS-PAGE due to their shift in molecular mass compared to polypeptides in their monomeric state. The purified PDZ domains of SYNPO2 and SYNPO2L were diluted in PDZ GF buffer containing a final concentration of 4 mM DTT. The final protein concentrations were 10 µM. Protein samples were mixed to a final volume of 50 µL and incubated at either 22 °C for 15 min or 4 °C for 30 min. The crosslinking reagent EGS dissolved in DMSO was added to a final concentration of 0.5 mM per reaction. In negative control samples, same volumes of DMSO were added. The crosslinking reactions were carried out at two different temperature conditions, 4 °C and 22 °C for 30 or 15 min, respectively. As quenching agent, 20 µL of 5× SDS sample buffer were added and incubated for additional 15 min at RT. Afterwards, all samples were boiled for 2 min at 98 °C.

2.3.9 Co-immunoprecipitations (co-IP)

Co-immunoprecipitation (co-IP) experiments represent another approach to study the interaction of two proteins *in vitro*. In contrast to protein pulldown assays, this method selectively immobilizes protein complexes on magnetic beads by using a specific antibody directed against a bait protein of interest (POI). The utilized beads carry covalently bound protein G which binds to the constant region of the antibodies, precipitating the POI. Interacting proteins forming protein complexes with the POIs are coprecipitated along with the proteins of interest. First, 2.5 µM of POIs and 7.5 µM of ligand proteins were diluted in a co-IP buffer and incubated for 1 h at 4 °C under agitation. Protein G-coupled *Dynabeads*™ (Invitrogen) were washed with co-IP buffer X and 0.75 µg/sample of either a T7-tag-directed antibody, or a control antibody (XR1B) were incubated for 15 min at RT. After removal of unbound antibodies by washing three times with co-IP wash buffer X, beads were resuspended in 20 µL PBS per sample, added to the protein mixture, and incubated for another 15 min at 25 °C. After three final washing steps, and

removing residual buffer, the beads were supplemented with pre-heated SDS sample buffer. Finally, samples were mixed and heated for 2 min at 98 °C. Experimental outcomes were determined as described above.

2.3.10 Co-immunoprecipitations (co-IP) with YAP1/TAZ constructs

Due to the hydrophobic character of assessed YAP1/TAZ interactions and the reduction of unspecific binding, YAP1/TAZ constructs used in biochemical procedures were washed in absence of harsh detergents. The sample preparation was carried out as described in section 2.3.7, with following modifications: during all steps, *Protein LoBind*™ tubes (Eppendorf) were used. Prior to antibody coupling, *Dynabeads*™ were pre-equilibrated with *PBS-based Intercept*™ blocking buffer (LI-COR) for 45 min at RT. After adding the antibody-coupled beads to the protein samples, the incubation time was reduced to 10 min at 4 °C. The samples were washed once with co-IP buffer T transferred to a new tube. After four final washing steps with co-IP buffer T and removal of residual buffer, the beads were supplemented with pre-heated SDS sample buffer. Finally, samples were mixed and heated for 2 min at 98 °C. Experimental outcomes were determined as described above.

2.3.11 Competitive binding assay

To study the competition of two proteins for an interaction with a bait POI, a competitive binding assay was performed. First, 2.5 µM of POIs and 7.5 µM of one ligand were diluted in a co-IP buffer and incubated for 1 h at 4 °C under agitation. The other ligand was titrated to samples in different concentrations, ranging from 0 to 8 µM. The samples were incubated again for 1 h at 4 °C. *Dynabeads*™ were washed with co-IP buffer X and equilibrated with *PBS-based Intercept*™ blocking buffer (LI-COR) for 45 min at RT. The beads were then loaded with 0.75 µg/sample of either a T7-tag-directed antibody, or a control antibody (XR1B) were incubated for 15 min at RT. After removal of unbound antibodies by washing three times with co-IP wash buffer X, beads were resuspended in 20 µL PBS per sample, added to the protein mixture, and incubated for another 15 min at RT. The samples were washed once with co-IP buffer NT transferred to a new tube. After

four final washing steps with co-IP buffer NT and removal of residual buffer, the beads were supplemented with pre-heated SDS sample buffer. Finally, samples were mixed and heated for 2 min at 98 °C. Experimental outcomes were determined as described above.

2.3.12 Peptide interaction assay

To examine protein-protein interactions with a certain motif of amino acids, peptide membranes (Peptides & Elephants) were probed with potentially interacting proteins according to the manufacturers protocol with slight modifications. All incubation steps were carried out at RT. The blocking of free binding sites was performed for 1 h, followed by two washing steps with TBST. Protein probes were diluted in TBST to a final concentration of 25 nM. Before incubating primary and secondary antibodies, membranes were washed with TBST in five consecutive steps instead of three. The immunodetection of the membranes was performed as previously described. Membranes were finally analyzed on a *ChemiDoc MP* imaging system (Bio-Rad Laboratories) after immunodetection.

2.3.13 SDS-Polyacrylamide gel electrophoresis (SDS-PAGE)

Electrophoretic separation via SDS gels provides a direct method of assessing protein preparations for sample purity and protein quantities. Prepared samples are treated with SDS, an anionic detergent that binds to polypeptide chains, eventually denaturing them (Laemmli, 1970). Bound SDS molecules confer a negative charge to proteins, masking their intrinsic charge. In an electric field, protein samples can be separated due to their differences in molecular masses in a polyacrylamide gel matrix. Prior to loading, all protein samples were diluted in 5× SDS sample buffer and boiled for 2 min at 98 °C.

2.3.13.1 Tris-glycine polyacrylamide gels

Separating gels (left) and stacking gels (right) were prepared as follows:

Tab. 2.16: Tris-glycine SDS gel composition

Solution	**8%**	**10%**	**12.5%**	**15%**	**Solution**	**4%**
Acrylamide (30%, 37.5:1)	1.33 mL	1.65 mL	2.08 mL	2.50 mL	Acrylamide	0.65 mL
1.5 M Tris pH 8.8	1.25 mL	1.25 mL	1.25 mL	1.25 mL	0.5 M Tris pH 6.8	1.25 mL
ddH2O	2.37 mL	2.05 mL	1.62 mL	2.40 mL	ddH2O	3.00 mL
SDS 10%	50 µL				SDS 10%	50 µL
TEMED	5 µL				TEMED	5 µL
APS	16 µL				APS	50 µL

Separating gels were overlaid with 2-propanol. Both parts of the gel were allowed to polymerize for at least 1 h at RT before continuing. Fully cast gels were stored at 4°C.

2.3.13.2 Bis-Tris polyacrylamide gels

For proteins with molecular masses below 20 kDa, a different discontinuous gel buffering system was used for sufficient separation. Preparation steps were carried out as previously described (see section 2.3.10.1).

Tab. 2.17: Bis-Tris SDS gel composition

Solution	**8%**	**10%**	**12.5%**	**15%**	**Solution**	**4%**
Acrylamide (30%, 29:1)	1.33 mL	1.65 mL	2.08 mL	2.50 mL	Acrylamide	0.65 mL
1.5 M Tris pH 8.8	1.42 mL	1.42 mL	1.42 mL	1.42 mL	0.5 M Tris pH 6.8	1.25 mL
ddH2O	2.25 mL	1.93 mL	1.50 mL	1.08 mL	ddH2O	3.00 mL
SDS 10%	50 µL				SDS 10%	50 µL
TEMED	5 µL				TEMED	5 µL
APS	16 µL				APS	50 µL

2.3.13.3 Coomassie Brilliant Blue staining

SDS gels were stained with Coomassie Brilliant blue G-250 according to the Rapid Coomassie Protein SDS-gel Staining protocol (Yan, 2011).

2.3.13.4 Stain-free analysis of SDS gels

Prior to transfer and immobilization of proteins, SDS gels of co-IPs could be analyzed with 2,2,2-trichloroethanol (TCE). Tryptophanes present in the separated proteins can be covalently modified by TCE incorporated into the SDS gel. When excited with UV/B light at 310 nm, modified proteins in the gel emit light at 410 nm (Ladner *et al.*, 2004; Chopra *et al.*, 2019). Therefore, 50 µL of TCE was incorporated per gel during SDS-gel preparation (see previous sections). After running, the gels were analyzed using the ChemiDoc MP Imaging System (Bio-Rad Laboratories) with settings adjusted for stain-free gels.

2.3.13.5 Protein Transfer

Proteins separated by SDS-PAGE were transferred to a *Whatman* nitrocellulose membrane (GE Healthcare) to facilitate accessibility for the detection of antibodies. A wet transfer was utilized as preferred method of choice. The gel was first equilibrated in transfer buffer (see section 2.2.2), then placed on a sheet of nitrocellulose membrane, cushioned with 3 filter papers and compressed in a support grid cassette. The cassettes were placed into a *TE22 Mighty Small* transfer tank (Hoefer, Harvard Bioscience) containing transfer buffer. Depending on the experiment, the transfer was performed with a constant current either at 250 mA for 16 h at 4 °C, or at 300 mA for 90 min at RT.

2.3.13.6 Immunodetection of western blots

After proteins were transferred to the nitrocellulose membrane, primary antibodies specific against the proteins of interests were used (Tab. 2.7). All incubation steps were

carried out at RT. Prior to antibody incubation, free binding sites on the membrane were blocked using 4% (w/v) milk powder diluted in TBST for 1 h. For primary antibody conjugates, 5% (w/v) milk powder in TBST was incubated for 90 min. Primary antibodies were diluted in TBS and incubated for 1 h. The membranes were then washed three times with TBST for 10 min each to remove unbound antibodies. Secondary antibodies were diluted in TBS and incubated for 1 h. Final washing steps were repeated three times with TBST for 10 min each. An enhanced chemiluminescence (ECL) solution (Thermo Fisher Scientific) was added to membranes incubated with secondary antibodies conjugated to a horseradish peroxidase (HRP) (Tab. 2.8) to facilitate a chemical reaction emitting light at 425 nm, enabling the analysis via the *ChemiDoc MP* imaging system.

For quantitative analyses of immunodetections, fluorophore conjugated antibodies (Tab. 2.8) were used. Fluorescence emissions were analyzed with the *ChemiDoc MP* imaging system with appropriate settings for antibodies used.

2.4 Methods in Cell Biology

2.4.1 Cultivation of mammalian cells

Mammalian cells were grown at 37 °C in a *Heracell 240i* incubator (Heracell) with a relative humidity of 100% and atmospheric conditions with 5% CO2 saturation. If not described otherwise, all cell culture media or solutions were pre-warmed and cell confluences for differentiation were estimated visually.

2.4.2 C2C12 murine myoblast cell line

Initially subcloned and established from a mouse myoblast cell line (Yaffe & Saxel, 1977; Blau *et al.*, 1985), the C2C12 cell line functioned as a model system for adherent skeletal myoblasts, eventually differentiating to myotubes. Cells were thawed in 1 mL aliquots at 37 °C, diluted in C2C12-GM, and centrifuged at 800×g for 3 min. Cell pellets were resuspended in 1–2 mL C2C12-GM and gently transferred to a plate containing C2C12-GM. Incubation was performed as described previously until the cells reached a confluence of approx. 85%. For subcultivation, a plate of cells was washed with PBS-EDTA, treated with 0.25% (w/v) trypsin in PBS until cells detached. Detaching cells were resuspended in C2C12-GM and centrifuged as described above. After centrifugation, the supernatant was removed by aspiration and the cell pellet was diluted in C2C12-GM. The cells were then seeded 1:10 onto new plates containing C2C12-GM. Differentiation was carried out exchanging the C2C12-GM to C2C12-DM at a visual confluence of approx. 100%.

2.4.3 A7r5 smooth muscle-like cell line

A7r5 cells were used to function as a model system of undifferentiated vascular smooth muscle cells (vSMC). These cells are derived from the thoracic aorta of 14–17-day old BDIX rat embryos, a strain used for, among other things, carcinogenic and teratogenic studies (Kimes & Brandt, 1976). A7r5 cells were thawed in 1 mL aliquots at 37 °C, diluted in A7r5-GM, and centrifuged at 800×g for 3 min. The cell pellets were resuspended in 1–2 mL A7r5-GM and gently transferred to a plate containing A7r5-GM. Incubation was

performed as described previously until the cells reached a visual confluence of approx. 85%. For subcultivation, a plate of cells was washed with PBS-EDTA, treated with 0.25% trypsin in PBS until cells detached. Detaching cells were resuspended in A7r5-GM and centrifuged as described above. After centrifugation, the supernatant was removed by aspiration and the cell pellet was diluted in A7r5-GM. The cells were then seeded 1:3 to 1:4 onto new plates containing A7r5-GM. For subcultivation on smaller plates, A7r5 cells were diluted appropriately depending on the surface area of the plates.

2.4.4 Cell density measurements

To minimize the cell density-dependent variations of YAP1 localization within cells for subsequent experiments, the density of A7r5 cells was assessed prior to transfection. Pre-plated A7r5 cells were grown on 35 mm cell culture dishes, with an additional sample dish for cell density measurements. The sample dish was washed and treated with 1 mL of trypsin as described above (see section 2.4.3). An aliquot of detached cells was mixed 1:1 with trypan blue stain (Invitrogen) for 2 min at RT and transferred to a disposable counting chamber slide (Invitrogen). By using trypan blue solution, only cells with a compromised membrane are stained. The density measurements were assessed using a *Countess Automated Cell Counter* (Invitrogen). The measured density of vital cells per plate was determined to be $3.39 \pm 0.58 \cdot 10^5 cells \cdot mL^{-1}$ which corresponds to the total number of vital cells per dish. It was assumed that the cell densities were distributed equally between the plates during subcultivation.

2.4.5 Transient transfection of myoblasts via electroporation (Nucleofection)

C2C12 cells to be transfected were grown until approx. 80% visual confluence. After a wash with DPBS, the cells were detached as previously described. Detached cells were resuspended in C2C12-GM and pelletized at 800 × g for 3 min. The supernatant was removed by aspiration. Transient transfections were performed with the *Amaxa Cell line Nucleofector Kit V* (Lonza Group) according to the manufacturer's protocol with following

modifications: Per plate of cells, 82 µL Nucleofection solution I and 18 µL Nucleofection supplement were combined with 4 µg of plasmid DNA to transfect. If two plasmids were transfected simultaneously, 2 µg of each plasmid DNA was used. The nucleofector program appropriate for C2C12 cells (B-032) was selected. After the transfection procedure, cells were seeded on fresh 35 mm plates containing C2C12-GM. Differentiation was induced 24h after transfection by exchanging the medium with C2C12-DM.

2.4.6 Transient transfection of cells via chemical compounds (JetPRIME)

A7r5 cells to be transfected were grown on 35 mm plates to a visual confluence of approx. 50–60%. Transfections were performed with the *JetPRIME transfection reagent* (Polyplus, Sartorius), following the manufacturer's instructions with following modifications: per reaction, 2 µg of plasmid DNA, 3 µL JetPRIME, and JetPRIME buffer were combined. If more than one plasmid was transfected per reaction, 1 µg for each plasmid DNA was used. The cells were fixed after 48 h post transfection.

2.4.7 Bimolecular fluorescence complementation assay (BiFC)

To provide a method for probing putative PPIs at a cellular level, a BiFC assay was used (Kerppola, 2006; Kerppola, 2008). The basic principle involves fusing each of two proteins of interest to complementary, non-fluorescent fragments of a fluorescent reporter protein (Hu *et al.*, 2002). When the proteins come into close proximity, during interaction, the reporter protein chimeras complement each other and become fluorescent. In this work, two protein fragments from a modified species of yellow fluorescent protein (YFP), named Venus were used. The fragments comprised an N-terminal (Venus1) and C-terminal (Venus2) part utilized in different mammalian expression vectors, respectively. The transfections of these plasmids into C2C12 and A7r5 cells were performed as described above (see. 2.4.4 and 2.4.5).

2.4.8 Fixation of cells with paraformaldehyde

Prior to antibody staining and microscopy, cultured cells were fixed with paraformaldehyde (PFA). Initial washing steps were performed by replacing the medium with DPBS and washing them twice, followed by a fixation step with a PFA solution for 10 min at 37 °C. Cells were then washed twice with DPBS, followed by permeabilization with 0.5% Triton X-100 in DPBS for 10 min at RT. Final washing steps were repeated three times with DPBS before the cells were stored in DPBS at 4 °C.

2.4.9 Electrical pulse stimulation (EPS)

In order to analyze the effects of contraction-induced mechanical stress exerted by EPS, C2C12 cells were grown and differentiated on 35 mm dishes as previously described. On day 7 of differentiation, the cells were transferred into a *C-dish* (Ion Optix) and electrically stimulated using *C-Pace EP Culture Pacer* (Ion Optix). The EPS protocol was applied for 3 h with 10 V and pulses of 20 ms. The program sequence consisted of a 5 s hold followed by continuous 20 ms pulses at 15 Hz, a 5 s delay, 5 s of pulses at 5 Hz followed by a 5 s delay (Orfanos *et al.*, 2016). After the EPS treatment, the cells were fixed followed by a immunofluorescence staining and fluorescence microscopic analysis.

2.4.10 Immunofluorescence staining of cells for microscopy

After fixation, cell dishes were prepared for fluorescence microscopy using an indirect immunofluorescence staining. All steps were carried out at RT. The cells were incubated for 30–60 min with an NGS/BSA solution for blocking, followed by adding primary antibodies diluted in PBS for 1 h (Tab. 2.7 and 2.8). After three washing steps with PBST, secondary fluorophore-conjugated antibodies, phalloidin and/or DAPI were added and incubated for 1 h. Prior to embedding with *Fluoromount-G* compound (Invitrogen, Thermo Fisher Scientific), three washing steps in PBST were carried out, followed by a desalting step in double-distilled water (ddH_2O). The dishes were stored in absence of light at RT for microscopic analyses.

2.4.11 Confocal laser scanning microscopy (CLSM)

Microscopic analyses of cells were performed using an LSM 900 confocal microscope (Carl Zeiss). The image acquisition was carried out with *Plan-Apochromat DIC 63x/1.4* and *Plan-Apochromat 40x/1.3 Oil DIC* lenses. Multi-channel images were acquired with separate fluorescence channels using the *Best Signal* setting according to the Zen Blue imaging software. Confocal image acquisition was performed using a pinhole size (diameter) of one *Airy unit*(AU) with 4-fold image averaging per channel, a scan speed setting of 4, and a bit depth of 8 bits per channel in LSM Plus mode. For YAP1 localization and colocalization analyses, previous settings were used, the digital pixel size quality was set to 0.076–0.092 µm, and the bit depth was increased to 16 bits per channel. Images acquired were processed in *Carl Zeiss Image* (*.czi*)-format.

2.5 Computational Biology and *in silico* analyses

2.5.1 Nuclear translocation measurements of YAP1

Images acquired for YAP1 localization analyses in the cytoplasm and nucleus of assessed cells were processed using the *FIJI* distribution of the *ImageJ2* analysis and processing software (Tab. 2.11). The acquired fluorescence channels were imported separately. In order to determine the mean fluorescence intensities (MFI) of YAP1 in the cytoplasm or the nucleus, the respective compartment areas and the YAP1 cumulative fluorescence intensities (CFI) were determined (Zhang *et al.*, 2021):
In C2C12 myotubes, the total area of myotubes within the image was determined using the titin Z-disc epitope imaging channel gated with a *Li* thresholding algorithm (Li *et al.*, 1998). In A7r5 cells, the total cell area was measured by gating with a *Minimum* (entropy) thresholding algorithm for the SYNPO2 imaging channel, and a *Triangle* thresholding algorithm for the BAG3 and GFP imaging channels (Kittler & Illingworth, 1986; Zack *et al.*, 1977). Areas of the nuclei were determined using the *Li* thresholding algorithm for the DAPI channel and subsequently subtracted from the myotubular/cellular areas:

$$A_{cytoplasm} = A_{total} - A_{nucleus} \;\; ; \;\; CFI_{cytoplasm} = CFI_{total} - CFI_{nucleus} \tag{2.4}$$

YAP1 CFIs within the given compartments of cytoplasm and nucleus were divided by their area, giving the MFIs of YAP1 in either the nucleus or the cytoplasm. Ratios of nuclear and cytoplasmic YAP1 intensities should eventually provide information on the (transcriptional) coactivation of YAP1 in the nucleus. To determine the fraction of total YAP1 in the nucleus, ratios were calculated from MFI values for nuclear and cytoplasmic YAP1:

$$YAP1\ ratio = \frac{CFI_{nucleus}/A_{nucleus}}{(CFI_{total} - CFI_{nucleus})/(A_{total} - A_{nucleus})} \tag{2.5}$$

As of now, the occurrence of YAP1 in the nucleus is termed YAP1 nuclear translocation. Elevated levels of YAP1 in the nucleus compared to its cellular localization are denoted as YAP1 nuclear import, whereas elevated levels of YAP1 in the cytoplasm are referred to as YAP1 cytoplasmic retention.

$$YAP1\ nucleus/cytoplasm\ <\ 1\ (cytoplasmic\ retention) \tag{2.6}$$

$$YAP1\ nucleus/cytoplasm\ >\ 1\ (nuclear\ import) \tag{2.7}$$

For each calculation, at least 20 cells from three biological replicates were examined.

2.5.2 Colocalization analyses

In order to assess the spatial correlation between SYNPO2-YAP1 complexes and immunofluorescence-labeled structures in smooth and skeletal muscle cells, colocalization analyses were performed utilizing the *Colocalization module* implemented in the Zen Blue software.

In A7r5 cells, the spatial relation between fluorescence intensities of immuno-labeled α-actinin and the BiFC constructs was examined for three regions of interest (ROIs): (1) at stress fibers, (2) in the cell periphery, and (3) at FAs.

In C2C12 cells, the spatial relation between fluorescence intensities of BiFC constructs and the immuno-labeled Z-disc epitope of titin were examined throughout an image fraction of the myotube. For each BiFC construct and ROI, Pearson correlation coefficients (PCC) of the spatial signal intensity distributions were determined and corrected with the Costes algorithm (Costes *et al.*, 2004; Dunn *et al.*, 2011). Each measurement was performed with at least 20 cells from three biological replicates.

2.5.3 Line plot analyses

To investigate the spatial relation between transfected, fluorescence-labeled SYNPO2 constructs and immunofluorescence-labeled structures in smooth and skeletal muscle cells, fluorescence intensity line profile analyses were performed. Image processing was

carried out utilizing the *Profile utility* implemented in the Zen Blue software.
In A7r5 cells, the spatial relation between SYNPO2 and α-actinin was assessed along actin stress fibers, while in C2C12 cells, the spatial relation between SYNPO2 and the Z-disc epitope of titin was examined along myofibrils. Therefore, respective fluorescence intensities were measured separately for each channel along a line profile of 25 µm length with a width of 20 pixels, corresponding to a width of 1.52–1.85 µm, denoted as line plot. For each line plot, a PCC was calculated.

2.5.4 In-Gel quantification of GST-Pulldowns

In-gel quantification and statistical analyses were performed as previously published (Mao *et al.*, 2021). Results were presented as arithmetic means and corresponding standard errors of the mean (SEM) for the indicated number (n) of experiments. Distribution tests and statistical analyses were performed with a one-way ANOVA using *GraphPad Prism 7* analysis software.

2.5.5 Quantification of co-IPs

Quantifications of band intensities was performed with the FIJI distribution of ImageJ. The acquired fluorescence images were imported separately and band intensities were scaled and normalized to SYNPO2 band intensities. The results were presented as arithmetic means and corresponding SEM for the indicated number of experiments.

2.5.6 Statistical Analyses

If not stated otherwise, distribution testing, statistical analyses, and visualization of corresponding data were performed with R and the RStudio GUI software, implementing the R packages (Tab. 2.11):
`tidyverse` (Wickham *et al.*, 2019), `readxl` (Wickham & Bryan, 2019), `fitdistrplus` (Delignette-Müller & Dutang, 2015), and `ggstatsplot` (Patil, 2021).

Chapter 3

Results

3.1 PDZ domain interactions of SYNPO2

Similar to other members of the synaptopodin family, SYNPO2 is mostly intrinsically disordered (Kwok *et al.*, 2019; van der Lee *et al.*, 2014). The N-terminal part of three human SYNPO2 isoforms (a, b, c) comprises the PDZ domain with a distinct, well-defined structure, while remaining regions of the protein are disordered (Fig. 1.10; Linnemann *et al.*, 2010). PDZ domains function in signaling and regulation, canonically binding to C-terminal motifs of potential ligands (see section 1.4.2; Songyang *et al.*, 1997). To elucidate the role of SYNPO2 in muscle cell development, signaling and mechanotransduction, it is crucial to understand the function of the PDZ domain of SYNPO2.

One way to achieve this goal is to identify and characterize PPIs with novel ligands. PDZ domains can be classified according to binding properties of preferred C-terminal motifs, allowing structurally similar, putative binding motifs to be predicted *in silico* (Hui *et al.*, 2013; Valgardson *et al.*, 2019), which will be covered later (see section 3.1.2). Another approach is to study non-canonical PDZ interactions involving PDZ domain mediated homo- or heterodimerization which can occur in different ways (Im *et al.*, 2002). In a tested subset of PDZ domains, nearly 30% of the probed domains were observed to form homo- and hetero-dimers (Chang *et al.*, 2011). Moreover, studies reported that in some reported cases, dimerization of PDZ domains may be necessary in order to recognize and bind potential ligands (Fanning *et al.*, 2007; Chen *et al.*, 2008). However, the underlying mechanisms for PDZ-PDZ-dimers formation remain still unknown (Liu & Fuentes, 2019).

3.1.1 The PDZ domain of SYNPO2 remains in a monomeric state

To test whether SYNPO2 undergoes PDZ-PDZ multimerization *in vitro*, the PDZ domain of SYNPO2, referred to as SYNPO2(1–85), was analyzed via size exclusion chromatography (SEC) upon purification. The PDZ domain of SYNPO2L, referred to as SYNPO2L(1–85), was analyzed in comparison as a prospective control. In aqueous solutions, the hydrodynamic radius (Stoke's radius) of monomeric PDZ domains is reduced compared to PDZ dimers. As a result, these monomers are retained on the size exclusion columns and elute with a shift in retention volume. However, upon SDS-PAGE analyses, protein fractions of both elution peaks should migrate at the same height due to the reducing and denaturing conditions during electrophoresis, rendering all molecules monomeric. Both, SYNPO2(1–85) and SYNPO2L(1–85) constructs were expressed and purified as described above (see section 2.3.1 and 2.3.4). The components of the processed sample prior to SEC were the 3C protease (42 kDa), cleaved GST-tag (26.8 kDa), uncleaved protein (37 kDa), and the cleaved and monomeric forms of SYNPO2(1–85) and SYNPO2L(1–85) with theoretical molecular masses of 11.14 and 11.17 kDa, respectively (Fig. 3.1, Input). The elution profiles from SYNPO2(1–85) during SEC showed a primary elution peak at approx. 55 mL, and a secondary peak at approx. 72 mL of retention volume. The chromatogram of SYNPO2L(1–85) revealed two elution peaks at approx. 57 and 80 mL (Fig. 3.1, upper panels). A subsequent SDS-PAGE aimed at determining whether the primary elution peaks during SEC contained any PDZ domains (Fig. 3.1, lower panels).

However, protein bands from primary elution peaks of both purifications analyzed solely migrated at approx. 26 kDa, corresponding to the cleaved GST-tag. The secondary elution peaks show protein bands corresponding to the expected molecular masses of the PDZ domains (Fig. 3.1, arrows). This indicates that during size exclusion chromatography, formation of PDZ homo-dimers did not occur. Both SYNPO2(1–85) and SYNPO2L(1–85) remained in a monomeric state under the tested conditions. To confirm results obtained via SEC but also to study potential heterodimer formation of SYNPO2 and SYNPO2L PDZ domains, a protein crosslinking assay was performed, using either SYNPO2(1–85), SYNPO2L(1–85), or a mixture of both proteins. Proteins in close proximity, e.g. when undergoing interactions may be covalently crosslinked (see section 2.3.8). Upon SDS PAGE analysis, both SYNPO2(1–85) and

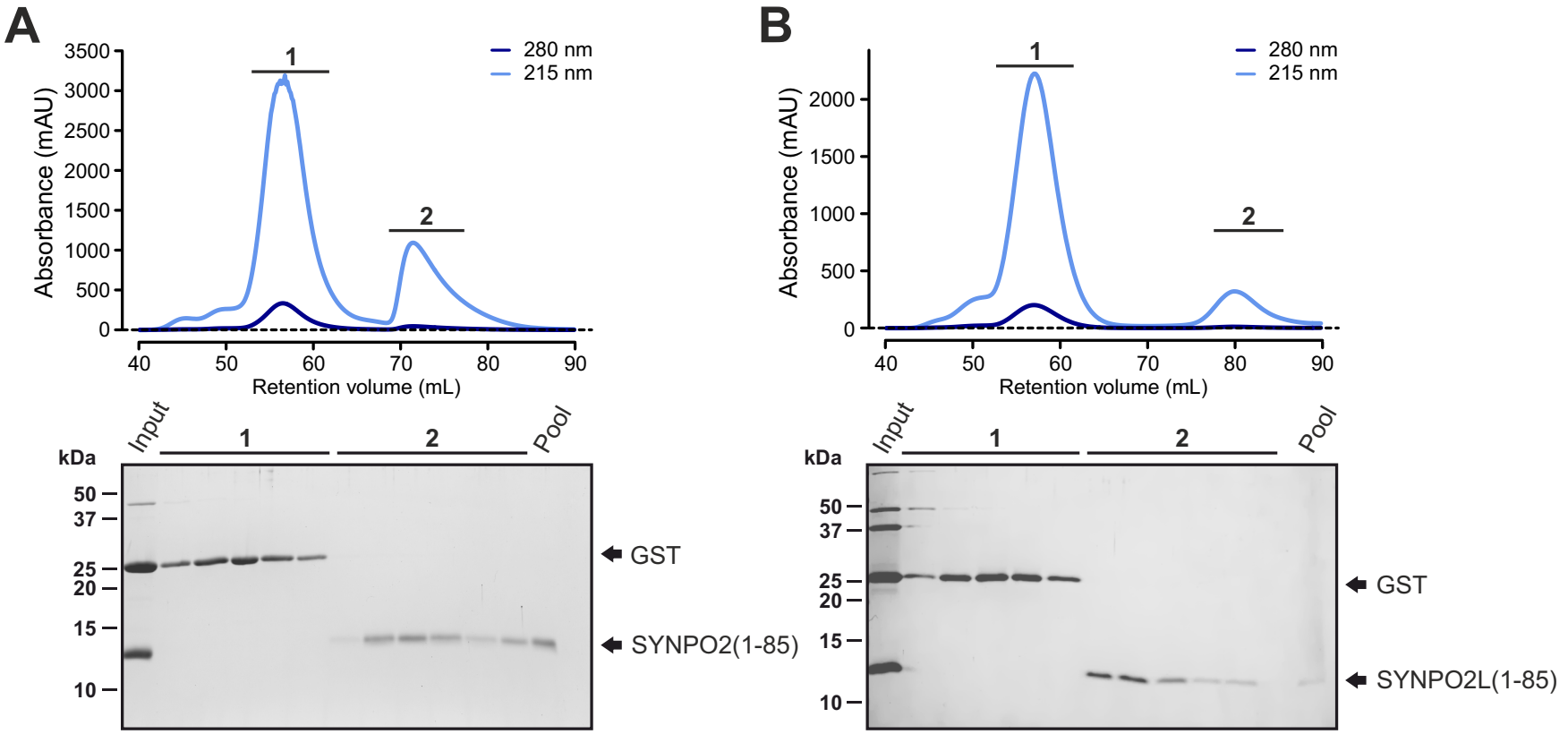


Fig. 3.1: SEC elution profiles of SYNPO2 and SYNPO2L during purification. (Upper panel) Chromatograms during size exclusion chromatography (SEC) of PDZ domains from SYNPO2 (A) and SYNPO2L (B), termed SYNPO2(1–85) and SYNPO2L(1–85). Each sample separated by SEC and resulted in two elution peaks, respectively. Fractions containing eluted proteins (labeled 1 and 2) were collected for analysis. (Lower panel) SDS-PAGE of elution peak fractions. A control sample after 3C cleavage but before SEC was loaded (Input). While primary elution peak fractions showed protein bands migrating at approx. 26 kDa, the secondary elution peak fractions showed bands migrating at approx. 12 kDa. The protein bands corresponded to GST eluted in the primary peak fractions. PDZ domains of SYNPO2 and SYNPO2L eluted during the secondary peak fractions, respectively. The primary peak fractions did not contain any PDZ domain proteins eluted, indicating that no dimerization occurred, featuring an increased hydrodynamic radius of PDZ domain populations.

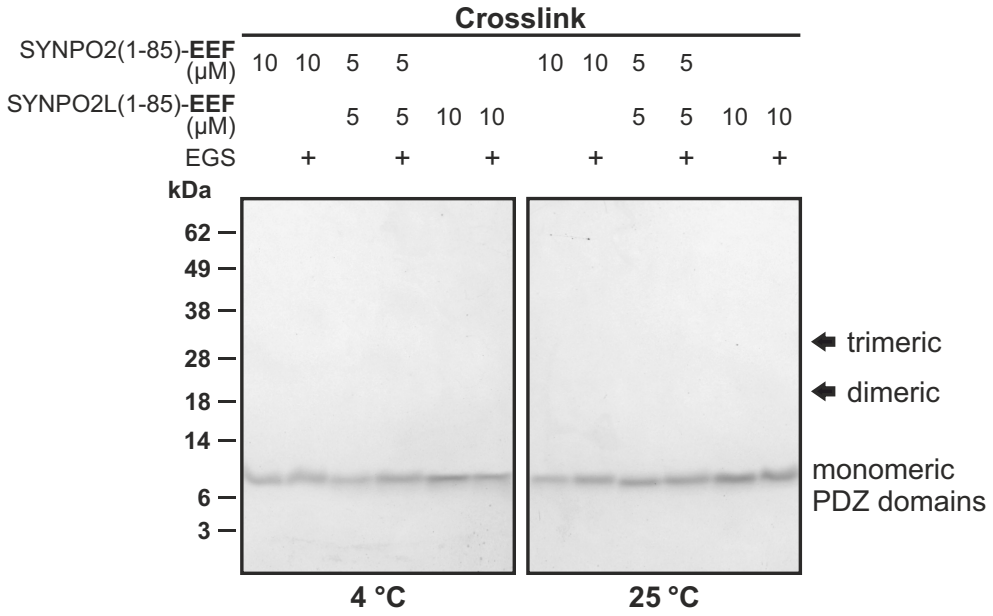


Fig. 3.2: PDZ domains of SYNPO2 and SYNPO2L remain in a monomeric state. SDS-PAGE analyzing purified PDZ domains of SYNPO2, abbreviated SYNPO2(1–85), and SYNPO2L, abbreviated SYNPO2L(1–85), in crosslinking assays. Samples containing PDZ domains of SYNPO2 and SYNPO2L labeled above, were chemically crosslinked with EGS. Reaction conditions are shown on the bottom. Control samples without crosslinking agent present were supplemented with DMSO. The band migration pattern of molecular weight markers is shown on the left. The expected migration of potential dimeric and trimeric PDZ domain protein complexes is indicated by arrows on the right.

SYNPO2L(1–85) proteins migrated at approx. 12 kDa (Fig. 3.2) corresponding to their monomeric molecular masses. No additional protein bands migrating at different heights were observed, indicating that neither SYNPO2, nor SYNPO2L form homo- or heterooligomers. Hence, a PDZ domain-mediated oligomerization did not occur under the conditions tested and both, SYNPO2 and SYNPO2L remained in a monomeric state.

3.1.2 YAP1 harbors a C-terminal motif that interacts with SYNPO2

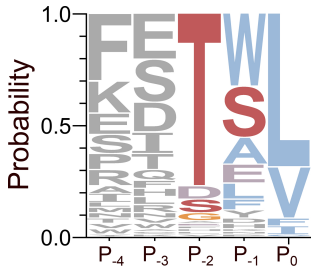
A starting point in order to identify novel SYNPO2 ligands was made by establishing a yeast-two-hybrid (Y2H) assay, screening the first 177 amino acids of SYNPO2 for new PPIs against a human protein library. The Y2H system provides an established, easy-to-use method with high throughput to identify PPIs (Fields & Song, 1989). Positive Yeast clones were screened for prey protein expression via a β-galactosidase-lift assay and prey plasmids from these clones were isolated and sequenced. The screen

carried out for this work resulted in positive yeast clones expressing the proteins synemin, TUSC1, or VPS18, which were found to bind the SYNPO2 PDZ domain bait construct. Protein alignments revealed that these proteins have canonical C-termini consisting of the amino acids W-L_{COOH} or W-F_{COOH}, suggesting the PDZ domain of SYNPO2 might specifically recognize ligands via a tryptophan-based motif (Fig. 3.3). In parallel, an *in silico* analysis of datasets based on support vector machine (SVM)-generated position weight matrix (PWM) ligand predictions for



Fig. 3.3: Protein alignment of positively screened ligands for SYNPO2. Multiple sequence alignments using the Clustal Omega algorithm in Jalview (Sievers *et al.*, 2018). Protein names (for Uniprot IDs, see Appendix) are displayed on the very left. The amino acid positions within proteins are shown on the left and right of each sequence. Colors are adapted from Clustal. C-termini of identified prey proteins sequenced featured a combination of tryptophan at P_{-1} in combination with either leucine or phenylalanine at P_0. Notably, positively screened ligands contained clusters of acidic residues between the P_{-6} and P_{-9} positions.

human PDZ domains was performed (Hui & Bader, 2010; Hui *et al.*, 2013). The datasets listed the five C-terminal amino acids of potential ligands, ranked according to a prediction score for recognition (Fig. 3.4; right). The dataset for predicted ligands of SYNPO2 yielded a few top scoring motifs, one of which was found to be F-L-T-W-L_{COOH}. This PDZ-BM was identified in two proteins, YAP1 and TAZ. Notably, predicted motifs were similar to ligand motifs identified in the Y2H assay (Fig. 3.4; left).



Motif	Protein	Score	Binding Class
FLTWL	YAP1/TAZ	1.164	
STTWL	MRPL43	0.756	
FSTYV	KALRN	0.658	X-[ST]-X-Φ_{COOH}
FETFL	ATAD2B	0.567	
KFTWF	R3HDML	0.524	

Fig. 3.4: *In silico* motif prediction and PDZ domain interactors. Consensus sequence of structure-based ligand motifs for the PDZ domain of SYNPO2 (left). Highest ranking scores of proteins from the in silico prediction (right). Both, the consensus motifs as well as C-terminal PDZ-BMs of screened ligands from the Y2H were based on the tryptophan at position P_{-1} to be crucial for recognition.

To characterize this predicted interaction biochemically, a protein pulldown assay was performed, as described above (see section 2.3.6). In this experiment, full-length YAP1,

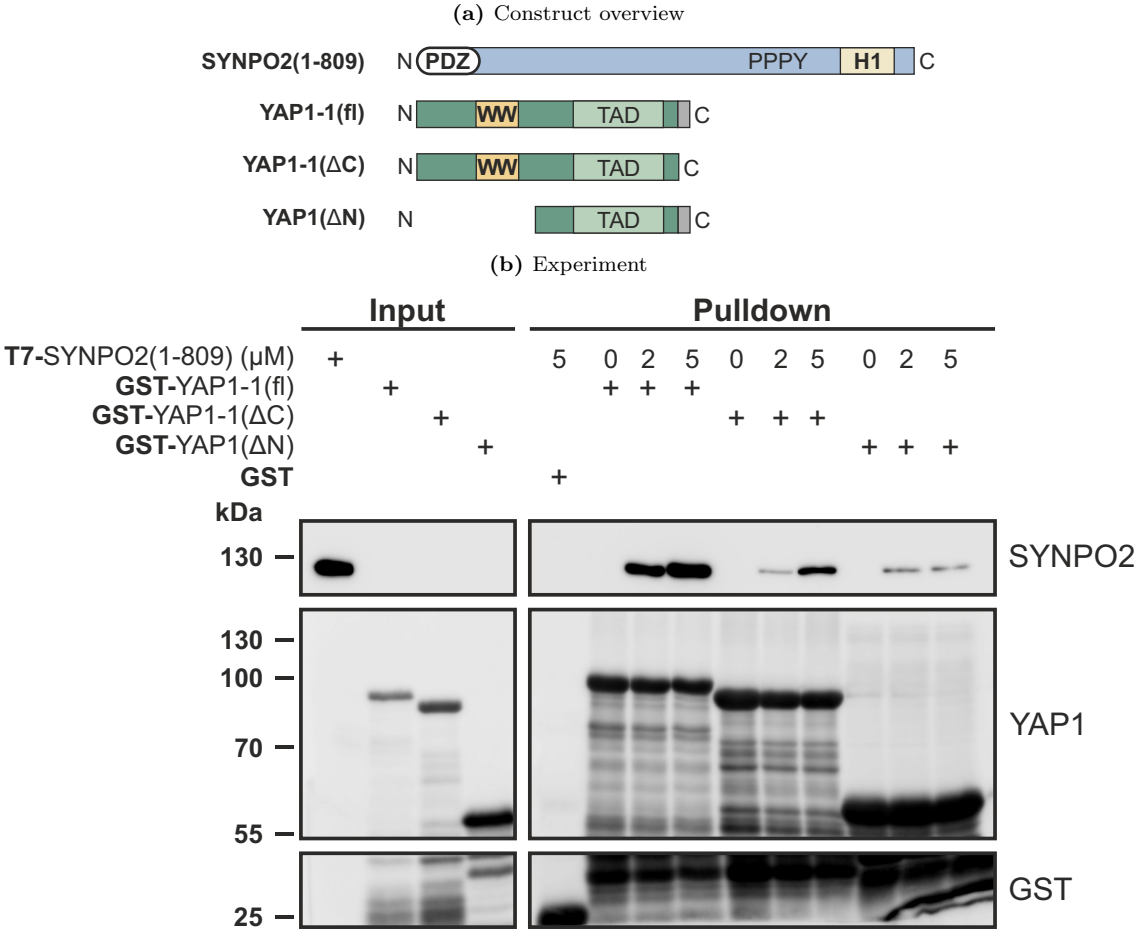


Fig. 3.5: YAP1 interacts with the PDZ domain of SYNPO2 *in vitro*. (a) Overview of precipitated constructs via protein pulldown assay. The first 809 amino acids of SYNPO2 fused to a T7-tag were probed (blue). GST-tagged YAP1 bait constructs were immobilized either without the N-terminus harboring the WW domain (ΔN), or without any truncations as full-length (fl) protein chimeras (green). (b) Digitally rearranged western blot of protein fractions from the Pulldown experiment. The sample composition in loading controls with fused tags (Input) and experimental samples after precipitation with anti-T7 antibody (Pulldown) is outlined on top. Immunotags fused to proteins for antibody detection are printed in bold. The band migration pattern of molecular weight markers is shown on the left. The expected migration of potential dimeric and trimeric PDZ domain protein complexes is indicated by arrows on the right. (Top panel) SYNPO2 probed in different concentrations. (Bottom panels) GST and YAP1 protein fractions from the same experiment. Probed SYNPO2 eluted together with immobilized YAP1 but not with GST itself, indicating an interaction between the proteins.

referred to as YAP1(fl), containing the C-terminal PDZ-BM was immobilized using an N-terminally fused GST-tag. Additionally, truncated YAP1 constructs lacking the PDZ-BM, referred to as YAP1(ΔC), or the N-terminal portion, referred to as YAP1(ΔN), were generated and immobilized using a N-terminal GST-tag as well. The immobilized constructs were probed with different concentrations of a SYNPO2 construct featuring the first 809 amino acids, referred to as SYNPO2(1–809), fused to a

T7-immunotag (Fig. 3.5; a). This construct harbored the PDZ domain and could be easily distinguished from the YAP1 constructs by its size. To ensure specificity of the interactions, the GST-tag itself was used as a control bait (Fig. 3.5). Immunoblotting exhibited bands in samples with coupled beads running at approx. 90 kDa, corresponding to YAP1(fl), detected with GST-directed antibodies (Fig. 3.5; b). Detection with a T7 tag-directed (T7-)antibody, revealed bands of a molecular mass of approx. 120 kDa in samples additionally probed with SYNPO2. These bands were absent in control sampled containing beads coupled with GST only. Thus, SYNPO2 eluted together with previously immobilized YAP1 but not with GST, indicating a specific complex formation between SYNPO2 and YAP1. Interestingly SYNPO2 also interacted with a YAP1 construct lacking the PDZ-BM, initially functioning as a control to exclude unspecific binding. This finding will be further investigated in section 3.2.

3.1.3 SYNPO2 functions as an adapter protein, forming a ternary complex with BAG3, and YAP1/TAZ

Previous studies have revealed versatile functions of SYNPO2, e.g. as adapter protein connecting BAG3 and VPS18. Thereby, membrane fusion complexes involving VPS18 are linked to the BAG3-mediated CASA machinery in muscle cells (Ulbricht *et al.*, 2013). SYNPO2 was shown to function as a linker of a ternary complex between VPS18, and BAG3. SYNPO2 simultaneously binds the C-terminus of VPS18 via its PDZ domain, while it interacts with the WW domain of BAG3 via its PPPY motif. With the identification of new interactions of the PDZ domain, versatile functions of SYNPO2 as adapter protein could become more eminent: Recent studies have highlighted the emerging role of Hippo pathway transcriptional coactivators for autophagy and mechanotransduction (Pavel *et al.*, 2018; Totaro *et al.*, 2019).
Similar to the complex formation with VPS18 and BAG3, SYNPO2 could therefore link the Hippo signaling pathway proteins YAP1/TAZ with the CASA complex core protein BAG3. To test the hypothesis of a putative complex formation between SYNPO2, BAG3, and YAP1/TAZ, a co-IP assay was performed as described above (see section 2.3.7). In this assay, the previously utilized T7-SYNPO2(1–809) construct

was simultaneously incubated with either GST-tagged YAP1, EEF-tagged BAG3, or both in order to study a putative ternary complex formation. These constructs were termed YAP1–1(fl) and BAG3(fl), respectively (Fig. 3.6; a). SYNPO2 was precipitated via its fused T7-immunotag. YAP1 and BAG3 were detected with anti-GST, and anti-EEF-directed antibodies, respectively. The western blot analysis

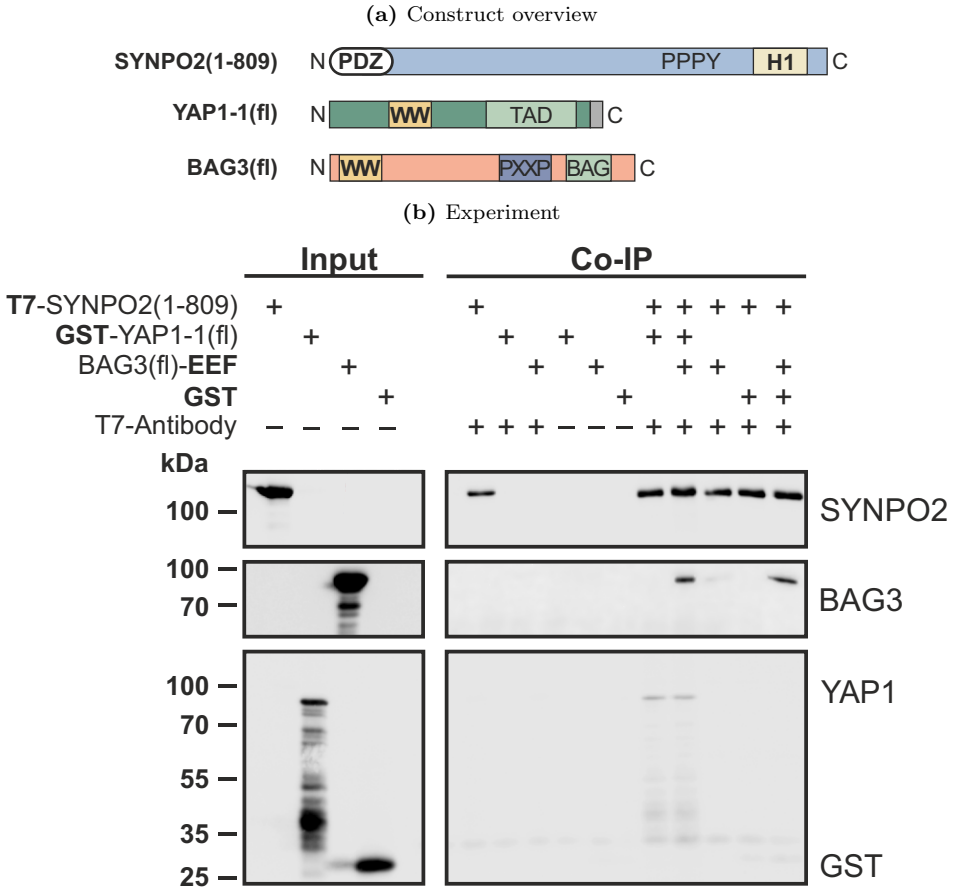


Fig. 3.6: SYNPO2, YAP1 and BAG3 form a ternary complex. (a) Overview of precipitated human T7-tagged SYNPO2 bait construct (blue), amino acids 1–809, harboring the PDZ domain and PPPY motif. GST-tagged human YAP1 harboring the first WW domain (YAP1–1) as full-length (fl) protein chimera (green) was coprecipitated along with human BAG3 (orange). (b) Digitally rearranged western blot of sample fractions from the co-IP experiment. The sample composition in loading controls (Input) and experimental samples after precipitation (co-IP) is outlined on top. Immunotags fused to proteins for antibody detection are printed in bold. The band migration pattern of molecular weight markers is shown on the left. (Top panel) SYNPO2 bait sample fractions from the co-IP experiment. (Middle panel) BAG3 protein sample fractions from the same experiment. (Bottom panel) YAP1 protein sample fractions from the same experiment. Samples without SYNPO2 bait protein or anti-T7 antibody did not show coprecipitation. Both YAP1 and BAG3 could be coprecipitated in samples containing anti-T7 antibody and SYNPO2, indicating the presence of a ternary complex. Furthermore, it was confirmed that YAP1 and BAG3 bind SYNPO2 separately.

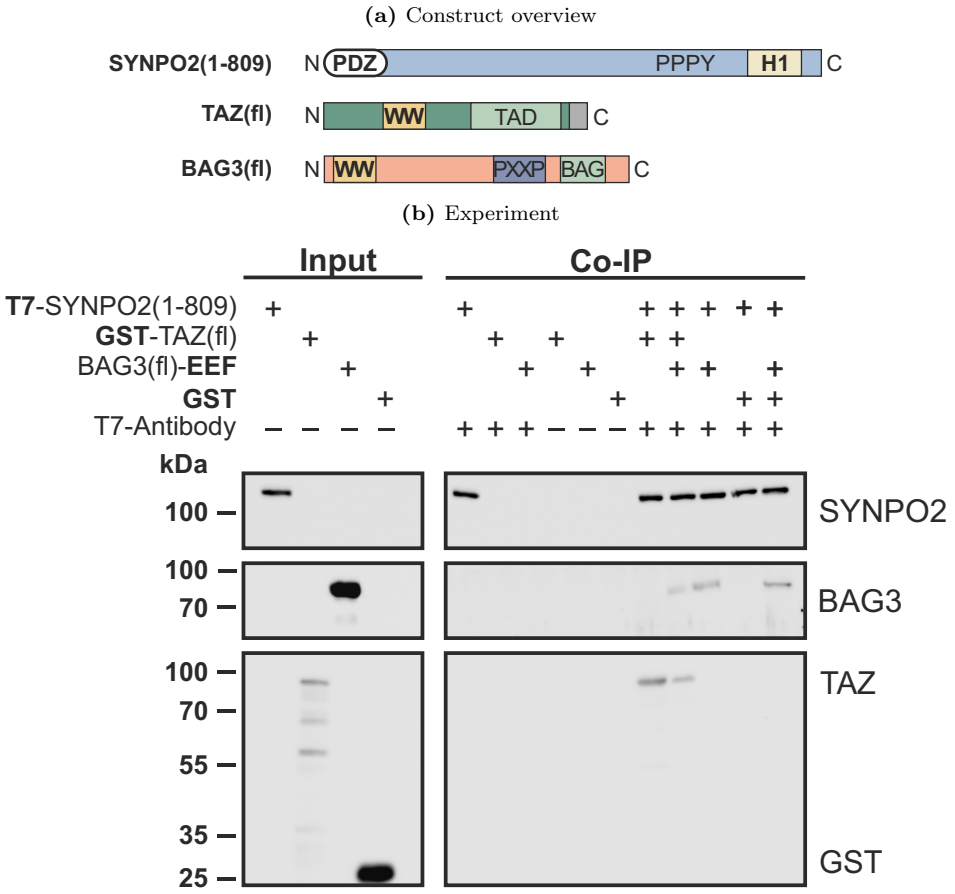


Fig. 3.7: SYNPO2, TAZ and BAG3 form a ternary complex. (a) Precipitated human T7-tagged SYNPO2 bait construct (blue), amino acids 1–809, harboring the PDZ domain and PPPY motif. Human GST-tagged TAZ protein chimera (green) was coprecipitated along with BAG3 (orange). (b) Digitally rearranged western blot of sample fractions from the co-IP experiment. The sample composition in loading controls (Input) and experimental samples after precipitation (co-IP) is outlined on top. Immunotags fused to proteins for antibody detection are printed in bold. The band migration pattern of molecular weight markers is shown on the left. (Top panel) SYNPO2 bait sample fractions from the co-IP experiment. (Middle panel) BAG3 protein sample fractions from the same experiment. (Bottom panel) TAZ protein sample fractions from the same experiment. Samples without SYNPO2 bait protein or anti-T7 antibody did not show coprecipitation. Both, TAZ and BAG3 could be coprecipitated in samples containing anti-T7 antibody and SYNPO2, indicating the presence of a ternary complex. Furthermore, it was confirmed that TAZ and BAG3 bind SYNPO2 separately.

showed bands for precipitated SYNPO2 migrating at around 120 kDa. Controls lacking the T7 antibody or SYNPO2 did not reveal any additional bands (Fig. 3.6; b). However, upon probing with YAP1 or BAG3, additional bands were detected, each migrating at 90 kDa, corresponding to either YAP1 or BAG3, respectively. In the sample probed with both, YAP1 and BAG3, two additional bands were detected simultaneously. These bands were identified as BAG3 and YAP1, indicating the coprecipitation of a ternary complex of SYNPO2, BAG3 and YAP1. Similarly, as observed previously in the protein

pulldown experiment, YAP1 itself coprecipitated along with SYNPO2, indicating a complex formation mediated by the PDZ domain of SYNPO2. In addition to that, BAG3 was found to co precipitate with SYNPO2, which confirms the findings of previous studies (see section 1.4.3). As a YAP1 paralog, TAZ is also involved in the Hippo signaling pathway. Both human proteins share about 47% of amino acid sequence identity as well as functional features. TAZ harbors the same C-terminal PDZ-BM, indicating a potential for a similar ternary complex formation between SYNPO2, TAZ and BAG3. Co-IP experiments were performed with SYNPO2, BAG3 and TAZ (Fig. 3.7; a). Similar to the previous assay, TAZ was fused to GST and subsequently detected with an anti-GST antibody. The western blot analysis showed results similar to the previous co-IP experiment (Fig. 3.7; b): Immunoblots of samples probed with either TAZ, BAG3, or both showed additional bands, each migrating at approx. 90 kDa. These bands were identified as BAG3 and TAZ, indicating the formation of a ternary complex between SYNPO2, BAG3 and TAZ as well. Thus, both YAP1/TAZ and BAG3 can bind SYNPO2 in an independent manner, but also form ternary complex with SYNPO2.

3.1.4 YAP1 and BAG3 bind SYNPO2 simultaneously, but independently

Previous research has demonstrated that a complex comprising of BAG3 and Hsp70 is capable of regulating the Hippo pathway by stimulating kinases such as LATS1 (Meriin *et al.*, 2018). In addition to that, this complex also mediates regulation of YAP1 itself by recruiting a LATS1-YAP1-angiomotin-like-2 (AMOTL2) complex (Varelas, 2014; Paramasivam *et al.*, 2011, Baldan *et al.*, 2021). Hence, YAP1 is directly linked to BAG3, suggesting a direct interaction between the two proteins (Baldan *et al.*, 2021). Therefore, a co-IP experiment was conducted to investigate the proposed interaction between BAG3 and YAP1. The BAG3 and YAP1 constructs previously utilized in this work were tested for binding (Fig. 3.8; a). Here, immunoblotting analyses did not reveal any coprecipitation of the tested YAP1 constructs (Fig. 3.8; b). As a result, it was not possible to demonstrate that YAP1 directly interacts with BAG3 under the conditions tested. Nonetheless, it can be concluded that the formation of a YAP1-SYNPO2-BAG3 complex involves two

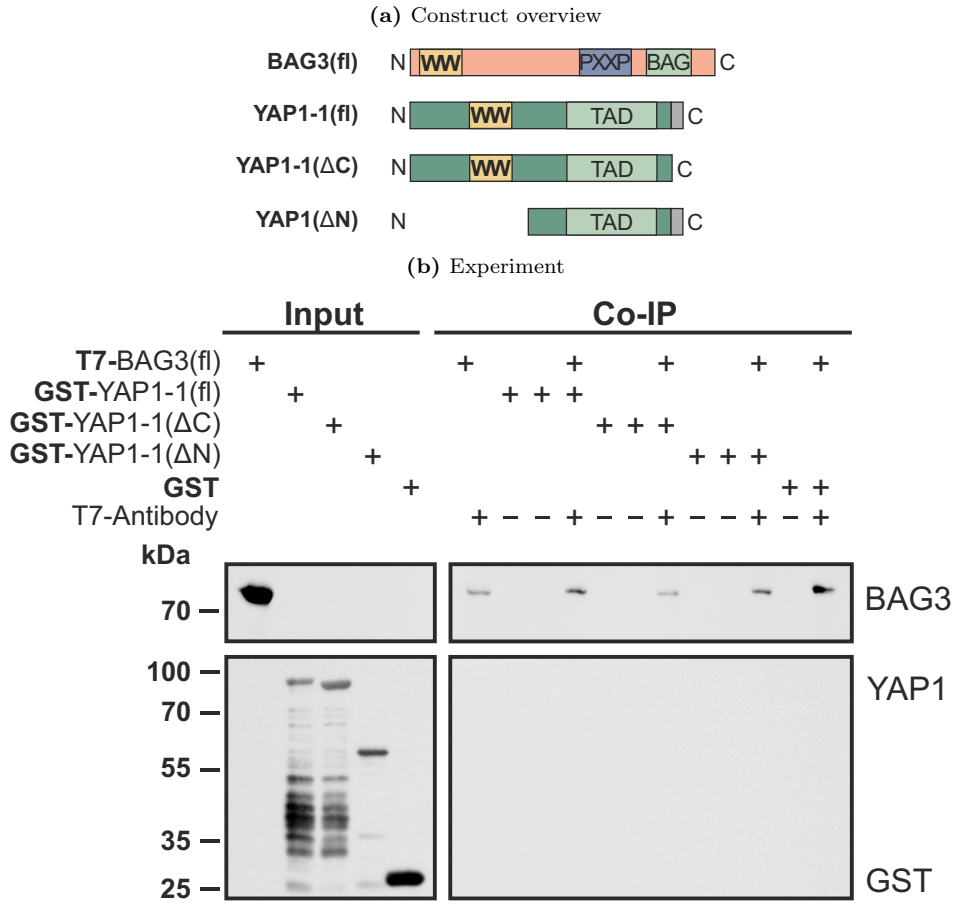


Fig. 3.8: YAP1 does not engage in PPIs with BAG3. (a) Overview of precipitated human T7-tagged full-length (fl) BAG3 bait construct (orange). Human GST-tagged YAP1 constructs were coprecipitated either without the PDZ-BM at the C-terminal end (ΔC), without the N-terminus harboring the WW domain (ΔN), or without any truncations as full-length (fl) protein chimeras (green). (b) Digitally rearranged western blot of protein fractions from the co-IP experiment. The sample composition in loading controls (Input) and experimental samples after precipitation (co-IP) is outlined on top. Immunotags fused to proteins for antibody detection are printed in bold. The band migration pattern of molecular weight markers is shown on the left. (Top panel) BAG3 bait protein fractions from the co-IP experiment probed with a monoclonal anti-T7 antibody. (Bottom panel) YAP1 protein fractions from the same experiment. Samples without BAG3 bait protein or precipitating antibody did not coprecipitate any of the YAP1 constructs, indicating the absence of BAG3 YAP1 complexes.

independent associations, one between SYNPO2 and BAG3, and another one between YAP1 and SYNPO2.

As a stepping stone to understanding the functional relation between SYNPO2 and YAP1, as well as its physiological relevance for muscle development at a cellular level, the potential effects of the PDZ-BM on YAP1 localization were investigated in muscle cells. It has been hypothesized that one way of regulating the nuclear translocation of YAP1/TAZ and its transcription activation might be regulated via interactions with the

PDZ-BM (Kanai *et al.*, 2000; Oha & Sudol, 2009). To elucidate its involvement in those regulatory processes, the localization of YAP1 in model systems for smooth and striated muscles was studied, in dependence of the presence of its PDZ-BM. Additionally, the effects of WW domains on YAP1 localization were also examined, as human isoforms of YAP1 either contain only the first WW domain (WW1) or both WW domains (see section 1.4.4). Therefore, human YAP1 constructs were genetically fused to an enhanced green fluorescent protein (eGFP)-tag and overexpressed in smooth and skeletal muscle cells (see section 2.4.2 and 2.4.3). Additional constructs with a deletion of the C-terminal 5 amino acids carrying the PDZ-BM (ΔC), with either one or both WW domains were generated (Fig. 3.9). A further YAP1 truncation construct had a deleted N-terminus (ΔN), missing both WW domains.

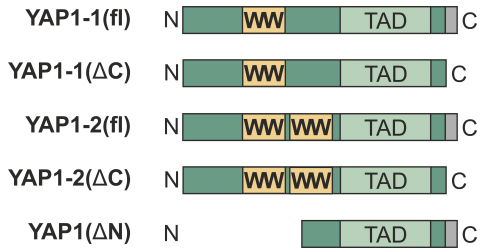


Fig. 3.9: Overview of YAP1 constructs for overexpression in muscle cells. Human eGFP-tagged YAP1 constructs expressed either without the PDZ-BM (gray) at the C-terminal end (ΔC) or without any truncations as full-length (fl) protein chimeras with the first WW domain (YAP1–1) or both WW domains (YAP1–2). An additional YAP1 truncation construct with a deletion of the N-terminus harboring the WW domain (ΔN) was generated. The fused eGFP-tags are not shown.

To specifically analyze the YAP1 localization in specific subcellular structures, such as the actin cytoskeleton and the nucleus, fluorophore-conjugated phalloidin, and DAPI were used (see section 2.4.10). For the experiment, rat aortic A7r5 cells were used which functioned as a model system for smooth muscle cells (see section 2.4.3). The transfected A7r5 cells exhibited different patterns of YAP1 localization: overexpressed YAP1(fl) constructs were localized both inside the nucleus and diffusely in the perinuclear region (Fig. 3.10; A). In the cell periphery, full-length YAP1 constructs were observed in association with the actin cytoskeleton. YAP1–1 and YAP1–2 showed a similar pattern in terms of actin cytoskeleton association (Fig. 3.10; A, D; C, F). Interestingly, YAP1(ΔC) was localized in the cytoplasm and associated with actin filaments only in the cell periphery. However, the nuclear translocation of YAP1(ΔC)

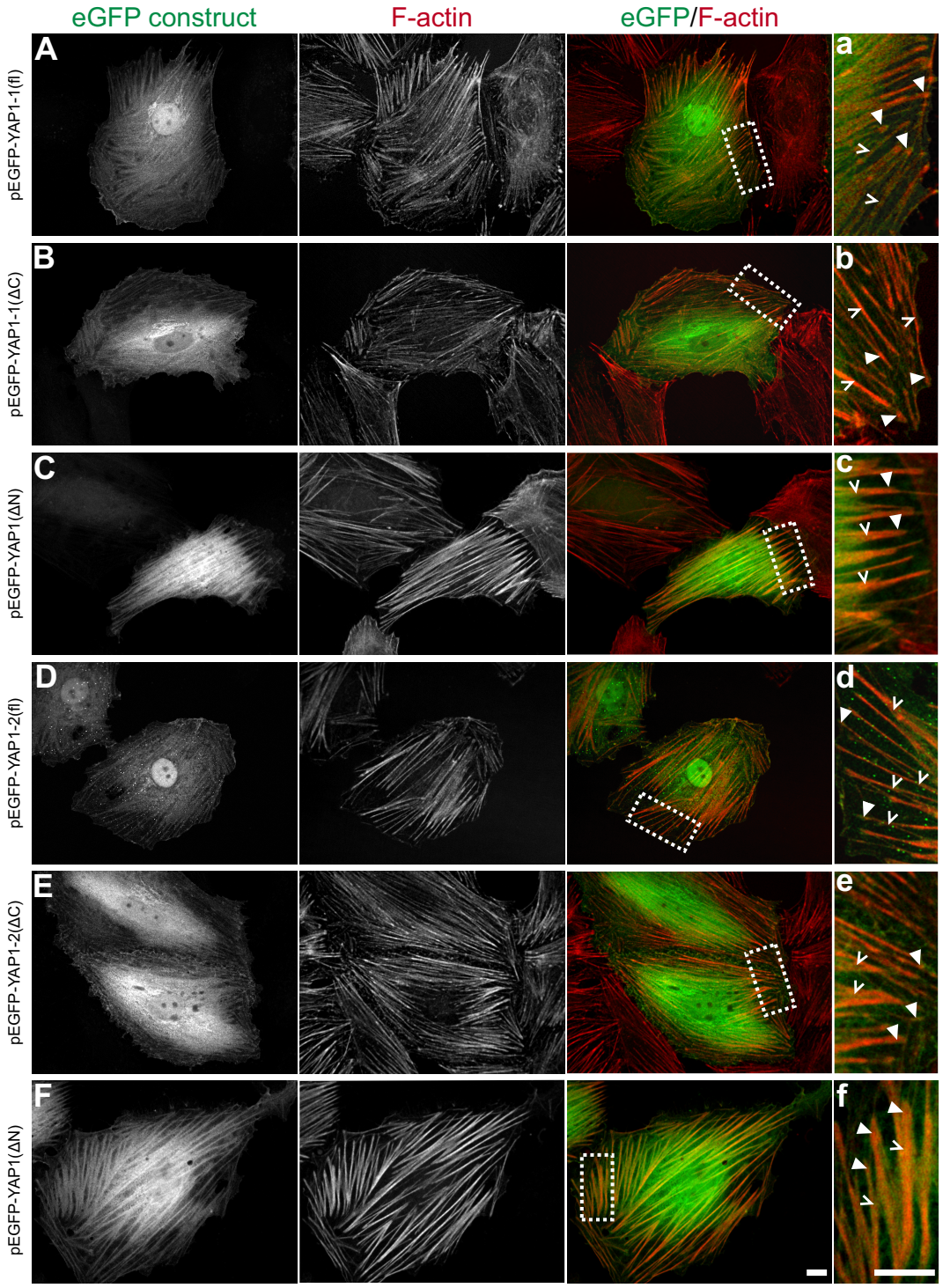


Fig. 3.10: YAP1 overexpression in smooth muscle cells. The row labels on the left side show YAP1 constructs that were transiently transfected and overexpressed. The column labels show the fluorescence channels for the eGFP-YAP1 chimeras (eGFP constructs), actin filaments (F-actin), and an overlay of both signals (eGFP/F-actin). The magnified regions in the far-right panel column are outlined by dashed lines in the overlay images. (A, D) Overexpressed YAP1(fl) with distinct nuclear and diffuse cytoplasmic localization. In the cell periphery, YAP1 appears to be targeted to the actin cytoskeleton (a,d; open arrows). (B, E) YAP1(ΔC) is diffusely localized at the actin filaments in the cell periphery with decreased nuclear import (b,d; open arrows). (C, F) N-terminally truncated YAP1(ΔN) localizes to the actin cytoskeleton rather than the nucleus (c,e; open arrows). In some cases, YAP1 localizes at the end of actin filaments, primarily at FAs (a-e; closed arrows). Scale bar: 5 µm

Fig. 3.11: YAP1 overexpression in skeletal muscle cells. The row labels on the left side show YAP1 constructs that were transiently transfected and overexpressed. The column labels show the fluorescence channels for the eGFP-YAP1 chimeras (eGFP constructs), Z-disc epitope of titin, referred to as titin (Z-disc), and an overlay of both signals (eGFP/titin (Z-disc)). (A, D) Overexpressed YAP1(fl) and with diffuse cytoplasmic localization. (B, E) YAP1(ΔC) is also diffusely localized in the cytoplasm, whereas N-terminally truncated YAP1(ΔN) shows weak localization to the Z-discs (C, F). In some cases, YAP1(ΔN) associated with a filamentous pattern. Scale bar: 10 µm.

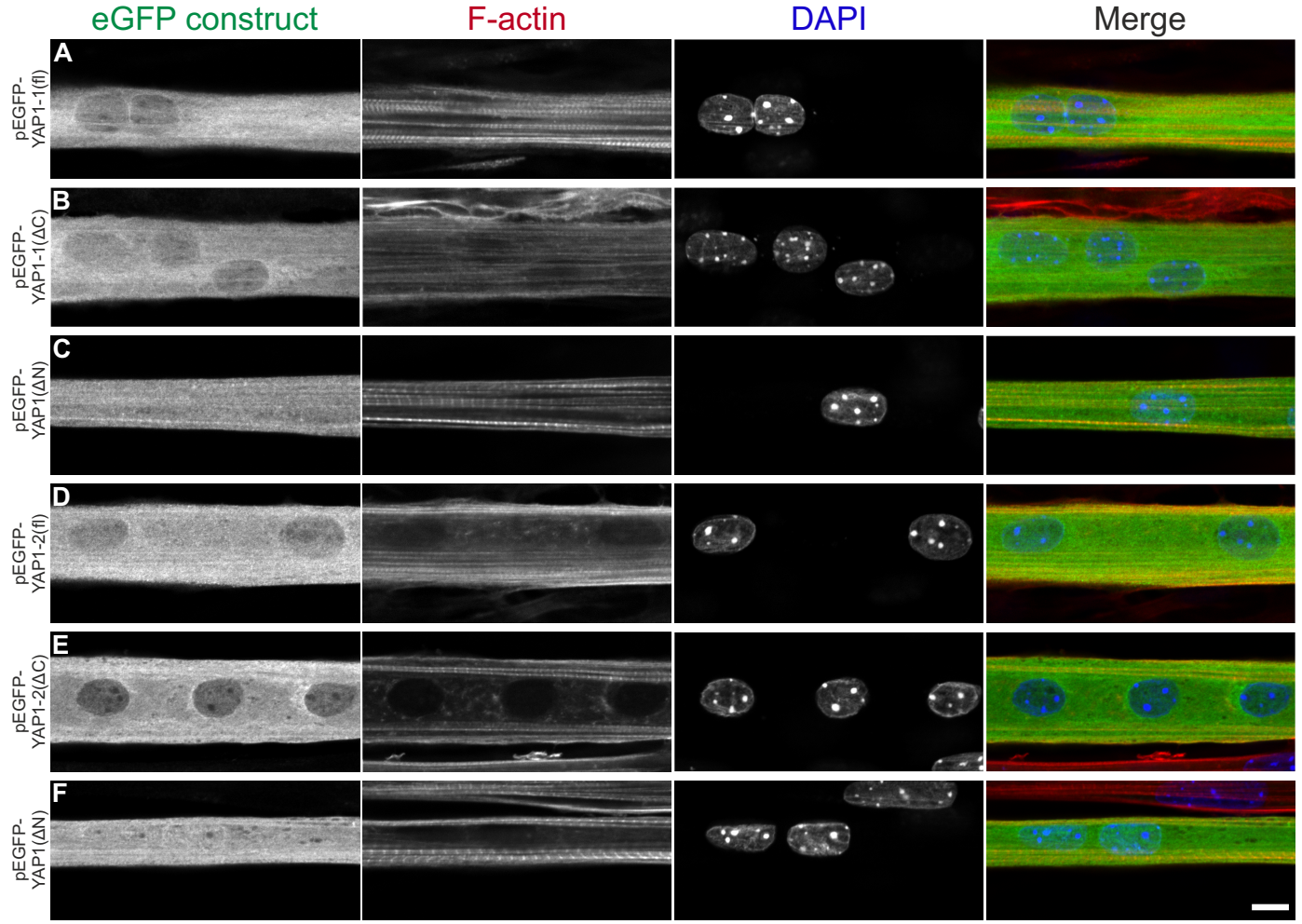


Fig. 3.12: YAP1 overexpression in C2C12 cells with regard to nuclear targeting. The row labels on the left side show YAP1 constructs that were transiently transfected and overexpressed. The column labels show the fluorescence channels for the eGFP-YAP1 chimeras (eGFP constructs), actin filaments (F-actin), nuclei (DAPI) and an overlay of these signals (Merge). (A, B; D, E) In myotubes, overexpressed YAP1 localize with distinct nuclear and diffuse cytoplasmic localization. In the cell periphery. (C, F) N-terminally truncated YAP1(ΔN) targets to the actin filaments, with increased nuclear localization. Compared to smooth muscle cells, overall less YAP1 targeted to the nucleus. Scale bar: 10 µm.

appeared to be reduced compared to full-length YAP1 (Fig. 3.10; B, D), suggesting that the absence of the PDZ-BM affects nuclear import. Furthermore, some YAP1 constructs appeared to associate more with the ends of actin filaments, particularly at FAs (Fig. 3.10; a, d; c, f). In contrast, N-terminally truncated YAP1(ΔN) primarily localized to the actin filament bundles. Here, a distinct localization to the nucleus was not observed (Fig. 3.10; C, F). Subsequently, an identical experiment was performed in C2C12 myotubes differentiated for seven days, utilized as a model system for the skeletal muscle (see section 2.4.2. The localization of YAP1 was studied with two main objectives: The localization of YAP1 in skeletal muscle cell structures such as the Z-disc (Fig. 3.11), and/or sarcomeric actin should be evaluated first. In addition, the localization in the cytoplasm and nuclear targeting should also be assessed and compared (Fig. 3.12). To analyze the YAP1 localization in myotubes, structures such as nuclei, and actin filaments were stained using fluorescence labeling probes, as described previously (see section 2.4.10). Additionally, myotubes were stained against a Z-disc epitope of titin to assess the degree of differentiation. In contrast to the staining obtained in smooth muscle cells, in myotubes, YAP1 constructs were mostly diffusely localized throughout the myotube cytoplasm (Fig. 3.11; A–F). Cells overexpressing YAP1(ΔC) showed augmented targeting with titin at the Z-discs (Fig. 3.11; B, E). Notably, YAP1–1 and YAP1–2 did not show distinct cellular localizations (Fig. 3.11; A, D; C, F). In contrast, the YAP1(ΔN) pattern of localization appeared filamentous in a number of myotubes (Fig. 3.11; C, F). An additional staining revealed an association with actin filament bundles (Fig. 3.12; C, F). Compared to smooth muscle cells, myotubes showed less translocation of YAP1 into their nuclei, with notable differences observed between YAP1(fl), YAP1(ΔC) and YAP1(ΔN), of which the latter exhibited the highest degree of nuclear translocation (Fig. 3.12; A-C; D-F).

To determine whether the degree of YAP1 nuclear translocation depended on the PDZ-BM, the mean fluorescence signal intensities in both the nucleus and cytoplasm were measured for both smooth and skeletal muscle cells, respectively. Ratios of nuclear and cytoplasmic YAP1 were calculated to measure the nuclear import of YAP1. As YAP1 activity relies on nuclear localization via phosphorylation, changes in nuclear import function as a direct read-out for YAP1 transcriptional activity (see section 2.5.1). While YAP1 mean ratios between 2.0 and 2.5 in A7r5 cells indicated nuclear import of

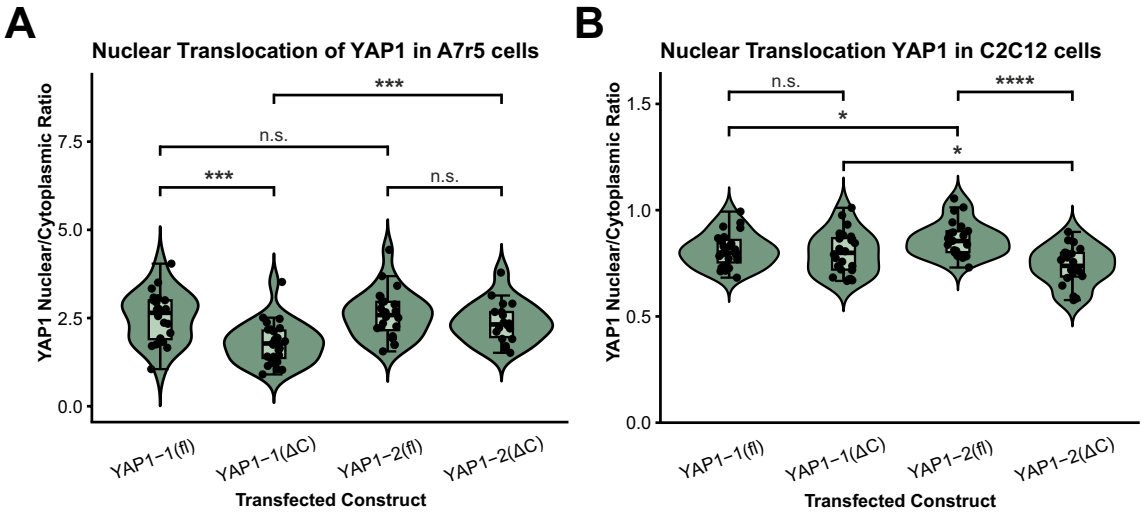


Fig. 3.13: Nuclear translocation of overexpressed YAP1 in smooth and skeletal muscles. Box and violin plots of average YAP1 intensities. Intensity ratios of nuclear and cytoplasmic YAP1 functioned as a direct readout of YAP1 nuclear import and YAP1 activity. Higher ratios of nuclear and cytoplasmic YAP1 indicate more YAP1 in the nucleus and higher YAP1 transcriptional activity. (A) Transfected human GFP-YAP1 constructs in A7r5 cells. (B) Transfected human GFP-YAP1 constructs in C2C12 cells. In both cell lines, YAP1 constructs without the PDZ-BM show decreased nuclear translocation than YAP1(fl) constructs. Statistical testing was performed via a two-sample t-test after distributions were tested for normality with a Shapiro-Wilk, Anderson-Darling and Kolmogorov-Smirnov test. n.s. $p > 0.05$; * $p \leq 0.05$; ** $p \leq 0.01$; *** $p \leq 0.001$; **** $p \leq 0.0001$.

YAP1, ratios in C2C12 cells showed cytoplasmic retention with mean ratios between 0.7 and 0.9 (Fig. 3.13). Truncated YAP1 constructs lacking the PDZ-BM showed decreased nuclear import in both, smooth and skeletal muscle cells. Notably, a significant decrease of YAP1–1(ΔC) activity was observed only in smooth muscle, while only the decrease of YAP1–2(ΔC) was significant in skeletal muscle cells. These findings highlight that the PDZ-BM promotes the nuclear import of YAP1 in both, smooth and skeletal muscle cells.

3.2 The relationship between SYNPO2, BAG3, and YAP1/TAZ

3.2.1 SYNPO2 harbors a novel binding motif for both YAP1 and TAZ independent of the PDZ domain

Even in absence of the PDZ-BM, YAP1 was shown to interact with SYNPO2 in the protein pulldown assay (see section 3.1.2). It was assumed that other existing motifs or additional structural features in YAP1 might mediate this interaction. Conspicuously, YAP1 shares its WW domains as a common structural feature with BAG3 (see section 1.4.3 and 1.4.4). As described above, WW domains can be divided into different groups according to the linear peptide motif that they specifically recognize (see section 1.5). To date, YAP1 and BAG3 are classified as group I WW domains, which specifically recognize SLIMs consisting of the four consecutive amino acids P-P-X-Y (Sudol *et al.*, 1995; Chen & Sudol, 1995; Macias *et al.*, 1996; Espanel & Sudol, 1999).

Based on these findings, it was hypothesized whether the WW domains of YAP1 could interact with the PPPY motif of SYNPO2 in a similar manner that BAG3 does. A protein alignment was made to investigate similar binding properties of the WW domains based on their primary structure. The human WW domains of BAG3, YAP1 (and its paralog TAZ) were compared to the group I WW domain-containing proteins E3 ubiquitin-protein ligase NEDD4, kidney and brain protein KIBRA, and E3 ubiquitin-protein ligase Itchy homolog ITCH (Fig. 3.14). Like YAP1/TAZ, these proteins are involved in the Hippo signaling pathway, engaging in interactions with PPXY motifs as well (Bae *et al.*, 2015; Genevet *et al.*, 2010; Ho *et al.*, 2011; Salah *et al.*, 2011). The alignment of the WW domains of BAG3, TAZ, and YAP1 revealed two interesting features: Firstly, WW1 of YAP1 shares 48.5 and 73.5% amino acid identity with the WW domains of BAG3 and TAZ, respectively. Secondly, the WW2 domain of YAP1 shows more similarity to WW domains of NEDD4, ITCH, or KIBRA. Based on these similarities between BAG3 and YAP1, it was hypothesized that the WW1 domain of YAP1 might also interact with the PPPY motif of SYNPO2. To analyze this putative interaction, a co-IP experiment involving SYNPO2 and YAP1

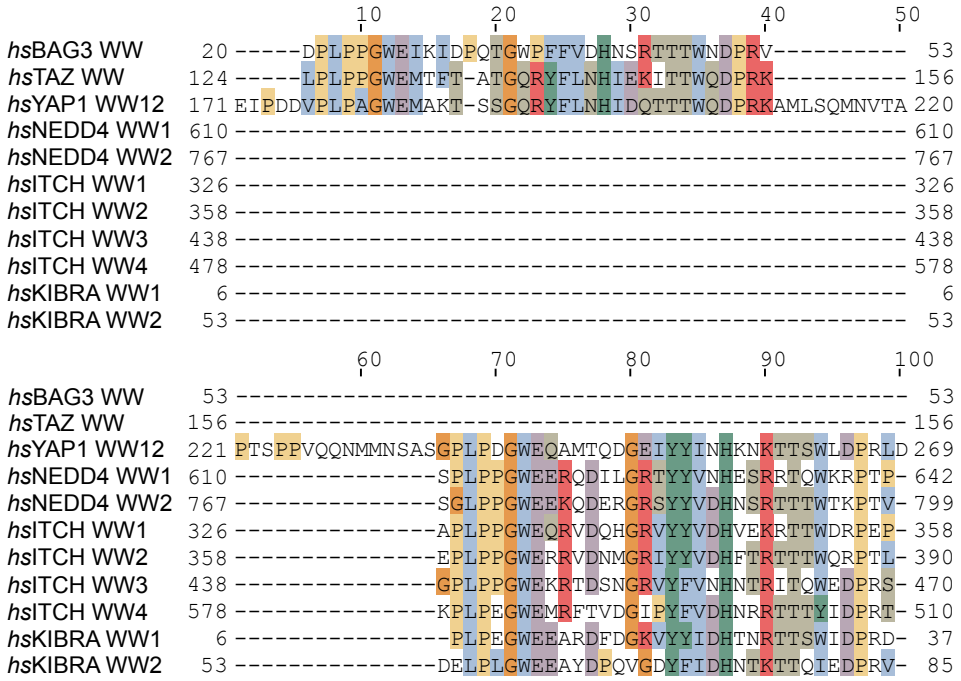


Fig. 3.14: Protein alignment of human group I WW domains. Group I WW domains of selected human proteins involved in the Hippo pathway aligned to YAP1 WW domains. Protein names are displayed on the left. The amino acid positions of each sequence are displayed on both sides. Colors are adapted from Clustal. While TAZ and BAG3 WW domains have high similarity with the first WW domain of YAP1 (upper panel), the WW domains of other Hippo pathway proteins like NEDD4, KIBRA, and ITCH have a high similarity with the second WW domain of YAP1 (lower panel). The WW domains were aligned according to the highest percentage identity scoring via pairwise alignment using the local alignment tool Matcher(EMBOSS) algorithm visualized in Jalview.

constructs containing the WW1 domain was conducted. Additional YAP1 constructs utilized in this experiment lacked either the WW domain, or the PDZ-BM (3.15; a). The subsequent western blot showed the expected bands for precipitated SYNPO2 at approx 120kDa (Fig. 3.15 b). Samples probed with YAP1 constructs revealed proteins migrating at approx. 90, 80, and 60 kDa, corresponding to YAP1–1(fl), YAP1–1(ΔC), and YAP1(ΔN), respectively. Controls lacking SYNPO2 exhibited bands of low intensity due to some unspecific binding. Most importantly, all YAP1 constructs tested coprecipitated with SYNPO2, revealing the existence of an additional binding motif independent of the PDZ-BM. Upon comparing the band intensities, it was assumed that more of the YAP1 constructs containing the PDZ-BM co precipitated than YAP1 lacking the PDZ-BM. Another pairwise alignment revealed that the WW domains of TAZ and BAG3 share 51.5% of amino acid identity. Therefore, it was assumed that the WW domain of TAZ is specific for the SYNPO2 PPPY motif as well. To verify this,

TAZ constructs corresponding to YAP1 constructs were utilized in a subsequent co-IP experiment (Fig. 3.16; a). The analyzed immunoblots revealed bands corresponding to SYNPO2 at around 120 kDa (Fig. 3.16 b). Samples probed with TAZ constructs

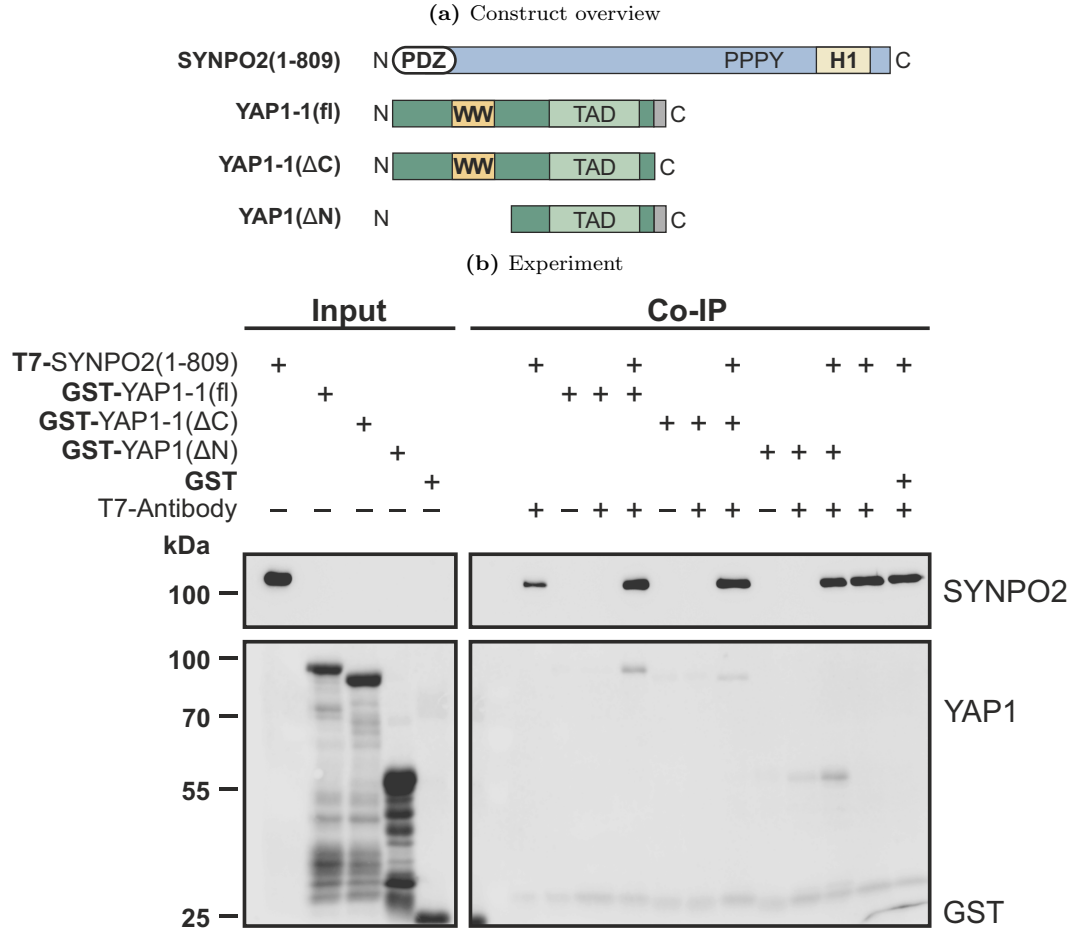


Fig. 3.15: SYNPO2 coprecipitates with YAP1 constructs lacking the PDZ-BM. (a) Overview of precipitated human T7-tagged SYNPO2 bait construct (blue), amino acids 1–809, harboring the PDZ domain and the PPPY motif. GST-tagged human YAP1 constructs were coprecipitated either without the PDZ-BM at the C-terminal end (ΔC), without the N-terminus including the WW1 domain (ΔN), or without any truncations as full-length (fl) protein chimeras (green). (b) Digitally rearranged western blot of sample fractions from the co-IP experiment. The sample composition in loading controls (Input) and experimental samples after precipitation (co-IP) is outlined on top. Immunotags fused to proteins for antibody detection are printed in bold. The band migration pattern of molecular weight markers is shown on the left. (Top panel) SYNPO2 bait protein fractions from the co-IP experiment. (Bottom panel) YAP1 protein fractions from the same experiment. Samples without SYNPO2 bait protein or anti-T7 antibody did not coprecipitate YAP1 constructs. Samples containing both precipitating antibody and SYNPO2 show coprecipitation of all YAP1 constructs, indicating interactions via two independent binding sites.

showed proteins migrating approx. 80, 70, and 55 kDa, corresponding to TAZ(fl), TAZ(ΔC), and TAZ(ΔN), respectively. Controls lacking either the T7 antibody or

SYNPO2 did not exhibit any bands potentially resulting from unspecific binding of theTAZ constructs. More strikingly, in this assay, the TAZ construct was also found to coprecipitate with SYNPO2, confirming the existence of an additional binding motif in TAZ that is independent of the PDZ-BM. Based on the band intensities, it was observed that more of the TAZ(fl) construct coprecipitated than its truncated variants. In conclusion, these results imply that these novel interactions of YAP1 and TAZ might be WW domain-mediated, similar to the interaction between BAG3 and SYNPO2.

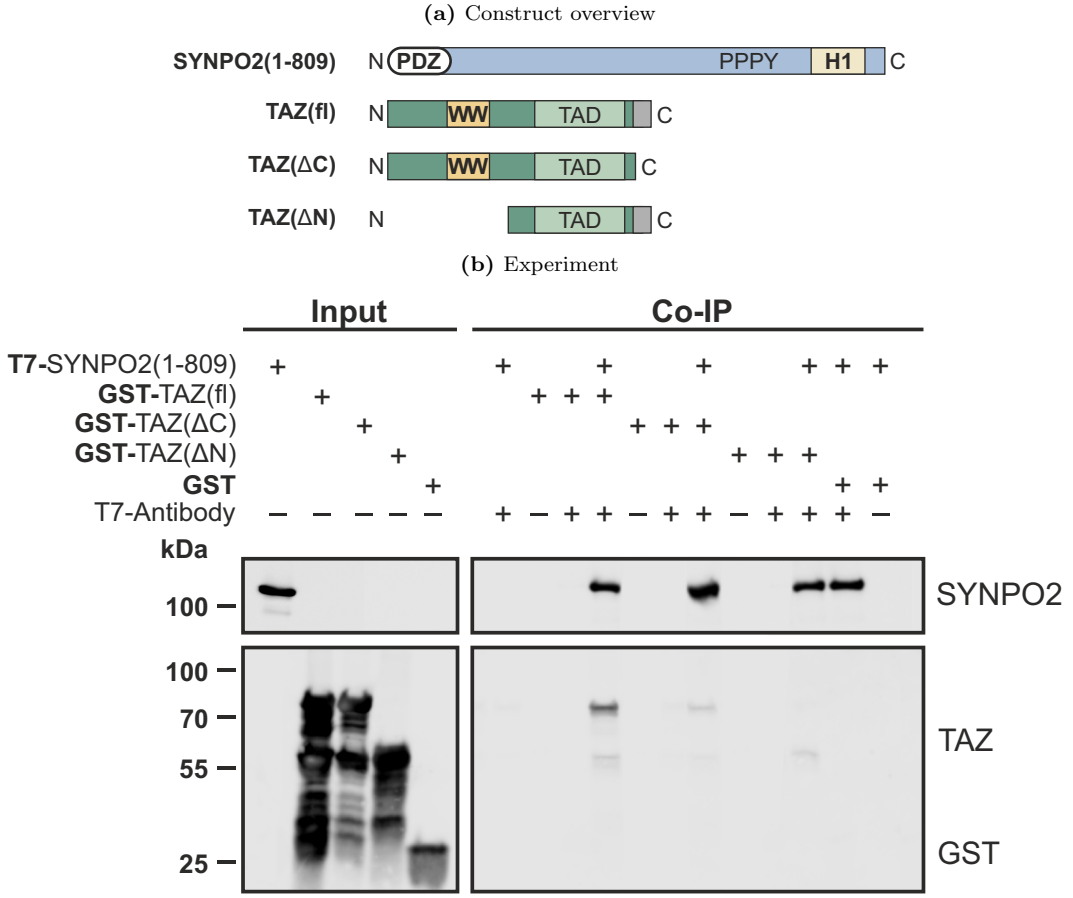


Fig. 3.16: SYNPO2 coprecipitates with TAZ constructs lacking the PDZ-BM. (a) Overview of precipitated human T7-tagged SYNPO2 bait construct (blue), amino acids 1–809, harboring the PDZ domain and the PPPY motif. GST-tagged human TAZ constructs (green) were coprecipitated either as full-length (fl) protein chimeras, lacking the PDZ-BM at the C-terminal end (ΔC), without the N-terminus including the WW domain (ΔN). (b) Digitally rearranged western blot of sample fractions from the co-IP experiment. The sample composition in loading controls (Input) and experimental samples after precipitation (co-IP) is outlined on top. Immunotags fused to proteins for antibody detection are printed in bold. The band migration pattern of molecular weight markers is shown on the left. (Top panel) SYNPO2 bait protein fractions from the co-IP experiment. (Bottom panel) TAZ protein fractions from the same experiment. Samples without SYNPO2 bait protein or anti-T7 antibody did not precipitate TAZ constructs, whereas samples containing both precipitating antibody and SYNPO2 show coprecipitation of all TAZ constructs tested, indicating interactions via two independent binding sites.

3.2.2 BAG3 competes with both YAP1 and TAZ for the PPPY motif in SYNPO2 *in vitro*

To support the assumption that the SYNPO2-YAP1 or SYNPO2-TAZ complex formation is mediated by WW domains, it was further investigated whether BAG3 and YAP1, or BAG3 and TAZ might compete for the PPPY motif. For this purpose, co-IP experiments were performed in the form of a competitive binding assay as described above (see section 2.3.7). In these assays, SYNPO2 was incubated with constant

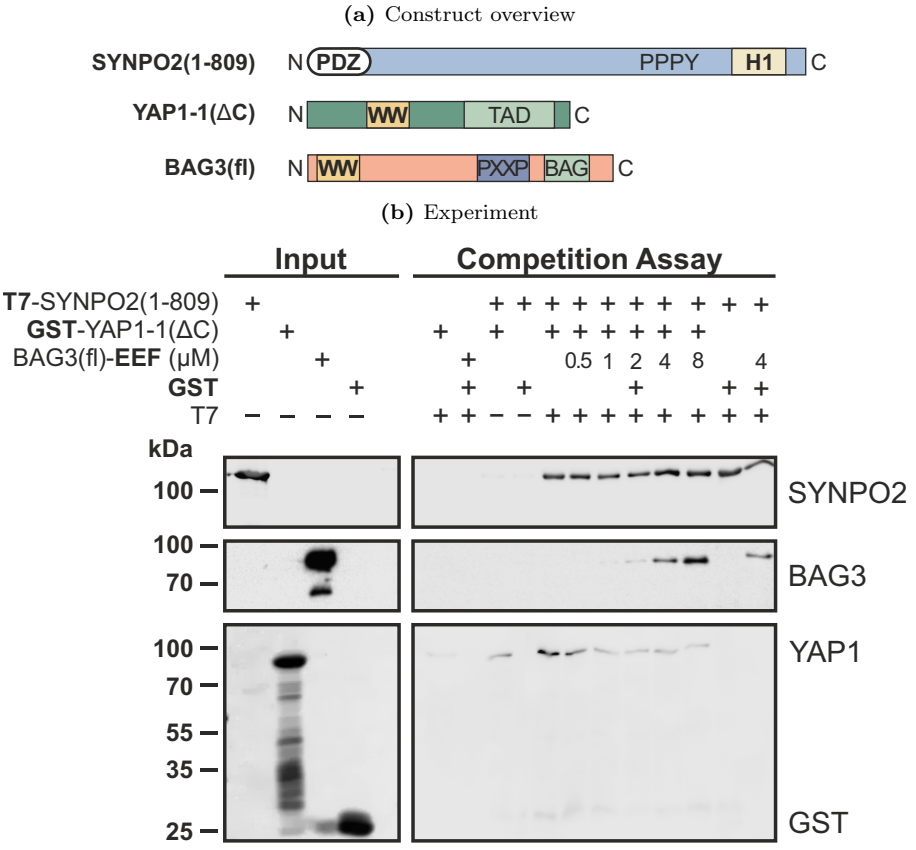


Fig. 3.17: Competitive binding assays of BAG3 and YAP1–1. (a) Overview of precipitated human T7-tagged SYNPO2, bait construct (blue), amino acids 1–809, harboring the PDZ domain and the PPPY motif. GST-tagged human YAP1–1 protein chimeras (green) lacking the PDZ-BM (ΔC) and EEF-tagged human full-length BAG3(fl) (orange) were coprecipitated. (b) Digitally rearranged western blot of sample fractions from the co-IP experiment. The sample composition in loading controls (Input) and experimental samples after precipitation (Competition assay) is outlined on top. Immunotags fused to proteins for antibody detection are printed in bold. The band migration pattern of molecular weight markers is shown on the left. (Top panel) SYNPO2 bait protein fractions from the co-IP experiment. (Middle panel) BAG3 protein sample fractions from the same experiment titrated in increasing concentrations. (Bottom panel) YAP1–1 protein sample fractions from the same experiment. Increased concentrations of BAG3 titrated in the samples hindered WW domain-mediated YAP1–1 binding to SYNPO2, resulting in increased BAG3 band intensities and decreasing YAP1 band intensities.

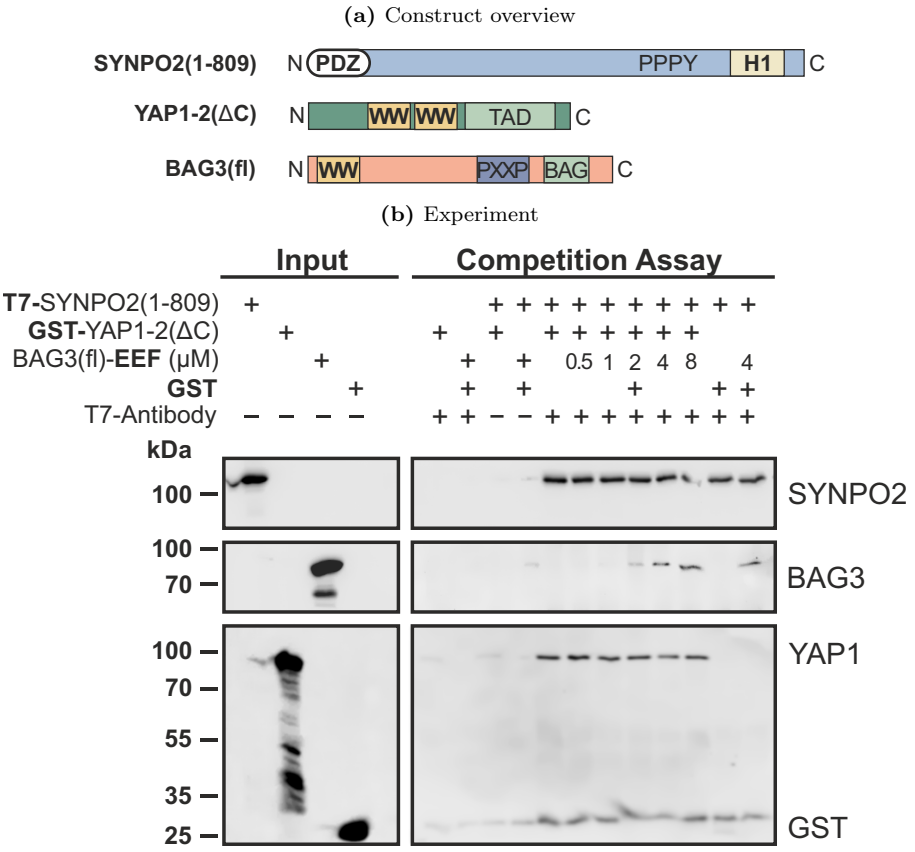


Fig. 3.18: Competitive binding assays of BAG3 and YAP1–2. (a) Overview of precipitated human T7-tagged SYNPO2, bait construct (blue), amino acids 1–809, harboring the PDZ domain and the PPPY motif. GST-tagged YAP1–2 protein chimeras (green) lacking the PDZ-BM (ΔC) and EEF-tagged human full-length BAG3(fl) (orange) were coprecipitated. (b) Digitally rearranged western blot of sample fractions from the co-IP experiment. The sample composition in loading controls (Input) and experimental samples after precipitation (Competition assay) is outlined on top. Immunotags fused to proteins for antibody detection are printed in bold. The band migration pattern of molecular weight markers is shown on the left. (Top panel) SYNPO2 bait protein fractions from the co-IP experiment. (Middle panel) BAG3 protein sample fractions from the same experiment titrated in increasing concentrations. (Bottom panel) YAP1 protein sample fractions from the same experiment. Despite the increased concentrations of BAG3 titrated, WW domain-mediated YAP1–2 binding to SYNPO2 was not obstructed, resulting in consistent YAP1–2 band intensities.

concentrations of YAP1 or TAZ, while BAG3 was titrated in increasing concentrations. To prevent interactions via the PDZ domain, the utilized YAP1 and TAZ constructs did not contain the PDZ-BMs in this experiment. In addition, YAP1 constructs with one (YAP1–1) and two WW domains (YAP1–2) were tested to investigate whether a tandem of WW domains would promote any changes in binding properties (Fig. 3.17 and 3.18; a). The immunoblot analyses from these co-IP experiments demonstrated that with increasing concentrations, BAG3 impeded the interaction between YAP1–1 and SYNPO2 (Fig. 3.17; b).

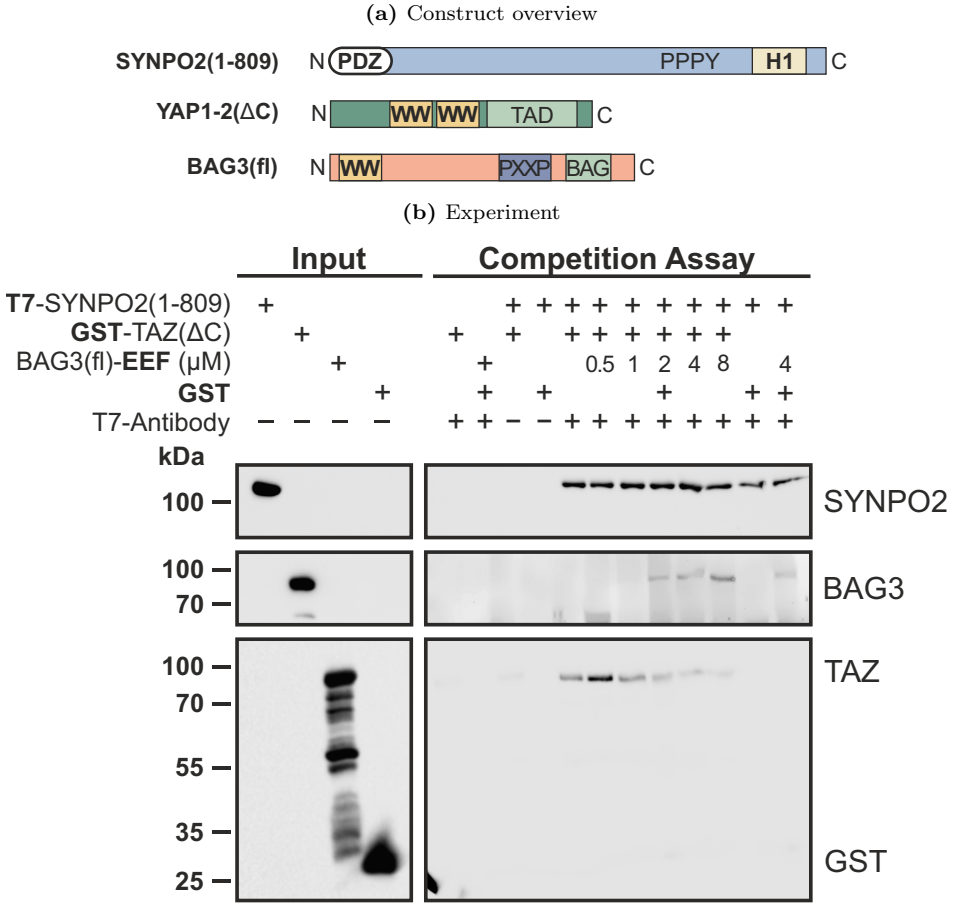


Fig. 3.19: Competitive binding assays of BAG3 and TAZ. (a) Overview of precipitated human T7-tagged SYNPO2 bait construct (blue), amino acids 1–809, harboring the PDZ domain and the PPPY motif. GST-tagged human TAZ protein chimera (green) lacking the PDZ-BM (ΔC) and EEF-tagged human full-length BAG3(fl) (orange) were coprecipitated. (b) Digitally rearranged western blot of sample fractions from the co-IP experiment. The sample composition in loading controls (Input) and experimental samples after precipitation (co-IP) is outlined on top. Immunotags fused to proteins for antibody detection are printed in bold. The band migration pattern of molecular weight markers is shown on the left. (Top panel) SYNPO2 bait protein fractions from the co-IP experiment. (Middle panel) BAG3 protein sample fractions from the same experiment titrated in increasing concentrations. (Bottom panel) TAZ protein fractions from the same experiment. Increased concentrations of BAG3 titrated in the samples hindered WW domain-mediated TAZ binding to SYNPO2, resulting in increased BAG3 band intensities and decreasing TAZ band intensities.

Similarly, a titration of BAG3 resulted in reduced binding of TAZ to SYNPO2 as evidenced by the competitive binding co-IP assays, where less TAZ co precipitated with SYNPO2 in the presence of increasing BAG3 concentrations (Fig. 3.19; b). In contrast, the interaction between YAP1–2 and SYNPO2 was not impaired by BAG3 (Fig. 3.18; b). These results might imply that either the presence of a second WW domain is sufficient to preclude a displacement of YAP1 or that the WW2 of YAP1 exhibits appreciably higher binding to the PPPY motif of SYNPO2 than BAG3.

Moreover, as human cells express different YAP1 isoforms containing either one or two WW domains, as well as TAZ containing a single WW domain, these findings might have more profound consequences, potentially affecting regulatory mechanisms involving BAG3 and the PPPY motif.

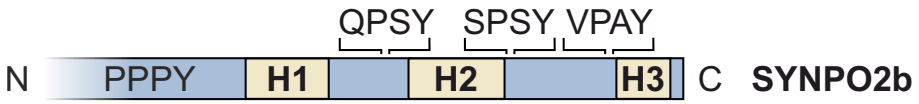


Fig. 3.20: Overview of C-terminal pseudo-PPXY motifs in human SYNPO2. Human SYNPO2 harbors three motifs similar to the N-terminally located PPPY motif. These three so-called pseudo-PPXY motifs might be as well specifically recognized by group I WW domain-containing proteins YAP1 or TAZ.

A phage display experiment revealed that motifs in addition to the canonical PPXY motif might also be recognized by YAP1-WW2 (Iglesias-Bexiga *et al.*, 2015). Since the primary structure of SYNPO2 is particularly rich in prolines, additional, more ambiguous proline-containing motifs might be present that could bind to YAP1 or TAZ WW domains (see section 1.4.3). An *in silico* analysis of the SYNPO2 amino acid sequence was conducted to assess the presence of such non-canonical WW domain binding motifs. Indeed, this analysis revealed three pseudo-PPXY motifs potentially specific for WW domains of either YAP1 or TAZ (Fig. 3.20). All of these motifs are located in the C-terminal part of SYNPO2, downstream of the PPPY motif. Similar to the PPPY motif itself, these pseudo-PPXY motifs occur in all human SYNPO2 isoforms and are conserved between man and mouse. A putative interaction with any of the pseudo-PPXY motifs of SYNPO2 with YAP1 and TAZ was therefore investigated by performing co-IP experiments. For these experiments, the C-terminal portion of SYNPO2b downstream of the PPPY motif, termed SYNPO2(664–1093) was used together with YAP1 and TAZ (Fig. 3.21; a and 3.22; a). The evaluation of the co-IP immunoblots did not reveal any coprecipitation of the tested YAP1 constructs with SYNPO2(664–1093) (Fig. 3.21; b). Consistent with these findings, another set of co-IPs carried out with TAZ constructs did not reveal any coprecipitation with SYNPO2(664–1093) (Fig. 22; b). Hence, it can be concluded that the PPPY motif is pivotal for a WW domain-mediated YAP1/TAZ interaction with SYNPO2 and that its C-terminal, proline-rich portion does not contain non-canonical YAP1/TAZ WW domain-binding motifs.

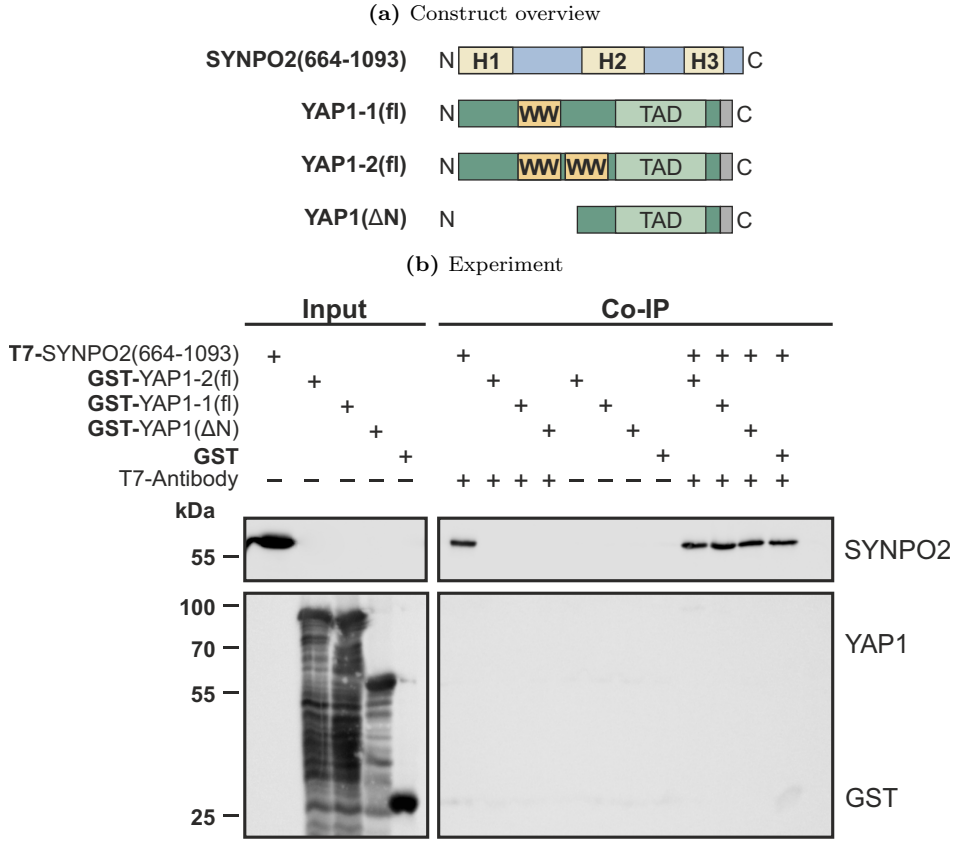


Fig. 3.21: Co-IPs of SYNPO2(664–1093) and YAP1. (a) Overview of T7-tagged SYNPO2 bait constructs (blue) harboring pseudo-PPXY motifs. GST-tagged YAP1 full-length (fl) protein chimeras (green) comprising either one (YAP1–1), both (YAP1–2), or no (ΔN) WW domains were coprecipitated. (b) Digitally rearranged western blot of sample fractions from the co-IP experiment. The sample composition in loading controls (Input) and experimental samples after precipitation (co-IP) is outlined on top. Immunotags fused to proteins for antibody detection are printed in bold. The band migration pattern of molecular weight markers is shown on the left. (Top panel) SYNPO2 bait protein fractions from the co-IP experiment. (Bottom panel) YAP1 protein fractions from the same experiment. Samples containing both precipitating antibody and SYNPO2 did not coprecipitate any of the YAP1 constructs, indicating the WW domains of YAP1 specifically recognizes the PPPY motif in SYNPO2.

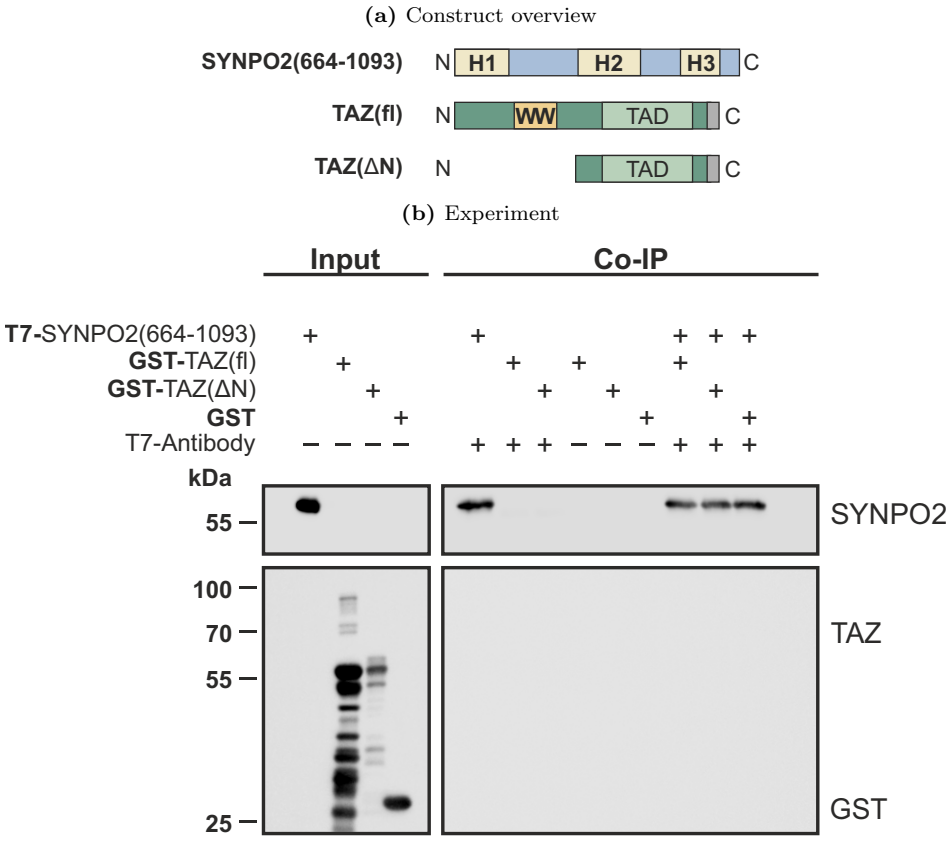


Fig. 3.22: Co-IPs of SYNPO2(664–1093) and TAZ. (a) Overview of T7-tagged SYNPO2 bait constructs (blue) harboring pseudo-PPXY motifs. GST-tagged YAP1 full-length (fl) protein chimeras (green) entailing either one or no (ΔN) WW domain were coprecipitated. (b) Digitally rearranged western blot of sample fractions from the co-IP experiment. The sample composition in loading controls (Input) and experimental samples after precipitation (co-IP) is outlined on top. Immunotags fused to proteins for antibody detection are printed in bold. The band migration pattern of molecular weight markers is shown on the left. (Top panel) SYNPO2 bait protein fractions from the co-IP experiment. (Bottom panel) TAZ protein fractions from the same experiment. Samples containing both precipitating antibody and SYNPO2 did not coprecipitate any of the TAZ constructs, indicating the WW domain of TAZ specifically recognized the PPPY motif in SYNPO2.

3.3 YAP1 and SYNPO2 have distinct interaction patterns in smooth and skeletal muscle cells

In the recent past, the role of SYNPO2 as an adapter protein involved in CASA in muscle cells has repeatedly been subject of research (Linnemann *et al.*, 2010; Linnemann *et al.*, 2013; Lohanadan *et al.*, 2021). One aim of the study presented here was to further examine the physiological relevance of the newly discovered interactions between SYNPO2 and YAP1 in muscle cells. Experiments in this thesis have already demonstrated that the YAP1 localization in the cytoplasm is associated with actin microfilament bundles (see section 3.1.5).

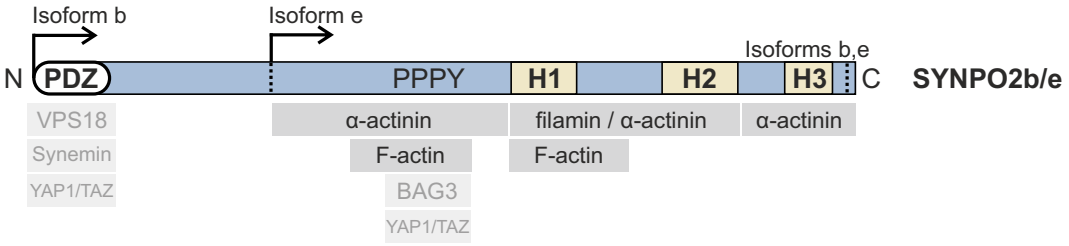


Fig. 3.23: Schematic overview of SYNPO2 isoforms predominantly expressed in striated muscle tissue. Arrows and dashed lines indicate the translational start and alternative splicing of the isoforms. (H1, H2, H3) Regions with synaptopodin family homology. (PPPY) WW domain-binding motif. The F-actin and α-actinin-binding regions of SYNPO2 are outlined in dark gray. Other previously identified interaction partners of interest are outlined in fade-gray.

As SYNPO2 entails C-terminally located filamin-, F-actin- and α-actinin-binding regions, it is suggested that SYNPO2 might link YAP1 to the actin cytoskeleton, particularly to dense bodies in smooth muscles or to the Z-discs of striated muscles (Fig. 3.23) (Linnemann *et al.*, 2010; Linnemann *et al.*, 2013). As a result, SYNPO2 might promote the cytoplasmic retention of YAP1.

To elucidate such a proposed role, the interaction between SYNPO2 and YAP1 should be visualized at the subcellular level by applying a bimolecular fluorescence complementation (BiFC) assay was performed in both smooth and skeletal muscle cells. More specifically, to investigate the effects of C-terminal F-actin and α-actinin binding regions of SYNPO2, proposed to facilitate YAP1 anchoring to the actin cytoskeleton, truncation variants lacking those motifs were generated (Fig. 3.24). As the role of tandem WW domains binding to the PPPY motif in SYNPO2 became more evident during this work, both YAP1–1 and YAP1–2 constructs were tested in these assays.

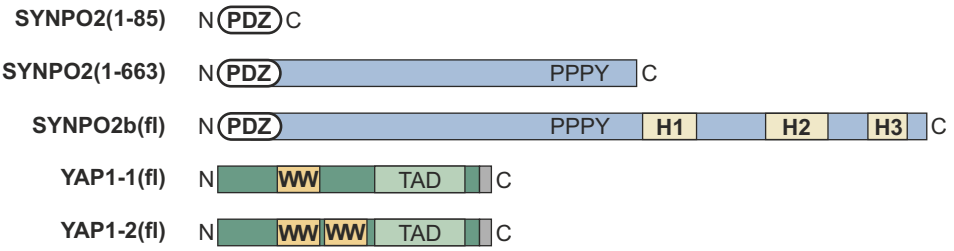


Fig. 3.24: Overview of transiently transfected BiFC constructs. SYNPO2 constructs with differentially truncated C-termini (blue) co-expressed with YAP1protein chimeras (green) comprising the first WW domain (YAP1–1) or both WW domains (YAP1–2). SYNPO2 and YAP1 constructs were fused to different parts of a complementary Venus-tag (see section 2.4.7). Amino acids of truncations are indicated in brackets, otherwise, full-length (fl) proteins were used.

3.3.1 SYNPO2-YAP1 complexes are recruited to dense bodies in smooth muscle cells

Smooth muscle cells overexpressing both SYNPO2(fl) and YAP1 exhibited interactions of these two proteins along actin microfilament bundles (Fig. 3.25; C and 3.26; C). Based on their appearance, size and, shape, these actin filament bundles were termed as stress fibers (Ridley & Hall, 1992; Brown *et al.*, 2006). The overexpression of SYNPO2(fl) with either YAP1–1 or YAP1–2 resulted in a similar BiFC localization pattern, *i. e.* the interaction occurred regardless of the presence of one or two WW domains. Staining against α-actinin revealed that SYNPO2(fl)-YAP1-complexes were associated with α-actinin-rich structures, specifically stress fiber dense bodies (Fig. 3.25 and 3.26; c, arrows). Depending on the extent of the removed α-actinin, and F-actin-binding regions, cells co-expressing either SYNPO2(1–663) or SYNPO2(1–85) together with YAP1 exhibited a predominantly diffuse localization of SYNPO2-YAP1 complexes in the cytoplasm, (Fig. 3.10, 3.25, and 3.26). However, a weak association of SYNPO2-YAP1 complexes with actin microfilament bundles was still observed (Fig. 3.25; A, B; a, b). It is worth noting that SYNPO2(fl)-YAP1 complexes were not localized in the nuclei, while interactions of truncated SYNPO2 variants with YAP1 did, in part, also occur in the nucleus of cells examined (Fig. 3.25 and 3.26; B, C).

To monitor whether overexpressed SYNPO2-YAP1 complexes colocalized with α-actinin along actin microfilament bundles, Pearson correlation coefficients (PCC) were determined between the BiFC fluorescence signal and the α-actinin signal.

Fig. 3.25: BiFC assays of YAP1–1 and SYNPO2 in smooth muscle cells. The row labels on the left side show BiFC constructs that were transiently double transfected and overexpressed. The column labels show the fluorescence channels for the Venus chimeras (BiFC constructs), actin filaments (F-actin), α-actinin, and an overlay of signals (BiFC/ α-actinin). The magnified regions in the far-right panel column are outlined by dashed lines in the overlay images. While full-length SYNPO2 interacts with YAP1–1 at dense bodies and FAs (C, arrows), SYNPO2 truncation variants interacted with YAP1–1 diffusely throughout the cytoplasm, depending on the extent of truncation (A, B). Scale bars: 10 µm, respectively.

Fig. 3.26: BiFC assays of YAP1–2 and SYNPO2 in smooth muscle cells. The row labels on the left side show BiFC constructs that were transiently double transfected and overexpressed. The column labels show the fluorescence channels for the Venus chimeras (BiFC constructs), actin filaments (F-actin), α-actinin, and an overlay of signals (BiFC/ α-actinin). The magnified regions in the far-right panel column are outlined by dashed lines in the overlay images. While full-length SYNPO2 interacts with YAP1–2 at dense bodies and FAs (C, arrows), SYNPO2 truncation variants interacted with YAP1–2 diffusely throughout the cytoplasm, depending on the extent of truncation (A, B). Scale bars: 10 µm, respectively.

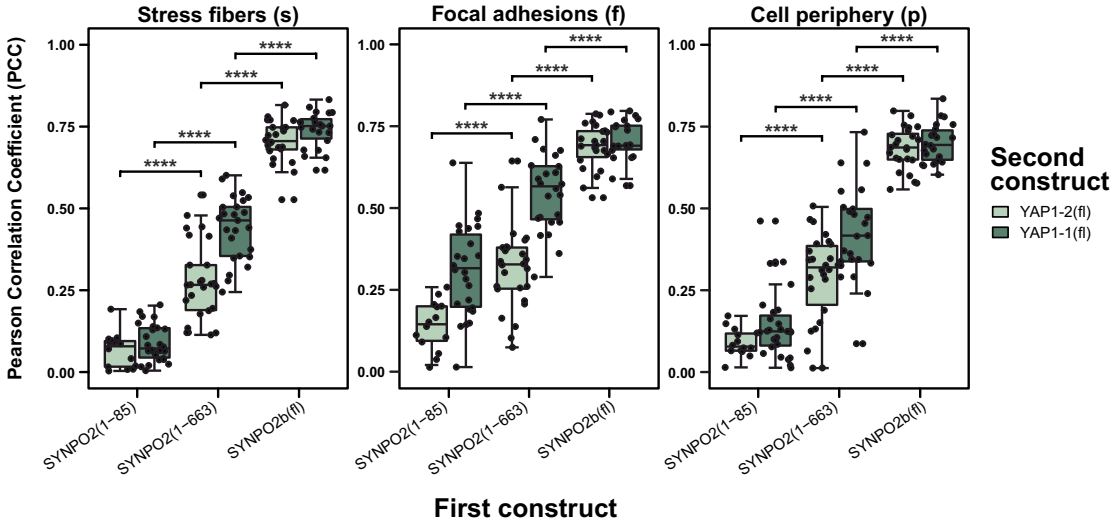


Fig. 3.27: SYNPO2-YAP1 colocalization with α-actinin in smooth muscle cells. Box plots with median, first and third quartile whiskers show Pearson correlation coefficient (PCC) measurements of α-actinin and BiFC constructs along actin microfilament bundles identified as stress fibers (s), at FAs (f) and in the cell periphery (c). Removed F-actin- and α-actinin-binding regions of SYNPO2 lead to a decreased mean correlation of SYNPO2-YAP1 complexes with α-actinin-rich structures. Notably, co-expression with YAP1–1 led to higher overall mean correlations of SYNPO2-YAP1 complexes with α-actinin compared to co-expression with YAP1–2, respectively. Statistical testing was performed via two-sample t-tests after distributions were tested for normality via Shapiro-Wilk tests. n.s. p>0.05; $^{*}p \leq 0.05$; $^{**}p \leq 0.01$; $^{***}p \leq 0.001$; $^{****}p \leq 0.0001$.

For that purpose, three different regions of interest (ROIs) containing α-actinin-rich structures were defined: (1) actin microfilament bundles spanning in between two FAs and previously denoted as stress fibers, (2) FAs, and (3) actin microfilament bundles in the cell periphery (Fig. 3.27) (see Appendix C). While SYNPO2(fl)-YAP1 complexes showed the highest correlation in all assessed ROIs, with mean values ranging from 0.68 to 0.74, the overexpression of SYNPO2 truncation variants with YAP1 resulted in significantly lower PCCs. The PCC mean values decreased from 0.28 at the actin stress fibers to 0.55 at FAs (Fig. 3.27). The correlation between SYNPO2(1–85) and YAP1 with α-actinin ranged from 0.07 to 0.31, with the highest correlation observed for SYNPO2 constructs co-expressed with YAP1–1. Therefore, SYNPO2 constructs lacking the α-actinin-binding regions, the colocalization of SYNPO2-YAP1 complexes with α-actinin was perturbed in smooth muscle cells. This implies that the recruitment of SYNPO2-YAP1 complexes to α-actinin-rich structures might be dependent on SYNPO2. To investigate this suggested role of SYNPO2 as a potential mediator for YAP1-SYNPO2 complex recruitment to α-actinin-rich structures, such as stress fiber dense bodies or FAs, the localization of SYNPO2 truncation constructs was examined in

smooth muscle cells (Fig. 3.28). Recent work has demonstrated that exon 6 of the SYNPO2a isoform itself targets to α-actinin at the dense bodies in smooth muscle cells due to an independent α-actinin-binding region (Lohanadan *et al.*, 2023).

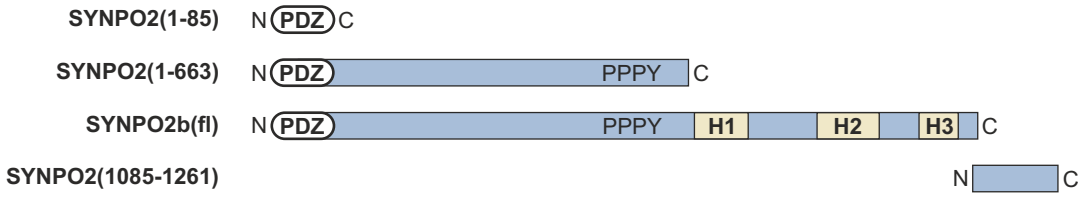


Fig. 3.28: Overview of transiently transfected SYNPO2 truncation constructs. Human eGFP-tagged SYNPO2 constructs differentially truncated and overexpressed in smooth muscle cells. Amino acids of truncations are indicated in brackets, otherwise, full-length (fl) proteins were used. SYNPO2 truncation constructs lacked different binding regions for cytoskeletal proteins, such as Filamin, F-actin, and α-actinin (see 3.3.1). SYNPO2 exon 6, referred to as SYNPO2(1085–1261), featuring an independent α-actinin-binding region, functioned as control. The fused eGFP-tags are not shown.

In this experiment, the localization of SYNPO2 exon 6, referred to as SYNPO2(1085–1261), functioned as a control. While SYNPO2(fl) was recruited to stress fiber dense bodies and FAs, truncated SYNPO2 constructs showed a diffuse localization in the cytoplasm of smooth muscle cells (Fig. 3.29; A–C). Similar to SYNPO2b(fl), SYNPO2 (1085–1261) was also recruited to stress fiber dense bodies due to the presence of the independent α-actinin binding region. In order to assess the degree of spatial (cor-)relation between overexpressed SYNPO2 constructs and α-actinin, line plot measurements were performed along actin microfilament bundles in selected ROIs (Fig. 3.29; dashed rectangles; Fig. 3.30). PCCs were calculated to quantify the correlation between generated line plots which revealed a spatial correlation between SYNPO2b(fl), and α-actinin of 0.56 and between SYNPO2(1085–1261), and α-actinin of 0.59, respectively (Fig. 3.30; E) Cells overexpressing SYNPO2(1–85) and SYNPO2(1–663) exhibited lower spatial correlations with α-actinin determined via PCCs (Fig. 3.30; E). All together, these results suggest that the interaction between SYNPO2 and YAP1 primarily occurs at α-actinin-rich structures in smooth muscle cells. SYNPO2 apparently mediates the recruitment of SYNPO2-YAP1 complexes in the presence of its F-actin- and α-actinin-binding regions, indicating that SYNPO2 facilitates YAP1 binding and anchoring to the actin cytoskeleton in smooth muscle cells.

Fig. 3.29: Overexpression of SYNPO2 constructs in smooth muscle cells. The row labels on the left side show transiently transfected SYNPO2 constructs that were overexpressed. The column labels show the fluorescence channels for the eGFP-SYNPO2 chimeras (eGFP constructs), actin filaments (F-actin), α-actinin and an overlay of both signals (eGFP/α-actinin). Dashed rectangles in the far-right panel column represent regions of interest (ROIs) measured in Fig. 3.27. While SYNPO2 truncation constructs exhibit a diffuse pattern of localization, SYNPO2(fl) and SYNPO2(1085–1261) were recruited to both dense bodies and FAs, associating with α-actinin. Scale bar: 10 µm.

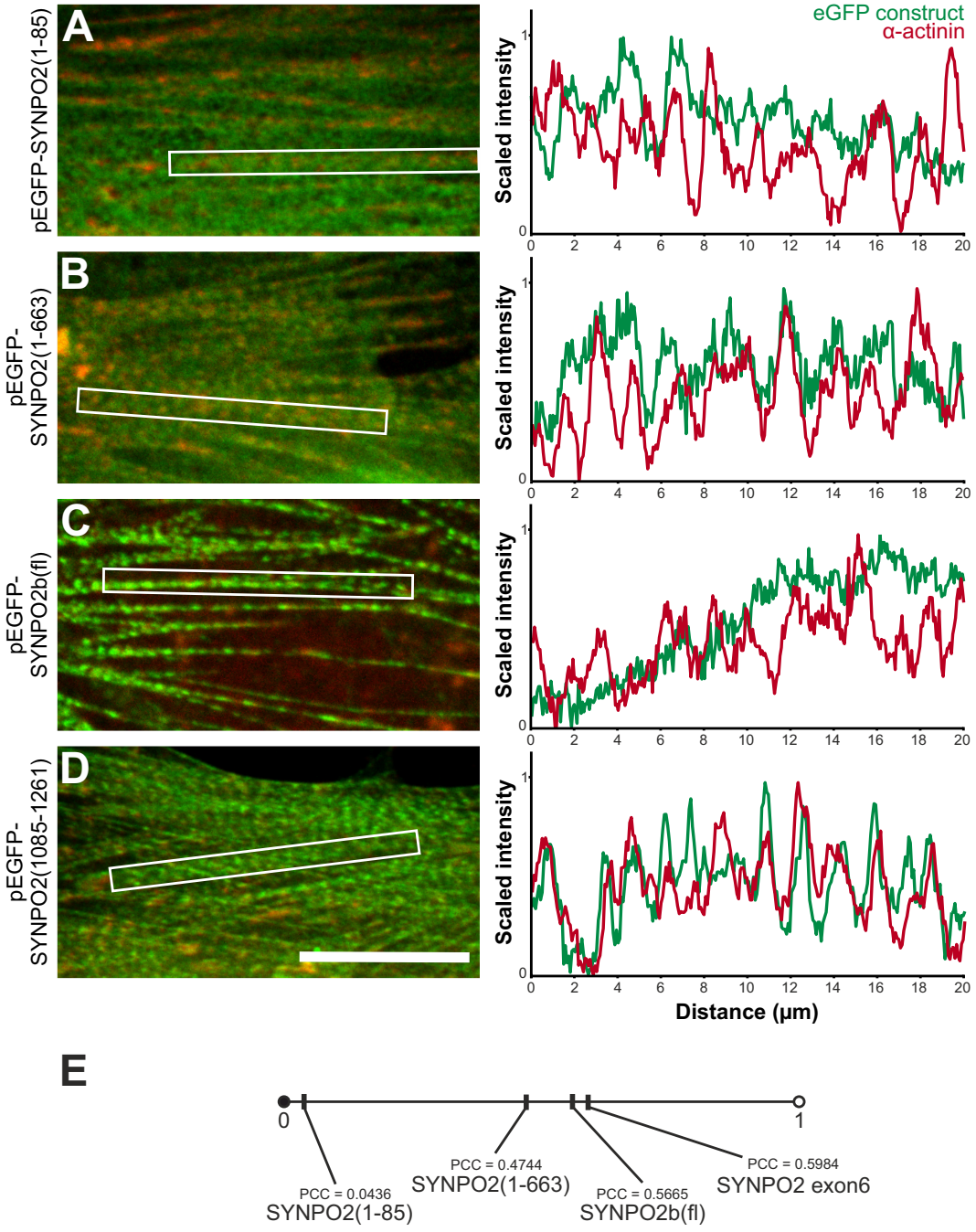


Fig. 3.30: Line plot measurements of SYNPO2 and α-actinin. ROIs (left panels) and Line plots (right panels) of actin microfilament bundles with measured signals of SYNPO2(1–85) (A), SYNPO2(1-663) (B), SYNPO2b(fl) (C), SYNPO2(1085–1261) (D) are shown in green. Line plots of α-actinin signals measured are shown in red. (E) Calculated Pearson correlation coefficient (PCC) indicated the special overlap of SYNPO2 and α-actinin. Both, SYNPO2b(fl) and SYNPO2(1085–1261) show the highest spatial correlation, whereas SYNPO2 truncations showed an abated correlation with α-actinin along actin microfilament bundles. Scale bar, 10 µm.

3.3.2 SYNPO2-YAP1 complexes are recruited to Z-discs in skeletal muscle cells

Similar to the recruitment of SYNPO2-YAP1 complexes to stress fiber dense bodies described above, SYNPO2 might facilitate a recruitment to Z-discs in skeletal muscle cells, specifically anchoring YAP1 to sarcomeres. To subsequently test this hypothesis, a similar BiFC assay was carried out in differentiated myoblasts in which the constructs utilized in smooth muscle cells were co-expressed (Fig. 3.24). Cells co-expressing SYNPO2 and YAP1 showed an interaction throughout the myotube (Fig. 3.31; A–F). Particularly, SYNPO2(fl)-YAP1 complexes were recruited to Z-discs (Fig. 3.31; C, F). Truncated SYNPO2 constructs also formed complexes with YAP1, albeit only partially localized to Z discs (Fig. 3.31; A, B, D; arrows). PCCs were calculated with the Z-disc epitope of titin in the assessed myotubes in order to determine the degree of colocalization between overexpressed SYNPO2-YAP1 complexes and Z discs. In the myotubes examined, complexes of truncated SYNPO2 and YAP1 showed a decreased mean correlation with the Z-disc titin epitope, ranging from 0.08 to 0.28, and 0.25 to 0.35 for SYNPO2(1–85) and SYNPO2(1–663), respectively (Fig. 3.32). SYNPO2(fl)-YAP1 complexes exhibited higher mean values of correlation, ranging from 0.43 to 0.60 (Fig. 3.32). In general, co-expression with YAP1–1 resulted in higher mean values of correlation compared to YAP1–2. However, there is a noticeable amount of SYNPO2-YAP1 interaction occurring throughout the myotubes, which may obscure precise correlation measurements at the Z-discs (Fig. 3.31).

To ascertain whether the correlation changes were dependent on SYNPO2, and to highlight the role of SYNPO2 as mediator for SYNPO2-YAP1 recruitment to Z-discs in skeletal muscles, the localization of truncated SYNPO2 constructs was examined (Fig. 3.33). As SYNPO2e is the isoform predominantly expressed in human skeletal muscle and localized to Z-discs (Lohanadan *et al.*, 2021; Linnemann, 2011), it was analyzed as a prospective control.

Both, overexpressed SYNPO2b(fl) and SYNPO2e(fl) predominantly localized at Z-discs (Fig. 3.34). However, both truncated constructs, SYNPO2(1–85) and SYNPO2(1–663), exhibited a diffuse localization pattern throughout the cytoplasm of myotubes. It should be noted that a fraction of overexpressed SYNPO2b(fl) also appeared to be distributed

Fig. 3.31: BiFC assays of YAP1 and SYNPO2 in skeletal muscle cells. The row labels on the left side show BiFC constructs that were transiently double transfected and overexpressed. The column labels show the fluorescence channels for the Venus chimeras (BiFC constructs), actin filaments (F-actin), Z-disc epitope of titin, denoted as titin (Z-disc), and an overlay of signals, referred to as BiFC/titin (Z-disc). While full-length SYNPO2 interacts with YAP1 at the Z-discs (C, F), SYNPO2 truncation constructs co-expressing with YAP1 showed less complex formation at Z-discs (A,B; D,E; arrows). Notably, SYNPO2-YAP1 complexes localized diffusely throughout the cytoplasm of myotubes. Scale bar: 10 µm.

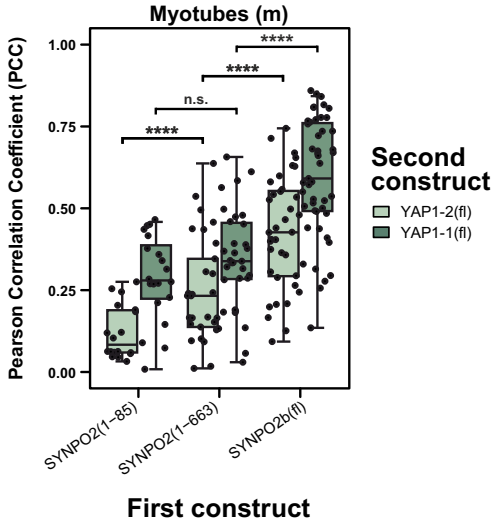


Fig. 3.32: SYNPO2-YAP1 colocalization with the Z-disc epitope of titin in skeletal muscle cells. Box plots with median, first and third quartile whiskers show Pearson correlation coefficient (PCC) measurements of the Z-disc epitope of titin and BiFC constructs throughout the myotube (m). Removed F-actin- and α-actinin-binding regions of SYNPO2 lead to a decreased mean correlation of SYNPO2-YAP1 complexes with titin at the Z-disc. Notably, co-expression with YAP1–1 led to higher overall mean correlations of SYNPO2-YAP1 complexes with Z-disc epitopes of titin compared to co-expression with YAP1–2, respectively. Statistical testing was performed via two-sample t-tests after distributions were tested for normality via Shapiro-Wilk tests. n.s. p> 0.05; $^{*}p \leq 0.05$; $^{**}p \leq 0.01$; $^{***}p \leq 0.001$; $^{****}p \leq 0.0001$.

in the cytoplasm (Fig. 3.34; C). Line plots of selected myofibrils were generated to assess the degree of a spatial relation between overexpressed SYNPO2 constructs and the titin epitope at the Z-disc (Fig.3.35; A–D). To quantify the correlation between generated line plots of SYNPO2 constructs and the titin fraction in Z-discs, PCCs were calculated (Fig. 3.34; dashed squares; Fig. 3.35; E). The quantifications showed decreased mean values of correlation when the SYNPO2 constructs lacked the binding regions for F-actin or α-actinin, while SYNPO2e(fl) and SYNPO2b(fl) correlated with the titin region of Z-discs in myofibrils examined (Fig. 3.35; E).

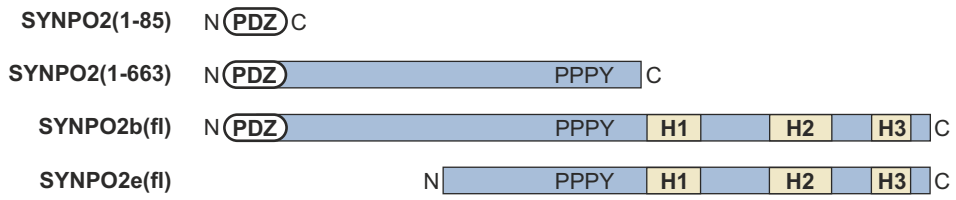


Fig. 3.33: Overview of transiently transfected SYNPO2 truncation constructs. Human eGFP-tagged SYNPO2 constructs differentially truncated and overexpressed in skeletal muscle cells. Amino acids of truncations are indicated in brackets, otherwise, full-length (fl) proteins were used. SYNPO2 truncation constructs lacked different binding regions for cytoskeletal proteins, such as filamin, F-actin, and α-actinin (see 3.23). SYNPO2e(fl) predominantly expressed in skeletal muscle cells functioned as a control. The fused eGFP-tags are not shown.

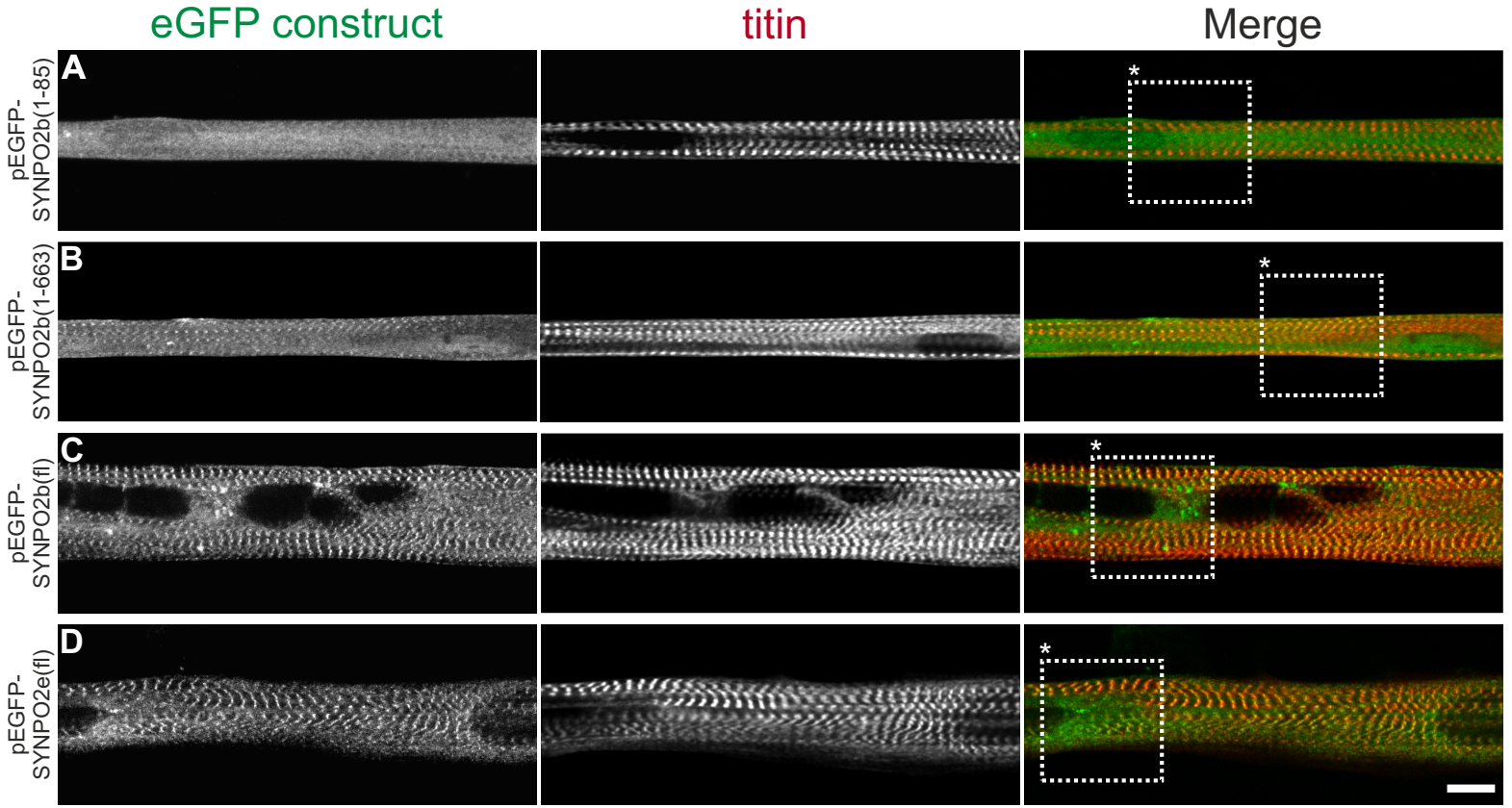


Fig. 3.34: Overexpression of SYNPO2 truncation constructs in skeletal muscle cells. The row labels on the left side show transiently transfected SYNPO2 constructs that were overexpressed. The column labels show the fluorescence channels for the eGFP-SYNPO2 chimeras (eGFP constructs) or the Z-disc epitope of titin, denoted as titin (Z-disc), and an overlay of both signals (merge). Dashed rectangles in the far-right panel column represent regions of interest (ROIs) measured in Fig. 3.3.2.5. While SYNPO2 truncation constructs exhibit a diffuse pattern of localization throughout the myotubes, both SYNPO2b(fl) and SYNPO2e(fl) were recruited to Z-discs, associating with titin. Scale bar: 10 µm.

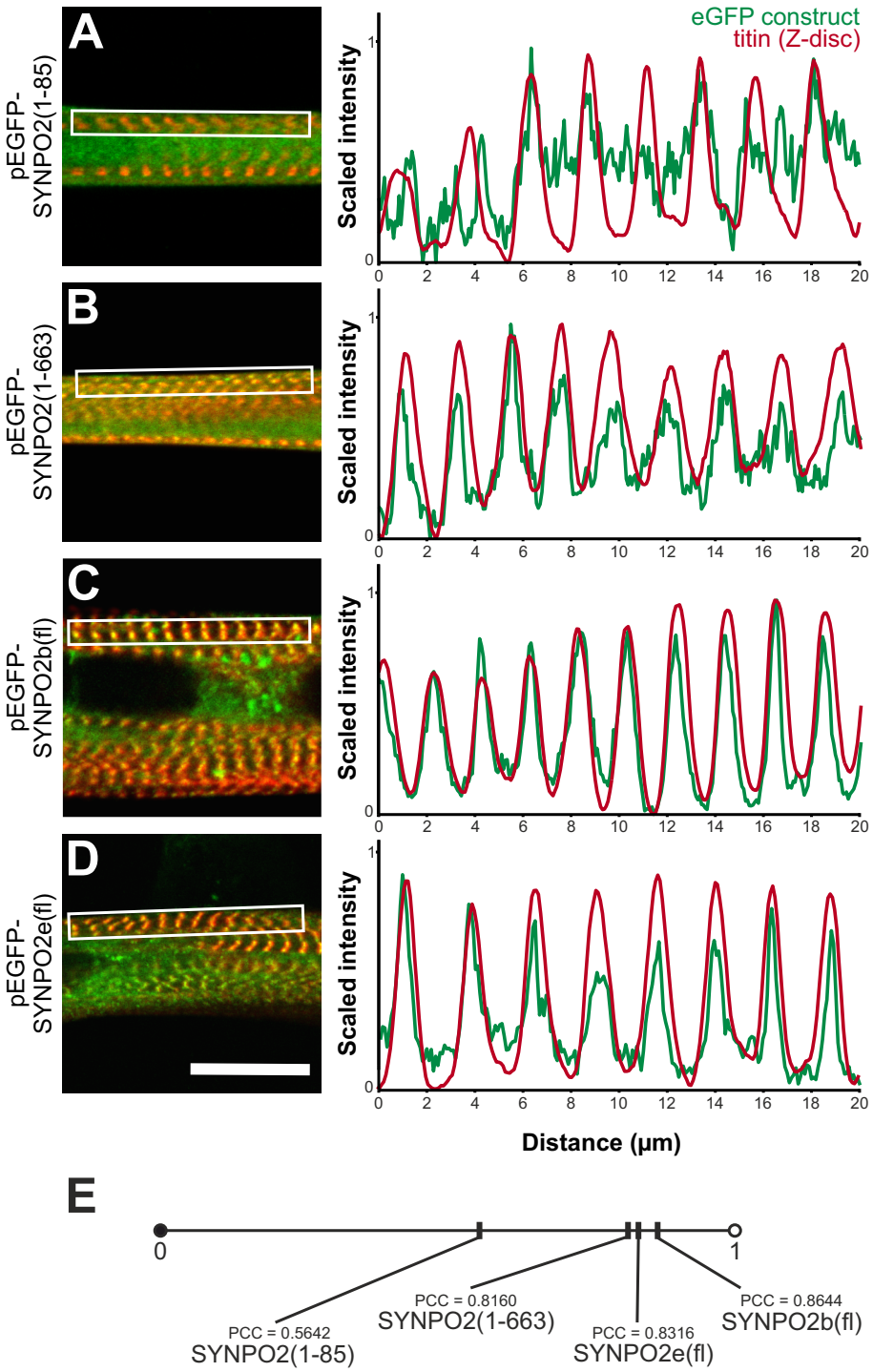


Fig. 3.35: Line plot measurements of SYNPO2 and the Z-disc epitope of titin. ROIs (left panels) and Line plots (right panels) of actin microfilament bundles with measured signals of SYNPO2(1-85) (A), SYNPO2(1–663) (B), SYNPO2b(fl) (C); SYNPO2e(fl) (D) are shown in green. Line plots of titin signals measured are shown in red. (E) Calculated Pearson correlation coefficients (PCC) indicated the spatial occupancy of SYNPO2 and the Z-disc epitope of titin. Both, SYNPO2b(fl) and SYNPO2e(fl) show the highest spatial correlation, whereas SYNPO2 truncations showed an abated correlation with titin in myofibrils.

In conclusion, SYNPO2 not only mediates the recruitment of YAP1 to stress fiber dense bodies in smooth muscle cells, but also to Z-discs in skeletal muscle cells. The results indicate that F-actin- and α-actinin-binding regions are required for this process. Nevertheless, a significant fraction of SYNPO2-YAP1 complexes remained diffusely localized throughout the cytoplasm, an effect which was only observed in skeletal muscle cells.

3.4 SYNPO2 interactions with BAG3, YAP1, and TAZ are regulated via phosphorylation

Tab. 3.1: SYNPO2 Phosphorylation sites in muscle cells upon mechanical stress

Identified Phosphopeptides	Site human	Site mouse	log_2 fold change	Reference
N-terminal of PPPY motif				
SVTSPISDFPA**PPPY**SAVSPPPEAFSR		S(603)	-0.267	Potts *et al.*, 2017
FSPTRNMTSPIADFP	T(610)		-0.055	Hofmann *et al.*, 2015
SPTRNMTSPIADFPA	S(611)		-0.031	Hofmann *et al.*, 2015
DFPA**PPPY**SAVTPPP	Y(622)		0.045	Hofmann *et al.*, 2015
C-terminal of PPPY motif				
FPA**PPPY**SAVTPPPD	S(623)		-0.032	Hofmann *et al.*, 2015
PPPYSAVTPPPDAFS	T(626)		0.073	Hofmann *et al.*, 2015
SVTSPISDFPA**PPPY**SAVSPPPEAFSR		S(618)	-1.234	Potts *et al.*, 2017

An objective of this work was to elucidate the underlying mechanisms for the regulation of interactions with SYNPO2 that occur at the PPPY motif. PTMs, such as phosphorylations of polypeptide chains, provide a key mechanism for regulating PPIs by altering protein stability or directly affecting a protein's function (Venerando *et al.*, 2017; Seok, 2021). Over the past decades, there have been several advances in studying the regulation of protein phosphorylation; in particular, one of the first studies specifically referring to murine SYNPO2 proposed that phosphorylation of SYNPO2 near the PPPY motif mediated binding to 14-3-3 proteins, eventually promoting nuclear shuttling of SYNPO2 (Faul *et al.*, 2005) (see section 1.4.2). More recently, further studies have identified various SYNPO2 peptides prone to phosphorylation in proximity to the PPPY motif in muscle upon induction of mechanical stress (Hoffman *et al.*, 2015; Potts *et al.*, 2017; Table 3.1). While the aforementioned studies aimed for a broad approach to unravel phosphorylation pathways via proteomic mapping, other studies specifically brought regulatory pathways that mediate phosphorylations of Z-disc protein into focus (Huttlin *et al.*, 2017; Reimann *et al.*, 2017). Taken together, these findings raise the question whether phosphorylatable sites might regulate binding with other interaction partners, such as the WW domain proteins BAG3, YAP1, and TAZ.

3.4.1 Phosphorylations in SYNPO2 regulate binding of different WW domains

Since WW domains are known to interact with SLIMs, 16-mer PPPY motif peptides of SYNPO2 were immobilized on membranes and overlaid with solutions of purified WW domains from BAG3, and YAP1/TAZ in a peptide binding assay (see section 2.3.11). To analyze potential effects of phosphorylations occurring proximal to the PPPY motif, SYNPO2 peptides were utilized by introducing phosphomimetic mutations. Phosphomimetic mutations in proteins are genetically engineered substitutions designed to mimic the structural and chemical properties of phosphorylated amino acids. These substitutions involve replacing a phosphorylatable amino acid residue in a protein by a non-hydrolyzable substitute that structurally resembles the phosphorylated state, despite lacking the actual phosphate group (Fig. 3.36).

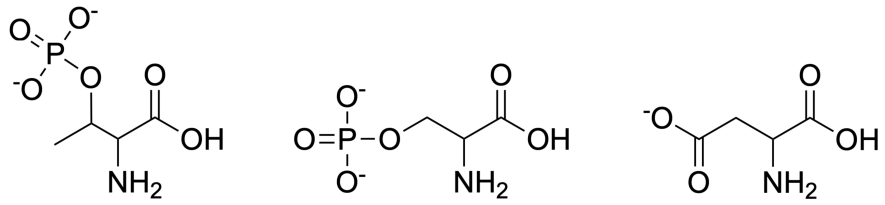


Fig. 3.36: Overview of Phosphomimetic substitute of serine and threonine. Modified amino acids phospho-threonine (A), phospho-serine (B), and aspartic acid (C) as phosphomimetic substitute. Similar to the phosphorylated amino acids, aspartic acid carries a negative charge, and is similar in terms of the sizes of the side chains.

To mimic phosphorylation of amino acids located N- (upstream) and C-terminally (downstream) to the PPPY motif identified by phosphoproteomics, serines and threonines were replaced by the acidic amino acid aspartic acid (Fig. 3.37; A, right panel). Furthermore, additional peptides were designed in which mutations were introduced into the PPPY motif of SYNPO2 to test for differences in specificity (Fig. 3.37; A, left panel). In the peptide binding assay, specific peptide recognition of WW domains derived from human YAP1, TAZ and BAG3 were tested. YAP1 constructs entailing both (WW12), or single WW domains (WW1 and WW2) were assessed separately.

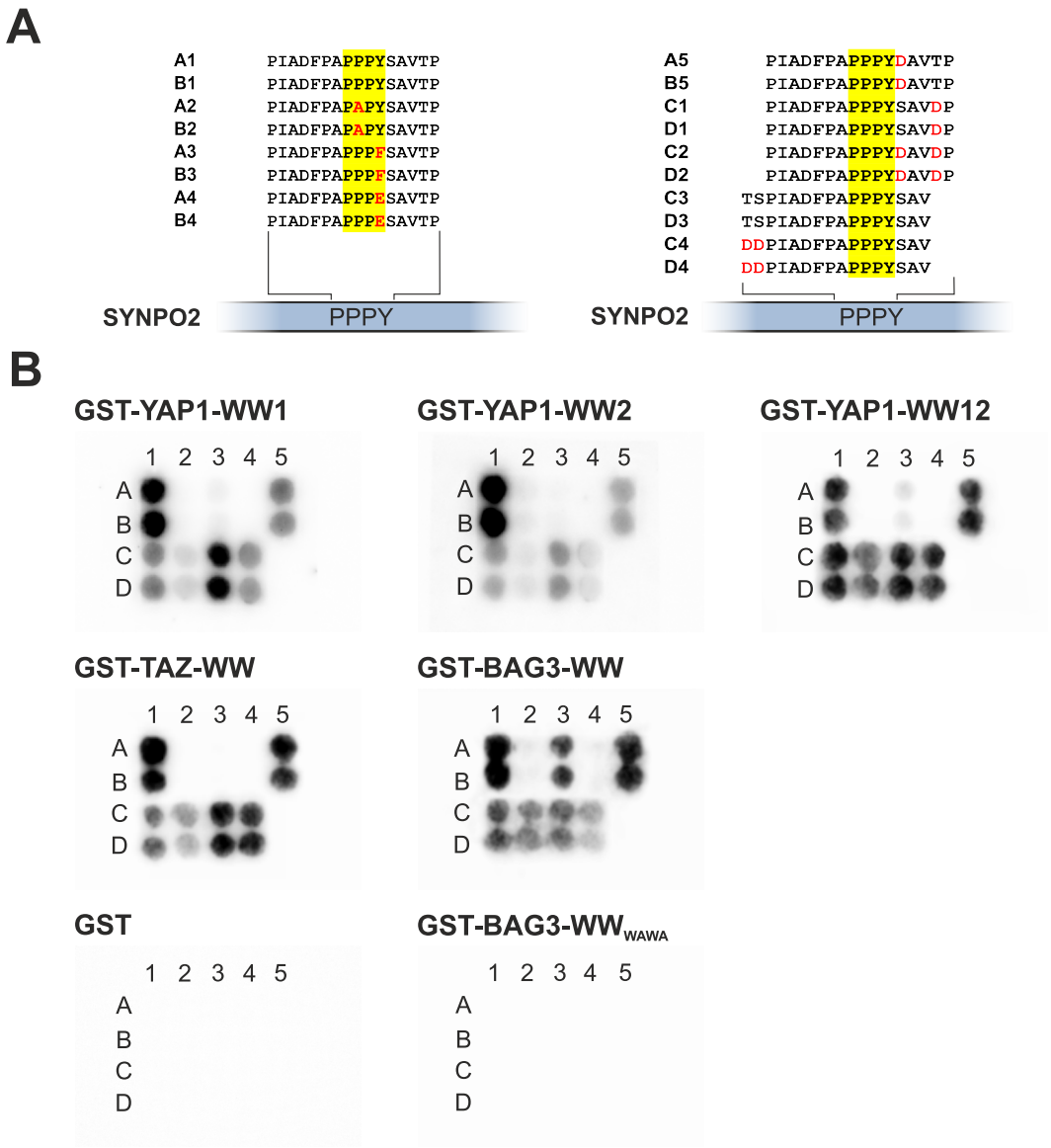


Fig. 3.37: Peptide binding assay of WW domain to the PPPY motif in SYNPO2. (A) Overview of SYNPO2 peptides spotted on the membranes. Mutations introduced into the PPPY motif should test for specificity (Left panel). Phosphomimetic mutations N- and C-terminally of the PPPY motif (B) Digitally rearranged images from peptide arrays. Proteins incubated are outlined on top. Immunotags fused to proteins for antibody detection are printed in bold. Column and row labels correspond to peptides shown above. While phosphorylations did not affect binding of YAP1 with both WW domains (WW12), phosphorylations at the PPPY motif can abrogate binding to single WW domains of YAP1, TAZ, and BAG3.

The peptide array experiments indicated that all WW domains show a specific binding to the wild-type PPPY motif, whereas mutations abrogated all of their interactions of all WW domains tested (Fig. 3.37; B). Upon evaluation of immunofluorescence analyses, the WW domain of BAG3 bound to peptides encompassing a phenylalanine-modified motif (Fig. 3.37; B, peptide A3/B3). Phosphomimetic mutations affected binding in different

ways: While single downstream serine to aspartate mutations impeded binding of BAG3, YAP1-WW1 and WW2, as well as TAZ, introducing two C-terminal mutations of this kind obstructed binding of those WW domains. Yet, N-terminal phosphomimic mutations impaired binding of BAG3, YAP-WW1, and YAP-WW2 but, in contrast, not the binding of TAZ. Interestingly, YAP1-WW12 binding to phosphomimetic mutants was not affected. Since tryptophans are crucial for WW domain binding, these two canonical tryptophan residues in the WW domain of BAG3 were replaced by alanines in an additional construct (BAG3-WAWA) to function as an additional control (Ingham *et al*, 2005; Jäger *et al*, 2009; Ulbricht *et al*, 2013). As demonstrated in previous studies, these substitutions completely abolished binding of this mutated domain to the PPPY peptides, rendering tryptophans in the WW domains crucial residues for PPPY motif recognition (Fig. 3.37; B, bottom panel). These findings indicate that a more complex mechanism regulating the displacement of YAP1 and TAZ through BAG3 or *vice versa* exists, involving phosphorylations downstream of the PPPY motif as an additional regulatory element. In contrast, YAP1 isoforms encompassing both WW domains might replace BAG3 at the PPPY motif independently of adjacent phosphorylations present.

3.4.2 Phosphorylations in SYNPO2 facilitate a replacement of YAP1 isoforms by BAG3 *in vitro*

To further biochemically characterize a potential displacement of YAP1 through BAG3 at the PPPY motif regulated by C-terminally located phosphorylations, competitive binding co-IPs were performed. Based on previous findings presented here, it was hypothesized that these phosphomimetic mutations might affect the substitution of YAP1 through BAG3 compared to the SYNPO2 wildtype (see section 3.4.1). For this purpose, a double phosphomimetic mutant of SYNPO2 spanning the PPPY motif was generated. In this mutant, denoted SYNPO2(527–663 TSDD, the residues S623 and T626 were replaced by aspartic acid (D), respectively (Fig. 3.37; C2-D2). This construct was compared to a wild type fragment of SYNPO2, referred to as SYNPO2(527–663) WT and tested for binding to WW domain constructs of YAP1 and BAG3 (Fig. 3.38; a).

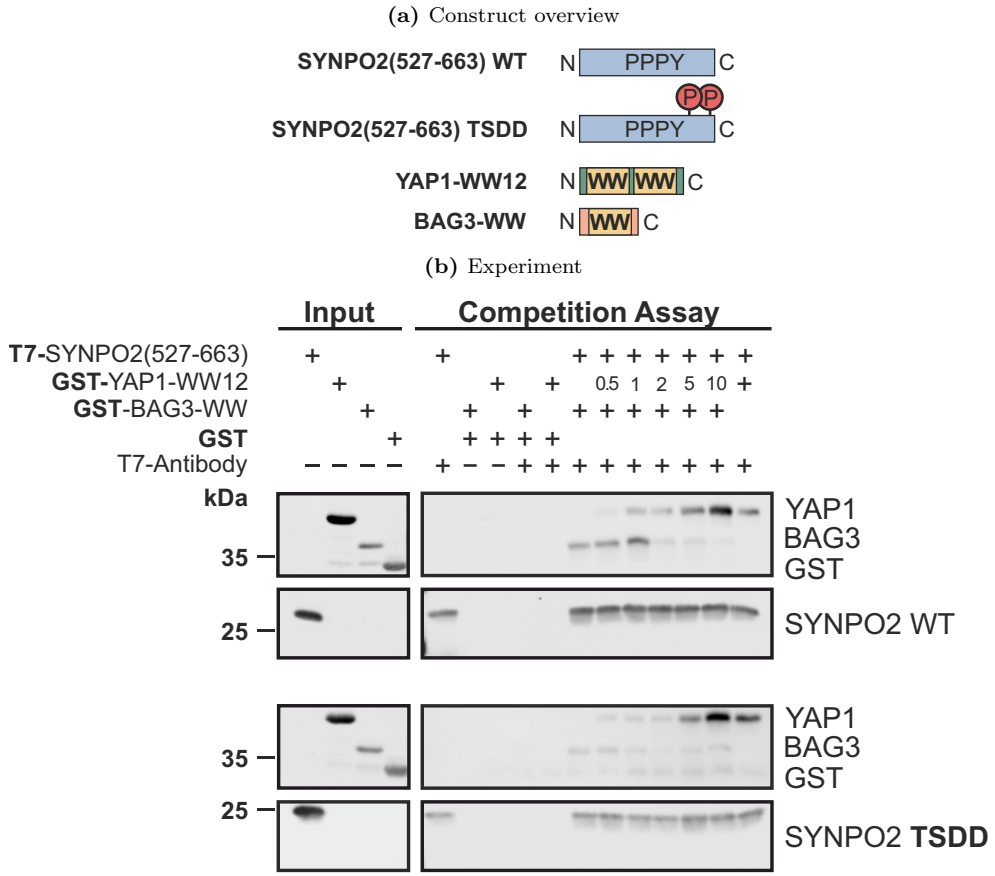


Fig. 3.38: Competitive binding assay of YAP1-WW12 and BAG3. (a) Overview of T7-tagged SYNPO2 bait constructs (blue), spanning amino acids 527–663. Red dots indicate phosphomimetic mutations in SYNPO2. GST-tagged YAP1 protein chimeras (green) and BAG3 (orange) were coprecipitated. The WW domains (WW) are outlined in yellow. (b) Digitally rearranged western blot of sample fractions from the co-IP experiment. The sample composition in loading controls (Input) and experimental samples after precipitation (Competition assay) is outlined on top. Immunotags fused to proteins for antibody detection are printed in bold. The band migration pattern of molecular weight markers is shown on the left. (Bottom panels) SYNPO2 bait protein fractions from the co-IP experiment. (Top panels) YAP1 and BAG3 protein sample fractions from the same experiment. Increased concentrations of YAP1 titrated in the samples replaced BAG3 at both, wildtype and phosphomimetic PPPY motif, resulting in increased band intensities of YAP1, while band intensities of BAG3 diminished.

Analyses of the immunoblots revealed a decrease in BAG3 band intensities with increasing concentrations of YAP1, which coprecipitated with both wildtype and phosphomimetic SYNPO2 variants (Fig. 3.38; b). This indicated that BAG3 displacement by YAP1 isoforms with two WW domains (YAP1-WW12) might not be mediated by C-terminal phosphorylations adjacent to the PPPY motif. However, YAP1 isoforms with a single WW domain might replace BAG3 in a phosphorylation-dependent manner. To test this hypothesis, a subsequent co-IP was carried out, in which the WW1 of YAP1 (YAP1-WW1) was co precipitated instead (Fig. 3.39; a). The western blot

analyses showed that phosphomimetic mutations in SYNPO2 impaired the binding of YAP1-WW1 compared to a SYNPO2 wild-type variant but hardly replaced bound BAG3 (Fig. 3.39; b).

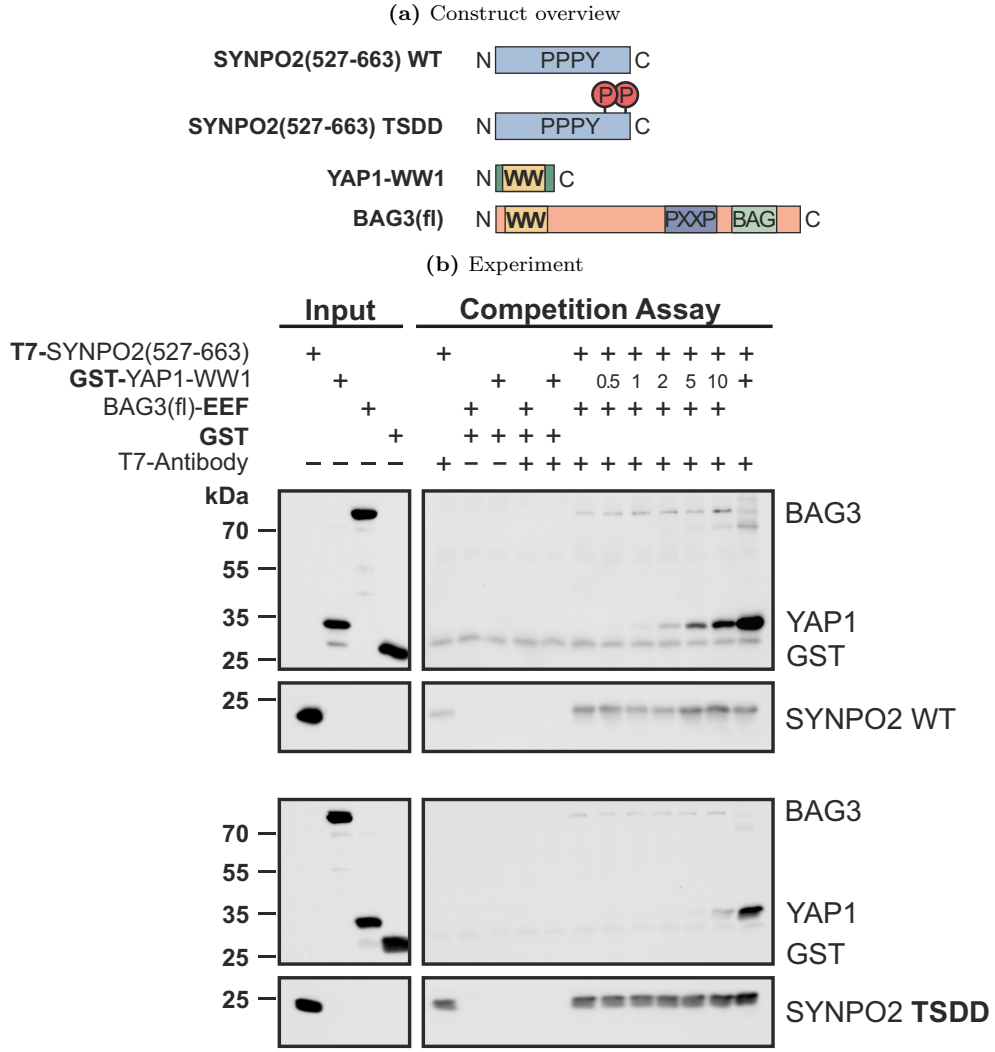


Fig. 3.39: Competitive binding assay of YAP1-WW1 and BAG3. (a) Overview of T7-tagged SYNPO2 bait constructs (blue), spanning amino acids 527–663. Red dots indicate phosphomimetic mutations in SYNPO2. GST-tagged YAP1 protein chimeras (green) and BAG3 (orange) were coprecipitated. The WW domains (WW) are outlined in yellow. (b) Digitally rearranged western blot of sample fractions from the co-IP experiment. The sample composition in loading controls (Input) and experimental samples after precipitation (Competition assay) is outlined on top. Immunotags fused to proteins for antibody detection are printed in bold. The band migration pattern of molecular weight markers is shown on the left. (Bottom panels) SYNPO2 bait protein fractions from the co-IP experiment. (Top panels) YAP1 and BAG3 protein sample fractions from the same experiment. Increased concentrations of YAP1 titrated in the samples replaced BAG3 at both, wildtype and phosphomimetic PPPY motif, resulting in increased band intensities of YAP1, while band intensities of BAG3 diminished.

These results suggest that there might be a distinct replacement mechanism of BAG3 by

YAP1 or *vice versa*, depending on the presence of the WW domains in YAP1. Phosphorylations downstream of the PPPY motif weaken YAP1–1 binding and promote replacement through BAG3, but BAG3 might also be substituted by YAP1–2 once SYNPO2 is phosphorylated in proximity to the PPPY motif. In general, this particular mechanism could only apply to a subset of human YAP1 isoforms expressing the first WW domain, since only the binding between SYNPO2 and YAP1–1, but not SYNPO2 and YAP1–2, was shown to be regulated in this SYNPO2 phosphorylation-dependent manner.

3.5 SYNPO2 phosphorylations specifically regulate its recruitment to the actin cytoskeleton in muscle cells

The potential phosphorylation sites located near the PPPY motif overlap with one of the α-actinin binding regions previously identified in SYNPO2 (Linnemann *et al.*, 2013; Fig. 3.23). Firstly, one may speculate that phosphorylations at these sites could alter the binding property of this SYNPO2 portion to WW domain-containing proteins. Secondly, these phosphorylations might also modulate the recruitment of SYNPO2 to Z-discs in skeletal muscle and/or stress fiber dense bodies in smooth muscle cells by affecting the binding to α-actinin.

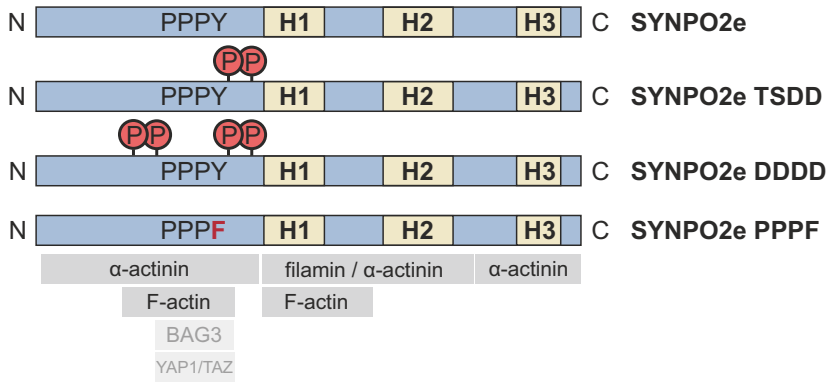


Fig. 3.40: Schematic overview of SYNPO2 phosphomimetic mutants. (H1, H2, H3) Regions with synaptopodin family homology. Red dots indicate the positions of phosphomimetic mutations in SYNPO2 near the PPPY motif. A mutated PPPY motif was generated to eliminate WW domain-binding (PPPF). Other binding regions of known interaction partners are outlined in dark gray.

In order to further assess effects potentially mediated by SYNPO2 phosphorylation, additional SYNPO2 mutant constructs were generated (Fig. 3.40). The design of these constructs was based on SYNPO2 isoform e (SYNPO2e), which contains binding regions for filamin, F-actin, and α-actinin, but while lacks the N-terminal PDZ domain-entailing portion. The following SYNPO2 mutant constructs encompassed: (1) two phosphomimetic serine/threonine to aspartic acid substitutions at the sites S623D and T626D (SYNPO2e TSDD), (2) four serine/threonine to aspartic acid substitutions at the sites T610D, S611D, S623D and T626D (SYNPO2e DDDD), or (3) a substitution of tyrosine (Y) in the PPPY motif to phenylalanine (F) (SYNPO2e PPPF) (Fig. 3.37).

3.5.1 SYNPO2 associates with the actin cytoskeleton in a phosphorylation-dependent manner

In smooth muscle cells, both overexpressed SYNPO2e WT and SYNPO2e DDDD localized along actin microfilament bundles and showed recruitment to stress fiber dense bodies as well as to FAs (Fig. 3.41; A, B). Despite only showing association with actin microfilament bundles, a localization of the SYNPO2e TSDD variant to dense bodies was not observed (Fig. 3.41; C). The tyrosine to phenylalanine substitution in the PPPY motif obstructed a recruitment to the actin microfilament cytoskeleton in smooth muscle cells (Fig. 3.41; D). A similar effect was observed when mutated SYNPO2 constructs were overexpressed in skeletal muscle cells: both, SYNPO2e WT and SYNPO2e DDDD mainly localized at the Z-discs, while SYNPO2e TSDD and SYNPO2e PPPF mutant constructs were found to be diffusely localized throughout the myotube (Fig. 3.43). The spatial relation between overexpressed SYNPO2 constructs and α-actinin enriched in dense bodies along stress fibers was determined via line plot measurements in smooth muscles (Fig. 3.42; A–D). Similarly, the assessment of a potential spatial relation between SYNPO2 constructs and a titin epitope at myofibrillar Z-discs was determined in skeletal muscle cells (Fig. 3.44; A–D). In both muscle cell types, the quantification of line plot measurements comparing SYNPO2 and either α-actinin (smooth muscles) or the Z-disc fraction of titin (skeletal muscles), showed similar mean PCCs of SYNPO2e WT and SYNPO2e DDDD, respectively (Fig. 3.42; E and 3.44; E). However, the line plot measurements revealed that the localization patterns of SYNPO2e TSDD and SYNPO2e PPPF mutant constructs correlated poorly with those of both, α-actinin and the Z disc epitope of titin, respectively (Fig. 3.42; E and 3.44; E).

In conclusion, SYNPO2 associates with either α-actinin or the Z-disc portion of titin in a phosphorylation-dependent manner in both skeletal and smooth muscle cells. These findings suggest that dephosphorylation of the phospho-acceptor sites T610 and S611 abolishes recruitment of SYNPO2e to these structures, while SYNPO2e localization is not affected by phosphorylations of all four phospho-acceptor sites. Moreover, the presence of the PPPY motif was found to be required for stress fiber dense body and Z-disc recruitment of SYNPO2 (Fig. 3.42; B, E and 3.44; B, E). Yet, these experiments could not reveal whether these phosphorylations were capable of directly modulating the

binding of SYNPO2 to α-actinin itself.

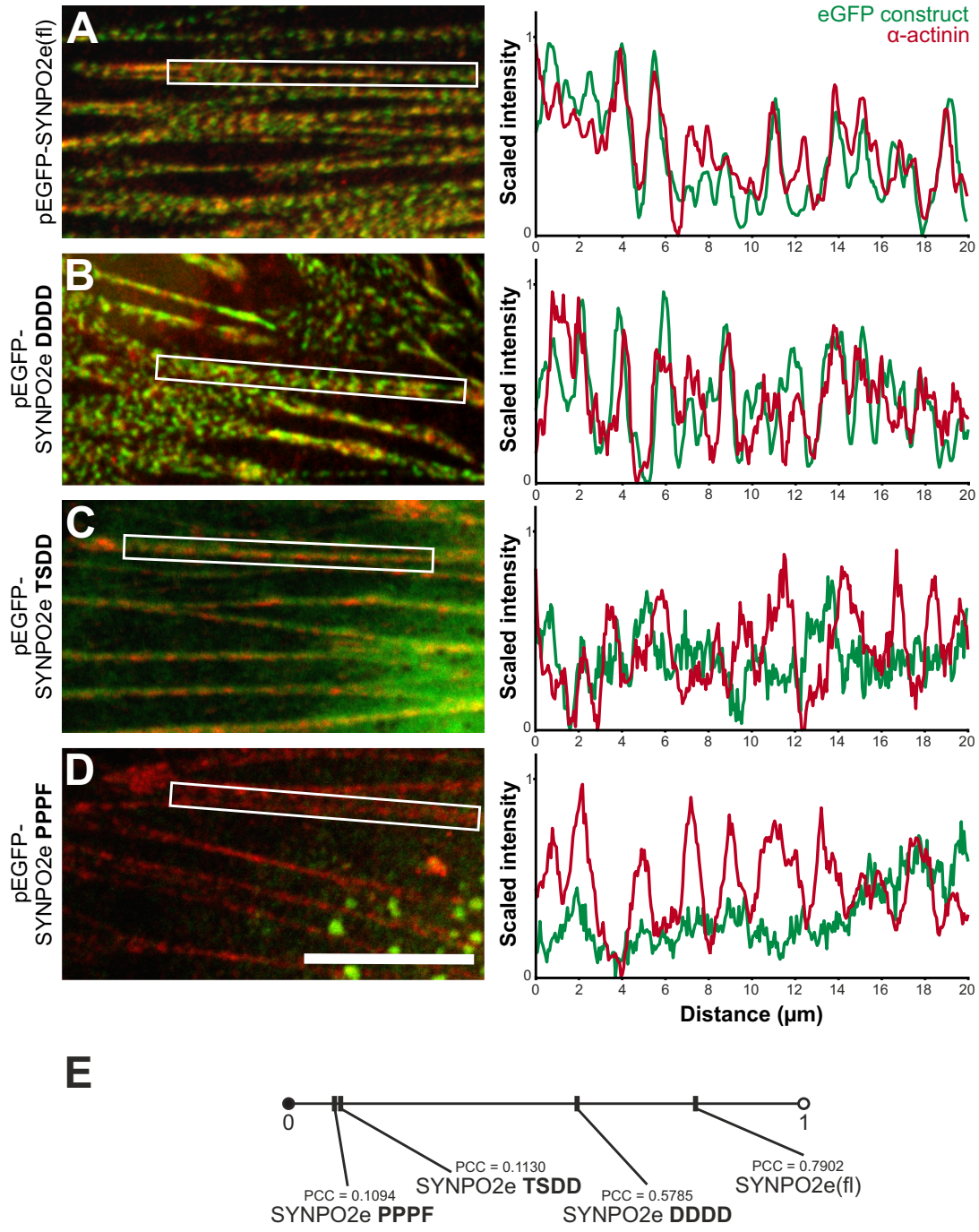


Fig. 3.42: Line plot measurements of SYNPO2 and α-actinin. ROIs (left panels) and Line plots (right panels) of actin microfilament bundles with measured signals of SYNPO2e WT (A), SYNPO2e DDDD (B), SYNPO2e TSDD (C); SYNPO2e PPPF (D) are shown in green. Line plots of α-actinin signals measured are shown in red. (E) Calculated Pearson correlation coefficient (PCC) indicated the special overlap of SYNPO2 and α-actinin. Both, SYNPO2e WT and SYNPO2e DDDD show the highest spatial overlap, whereas SYNPO2e TSDD and SYNPO2e PPPF showed an abated correlation with α-actinin along actin microfilament bundles. Scale bar: 10 µm.

Fig. 3.41: Overexpressing SYNPO2 mutant constructs in smooth muscle cells. The row labels on the left side show transiently transfected SYNPO2e mutant constructs that were overexpressed. The column labels show the fluorescence channels for the eGFP SYNPO2 chimeras (eGFP constructs), actin filaments (F-actin), α-actinin and an overlay of both signals (eGFP/α-actinin). Dashed rectangles in the far-right panel column represent regions of interest (ROIs) measured in Fig. 3.42. While SYNPO2e PPPF exhibited a diffuse pattern of localization, both SYNPO2e WT and SYNPO2e DDDD were recruited to dense bodies and FAs. Notably, SYNPO2e TSDD associated with actin microfilament bundles, but was not recruited to neither dense bodies nor FAs. Scale bar: 10 µm.

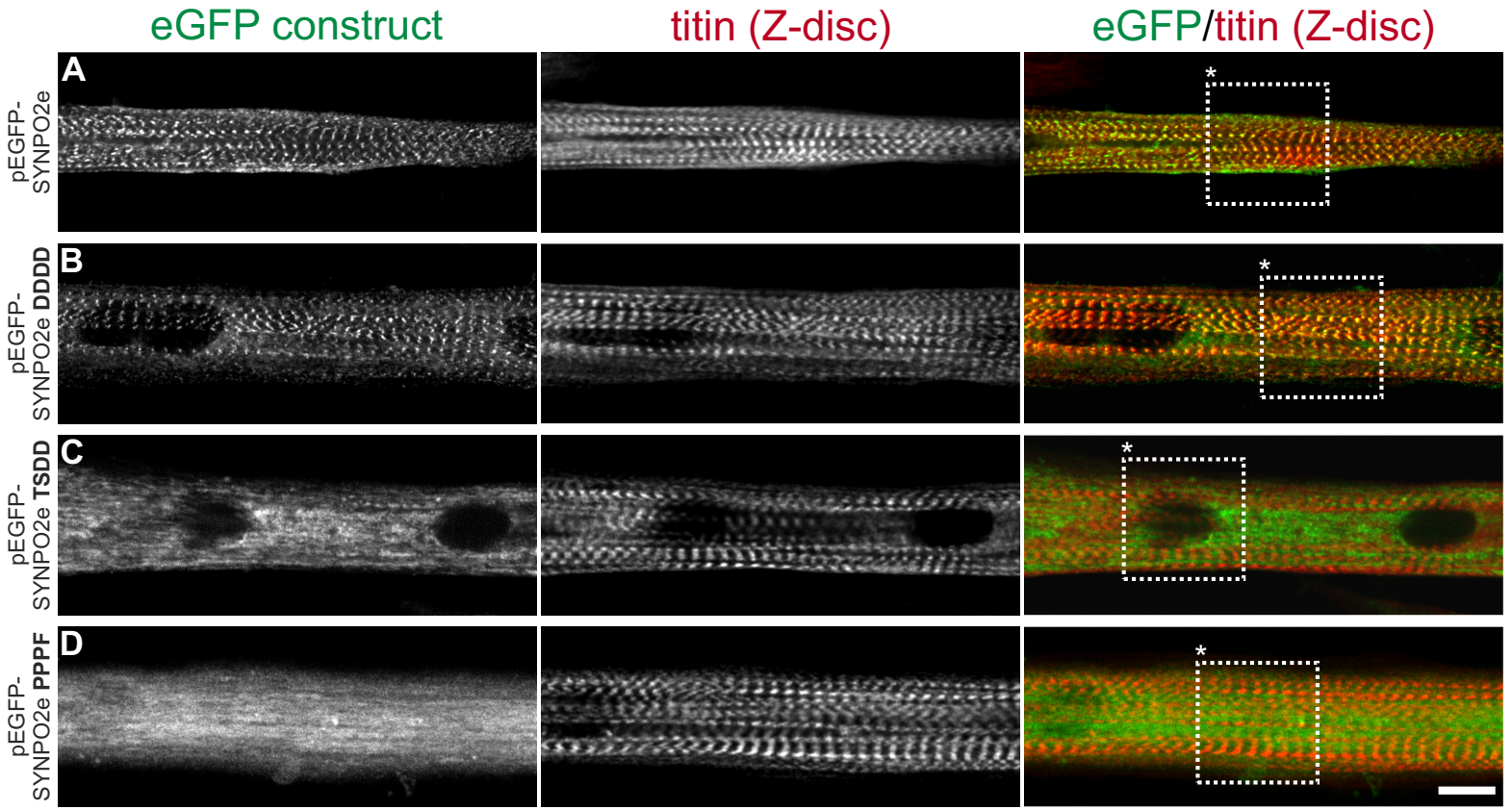


Fig. 3.43: Overexpressing SYNPO2 mutant constructs in skeletal muscle cells. The row labels on the left side show transiently transfected SYNPO2e mutant constructs that were overexpressed. The column labels show the fluorescence channels for the eGFP SYNPO2 chimeras (eGFP constructs), the Z-disc epitope of titin, referred to as titin (Z-disc), and an overlay of both signals (eGFP/ titin). Dashed rectangles in the far-right panel column represent regions of interest (ROIs) measured in Fig. 3.44. While both, SYNPO2e TSDD and SYNPO2e PPPF exhibited a diffuse pattern of localization within the myotube, both SYNPO2e WT and SYNPO2e DDDD were mainly recruited to Z-discs. Scale bar: 10 µm.

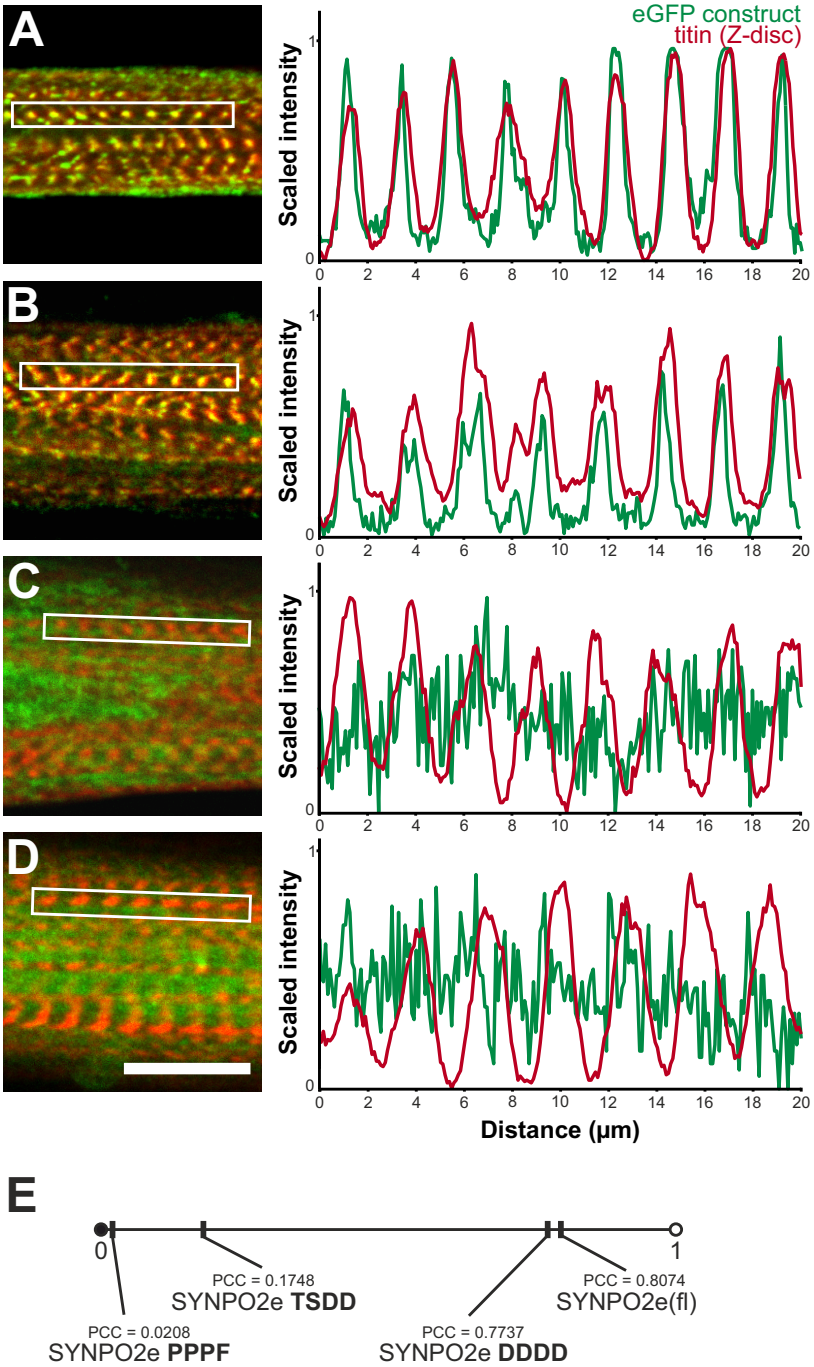


Fig. 3.44: Line plot measurements of SYNPO2 and the Z-disc epitope of titin. ROIs (left panels) and Line plots (right panels) of myofibrils with measured signals of SYNPO2e WT (A), SYNPO2e DDDD (B), SYNPO2e TSDD (C); SYNPO2e PPPF (D) are shown in green. Line plots of titin Z-disc epitope signal measured are shown in red. (E) Calculated Pearson correlation coefficients (PCC) indicated the spatial correlation of SYNPO2 and titin. Both, SYNPO2e WT and SYNPO2e DDDD show the highest correlation with titin, whereas SYNPO2e TSDD and SYNPO2e PPPF showed an abated correlation with titin in myofibrils. Scale bar: 10 µm.

3.5.2 Phosphorylations of SYNPO2 regulate its binding to α-actinin *in vitro*

In the previous chapter, it was demonstrated that phosphorylations adjacent to the PPPY motif affected the targeting of SYNPO2 in smooth and skeletal muscle cells. The phosphorylations affected its localization to dense bodies and to Z-discs which both contain α-actinin, a protein bundling actin microfilaments. In SYNPO2, an α-actinin-binding region overlaps with phosphorylation sites analyzed (Fig. 3.23 and 3.40). In addition to that, the N-terminal part of this binding region shares similarity with the α-actinin-binding regions of two other Z-disc-associated α-actinin-binding proteins, calsarcin 1 and calsarcin-2 (Frey *et al.*, 2000; Sponga *et al.*, 2021; Fig 3.45). Thus, it was hypothesized that phosphorylations located upstream of the PPPY motif might directly modulate the interaction between SYNPO2 and α-actinin, affecting the SYNPO2 targeting to α-actinin-rich structures in muscle cells.

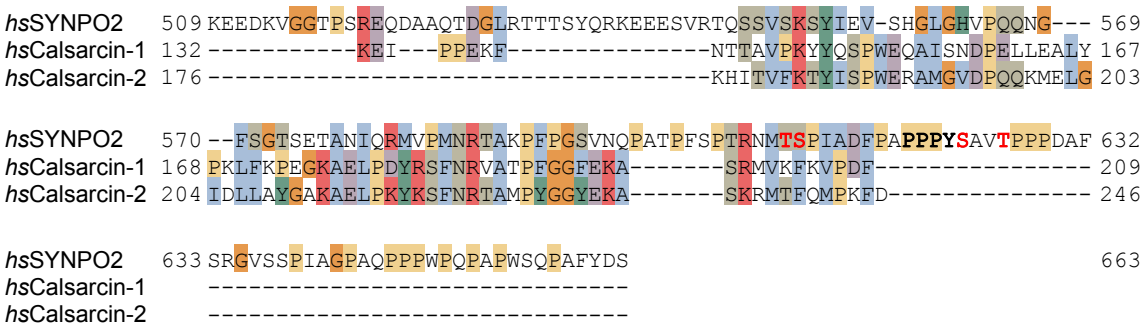


Fig. 3.45: Protein alignment of the N-terminal SYNPO2 α-actinin-binding region compared to Calsarcin-1, and Calsarcin-2. Multiple sequence alignments using the Clustal Omega algorithm in Jalview (Sievers *et al.*, 2018). Protein names are shown on the left. The amino acid positions of each protein are shown on both sides of each sequence. Colors were adapted from Clustal. The α-actinin-binding region of SYNPO2 flanking the PPPY motif is similar to linear α-actinin-binding motifs of calsarcins (Sponga *et al.*, 2021). The PPPY motif is printed in bold, adjacent SYNPO2 phosphor-acceptor sites T610, S611, S623, and T626 are printed in red.

Additional co-IP experiments were carried out to analyze the interaction between SYNPO2 and different α-actinin isoforms. In these experiments, α-actinin-1, 2, and 3 were tested, of which the first is expressed in smooth muscle cells while the latter two are isoforms expressed in skeletal muscle cells (see section 1.4.1). For these experiments, a shorter SYNPO2 variants was generated, referred to as SYNPO2(527–663), comprising of the N-terminal α-actinin binding region canonical for all SYNPO2 isoforms expressed in muscle tissues (Fig. 3.46; a).

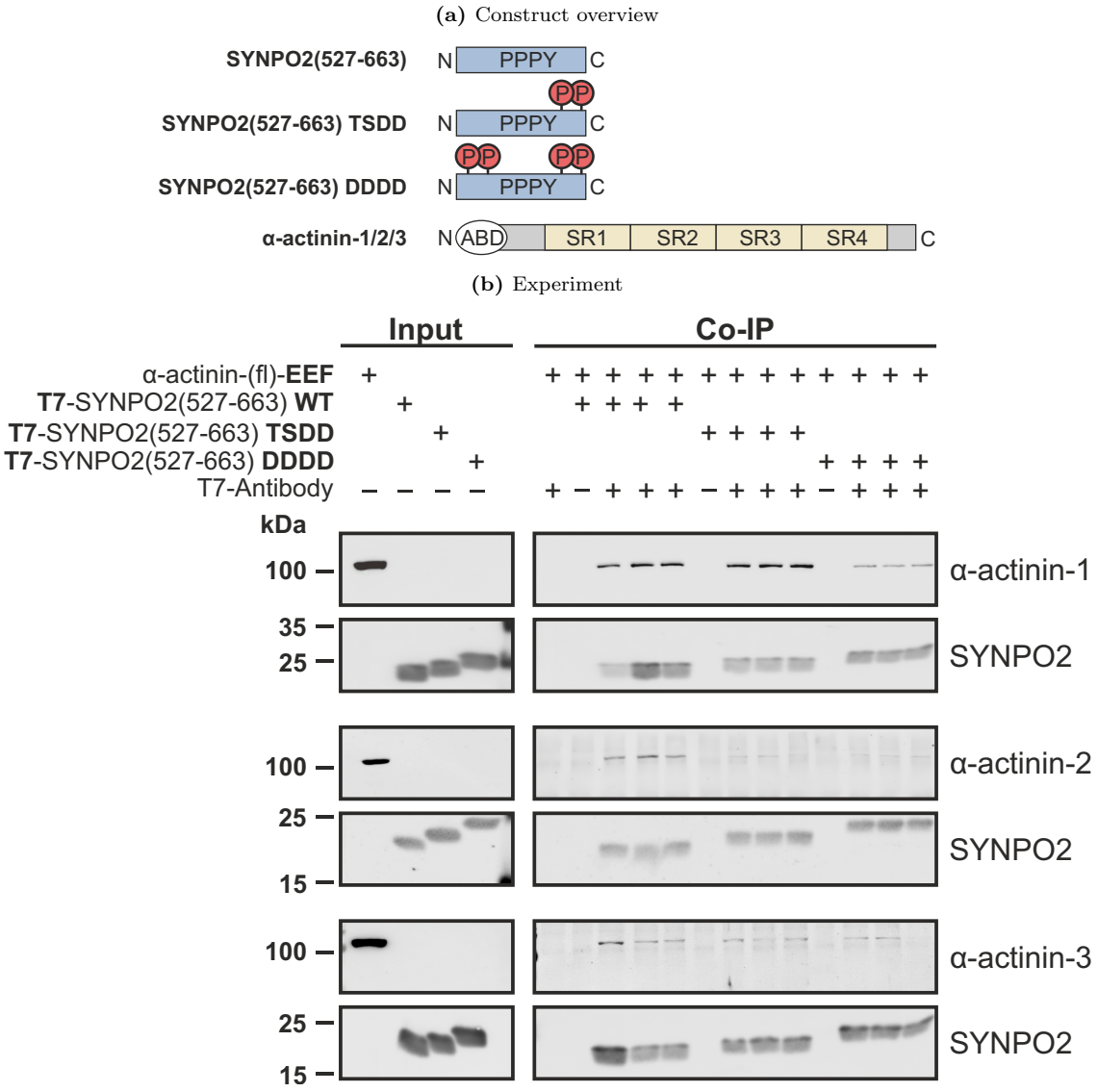


Fig. 3.46: Co-IPs of SYNPO2 with different α-actinin isoforms. (a) Overview of T7-tagged SYNPO2 bait constructs (blue), amino acids 537-663, harboring the α-actinin-binding region. Red dots indicate the positions of phosphomimetic mutations in SYNPO2 proximal to the PPPY motif. EEF-tagged full-length α-actinin(fl) protein chimeras (gray) were coprecipitated. Actin-binding domain (ABD) and spectrin repeats 1-4 (SR1-4). (b) Digitally rearranged western blot of sample fractions from the co-IP experiment. The sample composition in loading controls (Input) and experimental samples after precipitation (co-IP) is outlined on top. Immunotags fused to proteins for antibody detection are printed in bold. The band migration pattern of molecular weight markers is shown on the left. (Top panels) α-actinin isoform protein fractions from the co-IP experiments. (Bottom panels) SYNPO2 bait protein fractions from the same experiments. Samples containing both precipitating antibody and SYNPO2 showed different band intensities of coprecipitated α-actinin proteins. Notably, α-actinin-2, and α-actinin-3 showed reduced binding to SYNPO2 constructs compassing phosphomimetic mutations, while α-actinin-1 preferably bound to the SYNPO2(527–663) TSDD mutant.

Phosphomimetic mutations corresponding to SYNPO2 constructs utilized in the previous sections were introduced to analyze potential changes in α-actinin binding specificities (see section 3.5.1). When analyzed, co-IPs showed bands of the precipitated SYNPO2 constructs with molecular masses ranging between approx. 17 and 19 kDa (Fig. 3.46; b). Samples probed with α-actinin showed protein bands migrating at approx. 105 kDa, corresponding to the full-length proteins α-actinin-1, 2, and 3, respectively (Fig. 3.46; b). Based on their respective band intensities, both, α-actinin-2 and α-actinin-3 bound more wild-type SYNPO2(527–663) than corresponding SYNPO2 phosphomimetic mutants (Fig. 3.46; b, lower panels). In contrast, α-actinin-1 showed more coprecipitation with SYNPO2(527–663) TSDD (Fig. 3.46; b, upper panel).

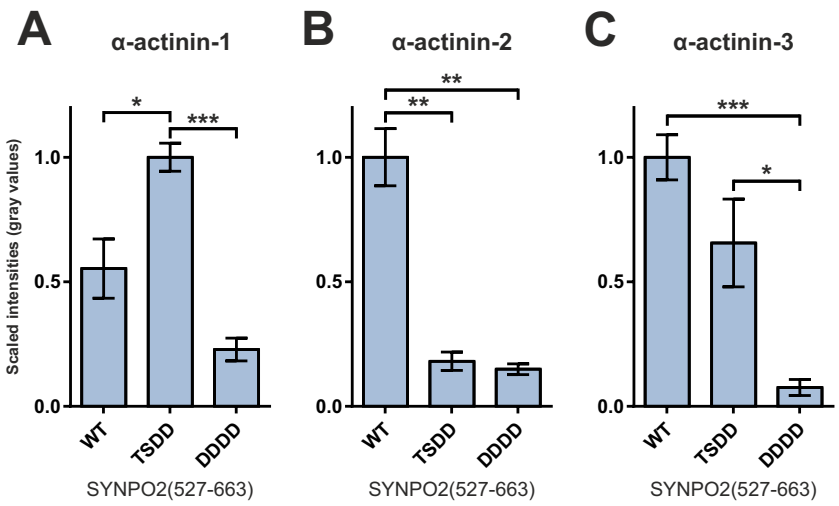


Fig. 3.47: Quantifying α-actinin isoform binding upon phosphorylation in SYNPO2. While SYNPO2 phosphorylations abrogated binding of α-actinin-2 and α-actinin-3, phosphorylations upstream of the PPPY motif ameliorated binding of α-actinin-1 compared to the wild-type SYNPO2 construct. Interestingly, four phosphorylations adjacent to the PPPY motif omitted the interactions between SYNPO2 and α-actinin isoform. Bars represent standard error of the mean (SEM) with n = 3. Statistical testing was performed via two-sample t-tests after distributions were tested for normality via Shapiro-Wilk tests. n.s. $p > 0.05$; * $p \leq 0.05$; ** $p \leq 0.01$; *** $p \leq 0.001$; **** $p \leq 0.0001$.

Subsequent quantification of α-actinin band intensities from the co-IP experiment found that phosphomimetic mutations downstream of the PPPY motif in SYNPO2 impaired binding to not only α-actinin-2, but also α-actinin-3 (Fig. 3.47; B, C). In contrast to α-actinin 2 and 3 binding, these mutations selectively ameliorated the binding between SYNPO2 and α-actinin-1 (Fig. 3.47; A). The phosphomimetic substitutions introduced both up- and downstream of the PPPY motif abrogated α-actinin binding to SYNPO2 in different manners (Fig. 3.47; A–C). However, in the previous chapter, only

phosphomimetic mutations downstream of the PPPY motif found to abrogate dense body and Z-disc targeting of SYNPO2 in smooth and skeletal muscle cells (seesection 3.5.1).

Taken together, these findings lead to two conclusions: On the one hand, phosphorylations adjacent to the PPPY motif may specifically regulate the recruitment of SYNPO2 to Z-discs and stress fiber dense bodies. On the other hand, this regulation might not be attributed to a change in binding of SYNPO2 to α-actinin isoforms. More strikingly, these phosphorylations may affect other F-actin- and α-actitin-binding regions in SYNPO2, or even promote the formation of charge clusters (Zhu & Karlin, 1996), potentially leading to differential targeting of SYNPO2 in smooth and skeletal muscle cells.

3.6 YAP1 activation regulation in muscles

Several studies widely addressed that YAP1 and TAZ, as effector proteins of the Hippo signaling pathway, are crucial mediators for cellular mechanical stress responses (Wada *et al.*, 2011; Calvo *et al.*, 2013; Zou *et al.*, 2020). Hippo signaling pathway-dependent mechanosensing was initially demonstrated in mesenchymal stem cells (MSCs), where matrix stiffness was found to modulate the subcellular localization of YAP1/TAZ (Dupont *et al.*, 2011). Within the past decade, systematic reviews emphasized the importance of YAP1/TAZ as key regulators for mechanosensing and force transduction in muscle tissues (Wackerhage *et al.*, 2014; Fischer *et al.*, 2016). Particularly in skeletal muscle cells, YAP1 was not only found to function as a key player positively regulating myogenesis but also to be essential for regulating muscle fiber size (Watt *et al.*, 2010; Watt *et al.*, 2015; Goodman *et al.*, 2015; Esteves de Lima *et al.*, 2016). In this work, SYNPO2 was characterized as a novel YAP1/TAZ interactor. In addition to its previously characterized multifunctional role, being associated to the cytoskeletal proteins actin, filamin C, and α-actinin in muscle, SYNPO2 emerged to be directly involved in YAP1-associated signaling via Hippo and Rho-ROCK signaling pathways (Lohanadan *et al.*, 2021; Kai *et al.*, 2012; OuYang *et al.*, 2021). Thus, a potential functional role of SYNPO2-dependent YAP1 activity regulation in skeletal and smooth muscle tissues was hypothesized. The potential effects of SYNPO2-dependent YAP1 regulation under mechanical stress in skeletal muscle cells will be addressed in the following chapter.

3.6.1 BAG3, but not SYNPO2 overexpression facilitates YAP1 activation in skeletal muscle cells

In skeletal muscle cells, YAP1 was shown to interact predominantly with SYNPO2 diffusely throughout the cytoplasm, while a fraction of SYNPO2-YAP1 complexes were still recruited to myofibrillar Z-discs (see section 3.4). Thus, SYNPO2 might be involved in indirectly regulating the transcription-promoting activity of YAP1 by facilitating its cytoplasmic retention, as SYNPO2-YAP1 complexes were recruited to the Z-discs. Subsequently, this raised the question whether elevated levels of SYNPO2 might be

capable of downregulating YAP1 activity in either smooth muscles or skeletal muscle cells. As YAP1 activity may be described as a function of YAP1 nuclear translocation, ratios of nuclear and cytoplasmic YAP1 were measured to test whether overexpression of particular SYNPO2 fragments affected the endogenous YAP1 activity (see section 1.4.4, 2.5.1, and 3.2.5). Therefore, different SYNPO2 variants genetically fused to GFP were transfected into C2C12 and A7r5 cells and subsequently, respective nuclear and cytoplasmic YAP1 ratios were compared with cells overexpressing only GFP (Fig. 3.48).

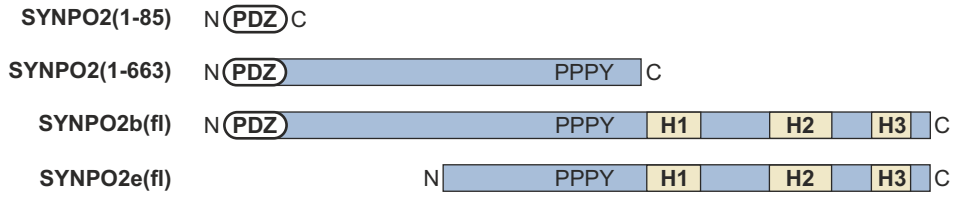


Fig. 3.48: Overview of transiently transfected SYNPO2 constructs. Human eGFP-tagged SYNPO2 constructs overexpressed in skeletal and smooth muscle cells. Amino acids of truncations are indicated in brackets, otherwise, full-length (fl) proteins were used. SYNPO2 truncation constructs lacked different binding regions for cytoskeletal proteins, (see 3.3.1). The fused eGFP-tags are not shown.

While smooth muscle cells overexpressing SYNPO2(1–663) showed decreased levels of YAP1 nuclear translocation, overexpression of other SYNPO2 variants did not affect YAP1 localization (Fig. 3.49; A). Notably, YAP1 nuclear translocation is 5-fold higher in smooth muscle cells compared to skeletal muscle cells. Yet, in skeletal muscle cells, overexpression of SYNPO2 did not alter the degree of YAP1 translocation into the nucleus (Fig. 3.49; B). More strikingly, these findings suggested that neither in skeletal nor in smooth muscle cells, YAP1 activity might be subject to regulation via SYNPO2 expression levels. These data are supported by the fact that SYNPO2 expression intensities measured in both cell types did not correlate with ratios of endogenously expressed nuclear and cytoplasmic YAP1 (data not shown). In 2013, Ulbricht *et al.* have previously proposed that BAG3 associates with the YAP1/TAZ inhibitors LATS1/2 and AMOTL1/2 through its WW domain. In this way, BAG3 is capable of interfering with the activity regulation of YAP1/TAZ signaling by binding to their inhibitors. Thereby, BAG3 might promote a positive regulation of YAP1/TAZ, allowing translocation to the nucleus to activate YAP1/TAZ-mediated gene expression. Notably, depletion of BAG3 in smooth muscle cells attenuated the expression

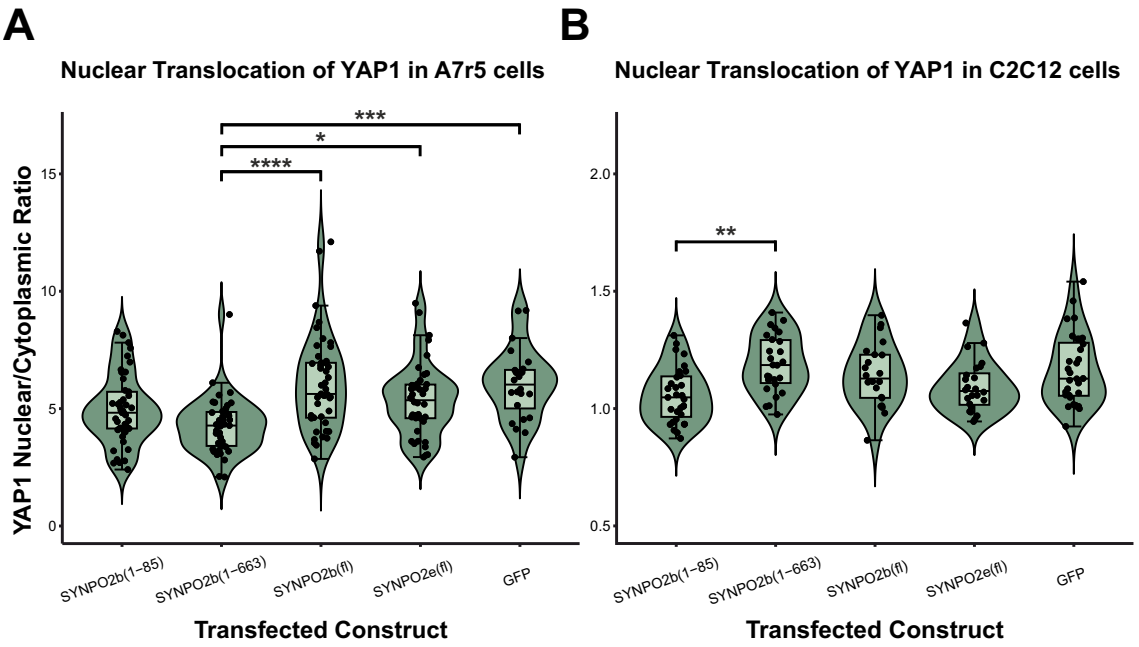


Fig. 3.49: Nuclear translocation of endogenous YAP1 in smooth and skeletal muscle cells. Box and violin plots of average endogenous YAP1 intensities. Intensity ratios of nuclear and cytoplasmic YAP1 functioned as a direct read-out of YAP1 activity. Higher ratios of nuclear and cytoplasmic YAP1 indicate more YAP1 in the nucleus as well as higher YAP1 transcriptional activity. (a) Transfected human GFP-SYNPO2 constructs in A7r5 cells. (B) Transfected human GFP-SYNPO2 constructs in C2C12 cells. A7r5 cells overexpressing SYNPO2(1–663) exhibited decreased nuclear translocation of YAP1, while overexpressing SYNPO2 constructs did not change YAP1 activities in C2C12 cells. Statistical testing was performed via a two-sample t-test with Bonferroni correction after distributions were tested for normality via Shapiro-Wilk, Anderson-Darling and Kolmogorov-Smirnov test. n.s. p> 0.05; * $p \leq 0.05$; ** $p \leq 0.01$; *** $p \leq 0.001$; **** $p \leq 0.0001$.

of YAP/TAZ target genes (Ulbricht *et al.*, 2013). Moreover, a complex of BAG3 and Hsp70 was found to associate with YAP1 via LATS1, and AMOTL2 (Baldan *et al.*, 2021). These findings suggest that BAG3 may act as a positive regulator of YAP1/TAZ-mediated transcription by potentially sequestering the inhibitors, hence facilitating the activation of YAP1/TAZ transcriptional activity (Ulbricht *et al.*, 2013; Baldan *et al.*, 2021). To assess potential effects of BAG3 overexpression on the YAP1 activity, subsequent experiments were performed in both smooth and skeletal muscle cells. In these experiments, the nuclear translocation of YAP1 was measured upon overexpression of human wild-type BAG3 fused to GFP, referred to as BAG3(fl). Since it was hypothesized that BAG3 might regulate YAP1 activity through WW domain interactions with YAP1 inhibitors, a BAG3 mutant construct, BAG3(fl) WAWA, harboring amino acid substitutions in the WW domain was generated (see section 3.4.1). In smooth muscle cells, neither the overexpression of BAG3(fl) nor BAG3(fl) WAWA did result in changes of YAP1 nuclear translocation compared to smooth muscle cells

overexpressing GFP, SYNPO2b(fl) or SYNPO2e(fl), respectively (Fig. 3.50; A). In contrast, skeletal muscle cells over-expressing BAG3(fl) showed a significant increase in YAP1 activity compared to cells overexpressing SYNPO2b(fl), SYNPO2e(fl), or a GFP control (Fig. 3.50; B). Interestingly, this effect was attenuated in cells overexpressing the BAG3(fl) WAWA construct (Fig. 3.50; B). These findings suggest that BAG3 might directly regulate YAP1 activity in skeletal muscle cells, whereas SYNPO2 may only exert indirect effects.

As these effects did not occur upon overexpression of the BAG3 WAWA mutant, one might conclude that BAG3 WW domain interactions mainly orchestrate the YAP1 activation by binding to Hippo signaling pathway-related inhibitors of YAP1, such as LATS1 or AMOTL2.

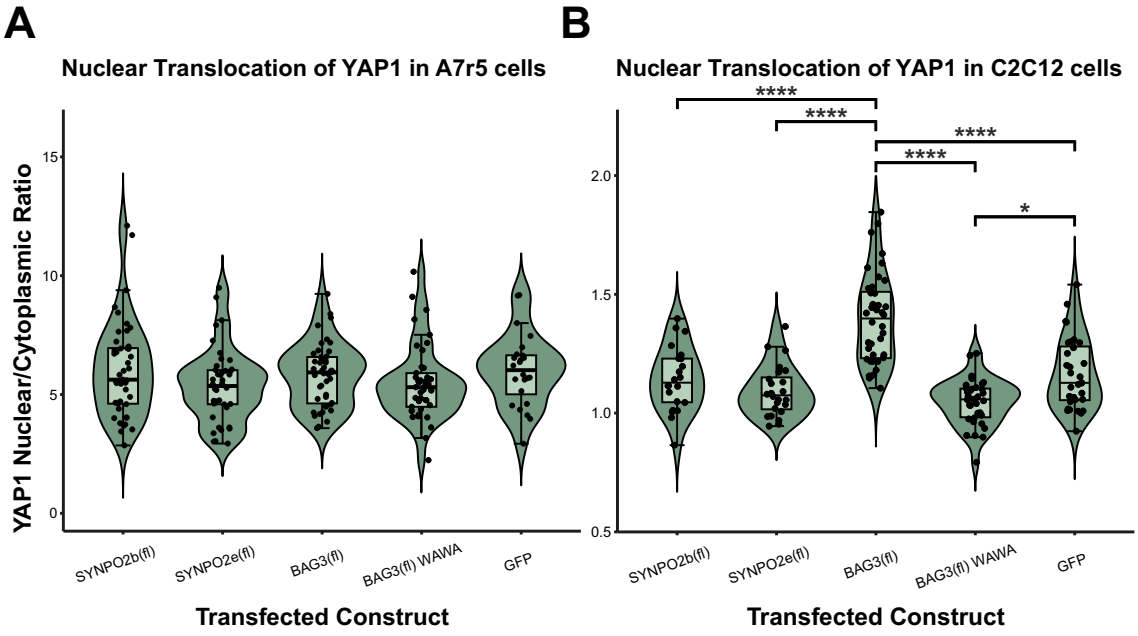


Fig. 3.50: Nuclear translocation of overexpressed YAP1 in smooth and skeletal muscle cells. Box and violin plots of average endogenous YAP1 intensities. Intensity ratios of nuclear and cytoplasmic YAP1 functioned as a direct read-out of YAP1 activity. Higher ratios of nuclear and cytoplasmic YAP1 indicate more YAP1 in the nucleus as well as higher YAP1 transcriptional activity. (A) Transfected human GFP-SYNPO2 and GFP-BAG3 constructs in A7r5 cells. (B) Transfected human GFP-SYNPO2 and GFP-BAG3 constructs in C2C12 cells. A7r5 cells overexpressing BAG3 constructs did not exhibit a change in nuclear translocation of YAP1, while overexpressing BAG3(fl) construct resulted in a tremendous elevated YAP1 activity in C2C12 cells. Statistical testing was performed via a two-sample t-test with Bonferroni correction after distributions were tested for normality via Shapiro-Wilk, Anderson-Darling and Kolmogorov-Smirnov test. n.s. $p > 0.05$; * $p \leq 0.05$; ** $p \leq 0.01$; *** $p \leq 0.001$; **** $p \leq 0.0001$.

3.6.2 Muscle damage exerted by EPS regulates YAP1 activation in skeletal muscle cells

To date, mechanical stimulation applied to cells has been demonstrated to increase YAP1 nuclear translocation and thus, YAP1 activity (Elosegui-Artola *et al.*, 2017). In order to further elucidate the role of YAP1 activation in skeletal muscle cells, it was investigated whether YAP1 might be regulated upon induction of mechanical stress. To achieve this, skeletal muscle cells were subjected to EPS in order to induce mechanical damage and eventually sarcomeric remodeling (Fig. 3.52) (Orfanos *et al.*, 2016).

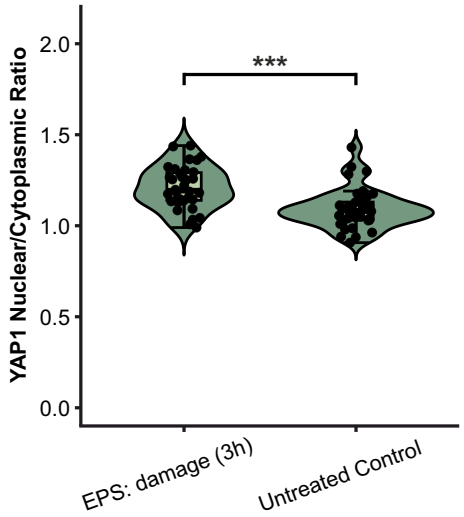


Fig. 3.51: Nuclear translocation of endogenous YAP1 in mechanically damaged C2C12 myotubes. Box and violin plots of average YAP1 intensities. Intensity ratios of nuclear and cytoplasmic YAP1 functioned as a direct readout of YAP1 nuclear import and YAP1 activity. Higher ratios of nuclear and cytoplasmic YAP1 indicate more YAP1 in the nucleus and higher YAP1 transcriptional activity. Mechanical damage via EPS resulted in increased nuclear import of YAP1 in myotubes. Statistical testing was performed via a two-sample t-test with Bonferroni correction after distributions were tested for normality via Shapiro-Wilk, Anderson-Darling and Kolmogorov-Smirnov test. n.s. $p > 0.05$; * $p \leq 0.05$; ** $p \leq 0.01$; *** $p \leq 0.001$; **** $p \leq 0.0001$.

Fluorescence microscopic analysis of untreated myotubes showed intact Z-discs which appeared as narrow, confined structures within myofibrils, indicating the presence of intact sarcomeres (Fig. 3.52; A, B). In contrast, damage in the myofibrillar apparatus induced by EPS exhibited areas of faded, disrupted myofibrillar Z-discs, each spanning around two to five sarcomeres (Fig. 3.52; C, D, arrowheads). These structures, previously characterized as lesions, indicated a focal disintegration of sarcomeres as a result of the mechanical damage and remodeling processes exerted by EPS

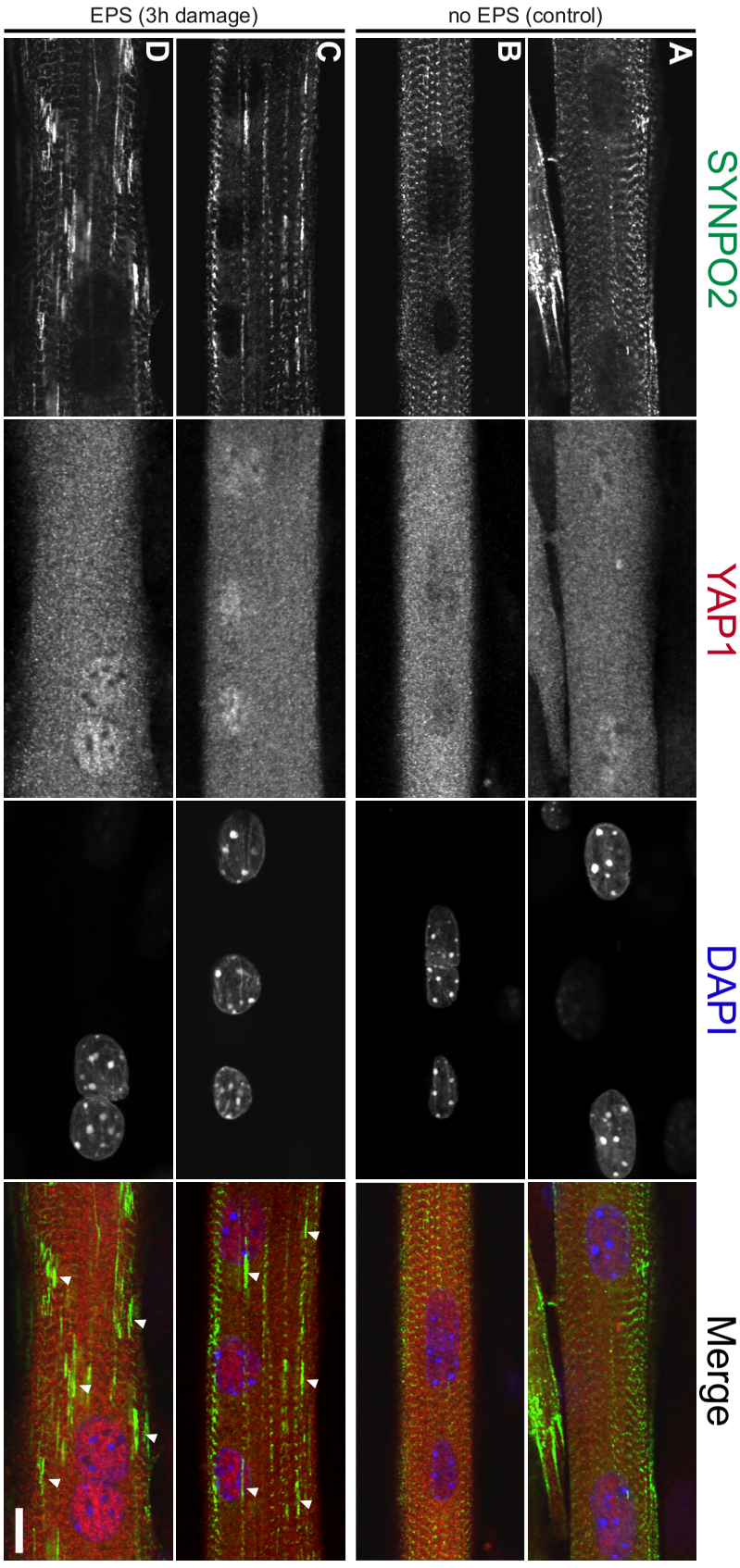


Fig. 3.52: YAP1 localization in skeletal muscle cells under mechanical stress. The row labels on the left side indicate the treatment conditions and duration, either without EPS (control) or after EPS treatment (damage 3h). The column labels show the fluorescence channels for SYNPO2, YAP1, nuclei (DAPI), and an overlay of signals (Merge). While untreated myotubes exhibited myofibrils with intact Z-discs, EPS treatment resulted in disruption of Z-discs in myofibrils (arrows). Compared to untreated cells (A, B), cells treated with EPS showed elevated levels of YAP1 localization in the nuclei (C, D). Scale bar, 10 µm, respectively.

(Orfanos *et al.*, 2016). Immunostaining against YAP1 revealed its accumulation in the nucleus upon mechanical damage (Fig. 3.52; A–D). To quantify the extent of nuclear translocation upon EPS treatment, YAP1 ratios in the nuclei and cytoplasm of myotubes were measured as described above (Fig. 3.51). EPS-treated cells clearly showed increased nuclear translocation of YAP1 compared to the untreated control which suggested that, as a result of mechanical damage and subsequent sarcomeric remodeling, YAP1 nuclear import is facilitated by simultaneously upregulated processes, such as the activation of the CASA complex.

3.7 Novel mutations in human SYNPO2 abrogate binding to α-actinin, eventually leading to disease

More recently, a novel discovery described two pathologically relevant, homozygous mutations in SYNPO2 in patients with childhood onset steroid-resistant nephrotic syndrome (SRNS), a form of kidney disease (Mao *et al.*, 2021). One of the discovered SYNPO2 mutations is a misssense mutation (p.A1134T), while the other mutation truncates the C-terminus of SYNPO2 (p.K1124*), both causing SRNS. These mutations occur in the sixth exon of SYNPO2 (exon 6, amino acids 1085–1261), which was found to be expressed in both podocytes and mesangial, smooth muscle-like cells. Immunofluorescence-labeled cryosections of kidney tissue from rat and adult human revealed a specific localization of SYNPO2 only in mesangial cells, where it was associated with α-actinin and filamin A-containing F-actin filament structures (Mao *et al.*, 2021). To examine potential effects of those mutations in SYNPO2 on its binding to different α-actinin isoforms, and thus eventually leading to disease, protein pulldown assays were performed. Therefore, short truncation variants of SYNPO2 containing the C-terminal portion of the exon 6, referred to as SYNPO2(1085–1261) fused to a GST-tag were generated.

The pulldown assays confirmed a direct interaction of the independent α-actinin-binding region within the exon 6 of SYNPO2 with α-actinin-1, α-actinin-2, and α-actinin-4. Both, α-actinin-1 and α-actinin-4 represent non muscle α-actinin isoforms expressed in podocytes (Fig. 3.7.1; A). Controls carried out did not exhibit unspecific binding (Fig. 3.7.1; B). The immunoblot analysis with regard to band intensities revealed that different amounts of the respective α-actinins bound to wild type SYNPO2, indicating differences in binding affinities between α-actinin-2, which bound strongest, and the weakly bound α-actinin-4 (Fig. 3.7.1; A, left panels). More strikingly, both mutations of SYNPO2, A1134T and K1124* impaired binding to α-actinin, leading to decreased band intensities in the pulldown experiments, respectively (Fig. 3.7.1; A, right panels). In order to quantify the extent of reduction caused by the SYNPO2 mutations, α-actinin band intensities from the pulldown assays were measured. The concentrations of bound α-actinin were normalized between the pulldowns and values were compared relative to α-actinin-2 bound to wild-type SYNPO2, which was set to 100% (Fig. 3.7.2).

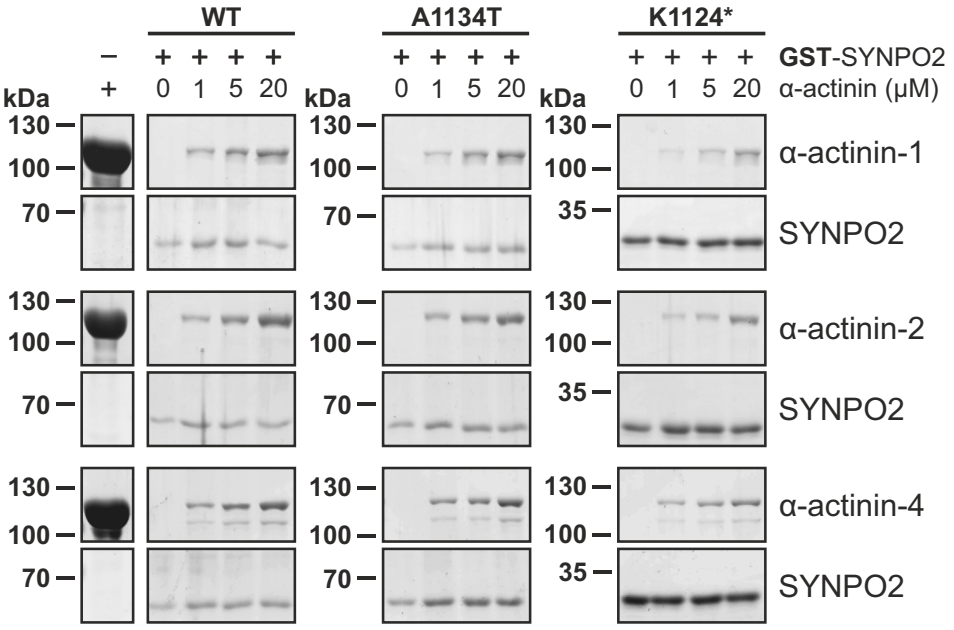


Fig. 3.53: Protein pulldown assay of SYNPO2 with α-actinins. Digitally rearranged SDS-gels. Sample composition is outlines on top of the panels, immunotags fused to proteins for antibody detection are printed in bold. The band migration pattern of molecular weight markers is shown on the left. (A) GST-tagged SYNPO2 wildtype (WT), missense mutant (A1134T) or truncation mutant (K1124*) constructs coupled to GSH-beads, incubated with increasing concentrations of α-actinin-1, 2, and 4. SYNPO2 mutants showed reduced amounts of α-actinins bound. In general, α-actinin-4 showed the weakest interaction with SYNPO2, whereas α-actinin-2 showed a strong interaction. (B) Controls with GST coupled to beads instead of SYNPO2. Background of unspecific interactions with α-actinin was used for correction during image analyses.

A subsequent quantification analysis of the protein pulldown assays revealed that the binding of the SYNPO2 truncation mutation K1124* to all tested α-actinins is significantly decreased (Fig. 3.7.2). In contrast, the SYNPO2 missense mutation A1134T only showed a significant reduction in binding to α-actinin-2, but not to α-actinin-1, nor α-actinin-4.

This indicated that both mutations affected the interaction between α-actinin and SYNPO2 in a different manner: the C-terminal deletion within exon 6 of SYNPO2 abolishes the interaction of SYNPO2 with non-muscle α-actinin isoforms expressed in podocytes. The A1134T substitution mutation in SYNPO2 impairs binding between non-muscle α-actinin isoforms and SYNPO2. As a result, both mutations might cause a loss of function of the α-actinin binding region encoded by the exon 6 of SYNPO2. This loss of function was found to be related to a α-actinin dysregulation, eventually affecting the α-actinin localization to the actin cytoskeleton in cells expressing SYNPO2 mutants (Mao *et al.*, 2021). Based on additional experiments, it was speculated that migration

defects in mesangial cells via an ARP2/3 related pathway as well as actin cytoskeleton remodeling due to SYNPO2 mutations contribute to the pathogenesis of SRNS (Mao *et al.*, 2021).

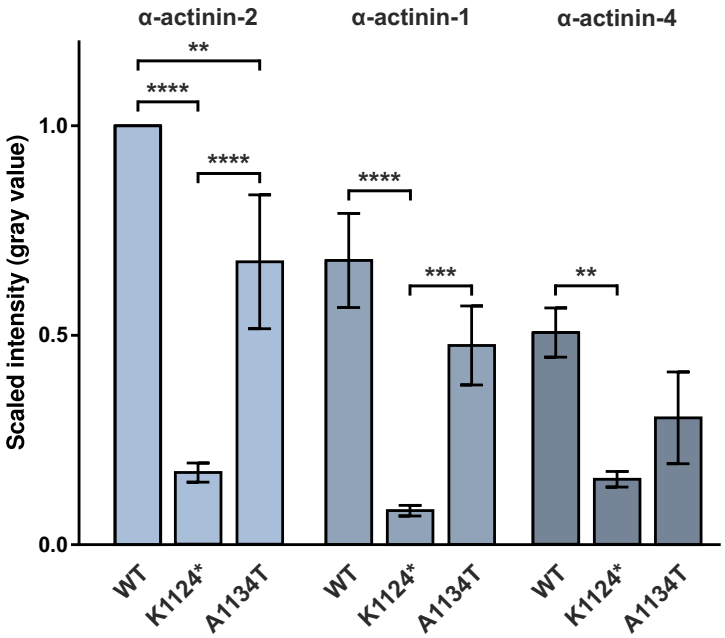


Fig. 3.54: Quantifying α-actinins bound to SYNPO2 exon 6 constructs. Band intensities of α-actinin-1, 2, and 4 from pulldown assays were measured and normalized to SYNPO2 exon 6 (amino acids 1085–1261) wildtype (WT), SYNPO2 missense mutant (A1134T), or SYNPO2 truncation mutant (K1124*) constructs bound to beads. Ratio values are relative to α-actinin-2. Both SYNPO2 mutants showed reduced amounts of α-actinins bound. Notably, only the SYNPO2 K1124* mutant showed significantly impaired binding for all α-actinins, including α-actinin-4, associated with SRNS. Bars represent standard error of the mean (SEM) with n = 3. Statistical testing was performed via a one-way ANOVA after distributions were tested for normality via Shapiro-Wilk. n.s. p> 0.05; * $p \leq 0.05$; ** $p \leq 0.01$; *** $p \leq 0.001$; **** $p \leq 0.0001$.

Chapter 4

Discussion

4.1 Novel interactors bind to the PDZ domain of SYNPO2

The main objective of this work was to elucidate the role of the Z-disc- and dense body-associated adapter protein SYNPO2 and its involvement in the signaling networks of both, smooth and skeletal muscle cells. As a structurally distinct element found in three of the six putative SYNPO2 isoforms characterized, the N-terminal PDZ domain represents a platform for PPIs critical to SYNPO2's function (see section 1.4.2) (Linnemann, 2011; De Ganck *et al.*, 2008). PDZ domains are not only capable of binding to C-termini of putative ligands, but also they may form homo- and heterodimers with other PDZ domains (Ivarsson, 2012). In order to identify new interaction partners that engage in PDZ domain-mediated PPIs with SYNPO2, it was crucial to study its potential for dimerization. A hallmark study found that 43 of the tested 157 PDZ domains engaged in homo- or heterodimerization (Chang *et al.*, 2011). The dimerization of PDZ domains is regarded to be involved in regulatory processes and might facilitate the assembly of larger protein complexes, directly linking Z-disc- or dense body-associated proteins, such as SYNPO2, to signaling pathways (Wu *et al.*, 2007, Xu *et al.*, 1998; Chen *et al.*, 2008). In order to identify new interaction partners engaging in PDZ domain-mediated PPIs with SYNPO2, it was therefore important to investigate its potential for dimerization in this study.

In this study presented here, SEC experiments of purified PDZ domains from SYNPO2 and another synaptopodin family protein, SYNPO2L, indicated the exclusive presence of monomers under the conditions tested. Further experiments in which a potential PDZ domain dimerization was examined via chemical crosslinking, also did not reveal the formation of protein complexes under different conditions including temperature and ionic strength, indicating that both, SYNPO2 and SYNPO2L are not engaged in PDZ

domain-mediated homo- or heterodimerization. However, the study by Chang *et al.* (2011) also revealed that the vast majority of PDZ domains does not engage in dimerization. In particular, Z-discs harbor a variety of other PDZ domain-containing proteins from the actin and α-actinin-associated PDLIM family, including PDLIM3, PDLIM5, the LIM domain-binding protein 3 (LDB3/PDLIM6/ZASP), and PDLIM7 (enigma) which may represent potential candidates for PDZ-PDZ dimerization screening (Xia *et al.*, 1997; Zhou *et al.*, 1999; Klaavuniemi *et al.*, 2004; Guy *et al.*, 1999; Nakagawa *et al.*, 2000; Faulkner *et al.*, 1999). Therefore, to shed light onto the interactome of the SYNPO2 PDZ domain, extensive screening via phage display assays or Y2H assays is may assist to unravel whether SYNPO2 might engage in dimerization with other PDZ domain-containing, Z-disc-associated proteins. To further investigate and eventually understand the role of the PDZ domain for SYNPO2 engaging in PPIs with C-terminal peptides of ligands, two stepping stones were elemental: (1) the identification of new interaction partners of its PDZ domain and (2) the classification of its preferred recognition motif in order to eventually predict interactions with further putative ligands. Since PDZ domains are capable of recognizing a variety of motifs beyond canonical binding, classification and prediction of a particular PDZ-BM specific for SYNPO2 might be cumbersome (Tonikian *et al.*, 2008; Velthuis *et al.*, 2011; Münz *et al.*, 2012; Gfeller, 2012; Zeng *et al.*, 2016). Previous efforts to predict proteome-wide PDZ-BM specificities of human PDZ domains were published under the PDZome database 1.0 & 2.0 (Belotti *et al.*, 2013; Castro-Cruz *et al.*, 2023). To date, these studies did not yet include data featuring the PDZ domains of the synaptopodin family proteins SYNPO2 and SYNPO2L.

A Y2H screen performed prior to this study identified the tumor suppressor TUSC1, the intermediate filament protein synemin, and VPS18 as new potential ligands. These proteins harbor a C-terminal PDZ-BM comprised of the amino acids WL_{COOH} or WF_{COOH} at positions P_{-1} and P_0 (Fig. 3.3). Bezerra (2015) demonstrated that the C-termini of both VPS18 and synemin specifically bind the PDZ domain of SYNPO2 (see section 3.2). Isothermal titration calorimetry (ITC) experiments and crystallization studies determined a perpendicular binding of octapeptides to the PDZ domain of SYNPO2. These octameric peptides corresponded to the PDZ-BMs of synemin and VPS18 with binding affinities of 8.84 ±0.86 µM, 0.75 ±0.10 µM, respectively. These

findings indicate that the PDZ domain of SYNPO2 is specific for tryptophan-containing PDZ-BM class I, III, or class IVa motifs (see Appendix B) (Bezerra, 2015). Furthermore, an *in silico* prediction database analysis carried out for this work revealed that the transcription coactivators YAP1 and TAZ share a PDZ-BM with TUSC1 and VPS18 (Hui & Bader, 2010; Hui *et al.*, 2013). Both, YAP1 and its paralog TAZ proteins were subsequently identified as novel SYNPO2 PDZ domain interaction partners in co-IP and pulldown experiments (see section 3.1.2). These findings were supported by additional ITC experiments which revealed a binding affinity between the PDZ domain of SYNPO2 and an octapeptide corresponding to the PDZ-BM of both YAP1 and TAZ of 5.33 ±0.78 µM (Djinovic-Carugo, personal communication). One may presume that YAP1 or TAZ might also engage in perpendicular binding with the PDZ domain of SYNPO2. These findings are in line with preliminary affinity purification-coupled mass spectrometry (AP-MS) experiments using the PDZ domain of SYNPO2 incubated with C2C12 skeletal muscle cell lysates which independently identified synemin, YAP1, and TAZ to be associated with SYNPO2 (Assent, 2020; data not published). Intriguingly, recent studies highlighted a further link of YAP1 and TAZ to two other Z-disc-associated proteins: PDLIM5 and the filamin C-interacting protein disheveled-2 (DVL2) involved in the Wnt signaling pathway. Similar to SYNPO2, both DVL2 and PDLIM5 are expressed in skeletal muscles, harbor a PDZ domain, and were also found to bind the C-termini of YAP1 and TAZ (Han *et al.*, 2021; Varelas *et al.*, 2010; Elbediwy *et al.*, 2018).

These findings suggest that the novel interaction partners VPS18, synemin, YAP1, and TAZ might link SYNPO2 to (1) membrane vesicle trafficking and autophagosome formation as part of the CASA machinery involved in BAG3-mediated macroautophagy, (2) the synemin-associated intermediate filament system, and (3) the Hippo signaling pathway involved in myogenesis, muscle regeneration and regulation of muscle fiber size (Ulbricht *et al.*, 2013; Lohanadan *et al.*, 2023; Goodman *et al.*, 2015; Watt *et al.*, 2010; Watt *et al.*, 2015).Previous research suggested a direct association between the Hippo signaling pathway protein YAP1 and BAG3 implying a link between the Hippo signaling pathway and the CASA machinery (Baldan *et al.*, 2021). However, biochemical interaction assays in terms of co-IPs in this thesis did not reveal a direct molecular interaction between YAP1 and BAG3 as initially proposed by Baldan *et al.* (2021). The capability of SYNPO2 to link the Hippo signaling pathway to BAG3-mediated

macroautophagy was further investigated biochemically in this thesis (see section 3.2): Similar to its simultaneous interaction with VPS18 and BAG3, co-IP experiments demonstrated that SYNPO2 was not only capable of simultaneously binding to BAG and YAP1 *in vitro*, but also BAG3 and TAZ. This formation of ternary YAP1/TAZ-SYNPO2-BAG3 complexes involves two independent associations, one between the PPPY motif of SYNPO2 and the BAG3 WW domain, and a second between the PDZ-BM of YAP1/TAZ and the PDZ domain of SYNPO2 (Fig. 3.6 and 3.7). Hence, this indicates a potential function of SYNPO2 as an adapter linking the Z-disc to the Hippo signaling pathway transcriptional coactivators YAP1/TAZ and the CASA machinery key player BAG3.

4.2 YAP1 and TAZ interactions with the PPPY motif of SYNPO2

In this work, a protein pulldown experiment demonstrated that YAP1 interacts with SYNPO2 even in absence of its PDZ-BM (see section 3.1.2). Based on these findings, it was speculated whether the interaction between SYNPO2 and YAP1 was mediated by other existing binding motifs in YAP1. As a distinct element of YAP1, the WW domain was first identified as novel protein domain (Sudol *et al.*, 1995, Bork & Sudol, 1995). Based on different types of proline-rich SLIMs recognized, WW domains were further categorized (Otte *et al.*, 2003; Schleinkofer *et al.*, 2004). Other studies characterized human YAP1 isoforms according to the presence of either one (YAP1–1) or two (YAP1–2) WW domains (Sudol, 2013; Guo *et al.*, 2020).

Here, an amino acid sequence alignment of BAG3 and other proteins associated with the Hippo signaling pathway revealed a high degree of similarity between the WW domains of BAG3, YAP1, and TAZ (Fig. 3.14). Previously classified as group I domains, these WW domains were found to be highly specific for PPXY-containing SLIMs (see Appendix B) (Otte *et al.*, 2003; Sudol *et al.*, 2001; Salah *et al.*, 2012). Additional co-IP experiments in this thesis demonstrated that similar to BAG3, both YAP1 and TAZ specifically bind the PPPY motif of SYNPO2 (Fig. 3.15 and 3.16). In contrast to the PDZ domain, the PPPY motif is present in all human SYNPO2 isoforms (Linnemann, 2011, pp. 61–65). In line with these experiments, peptide binding assays and additional co-IPs found clear support for the WW domain of TAZ, but also for both YAP1 WW domains to independently recognize the PPPY motif, but not similarly composed motifs in SYNPO2 (Fig. 3.37). Even though the binding to SYNPO2 is mediated via both the WW domains and PDZ-BM of YAP1 and TAZ, the stoichiometry and composition of this complex formation remains elusive. Firstly, results presented here indicate the formation of a ternary complex between YAP1/TAZ, SYNPO2, and BAG3 (Fig. 4.1; A). Secondly, additional findings allow for hypothesizing whether SYNPO2-YAP1/TAZ complexes might be composed of either a single YAP1/TAZ molecule simultaneously binding to both, the PDZ domain and the PPPY motif of SYNPO2, or alternatively, two YAP1/TAZ molecules binding independently to these SYNPO2 binding sites (Fig. 4.1; B, C). More recently, the cysteine residues in YAP1 (γ- and δ-isoforms) and TAZ were identified to be elemental for the

formation of YAP1/TAZ homo- and heterodimers *in vitro* and *in vivo* (Khanal *et al.*, 2018).

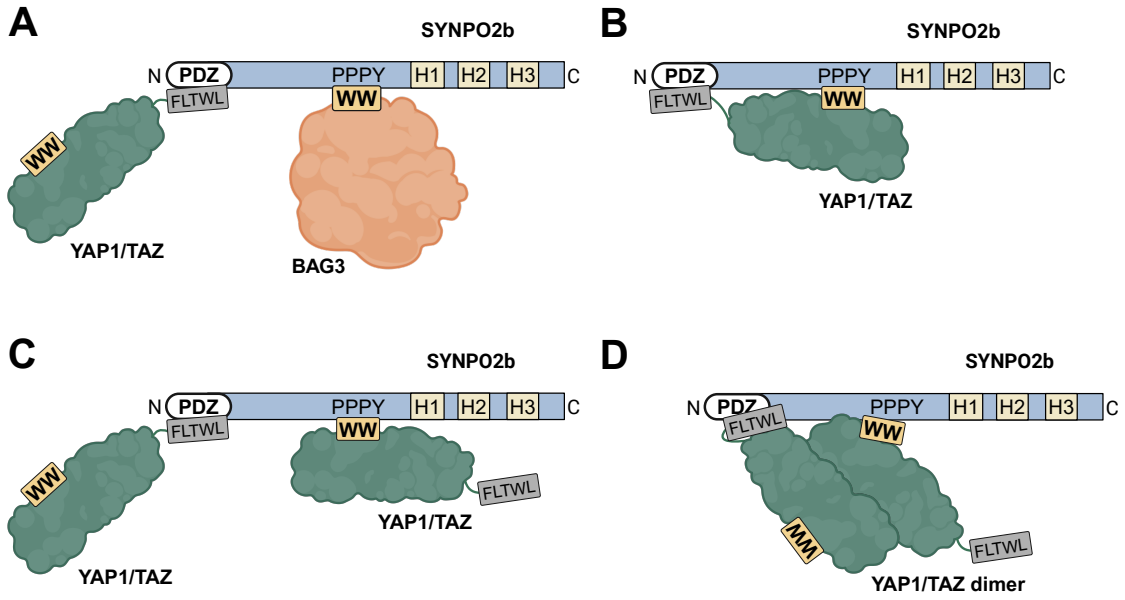


Fig. 4.1: Possible binding modes between YAP/TAZ and SYNPO2. (A) Formation of a ternary complex comprised of YAP1/TAZ-SYNPO2-BAG3 which was revealed through co-IP experiments (see section 3.2). (B) Formation of a 1:1 SYNPO2-YAP1/TAZ complex via simultaneous interactions via PDZ domain and PPPY motif. (C) Formation of a 1:2 SYNPO2-YAP1/TAZ complex with independent binding of YAP1/TAZ to the PDZ domain and PPPY motif of SYNPO2. (D) Formation of a 1:2 SYNPO2-YAP1/TAZ complex with disulfide bond-mediated dimerization of YAP1/TAZ. Created with BioRender.com.

Hence, the formation of SYNPO2-YAP1/TAZ complexes might also potentially involve the presence of YAP1/TAZ dimers (Fig. 4.1;D). However, to elucidate its composition, additional protein biochemical assays, such as SEC and protein crosslinking experiments, are required to obtain accurate data about the stoichiometry of these SYNPO2-YAP1/TAZ complexes. Notably, these hypothesized complex formations as well as a ternary complex require cells to express at least one of the SYNPO2 isoforms a, b, or c (Linnemann, 2011; De Ganck *et al.*, 2008).

This "dual-site binding specificity" of the Hippo signaling pathway effectors for (1) the PDZ domain and (2) a PPPY motif was previously characterized between TAZ and the protein DVL2 (Varelas *et al.*, 2010). Additional evidence proposed the link between the Hippo pathway and the Wnt signaling pathway to be crucial for modulating skeletal muscle development and regeneration processes (Moreira-Pais *et al.*, 2020, pp. 399–400; Brack *et al.*, 2008; Park *et al.*, 2015). This interplay is mediated by a stabilization of TAZ through DVL2 thus negatively regulating non-canonical Wnt signaling effectors,

such as β-catenin (Varelas *et al.*, 2010). The novel interactions between SYNPO2, YAP1 and TAZ identified here may hence imply a similar role for SYNPO2 by stabilizing cytoplasmic YAP1/TAZ. In this way, SYNPO2 might function as a regulatory element for muscle development potentially impeding Hippo signaling-mediated myoblast proliferation. Several studies postulated the C-terminal PDZ-BM to be important for nuclear import of YAP1/TAZ, since nuclear translocation is required to mediate the transcription of Hippo signaling downstream target genes (Oka & Sudol, 2009; Remue *et al.*, 2010; Kim *et al.*, 2020). However, the exact physiological role of these interactions is poorly understood.

Intriguingly, transfection assays in this work highlighted that the PDZ-BM is required for YAP1 nuclear translocation (see section 3.1.5). More strikingly, YAP1–1 and YAP1–2 show differences in A7r5 and C2C12 cells, potentially indicating distinct, cell type-specific roles of YAP1. A similar conclusion was reached by Guo *et al.* (2020), suggesting differential regulatory roles of YAP1 isoforms, e.g. for cell proliferation. Conspicuously, BiFC assays in smooth and skeletal muscle cells performed here did not reveal differences in intracellular targeting between SYNPO2-YAP1–1 and SYNPO2-YAP1–2 complexes (see section 3.3). Furthermore, these assays demonstrated that SYNPO2-YAP1 complexes targeted to stress fiber dense bodies and Z-discs in smooth and skeletal muscle, respectively, and that this targeting was solely dependent on SYNPO2 and required its α-actinin-binding regions (Fig. 3.29, 3.30; 3.34 3.35). Therefore, these findings support the previously suggested a primary role of SYNPO2 to stabilize cytoplasmic YAP1. Yet, it remains obscure whether this stabilization was mediated by the PDZ domain or the PPPY motif of SYNPO2. Further BiFC assays with SYNPO2 constructs lacking the PDZ domain (e.g. SYNPO2e) may address to unravel the underlying mechanisms of SYNPO2-YAP1 complex targeting in skeletal and smooth muscle cells.

4.3 SYNPO2 phosphorylations regulate binding of WW domain-containing proteins to its PPPY motif

Since BAG3, YAP1, and TAZ were found to specifically bind the PPPY motif, additional assays were performed revealing that BAG3 competes with both YAP1 and TAZ for SYNPO2 (see section 3.2.2). More strikingly, these experiments demonstrated that competitive binding of YAP1 and BAG3 at the PPPY motif is strongly influenced by the presence of one or two YAP1 WW domains, so that BAG3 could displace YAP1–1 and TAZ, but not YAP1–2 (Fig. 3.17, 3.18, and 3.19). These findings are in line with previous phage display and ITC experiments highlighting the WW domains of YAP1 as independent units with individual properties and binding preferences for PPPY motifs of its interactors LATS1/2 (Iglesias-Bexiga *et al.*, 2015). Other research pinpointed the WW2 domain in YAP1 as instrumental for forming regulatory YAP1–2-LATS-AMOT complexes by reinforcing the interaction between YAP1 and LATS (Guo *et al.*, 2020). Interestingly, that study particularly reported the YAP1–2 isoforms to be less stable at the protein level than the YAP1–1 isoforms (Guo *et al.*, 2020).

According to these findings, the presence of tandem WW domains in YAP1 might also have profound consequences for SYNPO2 binding, potentially affecting regulatory mechanisms involving BAG3 and YAP1 at the PPPY motif. Moreover, these results support a suggested stabilization of YAP1–2 via SYNPO2 *in vivo* since this YAP1 variant was not displaced by BAG3 in the competitive binding assays, as reported here. Regarding the limitations of co-IP experiments to assess exact binding properties to the PPPY motif of SYNPO2, further ITC experiments are required to determine the binding affinities for each individual WW domain of BAG3, YAP1, and TAZ.

Furthermore, studies reported phosphorylations in proximity to the PPPY motif of murine SYNPO2 mediated by CAMKII and PKA (Faul *et al.*, 2007). These phosphorylations facilitate the interaction between SYNPO2 and the regulatory adapter protein 14-3-3β associated with a number of phosphatases and other kinases (Faul *et al.*, 2005). Although not all phospho-acceptor sites are conserved even between murine and human SYNPO2, it was hypothesized in this thesis that phosphorylating the remaining, conserved phospho-acceptor site (T610) may still be capable of affecting interactions of SYNPO2 with other binding partners. To this end, peptide array

experiments of the SYNPO2 region proximal to the PPPY motif including mutations from tyrosine and serine to the phospho-mimicking aspartic acid demonstrated attenuated and abolished WW domain-binding properties. More precisely, downstream phosphorylations regulated WW domain-dependent binding of BAG3, YAP1 and TAZ, whereas phosphorylations upstream only affected the binding of BAG3 and YAP1 WW domains (Fig. 3.37). Interestingly, the interaction between a YAP1 tandem WW domain construct and SYNPO2 peptides was not affected by phosphorylations, indicating a more complex mechanism regulating the displacement of YAP1 through BAG3 or *vice versa*. Additional co-IP experiments presented here are in line with these findings, as SYNPO2 phosphorylations regulated a replacement of BAG3 by YAP1–1. Intriguingly, SYNPO2 phosphorylations proximal to the PPPY motif have been identified to be predominantly downregulated upon contraction-induced mechanical stress exerted by exercise or EPS (Potts *et al.*, 2017; Hoffman *et al.*, 2015; Reimann *et al.*, 2017). However, a respective regulation of these phospho-acceptor sites was not determined significant (see Tab. 3.1) (Potts *et al.*, 2017; Hoffman *et al.*, 2015). Notably, the PPPY motif is present in all human SYNPO2 isoforms, thus phosphorylations identified proximal to this site might affect all SYNPO2 isoforms expressed in both, cross-striated and smooth muscle cells (Linnemann, 2011; De Ganck *et al.*, 2008). Taken together, it remains elusive whether a dephosphorylation of SYNPO2 at the PPPY motif in response to mechanical stress is required *in vivo* to strengthen the interaction between BAG3 and SYNPO2.

Other studies showed that phosphorylations of YAP1, TAZ, and BAG3 similarly affected interactions with their respective binding partners. A considerable amount of literature points out different kinases, such as the tumor suppressor LATS1/2, NLK, and cyclin-dependent kinases (CDKs), to function as pivotal regulatory elements for the downstream Hippo pathway effectors YAP1/TAZ (Basu *et al.*, 2003; Zhao *et al.*, 2007; Lei *et al.*, 2008; Cho *et al.*, 2018; Moon *et al.*, 2017; Zhao & Yang, 2014). In particular, LATS kinase-mediated phosphorylations of the respective YAP1/TAZ phospho-acceptor sites S127/S89 promote their cytoplasmic retention, inactivation, and degradation by binding to 14-3-3 proteins (Zhao *et al.*, 2007; Hao *et al.*, 2008; Oka *et al.*, 2008; Lei *et al.*, 2008). Additionally, LATS1/2, Protein kinase B (PKB/Akt), and PRP4K were found to phosphorylate various other sites in YAP1/TAZ, including S164/S117 located in the respective WW domains. These phosphorylations are capable of

regulating YAP1/TAZ and inhibiting binding to PPXY motifs (Zhao *et al.*, 2010; Cho *et al.*, 2018; Clarke *et al.*, 2021). Furthermore, phosphorylations of BAG3 at two specific sites (T285 and S289) were found to weaken its interaction with HspB8 (Wördehoff, 2020, p. 46). Several phosphorylations in BAG3 were proposed to specifically regulate CASA machinery formation and association with translation factors (Höhfeld, personal communication). These findings provide substantial evidence for an intricate regulation mechanism of interactions between SYNPO2, YAP1/TAZ and BAG3 involving phosphorylations of all binding partners. Moreover, fluorescence microscopy-based quantifications presented here showed that SYNPO2 phosphorylations downstream of the PPPY motif may specifically regulate its recruitment to Z-discs and stress fiber dense bodies (see section 3.5.1). However, biochemical assays did not confirm those phosphorylations to account for the abrogated SYNPO2 targeting observed in skeletal and smooth muscle cells. Accordingly, phosphorylations adjacent to the PPPY motif may affect other F-actin- and α-actinin-binding regions in SYNPO2, or even promote the formation of charge clusters, impairing the targeting of SYNPO2 in smooth and skeletal muscle cells. Interestingly, the phosphorylations in murine SYNPO2 characterized by Faul *et al.*, (2005, 2007) not only facilitated a PPI between 14-3-3β and SYNPO2, but also promoted its shuttling into the nucleus. Contrary to these findings, a phosphorylation-dependent nuclear shuttling of SYNPO2 *in vivo* was not observed in this thesis and several other reports (Linnemann *et al.*, 2010; Linnemann, 2011; Lohanadan *et al.*, 2021; Lohanadan *et al.*, 2023).

Recent work from Lohanadan (2023) has highlighted other regulatory functions of phosphorylations in the podin homology regions H1 and H2 of SYNPO2. These portions of SYNPO2 are known to harbor additional α-actinin binding regions. In particular, SYNPO2 phosphorylations in the H1 region were required for SYNPO2 to bind LC3B, a microtubule-associated protein involved in autophagosome formation (Lohanadan, 2023, pp. 76–80). In addition to phospho-acceptor sites identified in this thesis, these findings put emphasis on further sites capable of regulating interactions between SYNPO2 and cytoskeletal proteins like α-actinin or F-actin.

For SYNPO2 it is still poorly understood which protein kinases or phosphatases mediate these SYNPO2 (de-)phosphorylations of phospho-acceptor sites investigated here. To analyze specifically regulated phospho-acceptor sites, the use of databases might

contribute to narrow down the number of potential candidates (Colinge *et al.*, 2014; Buljan *et al.*, 2020; Franciosa *et al.*, 2023). However, as kinase-substrate networks and proteome-based analyses provide vast amounts of robust data, ascribing particular kinases to specific phosphorylation events may be cumbersome.

4.4 Regulation of YAP1 in smooth and skeletal muscle cells

The Hippo signaling pathway is regulated by a variety of factors, including stiffness of the ECM, cell-cell contacts, morphological factors of the cell (density, polarity, shape, stretching), extracellular signals transduced by G-protein coupled receptors (GPCRs), and alternative Wnt signaling pathways (Park *et al.*, 2015; Fischer *et al.*, 2016; Wada *et al.*, 2011; Cai *et al.*, 2021; Das *et al.*, 2016). WW domain-mediated interactions play a key role in regulating and transducing signals mediated by Hippo kinases LATS1/2, and MST1/2. On the one hand, the phosphorylation-dependent inactivation of YAP1/TAZ by LATS relies on PPPY-WW domain interactions (Chen & Sudol, 1995; Sudol *et al.*, 2001; Oka *et al.*, 2008; Verma *et al.*, 2018; Wackerhage *et al.*, 2014). On the other hand, activating YAP1/TAZ via dephosphorylation is mediated by various phosphatases (Liu *et al.*, 2013; Schlegelmilch *et al.*, 2011; Wang *et al.*, 2011; Wang *et al.*, 2012; Hein *et al.*, 2019).

As this thesis identified YAP1 as novel binding partner of SYNPO2, it was speculated whether elevated SYNPO2 expression levels might modulate YAP1 activity in smooth or skeletal muscle cells. In these cells, ratios between fractions of nuclear and cytoplasmic YAP1 functions as a read-out for YAP1 activity (see sections 1.4.4 & 3.6). However, fluorescence microscopy-based quantifications of nuclear versus cytoplasmic YAP1 revealed that neither in skeletal nor in smooth muscle cells, YAP1 activity was affected by overexpressing SYNPO2. Hence, these findings support the previously presented idea that SYNPO2 might engage in stabilizing YAP1 reservoired in the cytoplasm rather than modulating its activity. In contrast, overexpression of BAG3 promoted a significant increase of nuclear YAP1 in skeletal, but not in smooth muscle cells. More strikingly, this effect did not occur when overexpressing a BAG3 WAWA mutant with two tryptophans replaced by alanines, rendering its WW domain dysfunctional. This suggests a fundamental role of the WW domain of BAG3 in regulating the activity of the Hippo signaling pathway effector YAP1 and its paralog TAZ as presented in this thesis. In line with this, Ulbricht et al. (2013) investigated the interaction between BAG3 and the Hippo signaling kinase LATS1, whereas another study found BAG3 to bind the LATS-related kinase NDR1 (Tang *et al.*, 2015). Therefore, by sequestering these YAP1/TAZ inhibitors, BAG3 acts as a positive regulator of YAP1/TAZ

(Ulbricht *et al.*, 2013; Baldan *et al.*, 2021; Tang *et al.*, 2015). Conversely, Hippo signaling key players may also regulate autophagy: the kinase NDR1 (STK38) was shown to interact with BAG3 and to subsequently impair BAG3-mediated autophagic degradation of the cytoskeleton in A7r5 smooth muscle-like cells (Klimek *et al.*, 2019).

As demonstrated in this thesis, ratios of cytoplasmic and nuclear YAP1 were lower in skeletal than in smooth muscle cells (Fig. 3.49). There are several possible explanations for this result. In differentiating C2C12 myoblasts, caspase-3 activation of the upstream Hippo kinase MST1 relays LATS-mediated phosphorylations, inhibiting YAP1/TAZ (Fernando *et al.*, 2002). Furthermore, during myogenic differentiation, YAP1 nuclear levels decrease as phosphorylations of YAP1 mediate its cytoplasmic retention (Watt *et al.*, 2010; Watt *et al.*, 2015). In A7r5 cells, ECM stiffness leads to tension-induced upregulation of autophagosomes and elevated BAG3 expression levels potentially increasing YAP1/TAZ activation (Ulbricht *et al.*, 2013). Therefore, the cultivation of smooth muscle cells on a different surface substrate (e.g. fibronectin) might induce a quantifiable decrease in YAP1 activation combined with SYNPO2/BAG3 overexpression or depletion (Disher *et al.*, 2005; Kim *et al.*, 2011). Additional quantifications of YAP1 activity while concomitantly depleting SYNPO2 and/or BAG3 in smooth or skeletal muscle cells may elucidate the mechanism of reciprocal buffering/stabilization dynamics of SYNPO2, BAG3, and YAP1/TAZ. Here, additional experiments performed on skeletal muscle cells found an increased nuclear translocation of YAP1 upon EPS-induced damage of the contractile apparatus. This local disruption of sarcomeres by mechanical stress is a result of mechanical unfolding and subsequent aggregation of proteins (Orfanos *et al.*, 2016). The increased YAP1 nuclear translocation implicates that activated YAP1 in the nucleus facilitates the transcription of downstream target genes through binding to TEAD complex proteins (Zhao *et al.*, 2008). This activation may be attributed to elevated levels of BAG3 during mechanical stress, as merely an interaction of BAG3 with Hippo pathway kinases is capable of activating YAP1/TAZ (Ulbricht *et al.*, 2013). Furthermore, BAG3 was shown to sense the conformational state of Z-disc proteins, such as filamin C, and to sequester damaged and unfolded proteins via the CASA machinery (Arndt *et al.*, 2010, Ulbricht *et al.*, 2013, Klimek *et al.*, 2019). In addition, it was demonstrated that BAG3 mediates the activation of the mTOR signaling pathway by interacting with the PPPY

motif of the mTOR inhibitor TSC1 (Kathage *et al.*, 2017). Components of a BAG3-TSC1-mediated active mTOR pathway might thereby further elevate the synthesis of YAP1/TAZ target genes in addition to activated YAP1/TAZ. Recent work on EPS-induced mechanical stress (twitch-EPS) identified mTORC1-associated components to be responsible for downregulated protein synthesis. In contrast, mTORC2-associated components responsible for cytoskeletal organization were found upregulated under twitch-EPS (Warscheid, personal communication). Notably, previous research identified overlapping YAP1/TAZ target genes in C2C12 myotubes, such as BAG3, while other genes like DVL2 or PDLIM1, PDLIM2, and PDLIM5 encoding Z-disc associated proteins were exclusively regulated by YAP1 (Sun *et al.*, 2017). Additionally, the FLNC gene, encoding the CASA machinery client filamin C, was not among identified target genes (Sun *et al.*, 2017). In line with this, filamin C levels were not found to be increased upon mechanical damage (Ulbricht *et al.*, 2013).

It is to note that - according to other investigations - the role of the Hippo pathway effectors is regarded ambiguous: Some studies showed that Hippo signaling pathway-dependent YAP1/TAZ activation inhibited the Wnt signaling pathway in cardiomyocytes and was linked to repression of processes involving cardiac regeneration and renewal (Heallen *et al.*, 2011; Heallen *et al.*, 2013). Other studies emphasized the YAP1/TAZ-dependent regulation of satellite cell proliferation essential for regenerating skeletal muscle cells (Meinhold *et al.*, 2024; Judson *et al.*, 2012, Sun *et al.*, 2017). This discrepancy might indicate cell type-specific differences, therefore the precise exact relationship of the regulatory interplay between YAP1/TAZ, BAG3, SYNPO2, and other Z-disc-associated proteins remains elusive. Future reporter gene assays as well as further mass spectrometry-based proteome analyses may contribute to shed light on these connections.

4.5 Novel SYNPO2 mutations and their role for human disease

Recently, several links of SYNPO2 to non-muscle-related human diseases were identified. SYNPO2 was suggested to function as a potential tumor suppressor regulating tumorigenesis of triple-negative breast cancer (TNBC), an aggressive form of mammary carcinomas, as well as colorectal cancer (CRC) (Liu *et al.*, 2018; OuYang *et al.*, 2021). While mutations in the SYNPO2-associated proteins filamin C or titin have been identified to be involved in serious pathological conditions, such as myofibrillar myopathies (MFM), no direct associations of SYNPO2 with skeletal muscle-related single-gene diseases have been described yet (Fürst *et al.*, 2013; Rees *et al.*, 2021).

This thesis presents a truncation mutation (K1124*) and a misssense mutation (A1134T), discovered in the exon 6 of human SYNPO2, which both illustrate a link to SRNS. This condition is a rare hereditary form of kidney disease in patients with earliest onset in childhood (Sadowski *et al.*, 2015). This identification is a fundamental novelty for the SYNPO2 gene, as no human pathogenic mutations were characterized before (Mao *et al.*, 2020). Consistent with previous findings from skeletal and smooth muscle cells in this thesis, SYNPO2 was demonstrated to colocalize with α-actinin isoforms expressed in rat mesangial cells (Linnemann *et al.*, 2010, Mao *et al.*, 2020). Additional pulldown experiments revealed interactions between the exon 6 of SYNPO2 and both, α-actinin-1 and -4. Both mutations impaired binding to these α-actinin isoforms, suggesting an α-actinin-related loss of SYNPO2's function which potentially results in a pathologic dysregulation of the actin cytoskeleton. Further results from this publication indicate that this loss of function causes cell migration defects due to decreased lamellipodia protrusion in mesangial cells via ARP2/3. ARP2/3 is responsible for mediating the regulation of actin filament bundle and branching dynamics inducing lamellipodia formation by SYNPO2 (Mao *et al.*, 2020; Kai *et al.*, 2015). In conclusion, these findings highlight an important role of SYNPO2 in α-actinin-associated actin cytoskeleton maintenance and unravels a novel link of SYNPO2 mutations leading to human disease.

Literature

Arndt, V., Dick, N., Tawo, R., Dreiseidler, M., Wenzel, D., Hesse, M., Fürst, D. O., Saftig, P., Saint, R., Fleischmann, B. K., Hoch, M., and Höhfeld, J. (2010). Chaperone-Assisted Selective Autophagy Is Essential for Muscle Maintenance. *Current Biology*, 20(2):143–148. Publisher: Elsevier.

Arndt, V., Rogon, C., and Höhfeld, J. (2007). To be, or not to be — molecular chaperones in protein degradation. *Cellular and Molecular Life Sciences*, 64(19):2525.

Bae, S. J., Kim, M., Kim, S.-H., Kwon, Y. E., Lee, J.-H., Kim, J., Chung, C. H., Lee, W.-J., and Seol, J. H. (2015). NEDD4 controls intestinal stem cell homeostasis by regulating the Hippo signalling pathway. *Nature Communications*, 6(1):6314. Number: 1 Publisher: Nature Publishing Group.

Baldan, S., Meriin, A. B., Yaglom, J., Alexandrov, I., Varelas, X., Xiao, Z.-X. J., and Sherman, M. Y. (2021). The Hsp70–Bag3 complex modulates the phosphorylation and nuclear translocation of Hippo pathway protein Yap. *Journal of Cell Science*, 134(23):jcs259107.

Bang, M. L., Mudry, R. E., McElhinny, A. S., Trombitás, K., Geach, A. J., Yamasaki, R., Sorimachi, H., Granzier, H., Gregorio, C. C., and Labeit, S. (2001). Myopalladin, a novel 145-kilodalton sarcomeric protein with multiple roles in Z-disc and I-band protein assemblies. *The Journal of Cell Biology*, 153(2):413–427.

Baron, M. D., Davison, M. D., Jones, P., and Critchley, D. R. (1987). The sequence of chick alpha-actinin reveals homologies to spectrin and calmodulin. *Journal of Biological Chemistry*, 262(36):17623–17629.

Basu, S., Totty, N. F., Irwin, M. S., Sudol, M., and Downward, J. (2003). Akt Phosphorylates the Yes-Associated Protein, YAP, to Induce Interaction with 14-3-3 and Attenuation of p73-Mediated Apoptosis. *Molecular Cell*, 11(1):11–23. Publisher: Elsevier.

Behl, C. (2011). BAG3 and friends: Co-chaperones in selective autophagy during aging and disease. *Autophagy*, 7(7):795–798. Publisher: Taylor & Francis _eprint: https://doi.org/10.4161/auto.7.7.15844.

Behl, C. (2016). Breaking BAG: The Co-Chaperone BAG3 in Health and Disease. *Trends in Pharmacological Sciences*, 37(8):672–688.

Belotti, E., Polanowska, J., Daulat, A. M., Audebert, S., Thomé, V., Lissitzky, J.-C., Lembo, F., Blibek, K., Omi, S., Lenfant, N., Gangar, A., Montcouquiol, M., Santoni, M.-J., Sebbagh, M., Aurrand-Lions, M., Angers, S., Kodjabachian, L., Reboul, J., and Borg, J.-P. (2013). The Human PDZome: A Gateway to PSD95-Disc Large-Zonula Occludens (PDZ)-mediated Functions. *Molecular & Cellular Proteomics : MCP*, 12(9):2587–2603.

Bennett, P. M., Maggs, A. M., Baines, A. J., and Pinder, J. C. (2006). The Transitional Junction: A New Functional Subcellular Domain at the Intercalated Disc. *Molecular Biology of the Cell*, 17(4):2091–2100. Publisher: American Society for Cell Biology (mboc).

Bezerra (2015). *Structural characterization and interaction studies of myopodin isoform A with Z-disc binding partners*. PhD thesis, Universität Wien, Vienna.

Blanchard, A., Ohanian, V., and Critchley, D. (1989). The structure and function of alpha-actinin. *Journal of Muscle Research and Cell Motility*, 10(4):280–289.

Blau, H. M., Pavlath, G. K., Hardeman, E. C., Chiu, C.-P., Silberstein, L., Webster, S. G., Miller, S. C., and Webster, C. (1985). Plasticity of the Differentiated State. *Science*, 230(4727):758–766. Publisher: American Association for the Advancement of Science.

Block, B. A., Imagawa, T., Campbell, K. P., and Franzini-Armstrong, C. (1988). Structural evidence for direct interaction between the molecular components of the transverse tubule/sarcoplasmic reticulum junction in skeletal muscle. *The Journal of Cell Biology*, 107(6 Pt 2):2587–2600.

Bond, M. and Somlyo, A. V. (1982). Dense bodies and actin polarity in vertebrate smooth muscle. *The Journal of Cell Biology*, 95(2):403–413.

Brack, A. S., Conboy, I. M., Conboy, M. J., Shen, J., and Rando, T. A. (2008). A Temporal Switch from Notch to Wnt Signaling in Muscle Stem Cells Is Necessary for Normal Adult Myogenesis. *Cell Stem Cell*, 2(1):50–59.

Brenman, J. E., Chao, D. S., Gee, S. H., McGee, A. W., Craven, S. E., Santillano, D. R., Wu, Z., Huang, F., Xia, H., Peters, M. F., Froehner, S. C., and Bredt, D. S. (1996). Interaction of Nitric Oxide Synthase with the Postsynaptic Density Protein PSD-95 and α1-Syntrophin Mediated by PDZ Domains. *Cell*, 84(5):757–767.

Brown, D., Dykes, A., Black, J., Thatcher, S., Fultz, M., and Wright, G. (2006). Differential actin isoform reorganization in the contracting A7r5 cell. *Canadian Journal of Physiology and Pharmacology*, 84(8-9):867–875. Publisher: NRC Research Press.

Buljan, M., Ciuffa, R., van Drogen, A., Vichalkovski, A., Mehnert, M., Rosenberger, G., Lee, S., Varjosalo, M., Pernas, L. E., Spegg, V., Snijder, B., Aebersold, R., and Gstaiger, M. (2020). Kinase Interaction Network Expands Functional and Disease Roles of Human Kinases. *Molecular Cell*, 79(3):504–520.e9.

Burridge, K. and Feramisco, J. R. (1981). Non-muscle α-actinins are calcium-sensitive actin-binding proteins. *Nature*, 294(5841):565–567. Publisher: Nature Publishing Group.

Burridge, K., Molony, L., and Kelly, T. (1987). Adhesion plaques: sites of transmembrane interaction between the extracellular matrix and the actin cytoskeleton. *Journal of Cell Science. Supplement*, 8:211–229.

Cabral, J. H. M., Petosa, C., Sutcliffe, M. J., Raza, S., Byron, O., Poy, F., Marfatia, S. M., Chishti, A. H., and Liddington, R. C. (1996). Crystal structure of a PDZ domain. *Nature*, 382(6592):649–652. Publisher: Nature Publishing Group.

Cai, X., Wang, K.-C., and Meng, Z. (2021). Mechanoregulation of YAP and TAZ in Cellular Homeostasis and Disease Progression. *Frontiers in Cell and Developmental Biology*, 9:673599.

Calvo, F., Ege, N., Grande-Garcia, A., Hooper, S., Jenkins, R. P., Chaudhry, S. I., Harrington, K., Williamson, P., Moeendarbary, E., Charras, G., and Sahai, E. (2013). Mechanotransduction and YAP-dependent matrix remodelling is required for the generation and maintenance of cancer-associated fibroblasts. *Nature Cell Biology*, 15(6):637–646.

Campbell, K. P. and Stull, J. T. (2003). Skeletal Muscle Basement Membrane-Sarcolemma-Cytoskeleton Interaction Minireview Series. *Journal of Biological Chemistry*, 278(15):12599–12600.

Carlsson, L. (2001). *The Muscle Cytoskeleton of Mice and Men*. PhD thesis, Umeå University, Umeå.

Carra, S., Seguin, S. J., Lambert, H., and Landry, J. (2008). HspB8 Chaperone Activity toward Poly(Q)-containing Proteins Depends on Its Association with Bag3, a Stimulator of Macroautophagy*. *Journal of Biological Chemistry*, 283(3):1437–1444.

Castro-Cruz, M., Lembo, F., Borg, J.-P., Travé, G., Vincentelli, R., and Zimmermann, P. (2023). The Human PDZome 2.0: Characterization of a New Resource to Test for PDZ Interactions by Yeast Two-Hybrid. *Membranes*, 13(8):737.

Chalovich, J. M. and Schroeter, M. M. (2010). Synaptopodin family of natively unfolded, actin binding proteins: physical properties and potential biological functions. *Biophysical Reviews*, 2(4):181. Publisher: Springer.

Chang, B. H., Gujral, T. S., Karp, E. S., BuKhalid, R., Grantcharova, V. P., and MacBeath, G. (2011). A Systematic Family-wide Investigation Reveals that 30% of Mammalian PDZ Domains Engage in PDZ-PDZ Interactions. *Chemistry & Biology*, 18(9):1143–1152.

Chen, H.-H., Chen, W.-P., Yan, W.-L., Huang, Y.-C., Chang, S.-W., Fu, W.-M., Su, M.-J., Yu, I.-S., Tsai, T.-C., Yan, Y.-T., Tsao, Y.-P., and Chen, S.-L. (2015). NRIP is newly identified as a Z-disc protein, activating calmodulin signaling for skeletal muscle contraction and regeneration. *Journal of Cell Science*, 128(22):4196–4209.

Chen, H. I. and Sudol, M. (1995). The WW domain of Yes-associated protein binds a proline-rich ligand that differs from the consensus established for Src homology 3-binding modules. *Proceedings of the National Academy of Sciences of the United States of America*, 92(17):7819–7823.

Chen, J., Pan, L., Wei, Z., Zhao, Y., and Zhang, M. (2008). Domain-swapped dimerization of ZO-1 PDZ2 generates specific and regulatory connexin43-binding sites. *The EMBO Journal*, 27(15):2113–2123.

Chi, R. J., Olenych, S. G., Kim, K., and Keller, T. C. S. (2005). Smooth muscle alpha-actinin interaction with smitin. *The International Journal of Biochemistry & Cell Biology*, 37(7):1470–1482.

Chi, R. J., Simon, A. R., Bienkiewicz, E. A., Felix, A., and Keller, T. C. S. (2008). Smooth Muscle Titin Zq Domain Interaction with the Smooth Muscle α-Actinin Central Rod. *The Journal of Biological Chemistry*, 283(30):20959–20967.

Cho, Y. s., Zhu, J., Li, S., Wang, B., Han, Y., and Jiang, J. (2018). Regulation of Yki/Yap subcellular localization and Hpo signaling by a nuclear kinase PRP4K. *Nature Communications*, 9(1):1657. Publisher: Nature Publishing Group.

Chopra, A., Willmore, W. G., and Biggar, K. K. (2019). Protein quantification and visualization via ultraviolet-dependent labeling with 2,2,2-trichloroethanol. *Scientific Reports*, 9(1):13923. Publisher: Nature Publishing Group.

Clark, K. A., McElhinny, A. S., Beckerle, M. C., and Gregorio, C. C. (2002). Striated muscle cytoarchitecture: an intricate web of form and function. *Annual Review of Cell and Developmental Biology*, 18:637–706.

Clarke, L. E., Cook, A., Mathavarajah, S., Bera, A., Salsman, J., Habib, E., Van Iderstine, C., Bydoun, M., Lewis, S. M., and Dellaire, G. (2021). Haploinsufficient tumor suppressor PRP4K is negatively regulated during epithelial-to-mesenchymal transition. *The FASEB Journal*, 35(11):e22001.

Colinge, J., César-Razquin, A., Huber, K., Breitwieser, F. P., Májek, P., and Superti-Furga, G. (2014). Building and exploring an integrated human kinase network: Global organization and medical entry points. *Journal of Proteomics*, 107(100):113–127.

Colomo, F., Piroddi, N., Poggesi, C., te Kronnie, G., and Tesi, C. (1997). Active and passive forces of isolated myofibrils from cardiac and fast skeletal muscle of the frog. *The Journal of Physiology*, 500 (Pt 2)(Pt 2):535–548.

Costes, S. V., Daelemans, D., Cho, E. H., Dobbin, Z., Pavlakis, G., and Lockett, S. (2004). Automatic and Quantitative Measurement of Protein-Protein Colocalization in Live Cells. *Biophysical Journal*, 86(6):3993–4003.

Couchman, J. R. and Rees, D. A. (1979). The behaviour of fibroblasts migrating from chick heart explants: changes in adhesion, locomotion and growth, and in the distribution of actomyosin and fibronectin. *Journal of Cell Science*, 39(1):149–165.

Cretoiu, D., Pavelescu, L., Duica, F., Radu, M., Suciu, N., and Cretoiu, S. M. (2018). Myofibers. In *Advances in Experimental Medicine and Biology*, volume 1088, pages 23–46. Springer Nature Singapore Pte Ltd.

Crippa, V., D'Agostino, V. G., Cristofani, R., Rusmini, P., Cicardi, M. E., Messi, E., Loffredo, R., Pancher, M., Piccolella, M., Galbiati, M., Meroni, M., Cereda, C., Carra, S., Provenzani, A., and Poletti, A. (2016). Transcriptional induction of the heat shock protein B8 mediates the clearance of misfolded proteins responsible for motor neuron diseases. *Scientific Reports*, 6:22827.

Curtis, B. M. and Catterall, W. A. (1984). Purification of the calcium antagonist receptor of the voltage-sensitive calcium channel from skeletal muscle transverse tubules. *Biochemistry*, 23(10):2113–2118.

Das, A., Fischer, R. S., Pan, D., and Waterman, C. M. (2016). YAP Nuclear Localization in the Absence of Cell-Cell Contact Is Mediated by a Filamentous Actin-dependent, Myosin II- and Phospho-YAP-independent Pathway during Extracellular Matrix Mechanosensing. *The Journal of Biological Chemistry*, 291(12):6096–6110.

Dave, H. D., Shook, M., and Varacallo, M. (2023). Anatomy, Skeletal Muscle. In *StatPearls*. StatPearls Publishing, Treasure Island (FL).

Davis, M. W. and Jorgensen, E. M. (2022). ApE, A Plasmid Editor: A Freely Available DNA Manipulation and Visualization Program. *Frontiers in Bioinformatics*, 2:818619.

De Ganck, A., Corte, V. D., Staes, A., Gevaert, K., Vandekerckhove, J., and Gettemans, J. (2008). Multiple isoforms of the tumor suppressor myopodin are simultaneously transcribed in cancer cells. *Biochemical and Biophysical Research Communications*, 370(2):269–273.

De Jongh, K. S., Warner, C., Colvin, A. A., and Catterall, W. A. (1991). Characterization of the two size forms of the alpha 1 subunit of skeletal muscle L-type calcium channels. *Proceedings of the National Academy of Sciences of the United States of America*, 88(23):10778–10782.

DeFelice, L. J. (1993). Molecular and biophysical view of the Ca channel: a hypothesis regarding oligomeric structure, channel clustering, and macroscopic current. *The Journal of Membrane Biology*, 133(3):191–202.

Delhommel, F. (2017). *Etude structurale de la Whirline, protéine modulaire cruciale dans les mécanismes de la vision et de l'audition*. PhD thesis, Pierre and Marie Curie University Paris VI.

Delignette-Muller, M. L. and Dutang, C. (2015). fitdistrplus: An R Package for Fitting Distributions. *Journal of Statistical Software*, 64:1–34.

Diogo, R. and Abdala, V. (2010). *Muscles of vertebrates: comparative anatomy, evolution, homologies and development*. CRC press, Boca Raton (Fla.).

Discher, D. E., Janmey, P., and Wang, Y.-l. (2005). Tissue Cells Feel and Respond to the Stiffness of Their Substrate. *Science*, 310(5751):1139–1143. Publisher: American Association for the Advancement of Science.

Djinović-Carugo, K., Young, P., Gautel, M., and Saraste, M. (1999). Molecular Basis for Cross-Linking of Actin Filaments: Structure of the α-Actinin Rod. *Cell*, 98(4):537–546. Publisher: Elsevier.

Donadon, M. and Santoro, M. M. (2021). The origin and mechanisms of smooth muscle cell development in vertebrates. *Development*, 148(7):dev197384.

Dong, J., Feldmann, G., Huang, J., Wu, S., Zhang, N., Comerford, S. A., Gayyed, M. F., Anders, R. A., Maitra, A., and Pan, D. (2007). Elucidation of a Universal Size-Control Mechanism in Drosophila and Mammals. *Cell*, 130(6):1120–1133.

Dorland, Y. L. and Huveneers, S. (2017). Cell–cell junctional mechanotransduction in endothelial remodeling. *Cellular and Molecular Life Sciences*, 74(2):279–292.

Draeger, A., Amos, W. B., Ikebe, M., and Small, J. V. (1990). The cytoskeletal and contractile apparatus of smooth muscle: contraction bands and segmentation of the contractile elements. *The Journal of Cell Biology*, 111(6 Pt 1):2463–2473.

Draeger, A., Stelzer, E. H. K., Herzog, M., and Small, J. V. (1989). Unique geometry of actin-membrane anchorage sites in avian gizzard smooth muscle cells. *Journal of Cell Science*, 94(4):703–711.

Dunn, K. W., Kamocka, M. M., and McDonald, J. H. (2011). A practical guide to evaluating colocalization in biological microscopy. *American Journal of Physiology - Cell Physiology*, 300(4):C723–C742.

Dupont, S., Morsut, L., Aragona, M., Enzo, E., Giulitti, S., Cordenonsi, M., Zanconato, F., Le Digabel, J., Forcato, M., Bicciato, S., Elvassore, N., and Piccolo, S. (2011). Role of YAP/TAZ in mechanotransduction. *Nature*, 474(7350):179–183.

Elbediwy, A., Vanyai, H., Diaz-de-la Loza, M.-d.-C., Frith, D., Snijders, A. P., and Thompson, B. J. (2018). Enigma proteins regulate YAP mechanotransduction. *Journal of Cell Science*, 131(22):jcs221788.

Elosegui-Artola, A., Andreu, I., Beedle, A. E., Lezamiz, A., Uroz, M., Kosmalska, A. J., Oria, R., Kechagia, J. Z., Rico-Lastres, P., Le Roux, A.-L., Shanahan, C. M., Trepat, X., Navajas, D., Garcia-Manyes, S., and Roca-Cusachs, P. (2017). Force Triggers YAP Nuclear Entry by Regulating Transport across Nuclear Pores. *Cell*, 171(6):1397–1410.e14.

Erdõs, G., Pajkos, M., and Dosztányi, Z. (2021). IUPred3: prediction of protein disorder enhanced with unambiguous experimental annotation and visualization of evolutionary conservation. *Nucleic Acids Research*, 49(W1):W297–W303.

Ernst, A., Appleton, B. A., Ivarsson, Y., Zhang, Y., Gfeller, D., Wiesmann, C., and Sidhu, S. S. (2014). A Structural Portrait of the PDZ Domain Family. *Journal of Molecular Biology*, 426(21):3509–3519.

Ervasti, J. M. and Campbell, K. P. (1991). Membrane organization of the dystrophin-glycoprotein complex. *Cell*, 66(6):1121–1131.

Espanel, X. and Sudol, M. (1999). A Single Point Mutation in a Group I WW Domain Shifts Its Specificity to That of Group II WW Domains *. *Journal of Biological Chemistry*, 274(24):17284–17289. Publisher: Elsevier.

Esteves de Lima, J., Bonnin, M.-A., Birchmeier, C., and Duprez, D. (2016). Muscle contraction is required to maintain the pool of muscle progenitors via YAP and NOTCH during fetal myogenesis. *eLife*, 5:e15593. Publisher: eLife Sciences Publications, Ltd.

Fang, X., Bogomolovas, J., Trexler, C., and Chen, J. (2019). The BAG3-dependent and -independent roles of cardiac small heat shock proteins. *JCI Insight*, 4(4):e126464.

Fanning, A. S. and Anderson, J. M. (1996). Protein–protein interactions: PDZ domain networks. *Current Biology*, 6(11):1385–1388.

Fanning, A. S., Lye, M. F., Anderson, J. M., and Lavie, A. (2007). Domain Swapping within PDZ2 Is Responsible for Dimerization of ZO Proteins. *The Journal of biological chemistry*, 282(52):37710–37716.

Fatigati, V. and Murphy, R. A. (1984). Actin and tropomyosin variants in smooth muscles. Dependence on tissue type. *Journal of Biological Chemistry*, 259(23):14383–14388.

Faul, C., Dhume, A., Schecter, A. D., and Mundel, P. (2007). Protein Kinase A, Ca2+/Calmodulin-Dependent Kinase II, and Calcineurin Regulate the Intracellular Trafficking of Myopodin between the Z-Disc and the Nucleus of Cardiac Myocytes. *Molecular and Cellular Biology*, 27(23):8215–8227.

Faul, C., Hüttelmaier, S., Oh, J., Hachet, V., Singer, R. H., and Mundel, P. (2005). Promotion of importin alpha-mediated nuclear import by the phosphorylation-dependent binding of cargo protein to 14-3-3. *The Journal of Cell Biology*, 169(3):415–424.

Faulkner, G., Pallavicini, A., Formentin, E., Comelli, A., Ievolella, C., Trevisan, S., Bortoletto, G., Scannapieco, P., Salamon, M., Mouly, V., Valle, G., and Lanfranchi, G. (1999). Zasp: A New Z-band Alternatively Spliced PDZ-motif Protein. *The Journal of Cell Biology*, 146(2):465–476.

Fernando, P., Kelly, J. F., Balazsi, K., Slack, R. S., and Megeney, L. A. (2002). Caspase 3 activity is required for skeletal muscle differentiation. *Proceedings of the National Academy of Sciences*, 99(17):11025–11030. Publisher: Proceedings of the National Academy of Sciences.

Fields, S. and Song, O.-k. (1989). A novel genetic system to detect protein–protein interactions. *Nature*, 340(6230):245–246. Number: 6230 Publisher: Nature Publishing Group.

Fischer, M., Rikeit, P., Knaus, P., and Coirault, C. (2016). YAP-Mediated Mechanotransduction in Skeletal Muscle. *Frontiers in Physiology*, 7:41.

Foley, K. S. and Young, P. W. (2013). An analysis of splicing, actin-binding properties, heterodimerization and molecular interactions of the non-muscle α-actinins. *The Biochemical Journal*, 452(3):477–488.

Foley, K. S. and Young, P. W. (2014). The non-muscle functions of actinins: an update. *The Biochemical Journal*, 459(1):1–13.

Fontanella, B., Birolo, L., Infusini, G., Cirulli, C., Marzullo, L., Pucci, P., Turco, M. C., and Tosco, A. (2010). The co-chaperone BAG3 interacts with the cytosolic chaperonin CCT: New hints for actin folding. *The International Journal of Biochemistry & Cell Biology*, 42(5):641–650.

Fosset, M., Jaimovich, E., Delpont, E., and Lazdunski, M. (1983). [3H]nitrendipine receptors in skeletal muscle. *The Journal of Biological Chemistry*, 258(10):6086–6092.

Fowler, V. M., Sussmann, M. A., Miller, P. G., Flucher, B. E., and Daniels, M. P. (1993). Tropomodulin is associated with the free (pointed) ends of the thin filaments in rat skeletal muscle. *Journal of Cell Biology*, 120(2):411–420.

Franciosa, G., Locard-Paulet, M., Jensen, L. J., and Olsen, J. V. (2023). Recent advances in kinase signaling network profiling by mass spectrometry. *Current Opinion in Chemical Biology*, 73:102260.

Frank, D., Kuhn, C., Katus, H. A., and Frey, N. (2006). The sarcomeric Z-disc: a nodal point in signalling and disease. *Journal of Molecular Medicine (Berlin, Germany)*, 84(6):446–468.

Frank, E. D. and Warren, L. (1981). Aortic smooth muscle cells contain vimentin instead of desmin. *Proceedings of the National Academy of Sciences of the United States of America*, 78(5):3020–3024.

Frey, N., Richardson, J. A., and Olson, E. N. (2000). Calsarcins, a novel family of sarcomeric calcineurin-binding proteins. *Proceedings of the National Academy of Sciences of the United States of America*, 97(26):14632–14637.

Fuchs, M., Poirier, D. J., Seguin, S. J., Lambert, H., Carra, S., Charette, S. J., and Landry, J. (2009). Identification of the key structural motifs involved in HspB8/HspB6-Bag3 interaction. *The Biochemical Journal*, 425(1):245–255.

Fürst, D. O., Cross, R. A., De Mey, J., and Small, J. V. (1986). Caldesmon is an elongated, flexible molecule localized in the actomyosin domains of smooth muscle. *The EMBO Journal*, 5(2):251–257.

Fürst, D. O., Goldfarb, L. G., Kley, R. A., Vorgerd, M., Olivé, M., and van der Ven, P. F. M. (2013). Filamin C-related myopathies: pathology and mechanisms. *Acta neuropathologica*, 125(1):33–46.

Fürst, D. O., Osborn, M., Nave, R., and Weber, K. (1988). The organization of titin filaments in the half-sarcomere revealed by monoclonal antibodies in immunoelectron microscopy: a map of ten nonrepetitive epitopes starting at the Z line extends close to the M line. *The Journal of Cell Biology*, 106(5):1563–1572.

Gabella, G. and Blundell, D. (1978). Effect of stretch and contraction on caveolae of smooth muscle cells. *Cell and Tissue Research*, 190(2):255–271.

Gaffney, C. J., Oka, T., Mazack, V., Hilman, D., Gat, U., Muramatsu, T., Inazawa, J., Golden, A., Carey, D. J., Farooq, A., Tromp, G., and Sudol, M. (2012). Identification, basic characterization and evolutionary analysis of differentially spliced mRNA isoforms of human YAP1 gene. *Gene*, 509(2):215–222.

Gallardo, R., Ivarsson, Y., Schymkowitz, J., Rousseau, F., and Zimmermann, P. (2010). Structural Diversity of PDZ–Lipid Interactions. *ChemBioChem*, 11(4):456–467. _eprint: https://onlinelibrary.wiley.com/doi/pdf/10.1002/cbic.200900616.

Gamerdinger, M., Hajieva, P., Kaya, A. M., Wolfrum, U., Hartl, F. U., and Behl, C. (2009). Protein quality control during aging involves recruitment of the macroautophagy pathway by BAG3. *The EMBO Journal*, 28(7):889–901. Num Pages: 901 Publisher: John Wiley & Sons, Ltd.

Gao, Y. (2022). *Biology of Vascular Smooth Muscle: Vasoconstriction and Dilatation*. Springer Nature Singapore, Singapore.

Gee, S. H., Sekely, S. A., Lombardo, C., Kurakin, A., Froehner, S. C., and Kay, B. K. (1998). Cyclic peptides as non-carboxyl-terminal ligands of syntrophin PDZ domains. *The Journal of Biological Chemistry*, 273(34):21980–21987.

Genevet, A., Wehr, M. C., Brain, R., Thompson, B. J., and Tapon, N. (2010). Kibra is a regulator of the Salvador/Warts/Hippo signaling network. *Developmental Cell*, 18(2):300–308.

Gfeller, D. (2012). Uncovering new aspects of protein interactions through analysis of specificity landscapes in peptide recognition domains. *FEBS Letters*, 586(17):2764–2772. _eprint: https://onlinelibrary.wiley.com/doi/pdf/10.1016/j.febslet.2012.03.054.

Goldstein, M. A., Michael, L. H., Schroeter, J. P., and Sass, R. L. (1987). Z band dynamics as a function of sarcomere length and the contractile state of muscle. *FASEB journal: official publication of the Federation of American Societies for Experimental Biology*, 1(2):133–142.

Goldstein, M. A., Schroeter, J. P., and Sass, R. L. (1990). Two structural states of the vertebrate Z band. *Electron Microscopy Reviews*, 3(2):227–248.

Goodman, C. A., Dietz, J. M., Jacobs, B. L., McNally, R. M., You, J.-S., and Hornberger, T. A. (2015). Yes-Associated Protein is up-regulated by mechanical overload and is sufficient to induce skeletal muscle hypertrophy. *FEBS Letters*, 589(13):1491–1497.

Grembecka, J., Cierpicki, T., Devedjiev, Y., Derewenda, U., Kang, B. S., Bushweller, J. H., and Derewenda, Z. S. (2006). The Binding of the PDZ Tandem of Syntenin to Target Proteins,. *Biochemistry*, 45(11):3674–3683. Publisher: American Chemical Society.

Grison, M., Merkel, U., Kostan, J., Djinović-Carugo, K., and Rief, M. (2017). α-Actinin/titin interaction: A dynamic and mechanically stable cluster of bonds in the muscle Z-disk. *Proceedings of the National Academy of Sciences of the United States of America*, 114(5):1015–1020.

Gunning, P., O'neill, G., and Hardeman, E. (2008). Tropomyosin-Based Regulation of the Actin Cytoskeleton in Time and Space. *Physiological Reviews*, 88(1):1–35. Publisher: American Physiological Society.

Gunst, S. J. and Tang, D. D. (2000). The contractile apparatus and mechanical properties of airway smooth muscle. *The European Respiratory Journal*, 15(3):600–616.

Gunst, S. J. and Zhang, W. (2008). Actin cytoskeletal dynamics in smooth muscle: a new paradigm for the regulation of smooth muscle contraction. *American Journal of Physiology-Cell Physiology*, 295(3):C576–C587. Publisher: American Physiological Society.

Guo, Q., Quan, M., Dong, J., Bai, J., Wang, J., Han, R., Wang, W., Cai, Y., Lv, Y.-Q., Chen, Q., Xu, H., Lyu, H.-D., Deng, L., Zhou, D., Xiao, X., Langhe, S. D., Billadeau, D. D., Lou, Z., and Zhang, J.-S. (2020). The WW domains dictate isoform-specific regulation of YAP1 stability and pancreatic cancer cell malignancy. *Theranostics*, 10(10):4422. Publisher: Ivyspring International Publisher.

Guy, P. M., Kenny, D. A., and Gill, G. N. (1999). The PDZ Domain of the LIM Protein Enigma Binds to β-Tropomyosin. *Molecular Biology of the Cell*, 10(6):1973–1984.

Hafen, B. B., Shook, M., and Burns, B. (2023). Anatomy, Smooth Muscle. In *StatPearls*. StatPearls Publishing, Treasure Island (FL).

Han, S., Cui, C., Zhao, X., Zhang, Y., Zhang, Y., Zhao, J., Shen, X., He, H., Wang, J., Ma, M., Li, D., Zhu, Q., and Yin, H. (2021). Filamin C regulates skeletal muscle atrophy by stabilizing dishevelled-2 to inhibit autophagy and mitophagy. *Molecular Therapy. Nucleic Acids*, 27:147–164.

Hao, Y., Chun, A., Cheung, K., Rashidi, B., and Yang, X. (2008). Tumor Suppressor LATS1 Is a Negative Regulator of Oncogene YAP*. *Journal of Biological Chemistry*, 283(9):5496–5509. Publisher: Elsevier.

Heallen, T., Morikawa, Y., Leach, J., Tao, G., Willerson, J. T., Johnson, R. L., and Martin, J. F. (2013). Hippo signaling impedes adult heart regeneration. *Development (Cambridge, England)*, 140(23):4683–4690.

Heallen, T., Zhang, M., Wang, J., Bonilla-Claudio, M., Klysik, E., Johnson, R. L., and Martin, J. F. (2011). Hippo pathway inhibits Wnt signaling to restrain cardiomyocyte proliferation and heart size. *Science (New York, N.Y.)*, 332(6028):458–461.

Hein, A. L., Brandquist, N. D., Ouellette, C. Y., Seshacharyulu, P., Enke, C. A., Ouellette, M. M., Batra, S. K., and Yan, Y. (2019). PR55α regulatory subunit of PP2A inhibits the MOB1/LATS cascade and activates YAP in pancreatic cancer cells. *Oncogenesis*, 8(11):63.

Herrera, A., Mcparland, B., Bienkowska, A., Tait, R., Paré, P., and Seow, C. (2005). 'Sarcomeres' of smooth muscle: Functional characteristics and ultrastructural evidence. *Journal of cell science*, 118:2381–92.

Herzog, W. (2018). The multiple roles of titin in muscle contraction and force production. *Biophysical Reviews*, 10(4):1187–1199.

Herzog, W., Lee, E. J., and Rassier, D. E. (2006). Residual force enhancement in skeletal muscle. *The Journal of Physiology*, 574(Pt 3):635–642.

Hillier, B. J., Christopherson, K. S., Prehoda, K. E., Bredt, D. S., and Lim, W. A. (1999). Unexpected Modes of PDZ Domain Scaffolding Revealed by Structure of nNOS-Syntrophin Complex. *Science*, 284(5415):812–815. Publisher: American Association for the Advancement of Science.

Ho, K. C., Zhou, Z., She, Y.-M., Chun, A., Cyr, T. D., and Yang, X. (2011). Itch E3 ubiquitin ligase regulates large tumor suppressor 1 stability. *Proceedings of the National Academy of Sciences*, 108(12):4870–4875. Publisher: Proceedings of the National Academy of Sciences.

Höhfeld, J., Benzing, T., Bloch, W., Fürst, D. O., Gehlert, S., Hesse, M., Hoffmann, B., Hoppe, T., Huesgen, P. F., Köhn, M., Kolanus, W., Merkel, R., Niessen, C. M., Pokrzywa, W., Rinschen, M. M., Wachten, D., and Warscheid, B. (2021). Maintaining proteostasis under mechanical stress. *EMBO reports*, 22(8):e52507. Publisher: John Wiley & Sons, Ltd.

Hong, W. and Guan, K.-L. (2012). The YAP and TAZ transcription coactivators: key downstream effectors of the mammalian Hippo pathway. *Seminars in cell & developmental biology*, 23(7):785–793.

Hu, C.-D., Chinenov, Y., and Kerppola, T. K. (2002). Visualization of Interactions among bZIP and Rel Family Proteins in Living Cells Using Bimolecular Fluorescence Complementation. *Molecular Cell*, 9(4):789–798. Publisher: Elsevier.

Hui, S. and Bader, G. D. (2010). Proteome scanning to predict PDZ domain interactions using support vector machines. *BMC Bioinformatics*, 11(1):507.

Hui, S., Xing, X., and Bader, G. D. (2013). Predicting PDZ domain mediated protein interactions from structure. *BMC bioinformatics*, 14:27.

Huttlin, E. L., Jedrychowski, M. P., Elias, J. E., Goswami, T., Rad, R., Beausoleil, S. A., Villén, J., Haas, W., Sowa, M. E., and Gygi, S. P. (2010). A tissue-specific atlas of mouse protein phosphorylation and expression. *Cell*, 143(7):1174–1189.

Huxley, A. F. (1957). Muscle structure and theories of contraction. *Progress in Biophysics and Biophysical Chemistry*, 7:255–318.

Huxley, H. and Hanson, J. (1954). Changes in the Cross-Striations of Muscle during Contraction and Stretch and their Structural Interpretation. *Nature*, 173(4412):973–976. Publisher: Nature Publishing Group.

Huxley, H. E. (1963). ELECTRON MICROSCOPE STUDIES ON THE STRUCTURE OF NATURAL AND SYNTHETIC PROTEIN FILAMENTS FROM STRIATED MUSCLE. *Journal of Molecular Biology*, 7:281–308.

Iglesias-Bexiga, M., Castillo, F., Cobos, E. S., Oka, T., Sudol, M., and Luque, I. (2015). WW Domains of the Yes-Kinase-Associated-Protein (YAP) Transcriptional Regulator Behave as Independent Units with Different Binding Preferences for PPxY Motif-Containing Ligands. *PLoS ONE*, 10(1):e0113828.

Im, Y. J., Park, S. H., Rho, S.-H., Lee, J. H., Kang, G. B., Sheng, M., Kim, E., and Eom, S. H. (2003). Crystal structure of GRIP1 PDZ6-peptide complex reveals the structural basis for class II PDZ target recognition and PDZ domain-mediated multimerization. *The Journal of Biological Chemistry*, 278(10):8501–8507.

Ingham, R. J., Colwill, K., Howard, C., Dettwiler, S., Lim, C. S. H., Yu, J., Hersi, K., Raaijmakers, J., Gish, G., Mbamalu, G., Taylor, L., Yeung, B., Vassilovski, G., Amin, M., Chen, F., Matskova, L., Winberg, G., Ernberg, I., Linding, R., O'Donnell, P., Starostine, A., Keller, W., Metalnikov, P., Stark, C., and Pawson, T. (2005). WW Domains Provide a Platform for the Assembly of Multiprotein Networks. *Molecular and Cellular Biology*, 25(16):7092–7106.

Ivarsson, Y. (2012). Plasticity of PDZ domains in ligand recognition and signaling. *FEBS Letters*, 586(17):2638–2647. _eprint: https://onlinelibrary.wiley.com/doi/pdf/10.1016/j.febslet.2012.04.015.

Ivarsson, Y., Wawrzyniak, A. M., Kashyap, R., Polanowska, J., Betzi, S., Lembo, F., Vermeiren, E., Chiheb, D., Lenfant, N., Morelli, X., Borg, J.-P., Reboul, J., and Zimmermann, P. (2013). Prevalence, Specificity and Determinants of Lipid-Interacting PDZ Domains from an In-Cell Screen and In Vitro Binding Experiments. *PLOS ONE*, 8(2):e54581. Publisher: Public Library of Science.

Jäger, M., Dendle, M., and Kelly, J. W. (2009). Sequence determinants of thermodynamic stability in a WW domain—An all-β-sheet protein. *Protein Science : A Publication of the Protein Society*, 18(8):1806–1813.

Jäger, M., Nguyen, H., Crane, J. C., Kelly, J. W., and Gruebele, M. (2001). The folding mechanism of a beta-sheet: the WW domain. *Journal of Molecular Biology*, 311(2):373–393.

Jäger, M., Nguyen, H., Dendle, M., Gruebele, M., and Kelly, J. W. (2007). Influence of hPin1 WW N-terminal domain boundaries on function, protein stability, and folding. *Protein Science : A Publication of the Protein Society*, 16(7):1495–1501.

Janssen, I., Heymsfield, S. B., Wang, Z., and Ross, R. (2000). Skeletal muscle mass and distribution in 468 men and women aged 18–88 yr. *Journal of Applied Physiology*, 89(1):81–88. Publisher: American Physiological Society.

Jeon, Y. H., Park, Y. H., Lee, J. H., Hong, J.-H., and Kim, I. Y. (2014). Selenoprotein W enhances skeletal muscle differentiation by inhibiting TAZ binding to 14-3-3 protein. *Biochimica et Biophysica Acta (BBA) - Molecular Cell Research*, 1843(7):1356–1364.

Jeong, H., Bae, S., An, S. Y., Byun, M. R., Hwang, J.-H., Yaffe, M. B., Hong, J.-H., and Hwang, E. S. (2010). TAZ as a novel enhancer of MyoD-mediated myogenic differentiation. *FASEB journal: official publication of the Federation of American Societies for Experimental Biology*, 24(9):3310–3320.

Ji, C., Tang, M., Zeidler, C., Höhfeld, J., and Johnson, G. (2019). BAG3 and SYNPO (synaptopodin) facilitate phospho-MAPT/Tau degradation via autophagy in neuronal processes. *Autophagy*, 15.

Johansson, B., Eriksson, A., Virtanen, I., and Thornell, L. E. (1997). Intermediate filament proteins in adult human arteries. *The Anatomical Record*, 247(4):439–448.

Judson, R. N., Tremblay, A. M., Knopp, P., White, R. B., Urcia, R., De Bari, C., Zammit, P. S., Camargo, F. D., and Wackerhage, H. (2012). The Hippo pathway member Yap plays a key role in influencing fate decisions in muscle satellite cells. *Journal of Cell Science*, 125(24):6009–6019.

Kai, F., Fawcett, J. P., and Duncan, R. (2015). Synaptopodin-2 induces assembly of peripheral actin bundles and immature focal adhesions to promote lamellipodia formation and prostate cancer cell migration. *Oncotarget*, 6(13):11162–11174. Publisher: Impact Journals.

Kanai, F., Marignani, P. A., Sarbassova, D., Yagi, R., Hall, R. A., Donowitz, M., Hisaminato, A., Fujiwara, T., Ito, Y., Cantley, L. C., and Yaffe, M. B. (2000). TAZ: a novel transcriptional co-activator regulated by interactions with 14-3-3 and PDZ domain proteins. *The EMBO Journal*, 19(24):6778–6791.

Kathage, B., Gehlert, S., Ulbricht, A., Lüdecke, L., Tapia, V. E., Orfanos, Z., Wenzel, D., Bloch, W., Volkmer, R., Fleischmann, B. K., Fürst, D. O., and Höhfeld, J. (2017). The cochaperone BAG3 coordinates protein synthesis and autophagy under mechanical strain through spatial regulation of mTORC1. *Biochimica et Biophysica Acta (BBA) - Molecular Cell Research*, 1864(1):62–75.

Kato, Y., Miyakawa, T., Kurita, J.-i., and Tanokura, M. (2006). Structure of FBP11 WW1-PL Ligand Complex Reveals the Mechanism of Proline-rich Ligand Recognition by Group II/III WW Domains*. *Journal of Biological Chemistry*, 281(52):40321–40329.

Kato, Y., Nagata, K., Takahashi, M., Lian, L., Herrero, J. J., Sudol, M., and Tanokura, M. (2004). Common Mechanism of Ligand Recognition by Group II/III WW Domains: REDEFINING THEIR FUNCTIONAL CLASSIFICATION *. *Journal of Biological Chemistry*, 279(30):31833–31841. Publisher: Elsevier.

Kausalya, P. J., Reichert, M., and Hunziker, W. (2001). Connexin45 directly binds to ZO-1 and localizes to the tight junction region in epithelial MDCK cells. *FEBS letters*, 505(1):92–96.

Kelly, R. E. and Rice, R. V. (1969). Ultrastructural studies on the contractile mechanism of smooth muscle. *The Journal of Cell Biology*, 42(3):683–694.

Kennedy, M. B. (1995). Origin of PDZ (DHR, GLGF) domains. *Trends in Biochemical Sciences*, 20(9):350.

Kerppola, T. K. (2006). Design and implementation of bimolecular fluorescence complementation (BiFC) assays for the visualization of protein interactions in living cells. *Nature Protocols*, 1(3):1278–1286.

Kerppola, T. K. (2008). Bimolecular fluorescence complementation: visualization of molecular interactions in living cells. *Methods in Cell Biology*, 85:431–470.

Khanal, P., Jia, Z., and Yang, X. (2018). Cysteine residues are essential for dimerization of Hippo pathway components YAP2L and TAZ. *Scientific Reports*, 8(1):3485. Publisher: Nature Publishing Group.

Kibbe, W. A. (2007). OligoCalc: an online oligonucleotide properties calculator. *Nucleic Acids Research*, 35(Web Server issue):W43–46.

Kim, H. R., Gallant, C., Leavis, P. C., Gunst, S. J., and Morgan, K. G. (2008). Cytoskeletal remodeling in differentiated vascular smooth muscle is actin isoform dependent and stimulus dependent. *American Journal of Physiology. Cell Physiology*, 295(3):C768–778.

Kim, J., Kwon, H., Shin, Y. K., Song, G., Lee, T., Kim, Y., Jeong, W., Lee, U., Zhang, X., Nam, G., Jeung, H.-C., Kim, W., and Jho, E.-h. (2020). MAML1/2 promote YAP/TAZ nuclear localization and tumorigenesis. *Proceedings of the National Academy of Sciences*, 117(24):13529–13540. Publisher: Proceedings of the National Academy of Sciences.

Kim, N.-G., Koh, E., Chen, X., and Gumbiner, B. M. (2011). E-cadherin mediates contact inhibition of proliferation through Hippo signaling-pathway components. *Proceedings of the National Academy of Sciences of the United States of America*, 108(29):11930–11935.

Kimes, B. W. and Brandt, B. L. (1976). Characterization of two putative smooth muscle cell lines from rat thoracic aorta. *Experimental Cell Research*, 98(2):349–366.

Kittler, J. and Illingworth, J. (1986). Minimum error thresholding. *Pattern Recognition*, 19(1):41–47.

Klaavuniemi, T., Kelloniemi, A., and Ylänne, J. (2004). The ZASP-like Motif in Actinin-associated LIM Protein Is Required for Interaction with the α-Actinin Rod and for Targeting to the Muscle Z-line *. *Journal of Biological Chemistry*, 279(25):26402–26410. Publisher: Elsevier.

Klimek, C., Jahnke, R., Wördehoff, J., Kathage, B., Stadel, D., Behrends, C., Hergovich, A., and Höhfeld, J. (2019). The Hippo network kinase STK38 contributes to protein homeostasis by inhibiting BAG3-mediated autophagy. *Biochimica et Biophysica Acta. Molecular Cell Research*, 1866(10):1556–1566.

Klimek, C., Kathage, B., Wördehoff, J., and Höhfeld, J. (2017). BAG3-mediated proteostasis at a glance. *Journal of Cell Science*, 130(17):2781–2788.

Knyazeva, A., Khudiakov, A., Vaz, R., Muravyev, A., Sukhareva, K., Sejersen, T., and Kostareva, A. (2020). FLNC Expression Level Influences the Activity of TEAD-YAP/TAZ Signaling. *Genes*, 11(11):1343. Number: 11 Publisher: Multidisciplinary Digital Publishing Institute.

Kofler, M. and Kapus, A. (2023). Nuclear Import and Export of YAP and TAZ. *Cancers*, 15(20):4956.

Kremerskothen, J., Plaas, C., Kindler, S., Frotscher, M., and Barnekow, A. (2005). Synaptopodin, a molecule involved in the formation of the dendritic spine apparatus, is a dual actin/α-actinin binding protein. *Journal of Neurochemistry*, 92(3):597–606. _eprint: https://onlinelibrary.wiley.com/doi/pdf/10.1111/j.1471-4159.2004.02888.x.

Kroemker, M., Rüdiger, A. H., Jockusch, B. M., and Rüdiger, M. (1994). Intramolecular interactions in vinculin control alpha-actinin binding to the vinculin head. *FEBS letters*, 355(3):259–262.

Kruger, M., Wright, J., and Wang, K. (1991). Nebulin as a length regulator of thin filaments of vertebrate skeletal muscles: correlation of thin filament length, nebulin size, and epitope profile. *Journal of Cell Biology*, 115(1):97–107.

Kwok, E., Rodriguez, D. J., Kremerskothen, J., and Nyarko, A. (2019). Intrinsic disorder and amino acid specificity modulate binding of the WW2 domain in kidney and brain protein (KIBRA) to synaptopodin. *The Journal of biological chemistry*, 294(46):17383–17394.

Labeit, S. and Kolmerer, B. (1995). Titins: Giant Proteins in Charge of Muscle Ultrastructure and Elasticity. *Science*, 270(5234):293–296. Publisher: American Association for the Advancement of Science.

Ladner, C. L., Yang, J., Turner, R. J., and Edwards, R. A. (2004). Visible fluorescent detection of proteins in polyacrylamide gels without staining. *Analytical Biochemistry*, 326(1):13–20.

Laemmli, U. K. (1970). Cleavage of Structural Proteins during the Assembly of the Head of Bacteriophage T4. *Nature*, 227(5259):680–685. Number: 5259 Publisher: Nature Publishing Group.

Larkin, M. A., Blackshields, G., Brown, N. P., Chenna, R., McGettigan, P. A., McWilliam, H., Valentin, F., Wallace, I. M., Wilm, A., Lopez, R., Thompson, J. D., Gibson, T. J., and Higgins, D. G. (2007). Clustal W and Clustal X version 2.0. *Bioinformatics (Oxford, England)*, 23(21):2947–2948.

Lee, H.-J., Wang, N. X., Shao, Y., and Zheng, J. (2009). Identification of Tripeptides Recognized by the PDZ domain of Dishevelled. *Bioorganic & medicinal chemistry*, 17(4):1701–1708.

Lee, H.-J. and Zheng, J. J. (2010). PDZ domains and their binding partners: structure, specificity, and modification. *Cell Communication and Signaling : CCS*, 8:8.

Lehman, W. and Morgan, K. G. (2012). Structure and Dynamics of the Actin-Based Smooth Muscle Contractile and Cytoskeletal Apparatus. *Journal of muscle research and cell motility*, 33(6):461–469.

Lei, Q.-Y., Zhang, H., Zhao, B., Zha, Z.-Y., Bai, F., Pei, X.-H., Zhao, S., Xiong, Y., and Guan, K.-L. (2008). TAZ Promotes Cell Proliferation and Epithelial-Mesenchymal Transition and Is Inhibited by the Hippo Pathway. *Molecular and Cellular Biology*, 28(7):2426–2436.

Leinweber, B. D., Fredricksen, R. S., Hoffman, D. R., and Chalovich, J. M. (1999). Fesselin: a novel synaptopodin-like actin binding protein from muscle tissue. *Journal of Muscle Research & Cell Motility*, 20(5):539–545.

Levy, D., Adamovich, Y., Reuven, N., and Shaul, Y. (2008). Yap1 Phosphorylation by c-Abl Is a Critical Step in Selective Activation of Proapoptotic Genes in Response to DNA Damage. *Molecular Cell*, 29(3):350–361. Publisher: Elsevier.

Li, C. H. and Tam, P. K. S. (1998). An iterative algorithm for minimum cross entropy thresholding. *Pattern Recognition Letters*, 19(8):771–776.

Lieber, R. L. (1993). Skeletal Muscle Architecture: Implications for Muscle Function and Surgical Tendon Transfer. *Journal of Hand Therapy*, 6(2):105–113.

Lieber, R. L. and Fridén, J. (2000). Functional and clinical significance of skeletal muscle architecture. *Muscle & Nerve*, 23(11):1647–1666. _eprint: https://onlinelibrary.wiley.com/doi/pdf/10.1002/1097-4598%28200011%2923%3A11%3C1647%3A%3AAID-MUS1%3E3.0.CO%3B2-M.

Liem, R. K. (2016). Cytoskeletal Integrators: The Spectrin Superfamily. *Cold Spring Harbor Perspectives in Biology*, 8(10):a018259.

Lin, F., Yu, Y.-P., Woods, J., Cieply, K., Gooding, B., Finkelstein, P., Dhir, R., Krill, D., Becich, M. J., Michalopoulos, G., Finkelstein, S., and Luo, J.-H. (2001). Myopodin, a Synaptopodin Homologue, Is Frequently Deleted in Invasive Prostate Cancers. *The American Journal of Pathology*, 159(5):1603–1612.

Linnemann, A. (2011). *Biochemische und zellbiologische Charakterisierung der Podin-Proteinfamilie als Adapterproteine des Aktinzytoskeletts in Muskelzellen*. Thesis, Rheinische Friedrich-Wilhelms-Universität Bonn, Bonn. Accepted: 2020-04-16T19:41:36Z.

Linnemann, A., Vakeel, P., Bezerra, E., Orfanos, Z., Djinović-Carugo, K., van der Ven, P. F. M., Kirfel, G., and Fürst, D. O. (2013). Myopodin is an F-actin bundling protein with multiple independent actin-binding regions. *Journal of Muscle Research and Cell Motility*, 34(1):61–69.

Linnemann, A., van der Ven, P. F. M., Vakeel, P., Albinus, B., Simonis, D., Bendas, G., Schenk, J. A., Micheel, B., Kley, R. A., and Fürst, D. O. (2010). The sarcomeric Z-disc component myopodin is a multiadapter protein that interacts with filamin and α-actinin. *European Journal of Cell Biology*, 89(9):681–692.

Littlefield, R. S. and Fowler, V. M. (2008). Thin filament length regulation in striated muscle sarcomeres: pointed-end dynamics go beyond a nebulin ruler. *Seminars in Cell & Developmental Biology*, 19(6):511–519.

Liu, J., Ye, L., Li, Q., Wu, X., Wang, B., Ouyang, Y., Yuan, Z., Li, J., and Lin, C. (2018). Synaptopodin-2 suppresses metastasis of triple-negative breast cancer via inhibition of YAP/TAZ activity. *The Journal of Pathology*, 244(1):71–83. _eprint: https://onlinelibrary.wiley.com/doi/pdf/10.1002/path.4995.

Liu, X. and Fuentes, E. J. (2019). Emerging Themes in PDZ Domain Signaling: Structure, Function, and Inhibition. *International review of cell and molecular biology*, 343:129–218.

Liu, X., Yang, N., Figel, S., Wilson, K., Morrison, C., Gelman, I., and Zhang, J. (2013). PTPN14 interacts with and negatively regulates the oncogenic function of YAP. *Oncogene*, 32(10):1266–1273.

Lohanadan, K. (2023). *Functions and regulation of synaptopodin-2 isoforms under mechanical stress in muscle cells*. Thesis, Rheinische Friedrich-Wilhelms-Universität Bonn, Bonn. Accepted: 2023-05-09T10:52:25Z.

Lohanadan, K., Assent, M., Linnemann, A., Schuld, J., Heukamp, L. C., Krause, K., Vorgerd, M., Reimann, J., Schänzer, A., Kirfel, G., Fürst, D. O., and Van der Ven, P. F. M. (2023). Synaptopodin-2 Isoforms Have Specific Binding Partners and Display Distinct, Muscle Cell Type-Specific Expression Patterns. *Cells*, 13(1):85.

Lohanadan, K., Molt, S., Dierck, F., van der Ven, P. F. M., Frey, N., Höhfeld, J., and Fürst, D. O. (2021). Isoform-specific functions of synaptopodin-2 variants in cytoskeleton stabilization and autophagy regulation in muscle under mechanical stress. *Experimental Cell Research*, 408(2):112865.

Lowy, J. and Small, J. V. (1970). The organization of myosin and actin in vertebrate smooth muscle. *Nature*, 227(5253):46–51.

Luther, P. K. (2000). Three-dimensional structure of a vertebrate muscle Z-band: implications for titin and alpha-actinin binding. *Journal of Structural Biology*, 129(1):1–16.

Luther, P. K. (2009). The vertebrate muscle Z-disc: sarcomere anchor for structure and signalling. *Journal of Muscle Research and Cell Motility*, 30(5-6):171–185.

Macias, M. J., Hyvönen, M., Baraldi, E., Schultz, J., Sudol, M., Saraste, M., and Oschkinat, H. (1996). Structure of the WW domain of a kinase-associated protein complexed

with a proline-rich peptide. *Nature*, 382(6592):646–649. Publisher: Nature Publishing Group.

Mao, Y., Schneider, R., Ven, P. F. M. v. d., Assent, M., Lohanadan, K., Klämbt, V., Buerger, F., Kitzler, T. M., Deutsch, K., Nakayama, M., Majmundar, A. J., Mann, N., Hermle, T., Onuchic-Whitford, A. C., Zhou, W., Margam, N. N., Duncan, R., Marquez, J., Khokha, M., Fathy, H. M., Kari, J. A., Desoky, S. E., Eid, L. A., Awad, H. S., Al-Saffar, M., Mane, S., Lifton, R. P., Fürst, D. O., Shril, S., and Hildebrandt, F. (2021). Recessive Mutations in SYNPO2 as a Candidate of Monogenic Nephrotic Syndrome. *Kidney International Reports*, 6(2):472–483. Publisher: Elsevier.

Maruyama, K., Kimura, S., Ishi, T., Kuroda, M., and Ohashi, K. (1977a). beta-actinin, a regulatory protein of muscle. Purification, characterization and function. *Journal of Biochemistry*, 81(1):215–232.

Maruyama, K., Kimura, S., Kuroda, M., and Handa, S. (1977b). Connectin, an elastic protein of muscle. Its abundance in cardiac myofibrils. *Journal of Biochemistry*, 82(2):347–350.

McElhinny, A. S., Kazmierski, S. T., Labeit, S., and Gregorio, C. C. (2003). Nebulin: The Nebulous, Multifunctional Giant of Striated Muscle. *Trends in Cardiovascular Medicine*, 13(5):195–201.

Meinhold, M., Verbrugge, S., Shi, A., Schönfelder, M., Becker, L., Jaspers, R. T., Zammit, P. S., and Wackerhage, H. (2024). Yap/Taz activity is associated with increased expression of phosphoglycerate dehydrogenase that supports myoblast proliferation. *Cell and Tissue Research*, 395(3):271–283.

Meissner, G. and Lu, X. (1995). Dihydropyridine receptor-ryanodine receptor interactions in skeletal muscle excitation-contraction coupling. *Bioscience Reports*, 15(5):399–408.

Melzer, W., Rios, E., and Schneider, M. (1984). Time course of calcium release and removal in skeletal muscle fibers. *Biophysical Journal*, 45(3):637–641.

Meriin, A. B., Narayanan, A., Meng, L., Alexandrov, I., Varelas, X., Cissé, I. I., and Sherman, M. Y. (2018). Hsp70-Bag3 complex is a hub for proteotoxicity-induced signaling that controls protein aggregation. *Proceedings of the National Academy of Sciences of the United States of America*, 115(30):E7043–E7052.

Milner, D. J., Weitzer, G., Tran, D., Bradley, A., and Capetanaki, Y. (1996). Disruption of muscle architecture and myocardial degeneration in mice lacking desmin. *The Journal of Cell Biology*, 134(5):1255–1270.

Moon, S., Kim, W., Kim, S., Kim, Y., Song, Y., Bilousov, O., Kim, J., Lee, T., Cha, B., Kim, M., Kim, H., Katanaev, V. L., and Jho, E. (2017). Phosphorylation by NLK inhibits YAP-14-3-3-interactions and induces its nuclear localization. *EMBO reports*, 18(1):61–71. Num Pages: 71 Publisher: John Wiley & Sons, Ltd.

Moreira-Pais, A., Amado, F., Vitorino, R., Coriolano, H.-J. A., Duarte, J. A., and Ferreira, R. (2020). The Signaling Pathways Involved in the Regulation of Skeletal Muscle Plasticity. In Silva, J. V., Freitas, M. J., and Fardilha, M., editors, *Tissue-Specific Cell Signaling*, pages 383–408. Springer International Publishing, Cham.

Morgan, M. R., Humphries, M. J., and Bass, M. D. (2007). Synergistic control of cell adhesion by integrins and syndecans. *Nature Reviews Molecular Cell Biology*, 8(12):957–969. Publisher: Nature Publishing Group.

Mu, Y., Cai, P., Hu, S., Ma, S., and Gao, Y. (2014). Characterization of Diverse Internal Binding Specificities of PDZ Domains by Yeast Two-Hybrid Screening of a Special Peptide Library. *PLoS ONE*, 9(2):e88286.

Mukund, K. and Subramaniam, S. (2020). Skeletal muscle: A review of molecular structure and function, in health and disease. *Wiley Interdisciplinary Reviews. Systems Biology and Medicine*, 12(1):e1462.

Muley, V. Y., Akhter, Y., and Galande, S. (2019). PDZ Domains Across the Microbial World: Molecular Link to the Proteases, Stress Response, and Protein Synthesis. *Genome Biology and Evolution*, 11(3):644–659.

Mullis, K., Faloona, F., Scharf, S., Saiki, R., Horn, G., and Erlich, H. (1986). Specific enzymatic amplification of DNA in vitro: the polymerase chain reaction. *Cold Spring Harbor Symposia on Quantitative Biology*, 51 Pt 1:263–273.

Münz, M., Hein, J., and Biggin, P. C. (2012). The Role of Flexibility and Conformational Selection in the Binding Promiscuity of PDZ Domains. *PLOS Computational Biology*, 8(11):e1002749. Publisher: Public Library of Science.

Murphy, R. A. (1976). Structural proteins in the myofilaments and regulation of contraction in vertebrate smooth muscle. *Federation Proceedings*, 35(6):1302–1306.

Nakagawa, N., Hoshijima, M., Oyasu, M., Saito, N., Tanizawa, K., and Kuroda, S. (2000). ENH, containing PDZ and LIM domains, heart/skeletal muscle-specific protein, associates with cytoskeletal proteins through the PDZ domain. *Biochemical and Biophysical Research Communications*, 272(2):505–512.

North, A. J., Galazkiewicz, B., Byers, T. J., Glenney, J. R., and Small, J. V. (1993). Complementary distributions of vinculin and dystrophin define two distinct sarcolemma domains in smooth muscle. *The Journal of Cell Biology*, 120(5):1159–1167.

North, A. J., Gimona, M., Cross, R. A., and Small, J. V. (1994a). Calponin is localised in both the contractile apparatus and the cytoskeleton of smooth muscle cells. *Journal of Cell Science*, 107(3):437–444.

North, A. J., Gimona, M., Lando, Z., and Small, J. V. (1994b). Actin isoform compartments in chicken gizzard smooth muscle cells. *Journal of Cell Science*, 107(3):445–455.

Noureddine, M. and Gehmlich, K. (2023). Structural and signaling proteins in the Z-disk and their role in cardiomyopathies. *Frontiers in Physiology*, 14:1143858.

Novak, I. and Truskinovsky, L. (2015). Nonaffine response of skeletal muscles on the 'descending limb'. *Mathematics and Mechanics of Solids*, 20(6):697–720. Publisher: SAGE Publications Ltd STM.

Ohtsuki, I. (1974). Localization of Troponin in Thin Filament and Tropomyosin Paracrystal. *The Journal of Biochemistry*, 75(4):753–765.

Ojima, K. (2019). Myosin: Formation and maintenance of thick filaments. *Animal Science Journal = Nihon Chikusan Gakkaiho*, 90(7):801–807.

Oka, T., Mazack, V., and Sudol, M. (2008). Mst2 and Lats Kinases Regulate Apoptotic Function of Yes Kinase-associated Protein (YAP)*. *Journal of Biological Chemistry*, 283(41):27534–27546.

Oka, T., Remue, E., Meerschaert, K., Vanloo, B., Boucherie, C., Gfeller, D., Bader, G. D., Sidhu, S. S., Vandekerckhove, J., Gettemans, J., and Sudol, M. (2010). Functional complexes between YAP2 and ZO-2 are PDZ domain-dependent, and regulate YAP2 nuclear localization and signalling1. *Biochemical Journal*, 432(3):461–478.

Oka, T. and Sudol, M. (2009). Nuclear localization and pro-apoptotic signaling of YAP2 require intact PDZ-binding motif. *Genes to Cells: Devoted to Molecular & Cellular Mechanisms*, 14(5):607–615.

Orfanos, Z., Gödderz, M. P. O., Soroka, E., Gödderz, T., Rumyantseva, A., van der Ven, P. F. M., Hawke, T. J., and Fürst, D. O. (2016). Breaking sarcomeres by in vitro exercise. *Scientific Reports*, 6(1):19614. Number: 1 Publisher: Nature Publishing Group.

Otte, L., Wiedemann, U., Schlegel, B., Pires, J. R., Beyermann, M., Schmieder, P., Krause, G., Volkmer-Engert, R., Schneider-Mergener, J., and Oschkinat, H. (2003). WW domain sequence activity relationships identified using ligand recognition propensities of 42 WW domains. *Protein Science : A Publication of the Protein Society*, 12(3):491–500.

OuYang, C., Xie, Y., Fu, Q., and Xu, G. (2021). SYNPO2 suppresses hypoxia-induced proliferation and migration of colorectal cancer cells by regulating YAP-KLF5 axis. *Tissue and Cell*, 73:101598.

Pandey, P., Hawkes, W., Hu, J., Megone, W. V., Gautrot, J., Anilkumar, N., Zhang, M., Hirvonen, L., Cox, S., Ehler, E., Hone, J., Sheetz, M., and Iskratsch, T. (2018). Cardiomyocytes Sense Matrix Rigidity through a Combination of Muscle and Non-muscle Myosin Contractions. *Developmental Cell*, 44(3):326–336.e3.

Paramasivam, M., Sarkeshik, A., John R. Yates, I. I. I., Fernandes, M. J. G., and McCollum, D. (2011). Angiomotin family proteins are novel activators of the LATS2 kinase tumor suppressor. *Molecular Biology of the Cell*, 22(19):3725. Publisher: American Society for Cell Biology.

Pardo, J. V., Siliciano, J. D., and Craig, S. W. (1983). A vinculin-containing cortical lattice in skeletal muscle: transverse lattice elements ("costameres") mark sites of attachment between myofibrils and sarcolemma. *Proceedings of the National Academy of Sciences of the United States of America*, 80(4):1008–1012.

Park, H. W., Kim, Y. C., Yu, B., Moroishi, T., Mo, J.-S., Plouffe, S. W., Meng, Z., Lin, K. C., Yu, F.-X., Alexander, C. M., Wang, C., and Guan, K.-L. (2015). Alternative Wnt Signaling Activates YAP/TAZ. *Cell*, 162(4):780–794.

Patel, T. J. and Lieber, R. L. (1997). Force transmission in skeletal muscle: from actomyosin to external tendons. *Exercise and Sport Sciences Reviews*, 25:321–363.

Patil, I. (2021). Visualizations with statistical details: The 'ggstatsplot' approach. *Journal of Open Source Software*, 6(61):3167.

Pavel, M., Renna, M., Park, S. J., Menzies, F. M., Ricketts, T., Füllgrabe, J., Ashkenazi, A., Frake, R. A., Lombarte, A. C., Bento, C. F., Franze, K., and Rubinsztein, D. C. (2018). Contact inhibition controls cell survival and proliferation via YAP/TAZ-autophagy axis. *Nature Communications*, 9:2961.

Pham, M. and Chalovich, J. M. (2006). Smooth muscle α-actinin binds tightly to fesselin and attenuates its activity toward actin polymerization. *Journal of Muscle Research & Cell Motility*, 27(1):45–51.

Pham, S. and Puckett, Y. (2024). Physiology, Skeletal Muscle Contraction. In *StatPearls*. StatPearls Publishing, Treasure Island (FL).

Ponting, C. P. and Phillips, C. (1995). DHR domains in syntrophins, neuronal NO synthases and other intracellular proteins. *Trends in Biochemical Sciences*, 20(3):102–103.

Potts, G. K., McNally, R. M., Blanco, R., You, J.-S., Hebert, A. S., Westphall, M. S., Coon, J. J., and Hornberger, T. A. (2017). A map of the phosphoproteomic alterations that occur after a bout of maximal-intensity contractions. *The Journal of Physiology*, 595(15):5209–5226.

Primeau, J. O., Armanious, G. P., Fisher, M. E., and Young, H. S. (2018). The SarcoEndoplasmic Reticulum Calcium ATPase. In Harris, J. R. and Boekema, E. J., editors, *Membrane Protein Complexes: Structure and Function*, Subcellular Biochemistry, pages 229–258. Springer, Singapore.

Purbey, P. K., Singh, S., Kumar, P. P., Mehta, S., Ganesh, K. N., Mitra, D., and Galande, S. (2008). PDZ domain-mediated dimerization and homeodomain-directed specificity are required for high-affinity DNA binding by SATB1. *Nucleic Acids Research*, 36(7):2107–2122.

Rauch, J. N. and Gestwicki, J. E. (2014). Binding of Human Nucleotide Exchange Factors to Heat Shock Protein 70 (Hsp70) Generates Functionally Distinct Complexes in Vitro. *The Journal of Biological Chemistry*, 289(3):1402–1414.

Rees, M., Nikoopour, R., Fukuzawa, A., Kho, A. L., Fernandez-Garcia, M. A., Wraige, E., Bodi, I., Deshpande, C., Özdemir, Ö., Daimagüler, H.-S., Pfuhl, M., Holt, M., Brandmeier, B., Grover, S., Fluss, J., Longman, C., Farrugia, M. E., Matthews, E., Hanna, M., Muntoni, F., Sarkozy, A., Phadke, R., Quinlivan, R., Oates, E. C., Schröder, R., Thiel, C., Reimann, J., Voermans, N., Erasmus, C., Kamsteeg, E.-J., Konersman, C., Grosmann, C., McKee, S., Tirupathi, S., Moore, S. A., Wilichowski, E., Hobbiebrunken, E., Dekomien, G., Richard, I., Van den Bergh, P., Domínguez-González, C., Cirak, S., Ferreiro, A., Jungbluth, H., and Gautel, M. (2021). Making sense of missense variants in TTN-related congenital myopathies. *Acta Neuropathologica*, 141(3):431–453.

Reimann, L., Wiese, H., Leber, Y., Schwäble, A. N., Fricke, A. L., Rohland, A., Knapp, B., Peikert, C. D., Drepper, F., van der Ven, P. F. M., Radziwill, G., Fürst, D. O., and Warscheid, B. (2017). Myofibrillar Z-discs Are a Protein Phosphorylation Hot Spot with Protein Kinase C (PKCα) Modulating Protein Dynamics. *Molecular & cellular proteomics: MCP*, 16(3):346–367.

Remue, E., Meerschaert, K., Oka, T., Boucherie, C., Vandekerckhove, J., Sudol, M., and Gettemans, J. (2010). TAZ interacts with zonula occludens-1 and -2 proteins in a PDZ-1 dependent manner. *FEBS Letters*, 584(19):4175–4180.

Renley, B. A., Rybakova, I. N., Amann, K. J., and Ervasti, J. M. (1998). Dystrophin binding to nonmuscle actin. *Cell Motility and the Cytoskeleton*, 41(3):264–270.

Ribeiro, E. d. A., Pinotsis, N., Ghisleni, A., Salmazo, A., Konarev, P. V., Kostan, J., Sjöblom, B., Schreiner, C., Polyansky, A. A., Gkougkoulia, E. A., Holt, M. R., Aachmann, F. L., Žagrović, B., Bordignon, E., Pirker, K. F., Svergun, D. I., Gautel, M., and Djinović-Carugo, K. (2014). The Structure and Regulation of Human Muscle α-Actinin. *Cell*, 159(6):1447–1460. Publisher: Elsevier.

Ridley, A. J. and Hall, A. (1992). The small GTP-binding protein rho regulates the assembly of focal adhesions and actin stress fibers in response to growth factors. *Cell*, 70(3):389–399.

Roman, H. N., Zitouni, N. B., Kachmar, L., Ijpma, G., Hilbert, L., Matusovskiy, O., Benedetti, A., Sobieszek, A., and Lauzon, A.-M. (2013). Unphosphorylated calponin enhances the binding force of unphosphorylated myosin to actin. *Biochimica et biophysica acta*, 1830(10):4634–4641.

Rybakova, I. N., Amann, K. J., and Ervasti, J. M. (1996). A new model for the interaction of dystrophin with F-actin. *The Journal of Cell Biology*, 135(3):661–672.

Rybakova, I. N., Patel, J. R., and Ervasti, J. M. (2000). The Dystrophin Complex Forms a Mechanically Strong Link between the Sarcolemma and Costameric Actin. *The Journal of Cell Biology*, 150(5):1209–1214.

Sadowski, C. E., Lovric, S., Ashraf, S., Pabst, W. L., Gee, H. Y., Kohl, S., Engelmann, S., Vega-Warner, V., Fang, H., Halbritter, J., Somers, M. J., Tan, W., Shril, S., Fessi, I., Lifton, R. P., Bockenhauer, D., El-Desoky, S., Kari, J. A., Zenker, M., Kemper, M. J., Mueller, D., Fathy, H. M., Soliman, N. A., Hildebrandt, F., and Group, t. S. S. (2015). A Single-Gene Cause in 29.5% of Cases of Steroid-Resistant Nephrotic Syndrome. *Journal of the American Society of Nephrology*, 26(6):1279.

Salah, Z., Alian, A., and Aqeilan, R. (2012). WW domain-containing proteins: retrospectives and the future. *Frontiers in bioscience : a journal and virtual library*, 17:331–48.

Salah, Z., Melino, G., and Aqeilan, R. I. (2011). Negative Regulation of the Hippo Pathway by E3 Ubiquitin Ligase ITCH Is Sufficient to Promote Tumorigenicity. *Cancer Research*, 71(5):2010–2020.

Schindelin, J., Arganda-Carreras, I., Frise, E., Kaynig, V., Longair, M., Pietzsch, T., Preibisch, S., Rueden, C., Saalfeld, S., Schmid, B., Tinevez, J.-Y., White, D. J., Hartenstein, V., Eliceiri, K., Tomancak, P., and Cardona, A. (2012). Fiji: an open-source platform for biological-image analysis. *Nature Methods*, 9(7):676–682. Number: 7 Publisher: Nature Publishing Group.

Schlegelmilch, K., Mohseni, M., Kirak, O., Pruszak, J., Rodriguez, J. R., Zhou, D., Kreger, B. T., Vasioukhin, V., Avruch, J., Brummelkamp, T. R., and Camargo, F. D. (2011). Yap1 acts downstream of α-catenin to control epidermal proliferation. *Cell*, 144(5):782–795.

Schleinkofer, K., Wiedemann, U., Otte, L., Wang, T., Krause, G., Oschkinat, H., and Wade, R. C. (2004). Comparative Structural and Energetic Analysis of WW Domain–Peptide Interactions. *Journal of Molecular Biology*, 344(3):865–881.

Schroeter, M. M., Beall, B., Heid, H. W., and Chalovich, J. M. (2008). The Actin Binding Protein, Fesselin, is a Member of the Synaptopodin Family ,. *Biochemical and biophysical research communications*, 371(3):582–586.

Schroeter, M. M. and Chalovich, J. M. (2005). Fesselin binds to actin and myosin and inhibits actin-activated ATPase activity. *Journal of Muscle Research & Cell Motility*, 26(4):183–189.

Seok, S.-H. (2021). Structural Insights into Protein Regulation by Phosphorylation and Substrate Recognition of Protein Kinases/Phosphatases. *Life*, 11(9):957.

Sievers, F. and Higgins, D. G. (2018). Clustal Omega for making accurate alignments of many protein sequences. *Protein Science : A Publication of the Protein Society*, 27(1):135–145.

Sit, B., Gutmann, D., and Iskratsch, T. (2019). Costameres, dense plaques and podosomes: the cell matrix adhesions in cardiovascular mechanosensing. *Journal of Muscle Research and Cell Motility*, 40(2):197–209.

Sjöblom, B., Salmazo, A., and Djinović-Carugo, K. (2008). α-Actinin structure and regulation. *Cellular and Molecular Life Sciences*, 65(17):2688.

Small and Gimona (1998). The cytoskeleton of the vertebrate smooth muscle cell. *Acta Physiologica Scandinavica*, 164(4):341–348. _eprint: https://onlinelibrary.wiley.com/doi/pdf/10.1046/j.1365-201X.1998.00441.x.

Small, J. (1985). Geometry of actin-membrane attachments in the smooth muscle cell: the localisations of vinculin and alpha-actinin. *The EMBO Journal*, 4(1):45–49. Num Pages: 49 Publisher: John Wiley & Sons, Ltd.

Small, J. V. and North, A. J. (1995). - Architecture of the Smooth Muscle Cell. In Schwartz, S. M. and Mecham, R. P., editors, *The Vascular Smooth Muscle Cell*, Biology of Extracellular Matrix, pages 169–188. Academic Press, San Diego.

Somlyo, A. P. and Somlyo, A. V. (2003). Ca2+ Sensitivity of Smooth Muscle and Nonmuscle Myosin II: Modulated by G Proteins, Kinases, and Myosin Phosphatase. *Physiological Reviews*, 83(4):1325–1358. Publisher: American Physiological Society.

Songyang, Z., Fanning, A. S., Fu, C., Xu, J., Marfatia, S. M., Chishti, A. H., Crompton, A., Chan, A. C., Anderson, J. M., and Cantley, L. C. (1997). Recognition of Unique Carboxyl-Terminal Motifs by Distinct PDZ Domains. *Science*, 275(5296):73–77. Publisher: American Association for the Advancement of Science.

Sponga, A., Arolas, J. L., Schwarz, T. C., Jeffries, C. M., Rodriguez Chamorro, A., Kostan, J., Ghisleni, A., Drepper, F., Polyansky, A., De Almeida Ribeiro, E., Pedron, M., Zawadzka-Kazimierczuk, A., Mlynek, G., Peterbauer, T., Doto, P., Schreiner, C., Hollerl, E., Mateos, B., Geist, L., Faulkner, G., Kozminski, W., Svergun, D. I., Warscheid, B., Zagrovic, B., Gautel, M., Konrat, R., and Djinović-Carugo, K. (2021).

Order from disorder in the sarcomere: FATZ forms a fuzzy but tight complex and phase-separated condensates with α-actinin. *Science Advances*, 7(22):eabg7653.

Stricker, N. L., Christopherson, K. S., Yi, B. A., Schatz, P. J., Raab, R. W., Dawes, G., Bassett, D. E., Bredt, D. S., and Li, M. (1997). PDZ domain of neuronal nitric oxide synthase recognizes novel C-terminal peptide sequences. *Nature Biotechnology*, 15(4):336–342.

Stromer, M. H. (1998). The cytoskeleton in skeletal, cardiac and smooth muscle cells. *Histology and Histopathology*, 13(1):283–291.

Studier, F. W. (2005). Protein production by auto-induction in high density shaking cultures. *Protein Expression and Purification*, 41(1):207–234.

Sudol, M. (1994). Yes-associated protein (YAP65) is a proline-rich phosphoprotein that binds to the SH3 domain of the Yes proto-oncogene product. *Oncogene*, 9(8):2145–2152.

Sudol, M. (2013). YAP1 oncogene and its eight isoforms. *Oncogene*, 32(33):3922–3922. Publisher: Nature Publishing Group.

Sudol, M., Bork, P., Einbond, A., Kastury, K., Druck, T., Negrini, M., Huebner, K., and Lehman, D. (1995). Characterization of the mammalian YAP (Yes-associated protein) gene and its role in defining a novel protein module, the WW domain. *The Journal of Biological Chemistry*, 270(24):14733–14741.

Sudol, M., Sliwa, K., and Russo, T. (2001). Functions of WW domains in the nucleus. *FEBS Letters*, 490(3):190–195. _eprint: https://onlinelibrary.wiley.com/doi/pdf/10.1016/S0014-5793%2801%2902122-6.

Sugi, T., Oyama, T., Muto, T., Nakanishi, S., Morikawa, K., and Jingami, H. (2007). Crystal structures of autoinhibitory PDZ domain of Tamalin: implications for metabotropic glutamate receptor trafficking regulation. *The EMBO journal*, 26(8):2192–2205.

Sun, C., De Mello, V., Mohamed, A., Ortuste Quiroga, H. P., Garcia-Munoz, A., Al Bloshi, A., Tremblay, A. M., von Kriegsheim, A., Collie-Duguid, E., Vargesson, N., Matallanas, D., Wackerhage, H., and Zammit, P. S. (2017). Common and Distinctive Functions of the Hippo Effectors Taz and Yap in Skeletal Muscle Stem Cell Function. *Stem Cells (Dayton, Ohio)*, 35(8):1958–1972.

Swist, S., Unger, A., Li, Y., Vöge, A., von Frieling-Salewsky, M., Skärlén, Å., Cacciani, N., Braun, T., Larsson, L., and Linke, W. A. (2020). Maintenance of sarcomeric integrity in adult muscle cells crucially depends on Z-disc anchored titin. *Nature Communications*, 11(1):4479. Publisher: Nature Publishing Group.

Taggart, M. J. (2001). Smooth Muscle Excitation-Contraction Coupling: a Role for Caveolae and Caveolins? *Physiology*, 16(2):61–65. Publisher: American Physiological Society.

Takahashi, K. and Hattori, A. (1989). Alpha-actinin is a component of the Z-filament, a structural backbone of skeletal muscle Z-disks. *Journal of Biochemistry*, 105(4):529–536.

Takahashi, K., Hiwada, K., and Kokubu, T. (1988). Vascular smooth muscle calponin. A novel troponin T-like protein. *Hypertension*, 11(6_pt_2):620–626. Publisher: American Heart Association.

Takayama, S., Bimston, D., Matsuzawa, S.-I., Freeman, B., Aime-Sempe, C., Xie, Z., Morimoto, R., and Reed, J. (1997). BAG-1 modulates the chaperone activity of Hsp70/Hsc70. *EMBO Journal*, 16(16):4887–4896.

Takayama, S., Xie, Z., and Reed, J. C. (1999). An Evolutionarily Conserved Family of Hsp70/Hsc70 Molecular Chaperone Regulators*. *Journal of Biological Chemistry*, 274(2):781–786.

Tang, D. D. (2008). INTERMEDIATE FILAMENTS IN SMOOTH MUSCLE. *American journal of physiology. Cell physiology*, 294(4):C869–C878.

Tang, D. D. and Tan, J. (2003). Role of Crk-Associated Substrate in the Regulation of Vascular Smooth Muscle Contraction. *Hypertension*, 42(4):858–863. Publisher: American Heart Association.

Tang, F., Gill, J., Ficht, X., Barthlott, T., Cornils, H., Schmitz-Rohmer, D., Hynx, D., Zhou, D., Zhang, L., Xue, G., Grzmil, M., Yang, Z., Hergovich, A., Hollaender, G. A., Stein, J. V., Hemmings, B. A., and Matthias, P. (2015). The kinases NDR1/2 act downstream of the Hippo homolog MST1 to mediate both egress of thymocytes from the thymus and lymphocyte motility. *Science Signaling*, 8(397):ra100.

Taylor, K. A., Taylor, D. W., and Schachat, F. (2000). Isoforms of α-Actinin from Cardiac, Smooth, and Skeletal Muscle Form Polar Arrays of Actin Filaments. *The Journal of Cell Biology*, 149(3):635–646.

Terasaki, A. G., Morikawa, K., Suzuki, H., Oshima, K., and Ohashi, K. (2002). Characterization of Arp2/3 complex in chicken tissues. *Cell Structure and Function*, 27(5):383–391.

Tonikian, R., Zhang, Y., Sazinsky, S. L., Currell, B., Yeh, J.-H., Reva, B., Held, H. A., Appleton, B. A., Evangelista, M., Wu, Y., Xin, X., Chan, A. C., Seshagiri, S., Lasky, L. A., Sander, C., Boone, C., Bader, G. D., and Sidhu, S. S. (2008). A specificity map for the PDZ domain family. *PLoS biology*, 6(9):e239.

Totaro, A., Zhuang, Q., Panciera, T., Battilana, G., Azzolin, L., Brumana, G., Gandin, A., Brusatin, G., Cordenonsi, M., and Piccolo, S. (2019). Cell phenotypic plasticity requires autophagic flux driven by YAP/TAZ mechanotransduction. *Proceedings of the National Academy of Sciences of the United States of America*, 116(36):17848–17857.

Trombitás, K., Frey, L., and Pollack, G. H. (1993). Filament lengths in frog semitendinosus and tibialis anterior muscle fibres. *Journal of Muscle Research and Cell Motility*, 14(2):167–172.

Turner, C. E., Kramarcy, N., Sealock, R., and Burridge, K. (1991). Localization of paxillin, a focal adhesion protein, to smooth muscle dense plaques, and the myotendinous and neuromuscular junctions of skeletal muscle. *Experimental Cell Research*, 192(2):651–655.

Ulbricht, A., Eppler, F. J., Tapia, V. E., van der Ven, P. F., Hampe, N., Hersch, N., Vakeel, P., Stadel, D., Haas, A., Saftig, P., Behrends, C., Fürst, D. O., Volkmer, R., Hoffmann, B., Kolanus, W., and Höhfeld, J. (2013). Cellular Mechanotransduction Relies on Tension-Induced and Chaperone-Assisted Autophagy. *Current Biology*, 23(5):430–435.

van der Lee, R., Buljan, M., Lang, B., Weatheritt, R. J., Daughdrill, G. W., Dunker, A. K., Fuxreiter, M., Gough, J., Gsponer, J., Jones, D. T., Kim, P. M., Kriwacki, R. W., Oldfield, C. J., Pappu, R. V., Tompa, P., Uversky, V. N., Wright, P. E., and Babu, M. M. (2014). Classification of Intrinsically Disordered Regions and Proteins. *Chemical Reviews*, 114(13):6589–6631.

van der Ven, P. F. M., Ehler, E., Vakeel, P., Eulitz, S., Schenk, J. A., Milting, H., Micheel, B., and Fürst, D. O. (2006). Unusual splicing events result in distinct Xin isoforms that associate differentially with filamin c and Mena/VASP. *Experimental Cell Research*, 312(11):2154–2167.

Varelas, X. (2014). The Hippo pathway effectors TAZ and YAP in development, homeostasis and disease. *Development*, 141(8):1614–1626.

Varelas, X., Miller, B. W., Sopko, R., Song, S., Gregorieff, A., Fellouse, F. A., Sakuma, R., Pawson, T., Hunziker, W., McNeill, H., Wrana, J. L., and Attisano, L. (2010). The Hippo Pathway Regulates Wnt/β-Catenin Signaling. *Developmental Cell*, 18(4):579–591. Publisher: Elsevier.

Velthuis, A. J. W. t., Sakalis, P. A., Fowler, D. A., and Bagowski, C. P. (2011). Genome-Wide Analysis of PDZ Domain Binding Reveals Inherent Functional Overlap within the PDZ Interaction Network. *PLOS ONE*, 6(1):e16047. Publisher: Public Library of Science.

Venerando, A., Cesaro, L., and Pinna, L. A. (2017). From phosphoproteins to phosphoproteomes: a historical account. *The FEBS Journal*, 284(13):1936–1951. _eprint: https://onlinelibrary.wiley.com/doi/pdf/10.1111/febs.14014.

Verma, A., Jing-Song, F., Finch-Edmondson, M. L., Velazquez-Campoy, A., Balasegaran, S., Sudol, M., and Sivaraman, J. (2018). Biophysical studies and NMR structure of YAP2 WW domain - LATS1 PPxY motif complexes reveal the basis of their interaction. *Oncotarget*, 9(8):8068–8080.

Wackerhage, H., Del Re, D. P., Judson, R. N., Sudol, M., and Sadoshima, J. (2014). The Hippo signal transduction network in skeletal and cardiac muscle. *Science Signaling*, 7(337).

Wada, K.-I., Itoga, K., Okano, T., Yonemura, S., and Sasaki, H. (2011). Hippo pathway regulation by cell morphology and stress fibers. *Development*, 138(18):3907–3914.

Waites, G., Graham, I., Jackson, P., Millake, D., Patel, B., Blanchard, A., Weller, P., Eperon, I., and Critchley, D. (1992). Mutually exclusive splicing of calcium-binding domain exons in chick alpha-actinin. *Journal of Biological Chemistry*, 267(9):6263–6271.

Wang, J., Shaner, N., Mittal, B., Zhou, Q., Chen, J., Sanger, J. M., and Sanger, J. W. (2005). Dynamics of Z-Band Based Proteins in Developing Skeletal Muscle Cells. *Cell motility and the cytoskeleton*, 61(1):34–48.

Wang, P., Bai, Y., Song, B., Wang, Y., Liu, D., Lai, Y., Bi, X., and Yuan, Z. (2011). PP1A-Mediated Dephosphorylation Positively Regulates YAP2 Activity. *PLoS ONE*, 6(9):e24288.

Wang, W., Huang, J., Wang, X., Yuan, J., Li, X., Feng, L., Park, J.-I., and Chen, J. (2012). PTPN14 is required for the density-dependent control of YAP1. *Genes & Development*, 26(17):1959–1971.

Wang, Z., Grange, M., Wagner, T., Kho, A. L., Gautel, M., and Raunser, S. (2021). The molecular basis for sarcomere organization in vertebrate skeletal muscle. *Cell*, 184(8):2135–2150.e13.

Waterhouse, A. M., Procter, J. B., Martin, D. M. A., Clamp, M., and Barton, G. J. (2009). Jalview Version 2–a multiple sequence alignment editor and analysis workbench. *Bioinformatics (Oxford, England)*, 25(9):1189–1191.

Watt, K. I., Judson, R., Medlow, P., Reid, K., Kurth, T. B., Burniston, J. G., Ratkevicius, A., Bari, C. D., and Wackerhage, H. (2010). Yap is a novel regulator of C2C12 myogenesis. *Biochemical and Biophysical Research Communications*, 393(4):619–624.

Watt, K. I., Turner, B. J., Hagg, A., Zhang, X., Davey, J. R., Qian, H., Beyer, C., Winbanks, C. E., Harvey, K. F., and Gregorevic, P. (2015). The Hippo pathway effector YAP is a critical regulator of skeletal muscle fibre size. *Nature Communications*, 6(1):6048. Number: 1 Publisher: Nature Publishing Group.

Webb, R. C. (2003). Smooth muscle contraction and relaxation. *Advances in Physiology Education*, 27(4):201–206. Publisher: American Physiological Society.

Weins, A., Schwarz, K., Faul, C., Barisoni, L., Linke, W. A., and Mundel, P. (2001). Differentiation- and stress-dependent nuclear cytoplasmic redistribution of myopodin, a novel actin-bundling protein. *The Journal of Cell Biology*, 155(3):393–404.

Wickham, H., Averick, M., Bryan, J., Chang, W., McGowan, L. D., François, R., Grolemund, G., Hayes, A., Henry, L., Hester, J., Kuhn, M., Pedersen, T. L., Miller, E., Bache, S. M., Müller, K., Ooms, J., Robinson, D., Seidel, D. P., Spinu, V., Takahashi, K., Vaughan, D., Wilke, C., Woo, K., and Yutani, H. (2019). Welcome to the Tidyverse. *Journal of Open Source Software*, 4(43):1686.

Wiesner, S., Stier, G., Sattler, M., and Macias, M. J. (2002). Solution Structure and Ligand Recognition of the WW Domain Pair of the Yeast Splicing Factor Prp40. *Journal of Molecular Biology*, 324(4):807–822.

Williams, M. W. and Bloch, R. J. (1999). Extensive but coordinated reorganization of the membrane skeleton in myofibers of dystrophic (mdx) mice. *The Journal of Cell Biology*, 144(6):1259–1270.

Winder, S. J., Allen, B. G., Clément-Chomienne, O., and Walsh, M. P. (1998). Regulation of smooth muscle actin-myosin interaction and force by calponin. *Acta Physiologica Scandinavica*, 164(4):415–426.

Wördehoff, J. F. (2020). *Regulation des Cochaperons BAG3 durch Phosphorylierung und Dephosphorylierung*. PhD thesis, Rheinische Friedrich-Wilhelms-Universität Bonn, Bonn.

Wu, J., Yang, Y., Zhang, J., Ji, P., Du, W., Jiang, P., Xie, D., Huang, H., Wu, M., Zhang, G., Wu, J., and Shi, Y. (2007). Domain-swapped Dimerization of the Second PDZ

Domain of ZO2 May Provide a Structural Basis for the Polymerization of Claudins *. *Journal of Biological Chemistry*, 282(49):35988–35999. Publisher: Elsevier.

Xia, H., Winokur, S. T., Kuo, W.-L., Altherr, M. R., and Bredt, D. S. (1997). Actinin-associated LIM Protein: Identification of a Domain Interaction between PDZ and Spectrin-like Repeat Motifs. *The Journal of Cell Biology*, 139(2):507–515.

Xu, X.-Z. S., Choudhury, A., Li, X., and Montell, C. (1998). Coordination of an Array of Signaling Proteins through Homo- and Heteromeric Interactions Between PDZ Domains and Target Proteins. *The Journal of Cell Biology*, 142(2):545–555.

Yaffe, D. and Saxel, O. (1977). Serial passaging and differentiation of myogenic cells isolated from dystrophic mouse muscle. *Nature*, 270(5639):725–727.

Yamaguchi, M., Izumimoto, M., Robson, R. M., and Stromer, M. H. (1985). Fine structure of wide and narrow vertebrate muscle Z-lines: A proposed model and computer simulation of Z-line architecture. *Journal of Molecular Biology*, 184(4):621–643.

Yamin, R. and Morgan, K. G. (2012). Deciphering actin cytoskeletal function in the contractile vascular smooth muscle cell. *The Journal of Physiology*, 590(17):4145–4154.

Yan, Q. (2011). Rapid Coomassie Protein SDS-gel Staining. *BIO-PROTOCOL*, 1(12).

Yang, S., Zhang, L., Liu, M., Chong, R., Ding, S.-J., Chen, Y., and Dong, J. (2013). CDK1 Phosphorylation of YAP Promotes Mitotic Defects and Cell Motility and Is Essential for Neoplastic Transformation. *Cancer research*, 73(22):10.1158/0008–5472.CAN–13–2049.

Ylänne, J., Scheffzek, K., Young, P., and Saraste, M. (2001). Crystal structure of the alpha-actinin rod reveals an extensive torsional twist. *Structure (London, England: 1993)*, 9(7):597–604.

Young, P. and Gautel, M. (2000). The interaction of titin and alpha-actinin is controlled by a phospholipid-regulated intramolecular pseudoligand mechanism. *The EMBO journal*, 19(23):6331–6340.

Yu, Y. P. and Luo, J.-H. (2006). Myopodin-mediated suppression of prostate cancer cell migration involves interaction with zyxin. *Cancer Research*, 66(15):7414–7419.

Zack, G. W., Rogers, W. E., and Latt, S. A. (1977). Automatic measurement of sister chromatid exchange frequency. *Journal of Histochemistry & Cytochemistry*, 25(7):741–753. Publisher: Journal of Histochemistry & Cytochemistry.

Zambrano, N., Bruni, P., Minopoli, G., Mosca, R., Molino, D., Russo, C., Schettini, G., Sudol, M., and Russo, T. (2001). The β-Amyloid Precursor Protein APP Is Tyrosine-phosphorylated in Cells Expressing a Constitutively Active Form of the Abl Protoncogene *. *Journal of Biological Chemistry*, 276(23):19787–19792. Publisher: Elsevier.

Zeng, M., Shang, Y., Guo, T., He, Q., Yung, W.-H., Liu, K., and Zhang, M. (2016). A binding site outside the canonical PDZ domain determines the specific interaction between Shank and SAPAP and their function. *Proceedings of the National Academy of Sciences of the United States of America*, 113(22):E3081–3090.

Zhang, C., Zhu, H., Ren, X., Gao, B., Cheng, B., Liu, S., Sha, B., Li, Z., Zhang, Z., Lv, Y., Wang, H., Guo, H., Lu, T. J., Xu, F., Genin, G. M., and Lin, M. (2021). Mechanics-driven nuclear localization of YAP can be reversed by N-cadherin ligation in mesenchymal stem cells. *Nature Communications*, 12(1):6229. Publisher: Nature Publishing Group.

Zhang, M., Liu, J., Cheng, A., Deyoung, S. M., and Saltiel, A. R. (2007). Identification of CAP as a costameric protein that interacts with filamin C. *Molecular Biology of the Cell*, 18(12):4731–4740.

Zhao, B., Li, L., Tumaneng, K., Wang, C.-Y., and Guan, K.-L. (2010). A coordinated phosphorylation by Lats and CK1 regulates YAP stability through SCFβ-TRCP. *Genes & Development*, 24(1):72–85.

Zhao, B., Wei, X., Li, W., Udan, R. S., Yang, Q., Kim, J., Xie, J., Ikenoue, T., Yu, J., Li, L., Zheng, P., Ye, K., Chinnaiyan, A., Halder, G., Lai, Z.-C., and Guan, K.-L. (2007). Inactivation of YAP oncoprotein by the Hippo pathway is involved in cell contact inhibition and tissue growth control. *Genes & Development*, 21(21):2747–2761.

Zhao, B., Ye, X., Yu, J., Li, L., Li, W., Li, S., Yu, J., Lin, J. D., Wang, C.-Y., Chinnaiyan, A. M., Lai, Z.-C., and Guan, K.-L. (2008). TEAD mediates YAP-dependent gene induction and growth control. *Genes & Development*, 22(14):1962–1971.

Zhao, Y. and Yang, X. (2015). Regulation of sensitivity of tumor cells to antitubulin drugs by Cdk1-TAZ signalling. *Oncotarget*, 6(26):21906–21917.

Zheng, Z. and Song, Y. (2023). Synaptopodin-2: a potential tumor suppressor. *Cancer Cell International*, 23:158.

Zhou, Q., Ruiz-Lozano, P., Martone, M. E., and Chen, J. (1999). Cypher, a striated muscle-restricted PDZ and LIM domain-containing protein, binds to alpha-actinin-2 and protein kinase C. *The Journal of Biological Chemistry*, 274(28):19807–19813.

Zhu, Z. Y. and Karlin, S. (1996). Clusters of charged residues in protein three-dimensional structures. *Proceedings of the National Academy of Sciences of the United States of America*, 93(16):8350–8355.

Zou, R., Xu, Y., Feng, Y., Shen, M., Yuan, F., and Yuan, Y. (2020). YAP nuclear-cytoplasmic translocation is regulated by mechanical signaling, protein modification, and metabolism. *Cell Biology International*, 44(7):1416–1425.

Appendix A

Abbreviations

aa	Amino acid(s)
ABD	Actin-binding domain
AMOT1/2	Angiomotin-1/2
AMOTL1/2	Angiomotin-like-1/2
AP-MS	Affinity purification-coupled mass spectrometry
APS	Ammonium persulfate
ATP	Adenosine triphosphate
AU	Airy unit
BAG3	B-cell lymphoma-2-associated athanogene 3
BiFC	Bimolecular fluorescence complementation
BSA	Bovine serum albumin
bp	Base pairs
CAMD	Calmodulin-like domain
CaMKII	Ca^{2+}/calmodulin-dependent kinase II
CASA	Chaperone-assisted selective autophagy
cDNA	Complementary deoxyribonucleic acid
CDK	Cyclin-dependent kinase
CLSM	Confocal laser-scanning microscopy
Co-IP	Co-immuno precipitation
CRC	Colorectal cancer
DAPI	4,6-Diamidin-2-phenylindol
DGC	Dystrophin-glycoprotein complexes
DHPR	Dihydropyridine receptors
Dlg1	Disc large tumor suppressor
DM	Differentiation medium
DMEM	Dulbecco's modified eagle medium
DMSO	Dimethyl sulfoxide
DNA	Deoxyribonucleic acid

DPBS	Dulbecco's phosphate-buffered saline
DVL2	Disheveled-2
EC	Exitation-contraction coupling
ECL	Enhanced chemiluminescence
ECM	Extracellular matrix
EDTA	Ethylenediaminetetraacetic acid
eGFP	Enhanced green fluorescent protein
EGS	Ethylene glycol bis-(succinimidyl succinate)
EPS	Electrical pulse stimulation
FA	Focal adhesion
FCS	Fetal calf serum
FPLC	Fast liquid protein chromatography
FRAP	Fluorescence recovery after photobleaching
GF	Gel filtration chromatography
GFP	Green fluorescent protein
GM	Growth medium
GPCR	G-protein coupled receptors
GSH	Glutathione
GST	Glutathione-S-transferase
H1/2/3	Homology regions of synaptopodin family proteins
HRP	Horseradish peroxidase
HS	Horse serum
IF	Immunofluorescence
Ig	Immunoglobulin
IPTG	Isopropyl β-D-1-thiogalactopyranoside
ITCH	E3 ubiquitin-protein ligase Itchy homolog
jSR	Junctional sarcoplasmic reticulum
KIBRA	Kidney and brain protein
LATS1/2	Large tumor suppressor kinase 1/2
LB	Luria-Bertani
LC3	Microtubule-associated proteins 1A/1B light chain 3B
LDB3	LIM domain-binding protein 3
MEM	Modified eagle medium
MLC	Myosin light chain
MLCK	Myosin light chain kinase
MLCP	Myosin light chain phosphatase

MLP	Muscle LIM protein
mRNA	Messenger RNA
MSC	Mesenchymal stem cells
MST1/2	Mammalian STE20-like protein kinase 1/2
mTOR	Mammalian target of rapamycin
NDR1	Nuclear DBF2-related kinase 1 (also known as STK38)
NEAA	Non-essential amino acids
NEDD4	E3 ubiquitin ligase protein NEDD4
NGS	Normal goat serum
nNOS	Neuronal nitric oxide synthase
NTA	Nitrilotriacetic acid
NS	Nephrotic syndrome
PAGE	Polyacrylamide gel electrophoresis
PBS	Phosphate-buffered saline
PBST	Phosphate-buffered saline supplemented with Tween-20
PCC	Pearson correlation coefficient
PCR	Polymerase chain reaction
PDLIM	PDZ and LIM domain protein
PDZ-BM	PDZ domain-binding motif
PFA	Paraformaldehyde
PIC	Protease inhibitor complex
PKA	Protein kinase A
PKB	Protein kinase B (also known as Akt)
PKC	Protein kinase C
PMSF	Phenylmethylsulfonyl fluoride
POI	Protein of interest
PPI	Protein-protein interaction
PSD95	Post synaptic density protein
PTM	Post-translational modification
PWM	Position-weighted matrix
RNA	Ribonucleic acid
ROI	Region of interest
RT	Room temperature
RyR	Ryanodine receptor
SDS	Sodium dodecyl sulfate
SEC	Size-exclusion chromatography

SERCA	Sarco-/endoplasmic reticulum Ca^{2+}-ATPase
sHSP	Small heat-shock protein
SI	Système International, International system of units
SLIM	Short linear motifs
SNT1	α1-syntrophin
SOC	Super optimal broth with catabolite repression
SR	Sarcoplasmic reticulum
SR	Spectrin-repeat
SRNS	Steroid-resistant nephrotic syndrome
SVM	Support vector machine
SYNPO	Synaptopodin
SYNPO2	Synaptopodin-2
SYNPO2L	Synaptopodin-2-like
TAD	Transcription activation domain
TAE	Tris-acetic acid-EDTA
TAP	Tandem-affinity purification
TAZ	Transcriptional coactivator with PDZ-binding motif
TBE	Tris-boric acid-EDTA
TBS	Tris-buffered saline
TBST	Phosphate-buffered saline supplemented with Tween-20
TC	Terminal cisterna
TCE	2,2,2-trichloro ethanol
TEAD	TEA domain transcription factors
TEMED	N,N,N',N'-tetramethylethylendiamin
TNBC	Triple-negative breast cancer
Tris	Tris-(hydroxymethyl)-amino methane
TSC1	Tuberous sclerosis complex 1
UBC	Ubiquitin-conjugating enzymes
UV	Ultraviolet
VGCC	Voltage-gated Ca^{2+}-channels
vSMC	Vascular smooth muscle cells
WB	Western blotting
WWTR1	WW domain transcriptional cofactor 1
Y2H	Yeast-two-hybrid
YAP1	Yes-associated protein 1
YFP	Yellow fluorescent protein

ZASP	Z-band alternatively spliced PDZ-motif protein
ZO-1	Zonula occludens-1 protein
ZY	N-Z-amine medium supplemented with yeast extract

Amino acid code

1 letter code	Amino acid	Group
A	Alanine	
C	Cysteine	
D	Aspartate	
E	Glutamate	
F	Phenylalanine	
G	Glycine	
H	Histidine	
I	Isoleucine	
K	Lysine	
L	Leucine	
M	Methionine	
N	Asparagine	
P	Proline	
Q	Glutamine	
R	Arginine	
S	Serine	
T	Threonine	
V	Valine	
W	Tryptophan	
Y	Tyrosine	
X	Any amino acid	
Φ	V, I, L, F, W, Y, M	Hydrophobic
Ω	F, W, Y, H	Aromatic
Ψ	V, I, G, L, A, M	Aliphatic (non-aromatic)

SI-Prefixes

Symbol	Prefix	Decimal Factor
M	Mega-	10^{6}
k	Kilo-	10^{3}
c	Centi-	10^{-2}
m	Milli-	10^{-3}
µ	Micro-	10^{-6}
n	Nano-	10^{-9}
f	Femto-	10^{-12}

List of Units

Symbol	Unit
°C	Degrees Celsius
A	Amperes
Å	Ångströms
d	Days
Da	Daltons
g	Gravity acceleration
h	Hours
L	Liters
M	Molar (Molarity)
m	Meters
min	Minutes
mol	Moles
s	Seconds
U	Unit

Appendix B

Motifs and domain classes

Tab. B.1: PDZ domain classes

(Sub)class	Recognized PDZ-BM	Examples	References
I	X–X–[S/T]–X–Φ_{COOH}	ZO-2	Oka *et al.*, 2010
II	X–X–Φ–X–Φ_{COOH}	syntenin	Grembecka *et al.*, 2006
III	X–X–[D/E]–X–Φ_{COOH}	nNOS	Stricker *et al.*, 1997
			Songyang *et al.*, 1997
IVa	X–[D/E]–X–W–Φ_{COOH}	ZO-1	Kausalya *et al.*, 2001
		NHERF4	Ernst *et al.*, 2014
		DVL-2	Varelas *et al.*, 2010
			Tonikian *et al.*, 2008
			Ivarsson *et al.*, 2012

Taken and adapted from Songyang *et al.*, 1997; Tonikian *et al.*, 2008; Ivarsson *et al.*, 2012.

Tab. B.2: WW domain groups

Class	Recognized motif	Examples	References
I	[L/P]–P–X*–[Y/Y_{phos}]	YAP1/TAZ	Macias *et al.*, 1996
		BAG3	Otte *et al.*, 2003
II	P–P–L–P–X*	FBP11	Otte *et al.*, 2003
			Kato *et al.*, 2004
			Kato *et al.*, 2006
III	[P/F]–P–X–P–P–X*–R and	FE65/ABPP1	Zambrano *et al.*, 2001
	[P/F]–P–P–[R/K]–X–X*–P–X*		Otte *et al.*, 2003
			Kato *et al.*, 2004
IV	[S_{phos}/T_{phos}]–P	PIN1	Otte *et al.*, 2003
V	[P/F]–P–P–P–P–P	PRP40	Salah *et al.*, 2012
			Wiesner *et al.*, 2002

Taken and adapted from Salah *et al.*, 2012.

Tab. B.3: YAP1/TAZ phosphorylation sites and kinases

Protein	Site	Regulatory effect	Kinases	References
YAP1	S61	Inhibition by cytoplasmic retention	LATS1/2	Zhao *et al.*, 2010
				Clarke *et al.*, 2021
	S109	Inhibition by inactivating YAP1	LATS1/2	Zhao *et al.*, 2010
	T119	Cell cycle regulation	CDK1	Yang *et al.*, 2013
	S127	Cytoplasmic retention/14-3-3 interaction	LATS1/2	Zhao *et al.*, 2007
			NDR1	Zhang *et al.*, 2015
			PKB/Akt	Basu *et al.*, 2003
	S164	Inhibition by cytoplasmic retention	LATS1/2	Zhao *et al.*, 2010
	S381	Inhibition by cytoplasmic retention	LATS1/2	Zhao *et al.*, 2010
	Y389	Activation by stabilizing YAP1	c-Abl	Levy *et al.*, 2008
	S397	Inhibition by cytoplasmic retention	LATS1/2	Zhao *et al.*, 2010
TAZ	S66	Inhibition by cytoplasmic retention	LATS1/2	Lei *et al.*, 2008
	S89	Cytoplasmic retention/14-3-3 interaction	LATS1/2	Lei *et al.*, 2008
	S90	Cell cycle regulation	CDK1	Zhao & Yang, 2015
	S117	Inhibition by inactivating TAZ	LATS1/2	HRXXS motif
	S311	Inhibition by cytoplasmic retention	LATS1/2	Zhao *et al.*, 2010

All YAP1 amino acid positions refer to the human YAP1-2α isoform (UniProtID: *P46937-2*).

Appendix C

Supplementary Figures

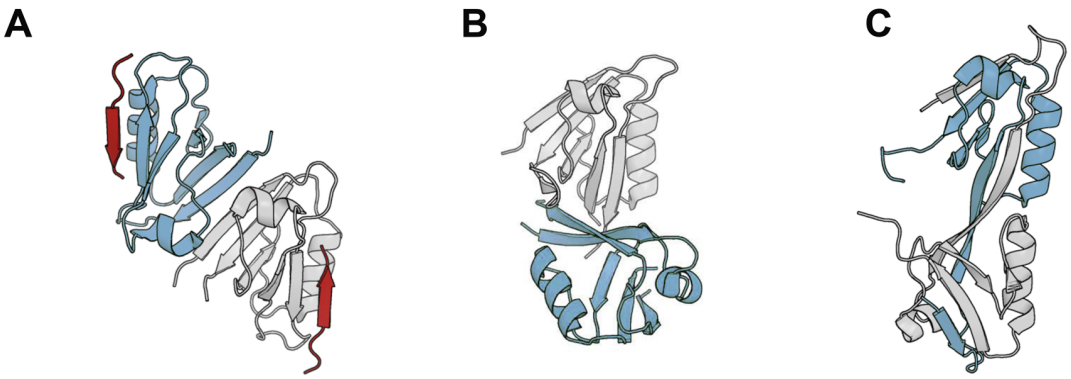


Fig. C.1: Species of PDZ-PDZ dimer complexes. Monomeric PDZ domain interaction partners are outlined in green and gray. Bound ligands are outlined in red. (A) Dimerization by formation of a β A–β E interprotomeric sheet at the interaction interface. (B) Dimerization by β B–β C strand interaction. (C) Dimerization by strand swapping, usually referred to as domain swapping (Wu *et al.*, 2007). Taken and modified from Delhommel, 2017, p.61.

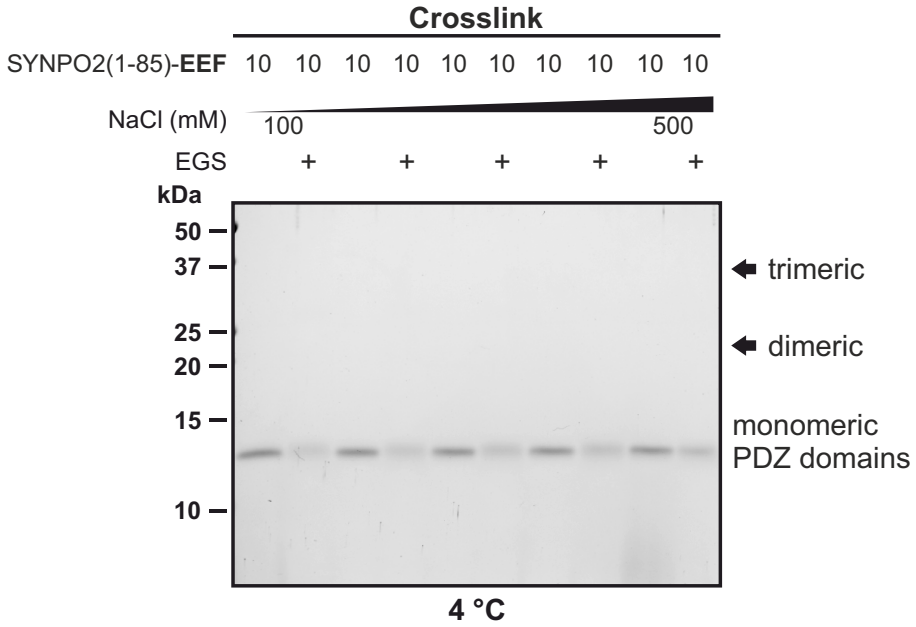


Fig. C.2: Protein crosslinks using the PDZ domain of SYNPO2 with increased ionic strength. SDS-PAGE analyzing purified PDZ domains of SYNPO2, abbreviated SYNPO2(1–85) in crosslinking assays. Ionic strength of NaCl and samples containing PDZ domains of SYNPO2 labeled above. Samples were chemically crosslinked with EGS. Reaction conditions are shown on the bottom. Control samples without crosslinking agent present were supplemented with DMSO. The band migration pattern of molecular weight markers is shown on the left. The expected migration of potential dimeric and trimeric PDZ domain protein complexes is indicated by arrows on the right.

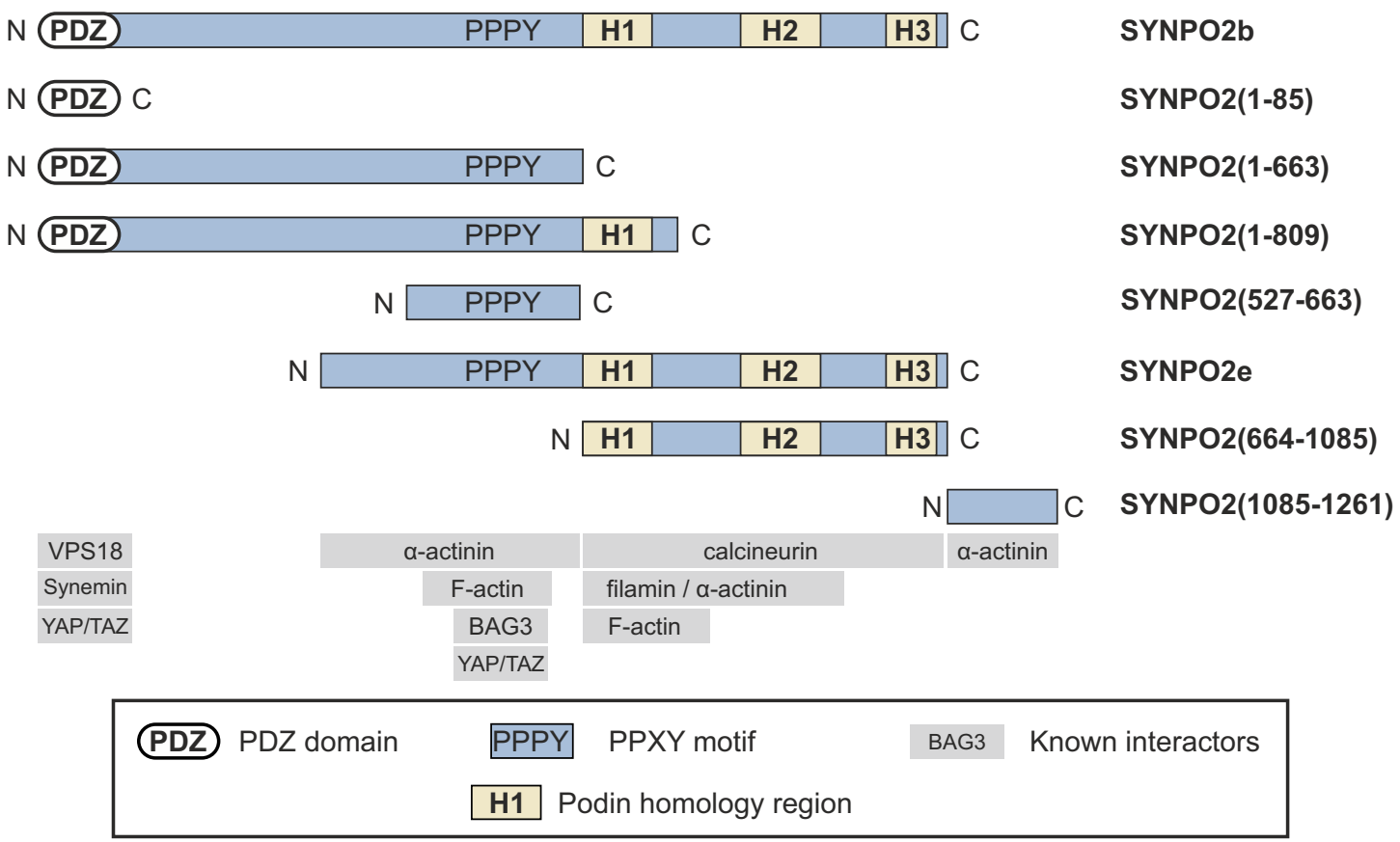


Fig. C.3: SYNPO2 constructs for biochemistry and cell biology experiments. Important domains are outlined. Construct names are denoted on the right. Amino acid positions refer to the human SYNPO2a isoform (UniProtID: *Q9UMS6*).

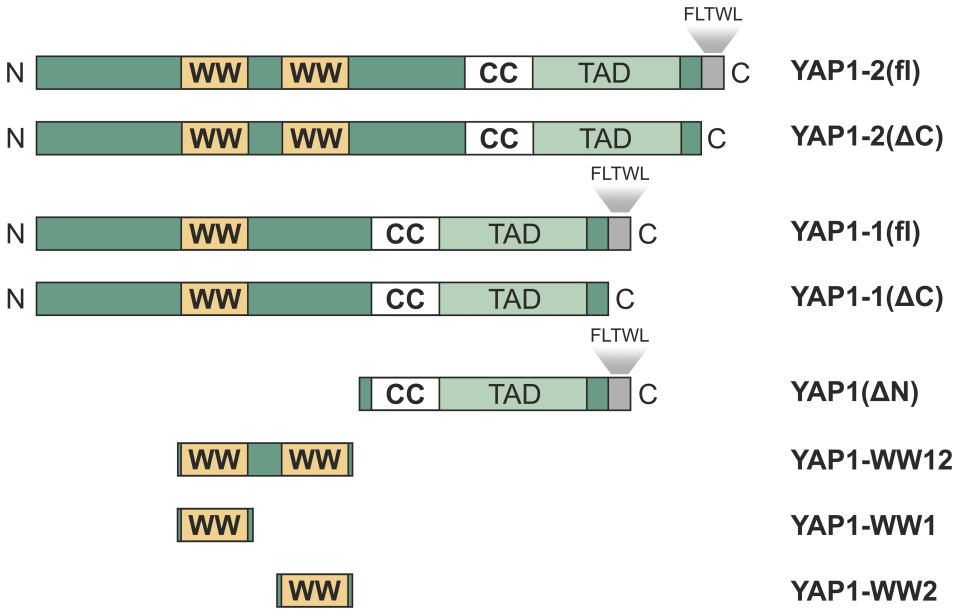


Fig. C.4: YAP1 constructs for biochemistry and cell biology experiments. Important domains are outlined. Construct names are denoted on the right. Amino acid positions refer to the human YAP1-2α isoform (UniProtID: *P46937-2*).

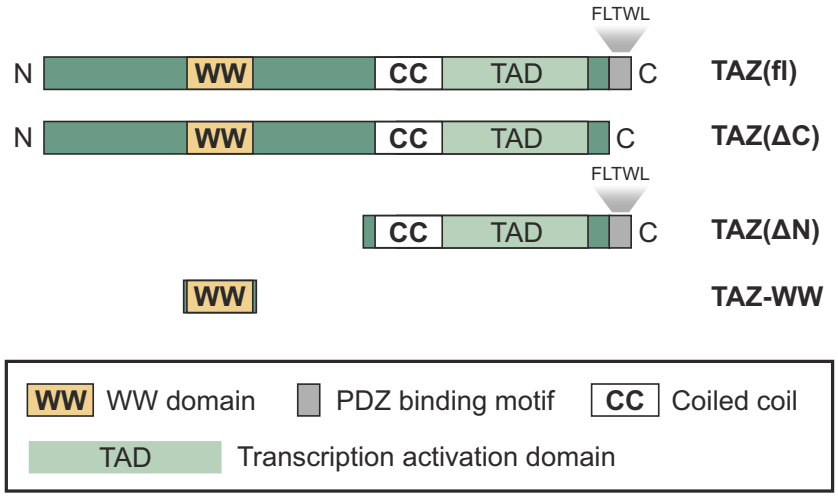


Fig. C.5: TAZ constructs for biochemistry and cell biology experiments. Important domains are outlined. Construct names are denoted on the right. Amino acid positions refer to human TAZ (UniProtID: *Q9GZV5*).

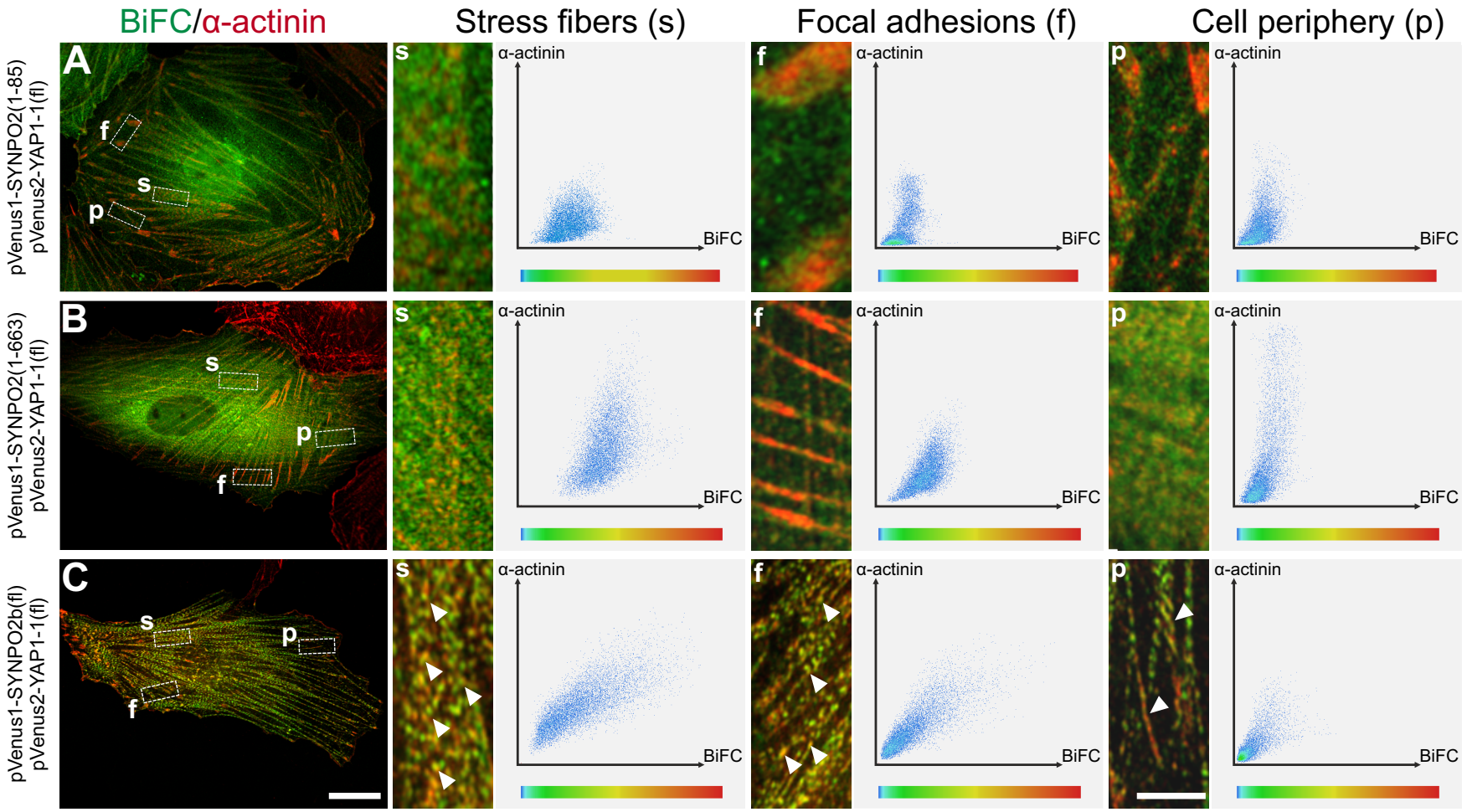


Fig. C.6: BiFC experiment of analyzed ROIs in A7r5 smooth muscle-like cells. (Left panels) A7r5 cells transfected with different combination of SYNPO2 and YAP1–1 constructs (A-C). (Right panels) Cell images and scatter plots from BiFC signal and the dense body marker α-actinin. Analyses were carried out in three different ROIs at the actin cytoskeleton: stress fibers (s), FAs (f), and the cell periphery (c). Scale bar: 10 µm and 5 µm, respectively.

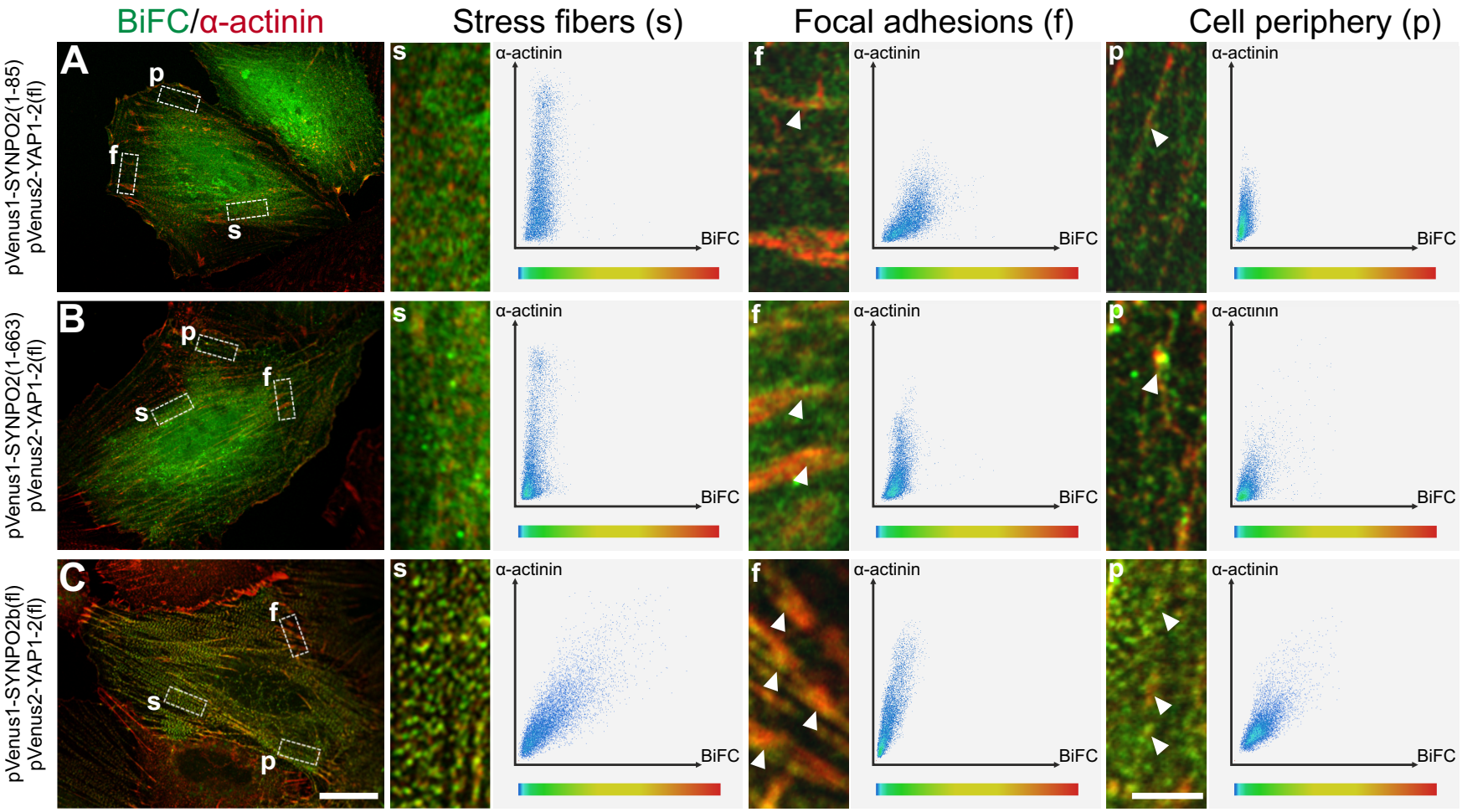


Fig. C.7: BiFC experiment of analyzed ROIs in A7r5 smooth muscle-like cells. (Left panels) A7r5 cells transfected with different combination of SYNPO2 and YAP1–2 constructs (A-C). (Right panels) Cell images and scatter plots from BiFC signal and the dense body marker α-actinin. Analyses were carried out in three different ROIs at the actin cytoskeleton: stress fibers (s), FAs (f), and the cell periphery (c). Scale bar: 10 µm and 5 µm, respectively.

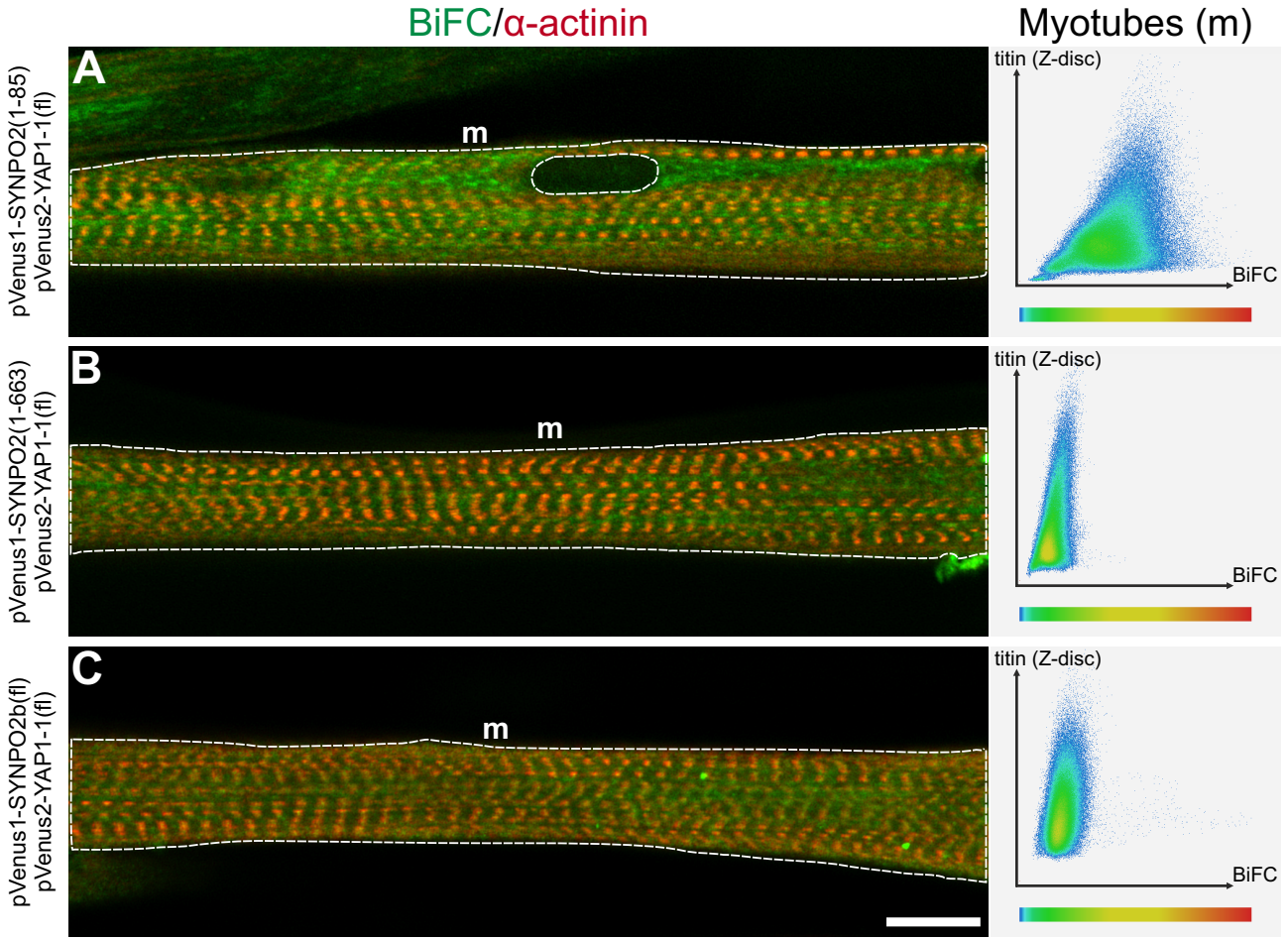


Fig. C.8: BiFC experiment of analyzed ROIs in C2C12 myotubes. (Left panels) C2C12 myotubes transfected with different combination of SYNPO2 and YAP1–1 constructs (A-C). (Right panels) Cell images and scatter plots from BiFC signal and the Z-disc epitope of titin. Analyses were carried out in a single ROI encompassing the myotube (m). Scale bar: 10 µm.

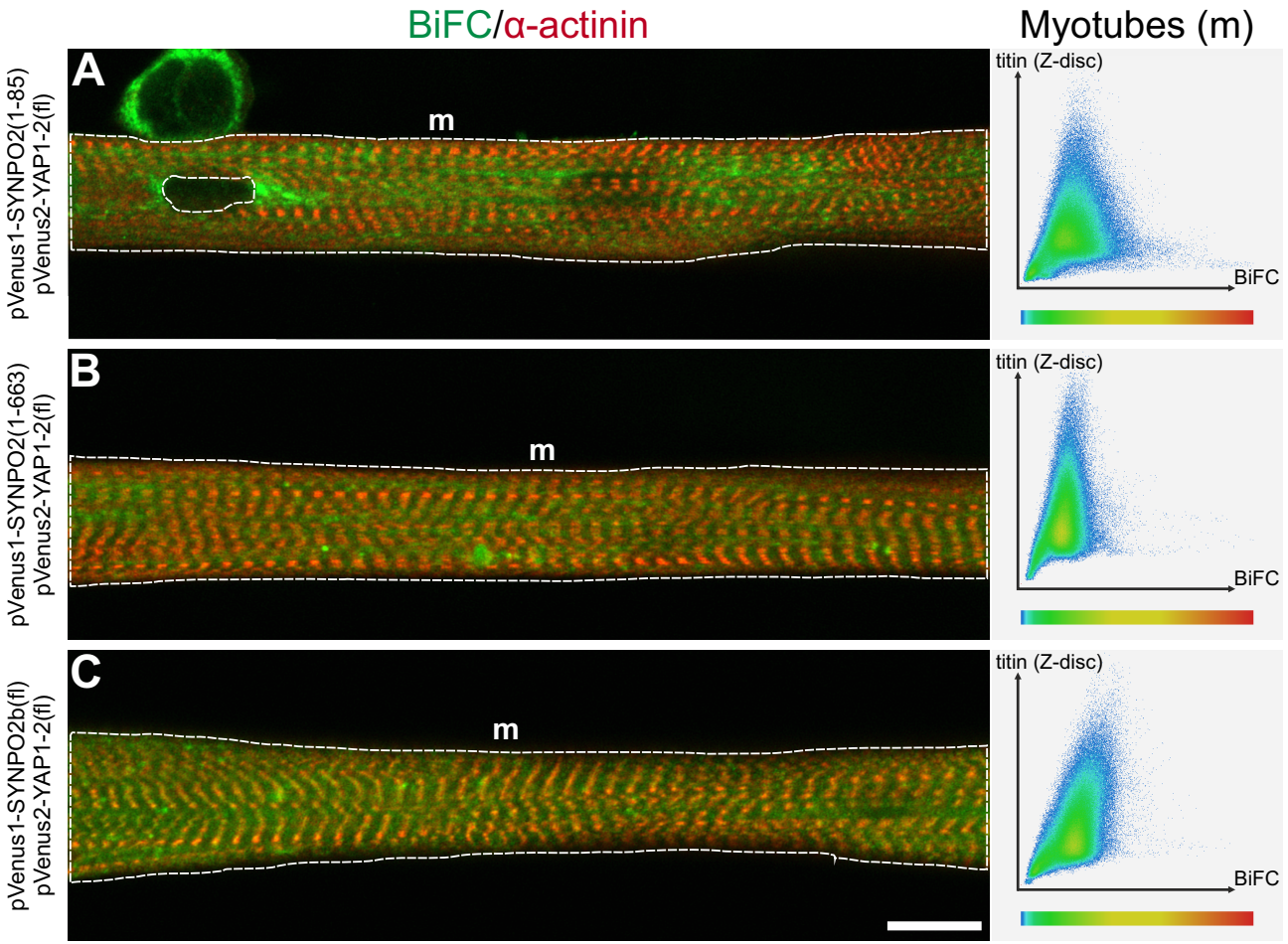


Fig. C.9: BiFC experiment of analyzed ROIs in C2C12 myotubes. (Left panels) C2C12 myotubes transfected with different combination of SYNPO2 and YAP1–2 constructs (A-C). (Right panels) Cell images and scatter plots from BiFC signal and the Z-disc epitope of titin. Analyses were carried out in a single ROI encompassing the myotube (m). Scale bar: 10 µm.

Appendix D

Sequences and primers

Tab. D.1: α-actinin cloning primer sequences

Primer name	Sequence	Amino acid position
huACTN1f	TTACGCGTATGGACCATTATGATTCTCAG	1
huACTN1endr	TTTGTCGACGAGGTCACTCTCGCCGTACAG	full-length
huACTN3_1f	TTTACGCGTATGATGATGGTTATGCAGCCC	1
huACTN3_endr	TTTGTCGACAAGGTCGCTCTCCCCATAGAG	full-length
huACTN4_1f	TTTACGCGTATGGTGGACTACCACGCGGCG	1
huACTN4_endr_*Xho*	TTTCTCGAGCAGGTCGCTCTCGCCATACAA	full-length

Tab. D.2: SYNPO2 cloning primer sequences

Primer name	Sequence	Amino acid position
LMYOP_1f	TTTGGATCCATGGGCACAGGGGATTTTATC	1
MYOP_ORFf	TTTACGCGTATGTTTAAGAAGCGACGTCGG	396
LMYOP_PDZr	TTTTGTCGACTTTGATGAGCATTTGGAGAG	85
MYOP_1482r	TTTGTCGACCGAATCGTAAAAGGCTGGCTG	663
MYOP_1990f	TTTACGCGTTCTGAGCGAATAGCTTCCCGA	803
MYOP_1920r	TTTGTCGACGGCTATTTTGATGGAGGAGAC	809
MYOP_1579f	TTTACGCGTACCGATGGCCTGAGAACCACG	527
MYOP_endr2	TTGTCGACCTCTTCCACAACAGATGGTTTC	1093
Exon 6 primer		
MYOP_ex5f	TTTACGCGTGAGAGTGGGCGCTCCCTTTCT	1085
altMYOPendr	TTTGTCGACTGTTTGGCGTCTCCATCCCC	1261

All amino acid positions refer to the human SYNPO2b isoform (UniProtID: *Q9UMS6-1*), exon 6 primers refer to the human SYNPO2a isoform (UniProtID: *Q9UMS6-2*).

Tab. D.3: YAP1 and TAZ cloning primer sequences

Primer name	Sequence	Amino acid position
huYAP1_1f	TTTACGCGTATGGATCCCGGGCAGCAGCCG	1
huYAP1_endr	TTTGTCGACCTATAACCATGTAAGAAAGCT	full-length
huYAP1_QELA_fw	TTTACGCGTCAGGAGTTAGCCCTGCGTAGC	327
huYAP1_deltaC_rev	TTTGTCGACGCCACCAAGCTAGATAAAGAAAGC	483
huTAZ1_1f	TTTACGCGTATGAATCCGGCCTCGGCGCCC	1
huTAZ1_endr	TTTCTCGAGTTACAGCCAGGTTAGAAAGGG	full-length
huTAZ1_ERER_fw	TTTACGCGTGAGAGAGAAAGGATTCGAATG	245
huTAZ1_deltaC_rev	TTTCTCGAGTTAGGGCTCACTTTTGTTCAGAGCAGA	400

All YAP1 amino acid positions refer to the human YAP1-2α isoform (UniProtID: *P46937-2*). TAZ amino acid positions refer to human TAZ (UniProtID: *Q9GZV5).*

Tab. D.4: SYNPO2L cloning primer sequences

Primer name	Sequence	Amino acid position
huTRITO_MGAEE_fw	TTTACGCGTATGGGTGCTGAGGAGGAGGTG	1
PDZ40b_PDZr	TTTGTCGACCTGCACAGTGAGGACAAGCTG	85

Amino acid positions refer to the human SYNPO2La isoform (UniProtID: *Q9H987-1*).

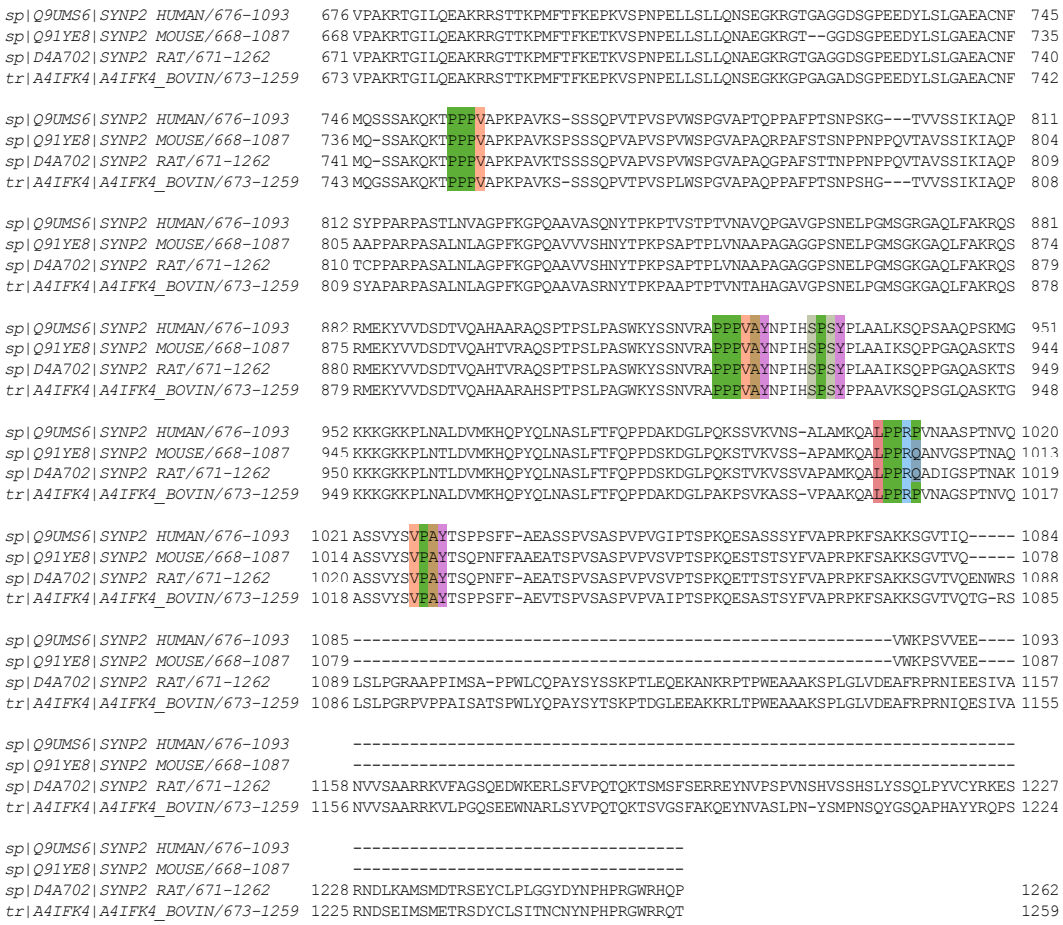


Fig. C.10: Sequence alignment of SYNPO2 proteins from different species. Conserved pseudo-PPXY motifs and prolinie-rich stretches specific for WW domains are outlined. Alignment performed via Clustal algorithm with default settings (Larkin *et al.*, 2007).

```
sp|P12814|ACTN1_HUMAN/1-892    1 --------------------MDHYDSQQTNDYMQPEEDWDRDLLLDPAWEKQQRKTFTAWCNSHLRKAGTQIENIEE  57
sp|P35609|ACTN2_HUMAN/1-894    1 ------MNQIEP------GVQYNYVYDEDEYMIQEEEWDRDLLLDPAWEKQQRKTFTAWCNSHLRKAGTQIENIEE  64
sp________ACTN3_HUMAN/1-901    1 -----MMMVMQPEGLGAGEGRFAGGGGGGEYMEQEEDWDRDLLLDPAWEKQQRKTFTAWCNSHLRKAGTQIENIEE  71
sp|O43707|ACTN4_HUMAN/1-911    1 MVDYHAANQSYQYGPSSAGNGAGGGGSMGDYMAQEDDWDRDLLLDPAWEKQQRKTFTAWCNSHLRKAGTQIENIDE  76

sp|P12814|ACTN1_HUMAN/1-892   58 DFRDGLKLMLLLEVISGERLAKPERGKMRVHKISNVNKALDFIASKGVKLVSIGAEEIVDGNVKMTLGMIWTIILR 133
sp|P35609|ACTN2_HUMAN/1-894   65 DFRNGLKLMLLLEVISGERLPKPDRGKMRFHKIANVNKALDYIASKGVKLVSIGAEEIVDGNVKMTLGMIWTIILR 140
sp________ACTN3_HUMAN/1-901   72 DFRNGLKLMLLLEVISGERLPRPDKGKMRFHKIANVNKALDFIASKGVKLVSIGAEEIVDGNLKMTLGMIWTIILR 147
sp|O43707|ACTN4_HUMAN/1-911   77 DFRDGLKLMLLLEVISGERLPKPERGKMRVHKINNVNKALDFIASKGVKLVSIGAEEIVDGNAKMTLGMIWTIILR 152

sp|P12814|ACTN1_HUMAN/1-892  134 FAIQDISVEETSAKEGLLLWCQRKTAPYKNVNIQNFHISWKDGLGFCALIHRHRPELIDYGKLRKDDPLTNLNTAF 209
sp|P35609|ACTN2_HUMAN/1-894  141 FAIQDISVEETSAKEGLLLWCQRKTAPYRNVNIQNFHTSWKDGLGLCALIHRHRPDLIDYSKLNKDDPIGNINLAM 216
sp________ACTN3_HUMAN/1-901  148 FAIQDISVEETSAKEGLLLWCQRKTAPYRNVNVQNFHTSWKDGLALCALIHRHRPDLIDYAKLRKDDPIGNLNTAF 223
sp|O43707|ACTN4_HUMAN/1-911  153 FAIQDISVEETSAKEGLLLWCQRKTAPYKNVNVQNFHISWKDGLAFNALIHRHRPELIEYDKLRKDDPVTNLNNAF 228

sp|P12814|ACTN1_HUMAN/1-892  210 DVAEKYLDIPKMLDAEDIVGTARPDEKAIMTYVSSFYHAFSGAQKAETAANRICKVLAVNQENEQLMEDYEKLASD 285
sp|P35609|ACTN2_HUMAN/1-894  217 EIAEKHLDIPKMLDAEDIVNTPKPDERAIMTYVSCFYHAFAGAEQAETAANRICKVLAVNQENERLMEEYERLASE 292
sp________ACTN3_HUMAN/1-901  224 EVAEKYLDIPKMLDAEDIVNTPKPDEKAIMTYVSCFYHAFAGAEQAETAANRICKVLAVNQENEKLMEEYEKLASE 299
sp|O43707|ACTN4_HUMAN/1-911  229 EVAEKYLDIPKMLDAEDIVNTARPDEKAIMTYVSSFYHAFSGAQKAETAANRICKVLAVNQENEHLMEDYEKLASD 304

sp|P12814|ACTN1_HUMAN/1-892  286 LLEWIRRTIPWLENRVPENTMHAMQQKLEDFRDYRRLHKPPKVQEKCQLEINFNTLQTKLRLSNRPAFMPSEGRMV 361
sp|P35609|ACTN2_HUMAN/1-894  293 LLEWIRRTIPWLENRTPEKTMQAMQKKLEDFRDYRRKHKPPKVQEKCQLEINFNTLQTKLRISNRPAFMPSEGKMV 368
sp________ACTN3_HUMAN/1-901  300 LLEWIRRTVPWLENRVGEPSMSAMQRKLEDFRDYRRLHKPPRIQEKCQLEINFNTLQTKLRLSHRPAFMPSEGKLV 375
sp|O43707|ACTN4_HUMAN/1-911  305 LLEWIRRTIPWLEDRVPQKTIQEMQQKLEDFRDYRRVHKPPKVQEKCQLEINFNTLQTKLRLSNRPAFMPSEGKMV 380

sp|P12814|ACTN1_HUMAN/1-892  362 SDINNAWGCLEQVEKGYEEWLLNEIRRLERLDHLAEKFRQKASIHEAWTDGKEAMLRQKDYETATLSEIKALLKKH 437
sp|P35609|ACTN2_HUMAN/1-894  369 SDIAGAWQRLEQAEKGYEEWLLNEIRRLERLEHLAEKFRQKASTHETWAYGKEQILLQKDYESASLTEVRALLRKH 444
sp________ACTN3_HUMAN/1-901  376 SDIANAWRGLEQVEKGYEDWLLSEIRRLQRLQHLAEKFRQKASLHEAWTRGKEEMLSQRDYDSALLQEVRALLRRH 451
sp|O43707|ACTN4_HUMAN/1-911  381 SDINNGWQHLEQAEKGYEEWLLNEIRRLERLDHLAEKFRQKASIHEAWTDGKEAMLKHRDYETATLSDIKALIRKH 456

sp|P12814|ACTN1_HUMAN/1-892  438 EAFESDLAAHQDRVEQIAAIAQELNELDYYDSPSVNARCQKICDQWDNLGALTQKRREALERTEKLLETIDQLYLE 513
sp|P35609|ACTN2_HUMAN/1-894  445 EAFESDLAAHQDRVEQIAAIAQELNELDYHDAVNVNDRCQKICDQWDRLGTLTQKRREALERMEKLLETIDQLHLE 520
sp________ACTN3_HUMAN/1-901  452 EAFESDLAAHQDRVEHIAALAQELNELDYHEAASVNSRCQAICDQWDNLGTLTQKRRDALERMEKLLETIDQLQLE 527
sp|O43707|ACTN4_HUMAN/1-911  457 EAFESDLAAHQDRVEQIAAIAQELNELDYYDSHNVNTRCQKICDQWDALGSLTHSRREALEKTEKQLEAIDQLHLE 532

sp|P12814|ACTN1_HUMAN/1-892  514 YAKRAAPFNNWMEGAMEDLQDTFIVHTIEEIQGLTTAHEQFKATLPDADKERLAILGIHNEVSKIVQTYHVNMAGT 589
sp|P35609|ACTN2_HUMAN/1-894  521 FAKRAAPFNNWMEGAMEDLQDMFIVHSIEEIQSLITAHEQFKATLPEADGERQSIMAIQNEVEKVIQSYNIRISSS 596
sp________ACTN3_HUMAN/1-901  528 FARRAAPFNNWLDGAVEDLQDVWLVHSVEETQSLLTAHDQFKATLPEADRERGAIMGIQGEIQKICQTYGLRPCST 603
sp|O43707|ACTN4_HUMAN/1-911  533 YAKRAAPFNNWMESAMEDLQDMFIVHTIEEIEGLISAHDQFKSTLPDADRFREAILAIHKEAQRIAESNHIKLSGS 608

sp|P12814|ACTN1_HUMAN/1-892  590 NPYTTITPQEINGKWDHVRQLVPRRDQALTEEHARQQHNERLRKQFGAQANVIGPWIQTKMEEIGRISIEMHGTLE 665
sp|P35609|ACTN2_HUMAN/1-894  597 NPYSTVTMDELRTKWDKVKQLVPIRDQSLQEELARQHANERLRRQFAAQANAIGPWIQNKMEEIARSSIQITGALE 672
sp________ACTN3_HUMAN/1-901  604 NPYITLSPQDINTKWDMVRKLVPSRDQTLQEALARQQVNERLRRQFAAQANAIGPWIQAKVEEVGRLAAGLAGSLE 679
sp|O43707|ACTN4_HUMAN/1-911  609 NPYTTVTPQIINSKWEKVQQLVPKRDHALLEEQSKQQSNEHLRRQFASQANVVGPWIQTKMEEIGRISIEMNGTLE 684

sp|P12814|ACTN1_HUMAN/1-892  666 DQLSHLRQYEKSIVNYKPKIDQLEGDHQLIQEALIFDNKHTNYTMEHIRVGWEQLLTTIARTINEVENQILTRDAK 741
sp|P35609|ACTN2_HUMAN/1-894  673 DQMNQLKQYEHNIINYKNNIDKLEGDHQLIQEALVFDNKHTNYTMEHIRVGWELLLTTIARTINEVETQILTRDAK 748
sp________ACTN3_HUMAN/1-901  680 EQMAGLRQQEQNIINYKTNIDRLEGDHQLLQESLVFDNKHTVYSMEHIRVGWEQLLTSIARTINEVENQVLTRDAK 755
sp|O43707|ACTN4_HUMAN/1-911  685 DQLSHLKQYERSIVDYKPNLDLLEQQHQLIQEALIFDNKHTNYTMEHIRVGWEQLLTTIARTINEVENQILTRDAK 760

sp|P12814|ACTN1_HUMAN/1-892  742 GISQEQMNEFRASFNHFDRDHSGTLGPEEFKACLISLGYDIGNDPQGEAEFARIMSIVDPNRLGVVTFQAFIDFMS 817
sp|P35609|ACTN2_HUMAN/1-894  749 GITQEQMNEFRASFNHFDRRKNGLMDHEDFRACLISMGYDL-----GEAEFARIMTLVDPNGQGTVTFQSFIDFMT 819
sp________ACTN3_HUMAN/1-901  756 GLSQEQLNEFRASFNHFDRKRNGMMEPDDFRACLISMGYDL-----GEVEFARIMTMVDPNAAGVVTFQAFIDFMT 826
sp|O43707|ACTN4_HUMAN/1-911  761 GISQEQMQEFRASFNHFDKDHGGALGPEEFKACLISLGYDVENDRQGEAEFNRIMSLVDPNHSGLVTFQAFIDFMS 836

sp|P12814|ACTN1_HUMAN/1-892  818 RETADTDTADQVMASFKILAGDKNYITMDELRRELPPDQAEYCIARMAPYTGPDSVPGALDYMSFSTALYGESDL  892
sp|P35609|ACTN2_HUMAN/1-894  820 RETADTDTAEQVIASFRILASDKPYILAEELRRELPPDQAQYCIKRMPAYSGPGSVPGALDYAAFSSALYGESDL  894
sp________ACTN3_HUMAN/1-901  827 RETAETDTTEQVVASFKILAGDKNYITPEELRRELPAKQAEYCIRRMVPYKGSGAPAGALDYVAFSSALYGESDL  901
sp|O43707|ACTN4_HUMAN/1-911  837 RETTDTDTADQVIASFKVLAGDKNFITAEELRRELPPDQAEYCIARMAPYQGPDAVPGALDYKSFSTALYGESDL  911
```

Fig. C.11: Sequence alignment of human α-actinin isoforms. Alignment performed via Clustal algorithm with default settings.



Fig. C.12: Sequence alignment of human YAP1 and TAZ isoforms. Alignment performed via Clustal algorithm with default settings.



Fig. C.13: Sequence alignment of human SYNPO2 constructs utilized. Alignment performed via Clustal algorithm with default settings.

Appendix E

Vector maps

pETW1-EEF

Vector size: 3638 bp

Origin: pET23a (Novagen/Sigma-Aldrich)

Features:

T7 promoter

5'-His_6-tag

EEF-tag

3'-His_6-tag

Ampicillin resistance cassette

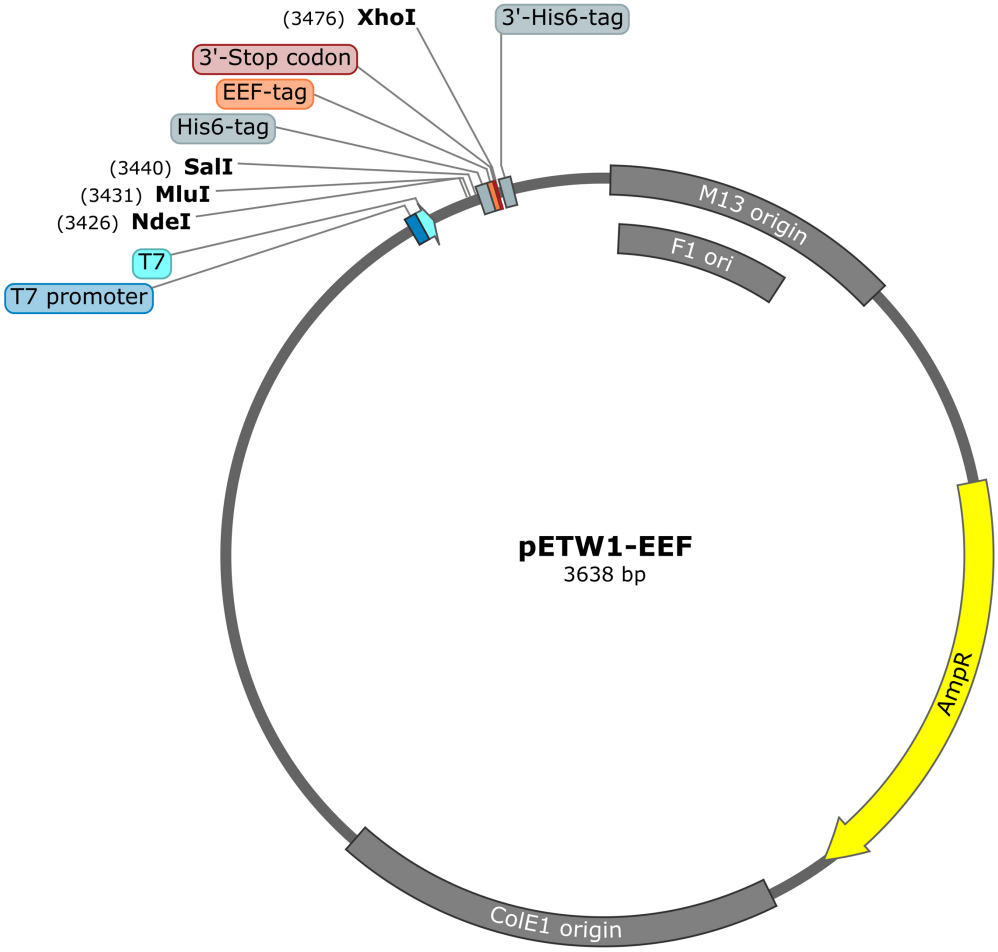


Fig. C.14

pETW2-T7

Vector size: 3644 bp

Origin: pET23a (Novagen/Sigma-Aldrich)

Features:

T7 promoter

T7 immuno-tag (T7-tag peptide)

3'-His_6-tag

Ampicillin resistance cassette

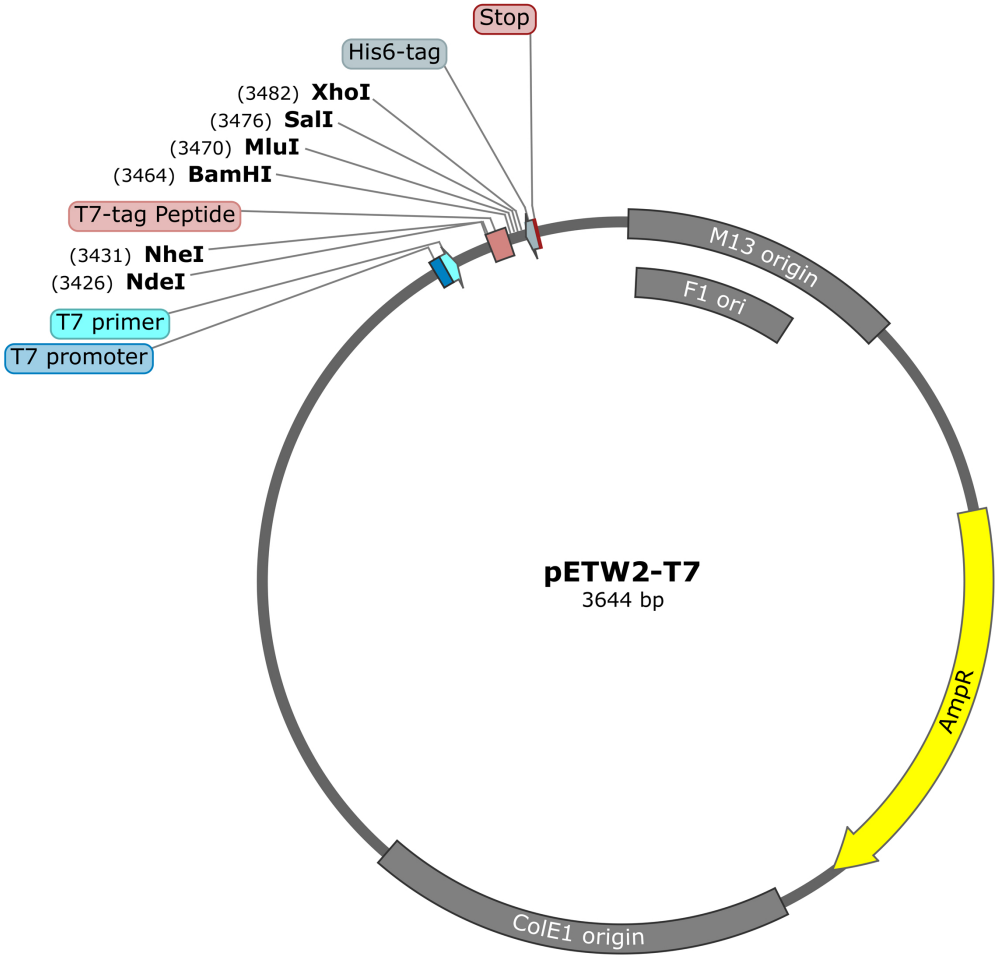


Fig. C.15

pGEX-6P

Vector size: 4985 bp

Origin: Novagen/Sigma-Aldrich

Features:

tac promoter

Glutathione-S-transferase (GST)-tag

3C/PreScission protease cleavage site

Ampicillin resistance cassette

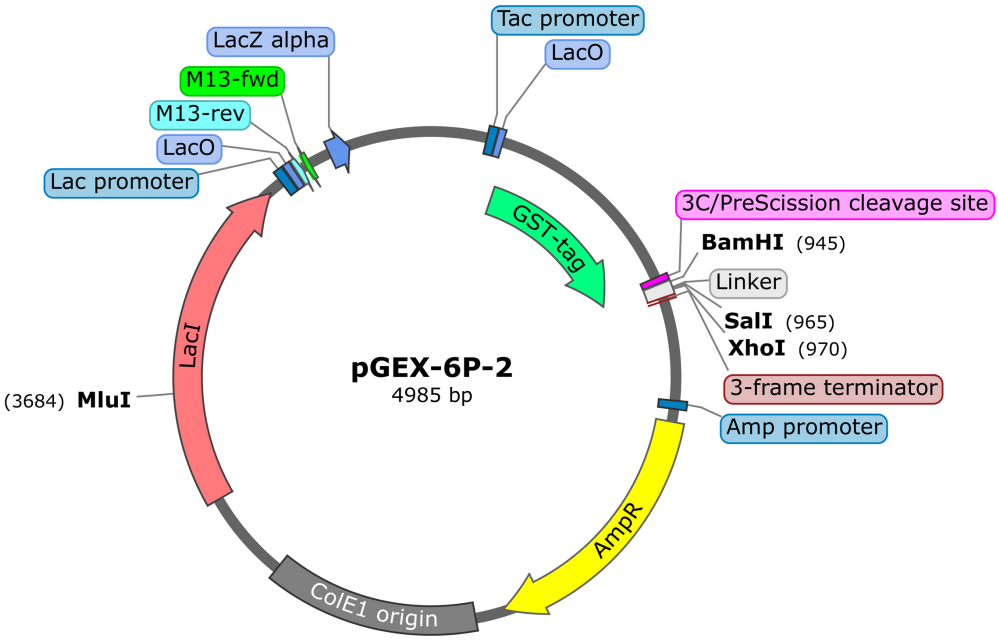


Fig. C.16

pGEX-W2-hybrid

Vector size: 5008 bp

Origin: Marvin Aßent, 2020

Features:

tac promoter

Glutathione-S-transferase (GST)-tag

3C/PreScission protease cleavage site

EEF-tag

3'-His_6-tag

Ampicillin resistance cassette

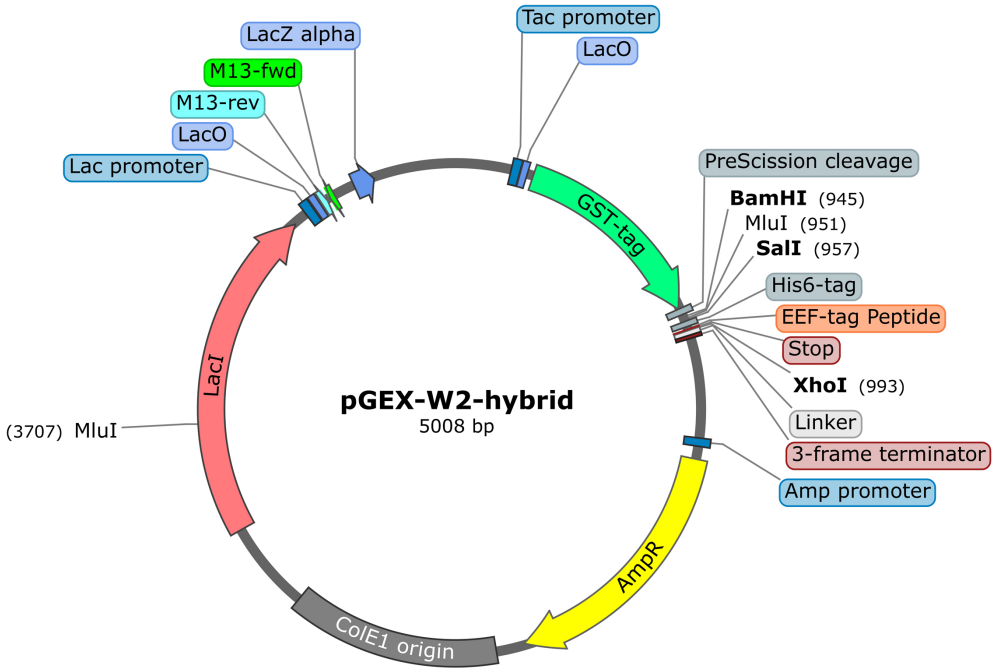


Fig. C.17

pEGFP-N1Pd

Vector size: 4710 bp

Origin: Clontech/Takara Bio

Features:

Cauliflower mosaic virus (CMV) promoter

enhanced GFP (eGFP)-tag

Kanamycin/Neomycin resistance cassette

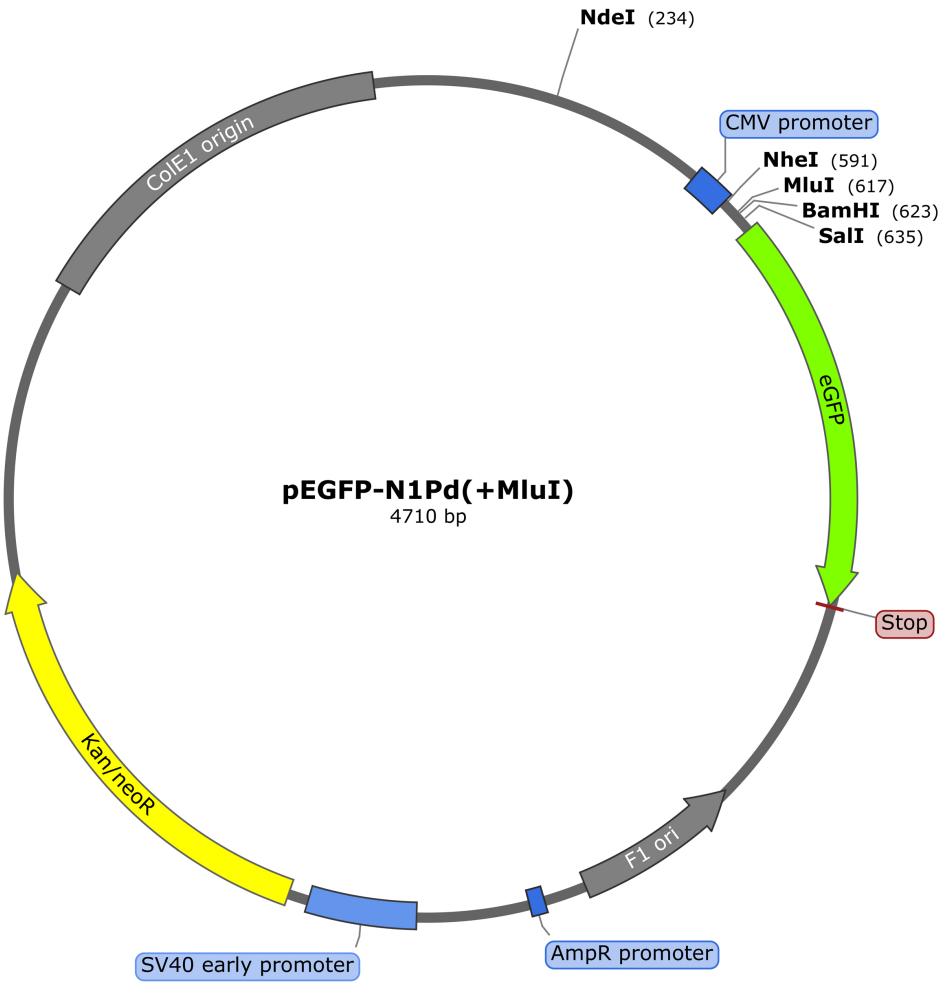


Fig. C.18

pEGFP-C1Pd

Vector size: 4732 bp

Origin: Clontech/Takara Bio

Features:

Cauliflower mosaic virus (CMV) promoter

Kozak sequence

enhanced GFP (eGFP)-tag

Kanamycin/Neomycin resistance cassette

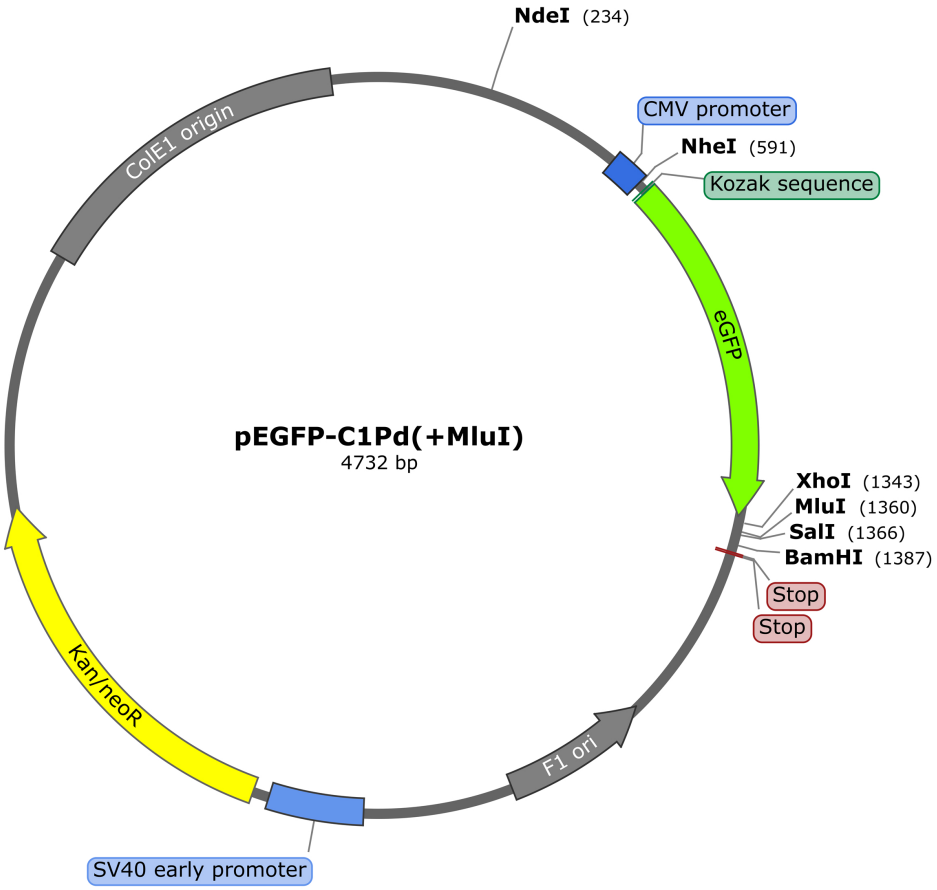


Fig. C.19

pVenus1-C

Vector size: 4461 bp

Origin: Clontech/Takara Bio

Features:

Cauliflower mosaic virus (CMV) promoter

Venus1-tag

FLAG-tag (FLAG peptide)

Kanamycin/Neomycin resistance cassette

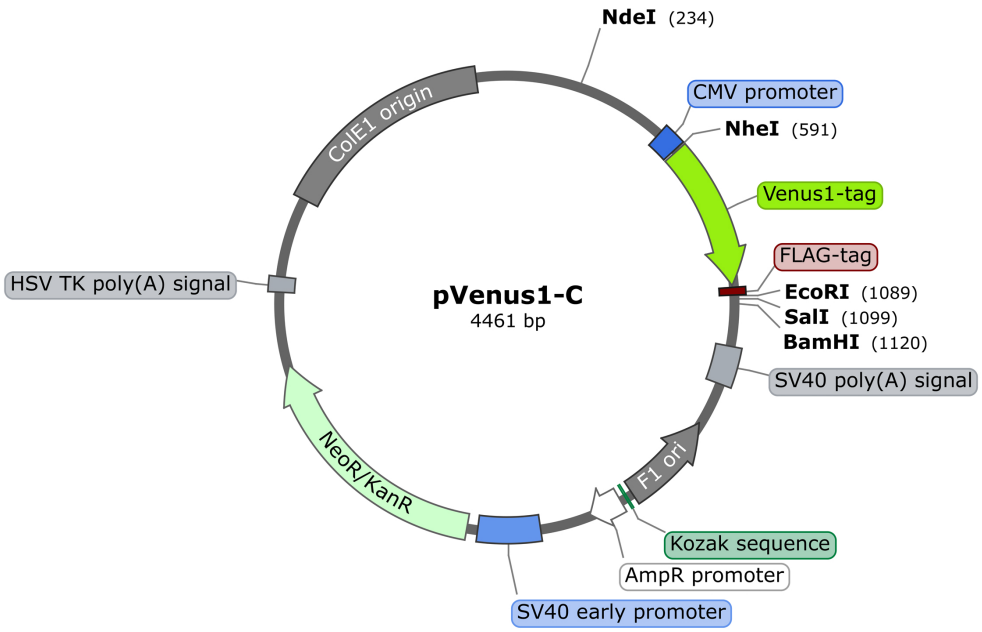


Fig. C.20

pVenus2-C

Vector size: 4266 bp

Origin: Clontech/Takara Bio

Features:

Cauliflower mosaic virus (CMV) promoter

Venus2-tag

Hemagglutinin (HA)-tag

Kanamycin/Neomycin resistance cassette

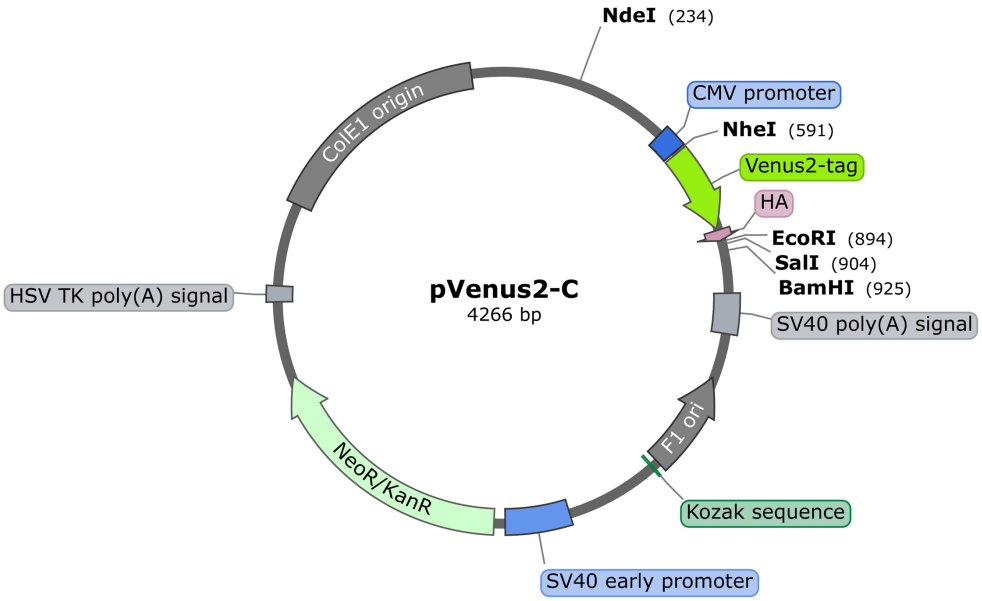


Fig. C.21

pVenus1-N3

Vector size: 4260 bp

Origin: Clontech/Takara Bio

Features:

Cauliflower mosaic virus (CMV) promoter

Venus1-tag

FLAG-tag (FLAG peptide)

Kanamycin/Neomycin resistance cassette

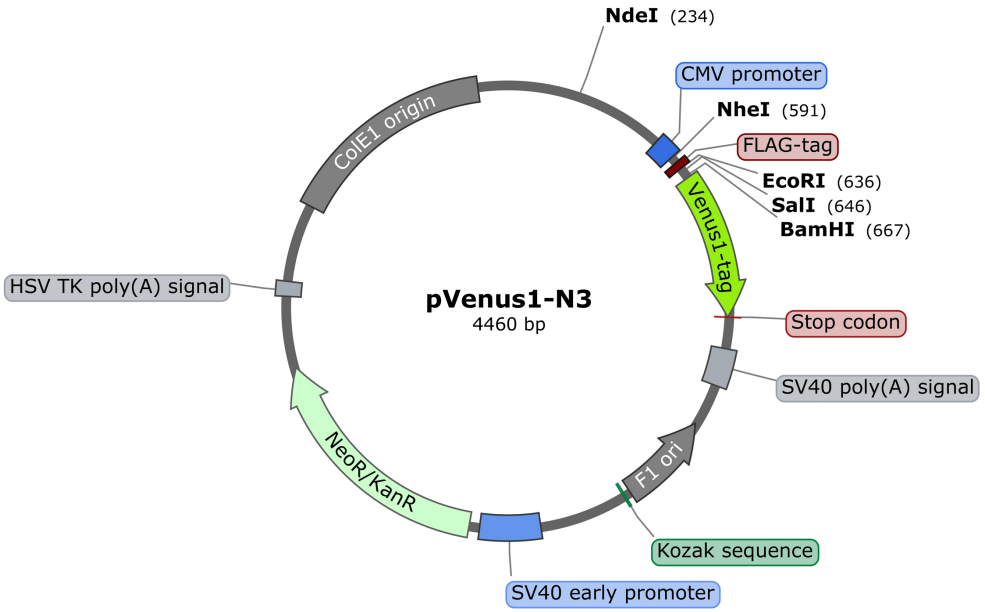


Fig. C.22

pVenus2-N3

Vector size: 4262 bp

Origin: Clontech/Takara Bio

Features:

Cauliflower mosaic virus (CMV) promoter

Venus2-tag

Hemagglutinin (HA)-tag

Kanamycin/Neomycin resistance cassette

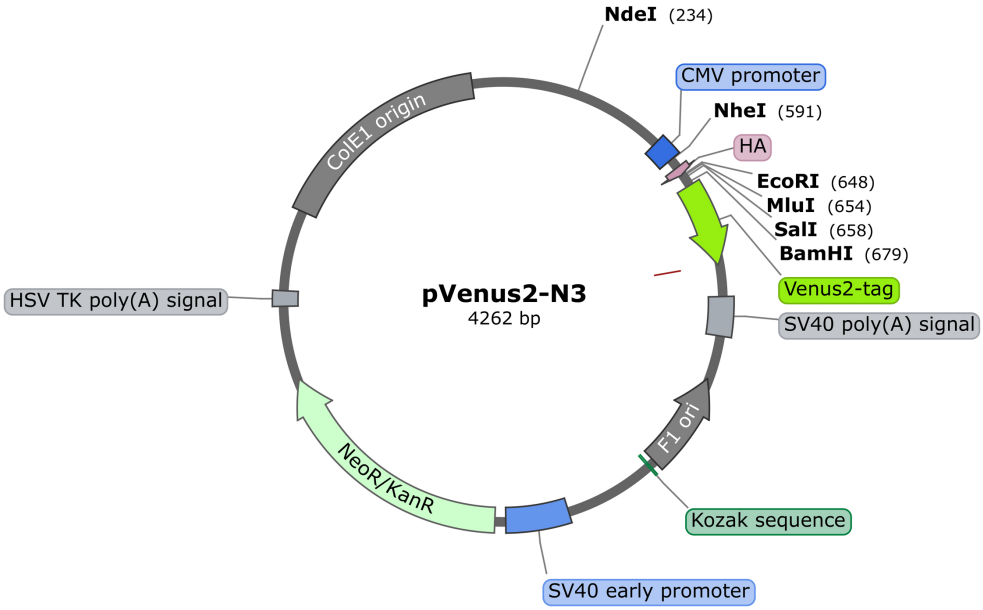


Fig. C.23

Appendix F

Suppliers, manufacturers, developers and publishers

Tab. E.1: Company list

Company name	**Place of incorporation, Country of origin**
Adobe Inc.	San José, California, USA
Agilent Technologies, Inc.	Santa Clara, California, USA
AppliChem GmbH	Darmstadt, Germany
ASV Sterilization GmbH	Trostberg, Germany
Avantor, Inc.	Radnor, Pennsylvania, USA
Beckman Coulter, Inc.	Brea, California, USA
Analytik Jena GmbH	Jena, Germany
Bio-Rad Laboratories, Inc.	Hercules, California, USA
Carl Zeiss AG	Oberkochen, Germany
Cell Signaling Technology, Inc.	Danvers, Massachusetts, USA
Cube Biotech	Monheim a.R., Germany
Corel Corporation	Ottawa, Ontario, Canada
Cytiva	Marlborough, Massachusetts, USA
Eppendorf AG	Hamburg, Germany
GE Healthcare	Chicago, Illinois, USA
GSL Biotech LLC	San Diego, California, USA
GraphPad Software, Inc.	San Diego, California, USA
Greiner Bio-One International GmbH	Kremsmünster, Austria
Heracell	Bremen, Germany
Hielscher Ultrasonics GmbH	Teltow, Germany
Implen GmbH	Munich, Germany
Invitrogen/Thermo Fisher	Carlsbad, California, USA
Ion Optix Corp.	Milton, Massachusetts, USA
Ismatec SA	Glattbrugg, Switzerland
Jackson ImmunoResearch Laboratories, Inc.	West Grove, Pennsylvania, USA
Köhler Chemie GmbH	Alsbach-Hähnlein, Germany
LI-COR Biosciences	Lincoln, Nebraska, USA
Lonza Group Ltd	Basel, Switzerland
Macherey-Nagel GmbH & Co. KG	Düren, Germany
Merck KGaA	Darmstadt, Germany

Tab. E.1: Company list

Company name	**Place of incorporation, Country of origin**
Microsoft Corporation	Redmond, Washington, USA
Novagen	Madison, Wisconsin, USA
Polyplus-transfection SA	Illkirch-Graffenstaden, France
Proteintech Group, Inc.	Manchester, United Kingdom
Qiagen	Hilden, Germany
Roche Diagnostics GmbH	Basel, Switzerland
Roth Industries GmbH & Co. KG	Karlsruhe, Germany
Santa Cruz Biotechnology, Inc.	Santa Cruz, California, USA
Sarstedt AG & Co.	Nümbrecht, Germany
Schlüter GmbH	Hamburg, Germany
Sigma-Aldrich	St. Louis, Missouri, USA
Snapgene.com/GSL Biotech LLC	San Diego, California, USA
Solis BioDyne	Tartu, Estonia
Starlab Group	Hamburg, Germany
Takara Bio Inc.	Kusatsu, Shiga, Japan
TPP Techno Plastic Products AG	Trasadingen, Switzerland
Th. Geyer GmbH & Co. KG	Renningen, Germany
Thermo Fisher Scientific Inc.	Waltham, Massachusetts, USA
VWR International GmbH	Radnor, Pennsylvania, USA